Thermo-hydro-mechanical behavior of an embankment to store thermal energy

Mojdeh Lahoori




UNIVERSITÉ DE LORRAINE

École doctorale SIMPPÉ
Science et Ingénierie des Molécules, des Produits,
des Procédés et de l'énergie
Laboratoire d'Énergétique et de
Mécanique Théorique et Appliquée

THÈSE

Présentée en vue de l'obtention du grade de
Docteur de l'Université de Lorraine
Spécialité : Énergie et Mécanique

Par

Mojdeh LAHOORI

Thermo-hydro-mechanical behavior of an embankment to store thermal energy

Soutenue le 17 Décembre 2020 devant la commission d'examen :

M. Akbar Javadi	Professeur-Université de Exeter	Rapporteur
M. Anh Minh TANG	Directeur de recherche-Ecole des Ponts ParisTech	Rapporteur
M. Daniel Dias	Professeur-Université de Grenoble-Alpes	Examinateur
M. Hossein Nowamooz	Maître de Conferences- INSA de Strasbourg	Examinateur
Mme. Farimah Masrouri	Professeur-Université de Lorraine	Directeur de Thèse
Mme. S. Rosin-Paumier	Maître de Conferences-Université de Lorraine	Co-directeur de Thèse

To my Mum and Dad,
To my Brothers,
To Soheib,

Acknowledgment

The research included in this thesis could not been performed if not for the assistance, patience and support of many individuals. I would like to express my appreciation to Professor Farimah Masrouri for supervising my thesis through these three years and for scientific discussions and advices all along my doctoral study. I would like to thank my co-supervisor, Dr. Sandrine Rosin for being always available and editing the thesis.

I would like express my thanks to Dr. Yves Jannot for fruitful discussions on thermal behavior of materials. Your great scientific qualities, listening skills and calm personality allowed me to grow and learn pleasantly. I appreciate the work that I have done with you.

My deep gratitude to Dr. Adel Abadallah, for valuable suggestions to overcome difficulties encountered during my PhD thesis.

I should express my thanks to the members of jury; Prof. Akbar Javadi, Prof. Daniel Dias, Dr. Anh-Minh Tang, Dr. Hossein Nowamooz for their time and precious comments.

I should express my gratitude to Dr Hossein Nowamooz and Fojia Tang for warmly welcoming me in their engineering school. The collaboration with them was very professional.

I would like also to thank Sarah Feuillatre who helped me to advance my administrative stuff. Thanks Sarah for helping me in administrative issues while always smiling.

I would like also to extend my thanks to Moise, Marvin, Zayad, Ahmed, and Alice and all the others that I met in the laboratory during my thesis. I would like to additionally thank my Iranian friends which without them these three years of thesis would not have been so easy. I need to truly thank to two friends of mine Marie Christelle and Anges for all the moments that we shared and for all their supports and helps.

I would like to express an immeasurable amount of gratitude to my parents and my brothers Rouzbeh and Mazyar, for their endless love, support and encouragement through all my life.

Finally I would like to thank Soheib, my love, who always guided me when I was lost, encouraged me when I was down, supported and motivated me to go further while always stand next to me. Thank you for your endless help and great advice.

Mojdeh

Abstract

Nowadays, thermal energy storage in geostructures like embankments can be possible by installing the horizontal heat exchangers in different layers of compacted soil. In this system, the thermal energy is stored in summer via a fluid, circulating in the heat exchangers, to be extracted in the demand period. When the serviceability of embankment as a medium to store the thermal energy starts, the compacted soil will be subjected to the daily and seasonally temperature variations. These seasonal temperature variations could modify the thermo-hydro-mechanical performance of the compacted soil. Thus, the aim of this study is to investigate the thermal and mechanical performances of a compacted soil when it is subjected to monotonic and cyclic temperature variations.

The studied soil is a sandy lean clay that is frequently used in embankment constructions in France. The thermal and mechanical behavior of the soil are investigated at a compaction state corresponding to the optimal thermal properties. However, this compacted soil is unsaturated and the estimation of its thermal properties is complex. In this study, an inverse analytical model is proposed to estimate the thermal properties of the soil using temperature monitoring in the range of 20 to 50 ^oC in a soil compacted in a large container. The estimated thermal parameters were compared to classical laboratory measurements (transient and steady-state methods). The comparison showed that the estimated values were close to the results obtained in transient laboratory method. Using this method, the thermal efficiency of the compacted soil can be verified in the lifetime of the storage system.

To ensure the structure stability, long-term mechanical response of these systems subjected to monotonic and cyclic temperature variations should be investigated. To achieve this aim, using temperature-controlled oedometric and direct shear devices, consolidation and shear parameters of the studied soil at different monotonic (5, 20, and 50 ^oC) and cyclic (5 to 50 ^oC) temperatures were investigated. The results of temperature-controlled oedometric tests showed that the effect of the temperature variation is more pronounced under vertical pressures higher than the preconsolidation pressure. The compression and swelling indexes could be considered independent of temperature variations. Therefore, the overall settlement of the embankment due to thermal variation near the heat exchangers could be considered negligible.

The results of temperature-controlled direct shear tests showed that the temperature variations (monotonic heating or cooling, or temperature cycles) increased the cohesion which is beneficial for the bearing capacity and slope stability of embankments. These results can be

directly used in the design of embankments to store thermal energy exposed to similar thermo-mechanical paths.

Finally, the thermal performance of the compacted soil is verified using a numerical simulation considering the soil atmosphere interaction. Different depths installation of heat exchanger loops and different heat storage scenarios were simulated. The results showed that the compacted soil increases 8.5% the systems performance compared to the horizontal loop installation in the local soil. The results of two different scenarios show that an inlet fluid temperature of 50 ^oC in summer increases highly the system performance (13.7% to 41.4%) while the improvement is less significant (0% to 4.8%) for the ambient inlet temperature. Moreover, a deeper installation of horizontal loops increases the system performance. From the numerical simulation results can be concealed that the embankment is in interaction with the atmosphere from its upper and lateral surfaces, the thermal efficiency of the structure could be affected due to heat losses. Therefore, it is preferable to place the heat exchangers away from the top and side surfaces.

Keywords: Embankment, compacted soil, thermo-hydro-mechanical, soil thermal properties, analytical model, temperature-controlled oedometric tests, temperature-controlled direct shear tests, numerical simulations, soil-atmosphere interaction, installation depth.

Résumé

Le stockage de chaleur dans des géostructures énergétiques telles que des remblais est réalisable en installant des échangeurs horizontaux au sein des différentes couches de sol compacté. Dans ce système, l'énergie thermique qui est injectée en été via un fluide caloporteur circulant dans les échangeurs de chaleur, peut être extraite en période hivernale. Dans ces conditions, lors de la mise en service, le sol compacté est soumis à des variations de température quotidiennes et saisonnières. Ces variations pourraient modifier les performances thermo-hydro-mécaniques du sol compacté. Ainsi, le but de cette étude est d'étudier les performances thermiques et mécaniques d'un sol compacté lorsqu'il est soumis à des variations de température monotones et cycliques.

Le sol étudié est un limon fréquemment utilisé dans les constructions de remblais en France. Le comportement thermique et mécanique du sol est étudié à un état de compactage correspondant aux propriétés thermiques optimales. Dans cet état, le sol compacté est non saturé ce qui complexifie l'estimation de ses propriétés thermiques. Pour pallier à ces difficultés, dans cette étude, un modèle inverse est proposé pour estimer les propriétés thermiques du sol compacté. L'efficacité du modèle est testée sur un jeu de données acquises dans la gamme de 20 à 50 ^oC dans un modèle réduit en laboratoire. Les valeurs obtenues sont ensuite comparées à des mesures classiques en laboratoire (méthodes en régime transitoire et en régime permanent). Cette méthode pourrait permettre de suivre l'évolution des propriétés thermiques du stockage et ainsi assurer son efficacité tout au long de sa durée de vie.

La question de la stabilité à long terme de ces structures soumises à des variations thermiques monotones (5, 20 et 50 ^oC) et cycliques (5 à 50 ^oC) est ensuite abordée à l'aide d'essais oedomètriques et d'essais de cisaillement direct à température contrôlée. Les résultats des essais de compressibilité ont montré que l'effet de la variation de température est plus prononcé sous une contrainte verticale supérieure à la pression de préconsolidation. Les indices de compression et de gonflement peuvent être considérés comme indépendants des variations de température. Donc le tassement global du remblai dû aux variations thermiques pourrait être considéré comme négligeable. Les résultats des essais de cisaillement direct ont montré que les variations de température (monotones ou cycliques) augmentent la cohésion ce qui est avantageux pour la capacité portante et la stabilité des pentes des remblais. Dans la phase de conception d'un remblai de stockage, ces résultats seraient utiles au dimensionnement du système si des trajectoires thermomécaniques similaires à celles de cette étude sont respectées.

Dans une dernière partie, une simulation numérique prenant en compte l'interaction sol-atmosphère est réalisée afin d'évaluer la performance thermique de ce sol compacté en conditions naturelles. Différentes profondeurs d'installation de boucles d'échangeurs de chaleur sont testéss ainsi que différents scénarios de stockage. Les résultats ont montré que le sol compacté augmente de 8.5% les performances du système par rapport à l'installation d'une boucle horizontale dans le sol naturel (non compacté). Les résultats de deux scénarios différents ont montré qu'en été avec un fluide ayant une température d'entrée de 50 ^oC augmente significativement la performance du système. De plus, une installation plus profonde des boucles horizontales améliore également la performance du système. Il convient de noter que le remblai est en interaction avec l'atmosphère depuis ses surfaces supérieure et latérale, l'efficacité thermique de la structure pourrait être affectée en raison des pertes de chaleur. Par conséquent, il est préférable de placer les échangeurs de chaleur loin des surfaces supérieures et latérales.

Mots clés: Géostructures énergétiques, sol compacté, thermo-hydro-mécaniques, propriétés thermiques du sol, modèle analytique, essais oedométriques à température contrôlée, essais de cisaillement direct à température contrôlée, simulations numériques, l'interaction sol-atomosphère, profondeur d'installation.

Publications

This study is a paper based thesis consists of 4 chapters and an appendix. Chapter I is dedicated to literature review. Chapter II, III and IV and appendix are the papers which are published or are under review in scientific journals.

Journal papers:

• **Lahoori, M.**, Jannot, Y., Rosin-Paumier, S., Boukelia, A., and Masrouri, F. Measurement of the thermal properties of unsaturated compacted soil by the transfer function estimation method. *Applied Thermal Engineering* 167, 114795. (2020): https://doi.org/10.1016/j.applthermaleng.2019.114795 (**Chapter II**).

• **Lahoori, M.**, Rosin-Paumier, S., and Masrouri, F. Effect of monotonic and cyclic temperature variations on mechanical behavior of a compacted soil. (Under review) (**Chapter III**)

• Tang, F., **Lahoori, M.**, Nowamooz, H., Rosin-Paumier, S., and Masrouri, F. Effect of compacted backfill soil and energy storage on the heat pump performance of a Horizontal Ground Heat Exchanger. (Under review) (**Chapter IV**).

• **Lahoori, M.**, Rosin-Paumier, S., Stoltz, G., and Jannot, Y. Thermal conductivity of non-woven needle-punched geotextiles: effect of stress and moisture . *Geosynthetics International*, (Jun 2020): https://doi.org/10.1680/jgein.20.00034 (**Appendix**).

Conference papers:

• **Lahoori, M.**, Stoltz, G., Rosin-Paumier, S., and Masrouri, F. (2019, March). Evaluation des performances des géotextiles non-tissés-aiguilletés pour l'isolation thermique des géostructures énergétiques. In 12e Rencontres Géosynthétiques (RGS). (oral presentation in French)

• **Lahoori, M.**, Rosin-Paumier, S., and Masrouri, F. Thermo-hydro-mechanical behavior of an embankment thermal storage (Accepted). CPEG2020– 3rd International Symposium on Coupled Phenomena in Environmental Geotechnics, Kyoto, Japan, March 17-19 2021.

• **Lahoori, M.**, Rosin-Paumier, S., Jannot, Y., Boukelia, A., and Masrouri, F. Thermal energy storage in embankments: Investigation of the thermal properties of an unsaturated compacted soil (Accepted). ICEGT-2021-2nd International Conference on Energy Geotechnics, California, USA, March 28-31 2021.

Contents

List of Figures

List of Tables

General Introduction

Thermal energy storage in mediums such as aquifers, rocks, natural and compacted soils is likely to reduce the dependency on fossil fuel and to contribute in producing renewable energy. Thermal energy is stored in these mediums during summer, to be preserved and later discharged for utilization in the demanded period. The source of the thermal energy can be solar energy which is a clean and affordable source. In storage systems, the heat will be exchanged with the ground via vertical or horizontal heat exchanger loops. Due to the cost-benefit and less environmental impact, the horizontal heat exchanger is more beneficial than the vertical one even if it needs more space. In this context, road and rail embankments show great potential to embed the horizontal heat exchanger loops due to their linear position on the ground. The embankments contain several layers of compacted soil that are made to achieve the desired level for construction of roads, highways, railways, and the base for buildings.

The proper design of an embankment to store the thermal energy requires the knowledge of soil compaction state, soil thermal properties and also the position of heat exchangers loops (depth, pattern, and spacing). Compacted soils are usually unsaturated but close to saturation state (degree of saturation between 85 to 95%). Therefore, adding temperature variations to this multi-phase medium, complicates the estimation or measurement of soil thermal properties such as volumetric heat capacity, thermal conductivity, and thermal diffusivity. Therefore, a reliable estimation and measurement method to determine the soil thermal properties is of paramount importance in the efficiency analysis of these structures.

Considering an embankment supposed to be used as a storage medium, the compacted soil will be subjected to daily and seasonally temperature variations from the atmosphere and heat exchangers. These cyclic temperature variations (5 to 50 ^oC) can modify the thermo-hydro-mechanical behavior of the compacted soil.

In terms of structural stability, the most important mechanical parameters of an embankment are the settlement and the mechanical stability of slopes. Several studies showed that temperature variations can provide more or less significant soil volumetric variations depending on the material and soil stress history. Therefore, even though the compacted soil can be selected based on its thermal performance, its mechanical behavior in different states (saturated and unsaturated), and under different stresses (in different depths of an embankment) should be investigated.

Until now, the thermo-hydro-mechanical behavior of storage mediums can be investigated

numerically using different finite-elements and finite-difference tools. However, the mass transfer in the soil medium due to the temperature variation has rarely been studied. In some studies, the soil medium is supposed to be homogeneous with constant thermal properties. Whereas, thermo-hydraulic transfer could change the thermal and mechanical properties of compacted soils. Therefore, in the design stage, a coupled thermo-hydro-mechanical simulation is generally required to investigate the stability and durability of the structure as a storage medium.

Four chapters are developed in this study to tackle the above-mentioned aspects. The aim of each chapter is summarized in the following:

Chapter I describes the different methods to store the thermal energy in soil, among them the thermal energy storage in embankments is presented as a newly proposed method. For a deep understanding of the thermal efficiency of this storage system, the mechanism of heat and mass transfer and soil thermal properties are presented in detail. Also, the evolution of soil thermal properties according to the soil physical and hydraulic properties are investigated. Then, to investigate the mechanical performance of a compacted soil due to temperature variations, a section is dedicated to introduce the thermal effects on hydraulic properties, consolidation parameters, and shear behavior of soil. Finally, the existing theoretical and constructive models to perform a coupled thermo-hydro-mechanical simulation of the storage system are presented. At the end, the most important issues concerning the thermal energy storage in an embankment are envisaged and developed in chapters II, III and IV.

Chapter II presents an inverse analytical model based on temperature monitoring in compacted soil, that can estimate the thermal properties of the compacted soil over the lifetime of the storage medium. Therefore, an experimental series was developed to monitor the temperature response using different temperature sensors at different levels in a compacted soil. The studied soil was a sandy lean clay, this type of soil is usually used in France for embankment construction. The temperatures were monitored during three successive temperature cycles in the range of 20 to 50 ^oC. Then the analytical model estimates the thermal diffusivity based on the temperature variations between two temperature sensors. Using the estimated thermal diffusivity and measured volumetric heat capacity in laboratory, the thermal conductivity is calculated. Finally, the calculated thermal conductivity is compared with two classical laboratory methods.

Chapter III presents the mechanical response of compacted soil to monotonic and cyclic temperature variations using temperature-controlled oedometer and direct shear devices. Tests at different temperatures were performed to evaluate the overall settlement and slope stability of the compacted soil due to heating during thermal charging seasons (20 to 50^oC) and cooling during thermal discharging seasons (20 to 5^oC). Then, under different constant vertical stress, several temperature cycles in the range of 5 to 50 ^oC were applied on compacted soil samples. These results reproduce the volumetric deformation of a compacted soil element in different depths of an embankment which is under seasonal temperature variations from the atmosphere and also from the horizontal heat exchangers. Finally, the compacted soil samples were sheared

to investigate the effect of temperature cycles on shear characteristics. These results were compared with the monotonic thermo-mechanical paths and discussed in terms of engineering application.

In **Chapter IV**, by using a validated constitutive model, the soil-atmosphere interaction on the soil surface was taken into account to show the performance of a compacted soil as a storage medium. The meteorological conditions corresponding to the local conditions in Alsace (France) were applied on soil surface. The hydro-thermal properties of the compacted soil were measured in laboratory and were used in the model. Different installation depths of horizontal heat exchangers were simulated. Two storage scenarios were considered and were compared with a scenario without storage.

Chapter 1

Literature review on thermal energy storage in soils

Introduction

Nowadays, most of the energy demand is supplied by fossil fuels which are limited and also have a negative impact on the environment. Therefore, the tendency is toward renewable energies that are infinite, affordable, and have a less environmental impact. Among different types of renewable energies, solar energy shows a great potential to provide a part of electrical and thermal energies for human needs. However, during a year in European regions, solar radiation is more pronounced from May to September, while the oil and gas consumption peaks are high during cold periods, from October to April. Therefore, seasonal thermal energy storage is considered as a solution to store the solar energy during summer, in a proper medium to be preserved and discharged in winter (ICAX, 2008).

In the first section (1.1) of this chapter the geologic mediums like aquifers, natural soils, compacted soil and rocks are proposed and presented as proper mediums to store thermal energy, due to the ease of access and also the capability to store heat for the long term (Xu et al. 2014; Stojanović and Akander 2010). Then, in the second section (1.2), the mechanism of heat and mass transfer, soil thermal properties, and the influencing factors on thermal properties are investigated. The thermal energy injection and extraction in storage mediums cause monotonic and cyclic temperature variations. These variations could have a non-negligible impact on the hydraulic and mechanical proper-

ties of soils. These aspects are developed in the third section (1.3), especially when the geostructure is designed to support mechanical loads. The thermal energy storage in geologic mediums raises questions about the long-term sustainability of these structures. Finally, in the fourth section (1.4), a literature review on existing numerical models to simulate the thermo-hydro-mechanical behavior of the energy storage system is presented, to investigate the mechanical performance in the design stage.

1.1 Different methods of thermal energy storage in soils

There are different methods to store thermal energy like boundary heat storage (thermal energy storage in chemical bonds), latent heat storage (thermal energy storage in phase change materials) and sensible heat storage (thermal energy storage in a material without changing phase)(H Abedin and A Rosen 2011). This study focuses on the thermal energy storage in geological mediums which is a sensible heat storage method. It includes, aquifer thermal energy storage, borehole thermal energy storage and thermal energy storage in compacted soils. The following parts are dedicated to explain these methods in which the heat flow, Q (J), is defined as:

$$Q = \int_{T_1}^{T_2} mc_p \, \mathrm{d}T \tag{1.1}$$

where T_1 and T_2 are the initial and final temperatures of the storage material respectively (K), m is the total mass of the material (kg) and c_p is the specific heat capacity of the material $(J.kg^{-1}.K^{-1})$.

1.1.1 Aquifer thermal energy storage method

In aquifer thermal energy storage (ATES), the natural water in the saturated and permeable part of an aquifer is used as a storage medium. In winter, the relatively warm water is extracted from the heat well to circulate through the heat distribution system in the building, where it cools down and is injected into the cold well (Figure 1.1). In summer, the water follow is reversed and the cold water in the cold well is extracted for cooling the building. The aquifer thermal energy storage method has been used successfully in a

number of projects including several hundred installations in Sweden, Germany, Belgium and some other European Countries (Lee 2010). In the past couple of years, the use of this method significantly raised in the Netherlands due to the high level of the underground water table (Caljé 2010). Since 2008, in Stockholm-Arlanda airport an aquifer is used to

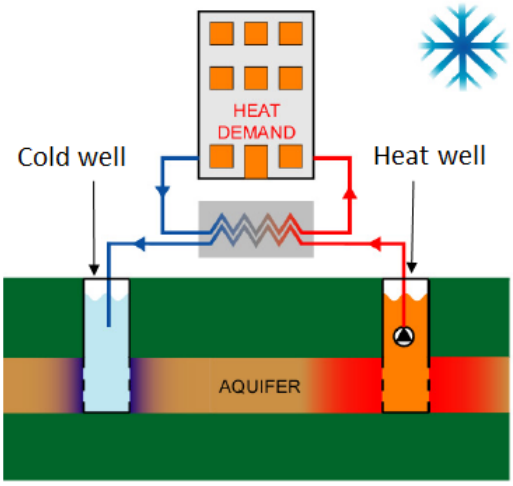

Figure 1.1: Aquifer thermal energy storage (Drijver and Willemsen 2001).

store the thermal energy for space heating or snowmelting in winter whereas in summer the cooling system is used for comfort cooling. The system is designed to cover a cooling and heating load of approximately 8 MW at a maximum underground water flow of 720 m^3/h. It has reduced the energy cost by 30% from an economic point of view (Wigstrand 2010). Beside the energy cost reducing of thermal energy storage in aquifers, however, the use of this method encounters some problems that are mentioned in the following (Schmidt et al. 2003):

• the well-clogging due to the groundwater flow;

• the variation in hydro-geological and engineering-geology conditions due to the water temperature rising in aquifers;

• the huge heat loss due to the natural groundwater flow and the interface between cool and heat wells, the cool well will impact on the heat one and vice versa.

Therefore, a good knowledge of the mineralogy, geochemistry and microbiology of the underground water is necessary to avoid the well-clogging. A correct scaling is also necessary to avoid the heat loss.

1.1.2 Borehole thermal energy storage method

Borehole thermal energy storage (BTES) is a way to store thermal energy in the ground by a series of U-tube loops placed in vertical wells (about 100 meters, Cao 2010). The boreholes are used to take advantage of the constant temperature (12 ^{0}C) of the ground below a certain depth (10-15 meters in Europe, Brandl 2006). This constant temperature can be used during winter using a ground source heat pump for space heating and during summer for cooling needs. The BTES provides an energy-efficient and environmental friendly solution. To increase its efficiency, solar energy can be stored during summer to increase the temperature of the ground, a schematic of combined solar energy and ground-source energy as hybrid energy is shown in Figure 1.2 (Gao et al. 2015). Several research

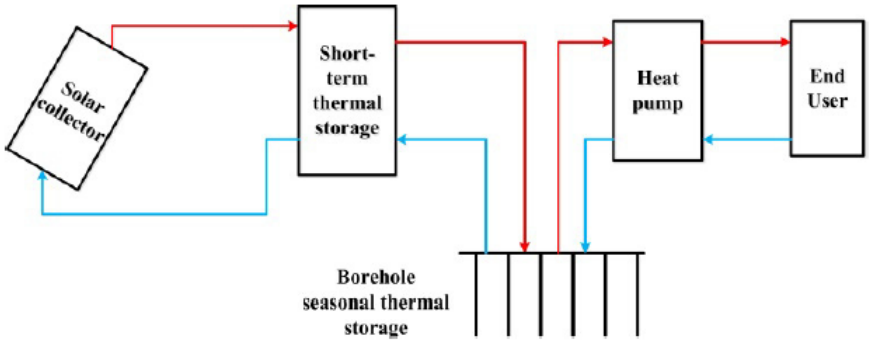

Figure 1.2: A schematic of borehole thermal energy storage by a combination of the solar energy and heat pump system (Gao et al. 2015).

studies investigated the thermal efficiency of the coupled heat pump and borehole solar energy storage numerically and experimentally (Xinguo et al. 2009, Sibbitt et al. 2012 and Wang and Qi 2008).

Girard et al. (2015) investigated the performance of the ground-source heat-pumps systems with and without solar assistance in 19 European cities. The coefficient of performance (COP_{sys}) which is the ratio between the useful energy production and energy demand varied from northern to southern locations. The COP_{sys} reached 4.3 to 5.1 without solar assistance and reached 4.4 to 5.8 with solar assistance. Results showed that solar collectors coupling with ground source heat pumps have more impact on performance improvement in regions that benefit from higher solar radiation. Due to the high thermal performance of this method, the number of boreholes in Germany raised from 24 in 1996 to approximately 18,000 in 2006. This method is also successfully used in the Netherlands

and the numbers of boreholes are almost 22500 in 2007 (Gao et al. 2015). Therefore the borehole thermal energy storage is one of the suitable methods to store solar energy in comparison with aquifer thermal energy storage method. However, the thermal energy storage in boreholes has different disadvantages:

• high cost of construction due to installation of vertical heat exchanger loops in the ground;

• environmental problems, such as increasing the groundwater temperature, and deep grouting acts as a barrier to groundwater flow;

• increase in thermal resistance between the circulating fluid and the borehole wall over time due to cracks occur in the grout above the groundwater table(Olafsen Lackey et al. 2009; Beier and Holloway 2015).

1.1.3 Thermal energy storage in compacted soils

In this section first the thermal energy storage in compacted backfill soil is introduced and then a new method to store thermal energy in embankments is also presented to point out the necessary research investigations have been carried out on it to the date.

1.1.3.1 Thermal energy storage in compacted backfill soil

In recent years, thermal energy storage in compacted soils in shallow depth of ground has been considered as a new and efficient method due to the ease of access, low cost of construction, less environmental impact and thermal energy efficiency (Gan 2013; Jradi et al. 2017). In this method, the thermal energy can be stored in compacted soil using horizontal heat exchanger loops, and then is released to heat the buildings in winter via heat pumps linked to underfloor heating (Figure 1.3).

Elminshawy et al. (2017) investigated experimentally the thermal performance of the earth-air pipe heat exchanger that was inserted in a compacted soil of the Madinah region (Saudi Arabia). The experimental setup consisted of inserting an exchanger tube in a cylindrical sample (Figure 1.4). The soil sample was compacted in the mold with target relative densities of 26, 70 and 91% (T1, T2 and T3 respectively) at an initial temperature of 20 to 25 ^oC. Then, the air was blown in the heat exchanger tube using a temperature-controlled air blow system. The imposed flow rate was in the range of 0.006 to 0.015

Figure 1.3: Thermal energy storage using horizontal heat exchanger loops (www.greenliving.lovetoknow.com).

$m^3.s^{-1}$ and its temperature was in the range of 40 to 55 ^oC.

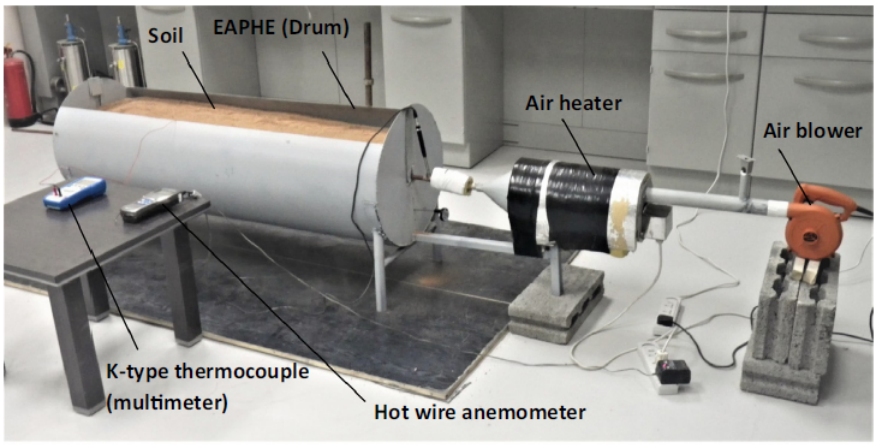

Figure 1.4: Experimental setup to investigate the horizontal air pipe heat exchanger in a compacted soil (Elminshawy et al. 2017).

The results compared the difference between inlet and outlet air temperature (ΔT). Figure 1.5 shows the results performed on soils at different densities (T1, T2 and T3) and different air flow rates but at a constant inlet air temperature of 50 ^oC. At air flow rate of 0.006 $m^3.s^{-1}$, the difference between inlet and outlet air temperature is higher than the other air flow rates and this difference increased by soil compaction level from T1 to T3. These results show that by increasing density the soil particle contact increases and consequently heat transfer by conduction increases which causes the temperature loss between the inlet and outlet air flow. This study shows that the thermal performance of this system highly depends on the soil density and air flow rate. These observations are in agreement with the study of Hurtado et al. (2012) who investigated the capacity of a

compacted soil to store thermal energy from the chimney power plant using an analytical model based on a finite volume procedure. They mentioned that the output power energy was increased by 10% when the soil compaction increased from loose to dense level.

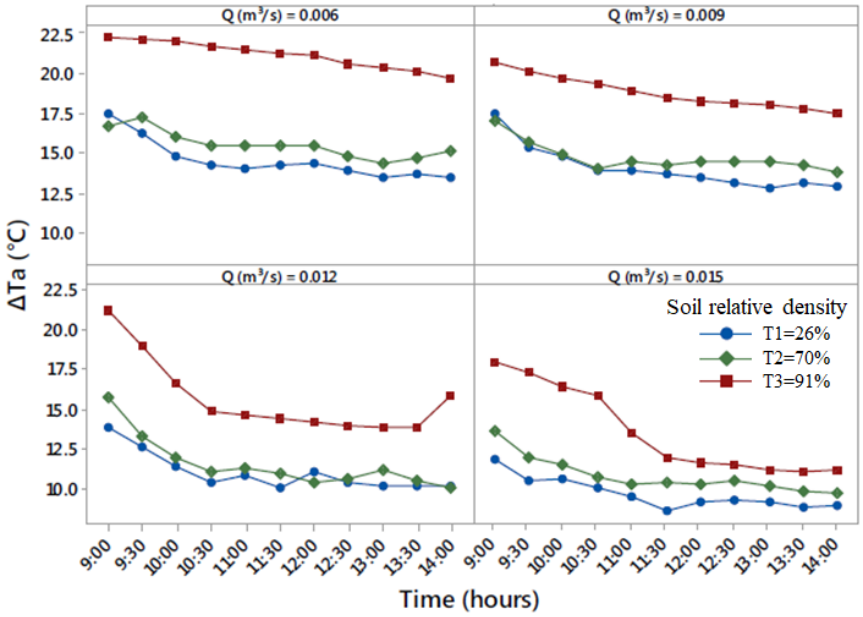

Figure 1.5: Effect of air flow rate across air pipe heat exchanger for various levels of soil compaction (modified from Elminshawy et al. 2017).

Heat exchanger loops are made of high density polyethylene material in different shapes such as linear, slinky, and spiral shape (Figure 1.6). Asgari et al. (2020) investigated numerically the thermal performance of different types of horizontal heat exchanger loops with various loop arrangements in the ground such as single, double, triple, and quadruple-layer arrangements. The thermal simulations were conducted by considering the heat transfer in the ground is coupled with mass transfer due to the fluid flow. They showed that the thermal performance of the linear and slinky types of horizontal heat exchangers increased by increasing the number of layers arrangement in the ground. For the spiral type (Figure 1.6c), the thermal performance does not change with increasing the number of layers.

1.1.3.2 Thermal energy storage in embankments

The position of heat exchanger loops in compacted soil is horizontal, therefore, a considerable area is needed which is one of the disadvantages of this method. In this content, road and rail embankments show great potential to embed the horizontal heat exchanger

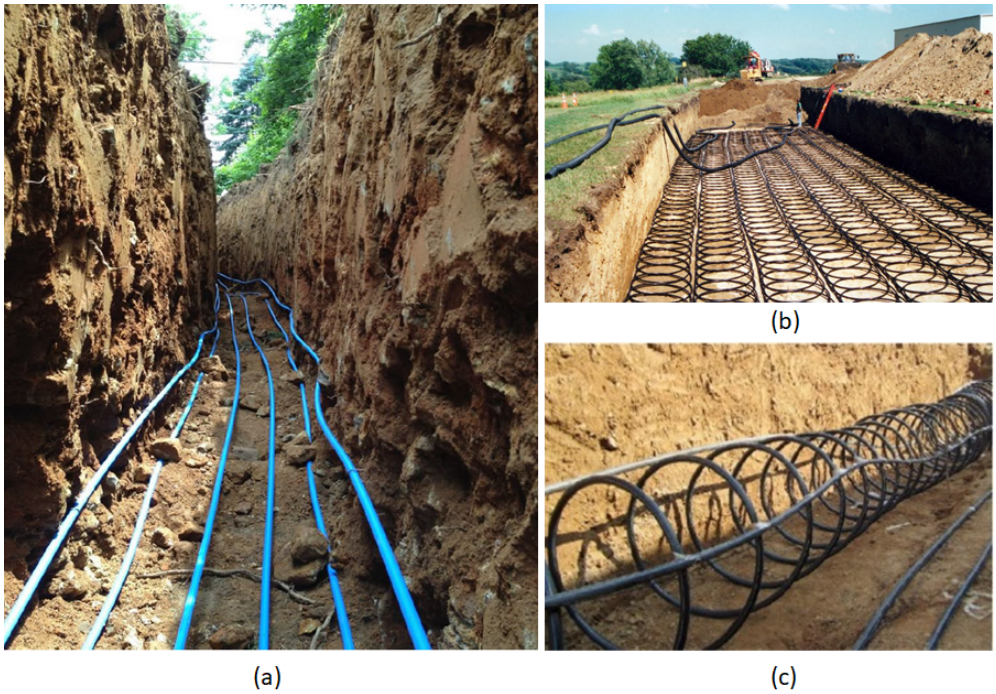

Figure 1.6: Horizontal heat exchangers (a) linear, (b) slinky shapes and (www.coloradocountrylife.coop) (c) spiral shapes (www.energyprofessionalsymposium.com).

loops due to their linear position on the ground. The embankments contain several layers of compacted soil that are made to achieve the desired level for construction of roads, highways, railways and the base for buildings. The installation of the horizontal heat exchangers is easy and feasible in the construction phase (Figure 1.7; Beier and Holloway 2015; Boukelia 2016b).

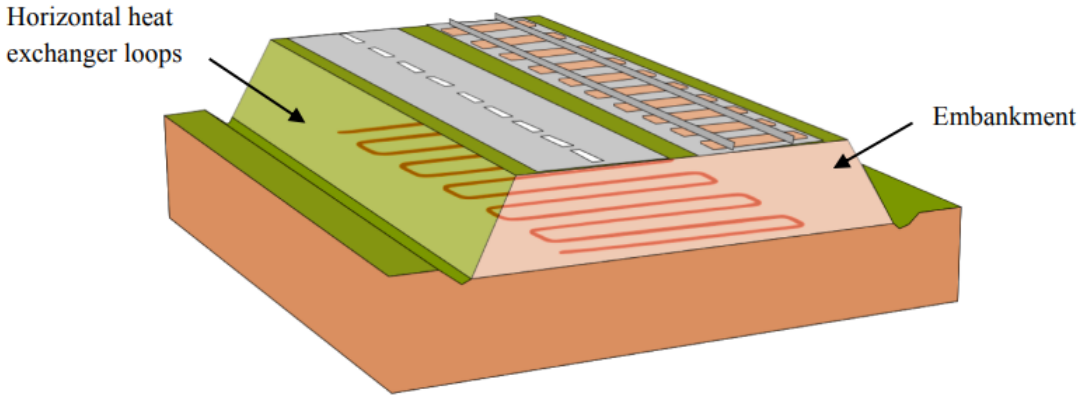

Figure 1.7: Forecast embankment thermal storage.

Gan (2013) investigated the thermal performance of a compacted soil using horizontal heat exchangers loops in various depths by a coupled thermo-hydraulic analytical method under variation of soil and atmosphere conditions. The author showed that during heat

extraction in winter, a deeper positioning of loops is more beneficial. This fact was also investigated in-situ by Beier and Holloway (2015) who studied the thermal performance of ten horizontal heat exchanger loops in an embankment made of clayey soil in Oklahoma (USA) (Figure 1.8). The Polymer-based loops penetrated in different depths of an embankment in the range of 1.9 to 3.4 m. The loops were parallel and the distance between each loop was 2 m and the length was 60 m. Six loops have been placed by a benotonite grout and four loops have been placed without grouting. In-situ thermal response tests (TRTs) were conducted using the inlet and outlet temperature fluid which is circulated through the horizontal loops in two times. The first one was within several months after loops installation (Summer, 2010) and the second one was after two years (Fall, 2012). The results of the first test showed that the ground thermal conductivity increased with increasing depth (Figure 1.9a). No significant differences in thermal resistances were observed for loops with or without grout (Figure 1.9b). The results from the second test after two years showed the ground thermal conductivity was reduced in some of the shallower loops (depths 1.9 and 2.4 m) by a factor greater than 2. Whereas for the two deeper loops (depths 2.9 and 3.4 m) a little change in ground thermal conductivity was observed (Figure 1.9a). The thermal resistance for some of the shallower loops increased by a factor of about 2 whereas for the deeper loops remained nearly unchanged (Figure1.9b). The results show that the thermal performance of this system strongly depends on the depth of loops positions. The soil moisture content decreased at shallow depths due to the soil atmosphere interaction, and consequently, the thermal conductivity of soil decreased.

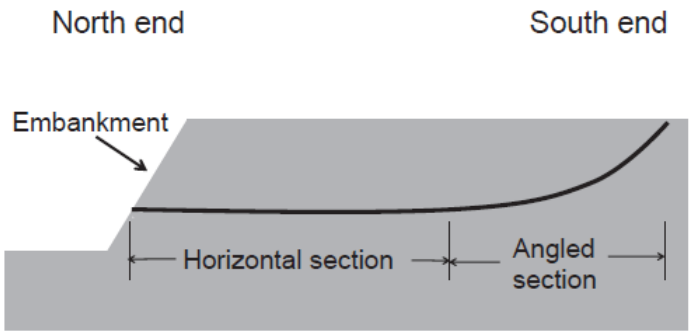

Figure 1.8: Linear horizontal heat exchanger loop in an embankment (Beier and Holloway 2015).

As it is mentioned in this part, compacted soil has shown a good capacity to store thermal energy but, however the cost of loops installation in the backfill method can be

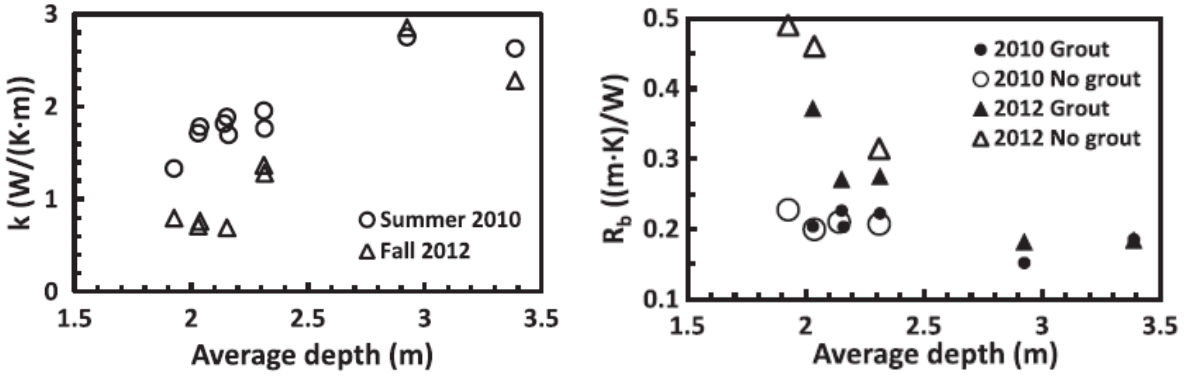

(a) (b)

Figure 1.9: (a) estimated ground thermal conductivity (K) and (b) estimated horizontal loops thermal resistance (R_b) according to the depth in an embankment, carried out in 2010 and 2012 (Beier and Holloway 2015).

significant. This can be compensated with thermal energy storage in embankments. In the construction phase of an embankment, the heat exchanger can be easily placed in different layers of compacted soil. Also the cost of solar energy collection can be reduced by the method of ICAX project which proposed a pipe network beneath the surface of black tarmac of road to collect the thermal energy (ICAX project, London). However, there are different aspects that should be taken into account:

• density variation along the profile of embankment can affect the thermal efficiency of the system;

• the soil-atmosphere interaction could be considerable, which leads to heat loss between charging and discharging seasons;

• the temperature variation could modify the structure stability.

1.1.4 Conclusion of thermal energy storage methods in geological mediums

In this section different methods to store thermal energy inside geological mediums are introduced. In terms of cost and environmental impact, the thermal energy storage in compacted soil is a efficient method compare to borehole and aquifer thermal energy storage methods. Thermal storage in an embankment is introduced as a new concept that may contribute to renewable energy production, but there are scientific issues to study. An important aspect of this system is the thermal efficiency. Several studies have indicated that the soil thermal properties, compaction state, water content and heat

exchanger depths, patterns and spacing are influencing parameters (Gan 2013; Boukelia 2016b; Jradi et al. 2017). Therefore, a comprehensive literature reviews is conducted in the following part to investigate:

- Heat and mass transfer mechanisms in soil;
- Thermal properties of soils and influencing parameters on them;
- Important parameters affecting the thermal efficiency of thermal energy storage in compacted soil.

1.2 Efficiency of thermal energy storage in compacted soil

By storing thermal energy in embankments using horizontal heat exchangers, heat may pass through the compacted soil due to the temperature gradient between the loops and the compacted soil. To increase the long-term efficiency of these systems, a good knowledge of coupled heat and mass transfer in soil, and soil thermal properties are required. In the following, these aspects are investigated in detail.

1.2.1 Coupled heat and mass transfer mechanism in soil

The heat transfer through soil provides the mass transfer. Therefore, in the beginning, the heat transfer mechanism and then the mass transfer in the porous media due to the moisture and temperature gradient are discussed in detail.

1.2.1.1 Heat transfer mechanism in soil

The main mechanisms which contribute to heat transfer within soils are (Figure 1.10):

- heat transfer by conduction;
- heat transfer by convection;
- heat transfer by radiation.

Heat transfer by conduction is a heat flow passed through the solids and liquids or vapor phases by vibration, the collision of molecules, and free electrons due to the temperature gradient between two different points. In compacted soils, the heat flow passes from particle to particle through their contacts. The rate of heat flow will be

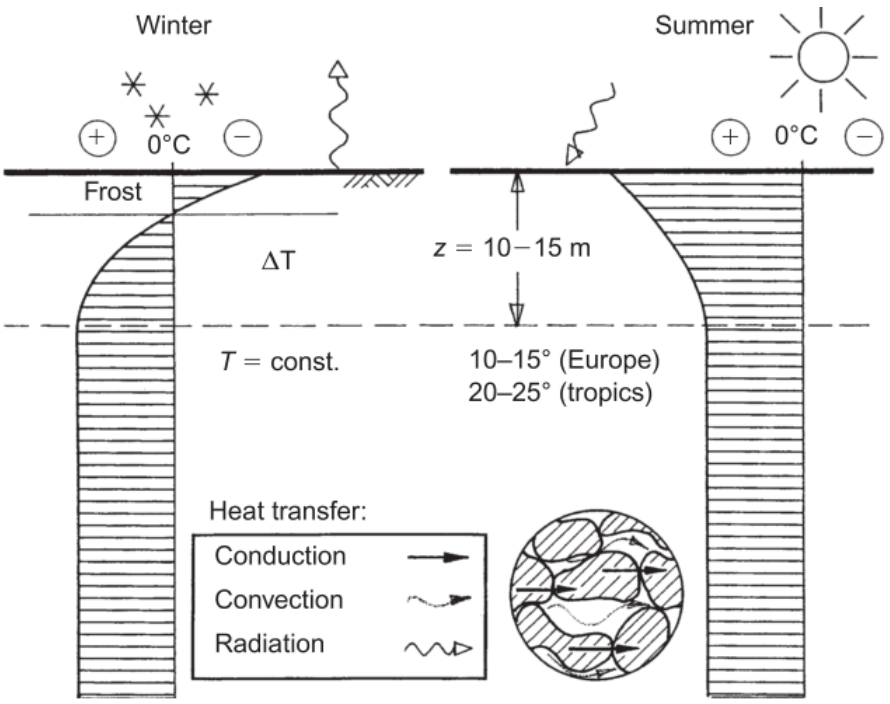

Figure 1.10: Heat transport in ground by different mechanisms (schematic) (Brandl 2006).

calculated by Fourier's Law:

$$q_{cond} = \frac{Q}{A} \tag{1.2}$$

where q_{cond} is the heat transfer by conduction ($W.m^{-2}$), Q is the heat flow ($J.s^{-1}$), A is the section of the material (m^2).

Heat transfer by convection occurs when a gas or liquid moves from one place to another place following a temperature gradient. The heat convection occurs inside the porosity of the soil, as the solid particles are static, the heat convection has to be distinguished from water flow or air flow inside the soil porosity. Heat transfer by water convection can be described by:

$$q_{w,conv} = c_w \rho_w \overline{\nu}_w (T - T^{'}) \tag{1.3}$$

where $q_{w,con}$ is the heat flow by water convection ($W.m^{-2}$), c_w is the water specific heat ($J.K^{-1}$), ρ_w is the water density ($kg.m^{-3}$), $\overline{\nu}_w$ is the vector of water velocity ($m.s^{-1}$) and

$T^{'}$ is a reference temperature (K). A similar equation can be described for air convection:

$$q_{v,conv} = c_v \rho_v \overline{\nu}_v (T - T^{'}) \tag{1.4}$$

where $q_{v,con}$ is the heat flow by air convection ($W.m^{-2}$), c_v is the vapor specific heat ($J.K^{-1}$), ρ_v is the vapor density ($kg.m^{-3}$) and $\overline{\nu}_v$ is the vector of vapor velocity ($m.s^{-1}$).

Heat transfer by radiation is the heat transfer due to the propagation of the electromagnetic waves or photons. The energy transferred by radiation moves at the speed of light. The solar radiation can be exchanged with the surface of the ground without heating the transitional space. The heat transfer by radiation can be described by the following equation:

$$q_r = \nabla D_\lambda \nabla T \tag{1.5}$$

where q_r is the heat transfer by radiation ($W.m^{-2}$) and D_λ is the dispersion coefficient which can be expressed as:

$$D_\lambda = c_w \rho_w \delta_v |v| \tag{1.6}$$

where δ_v is the heat dissipation.

Generally, heat radiation has a negligible contribution to the total heat transfer in the soil, because it occurs in a wavelength band between 0.5 and 30.0 μm at the surface of the soil (An 2017). Therefore, the total heat transfer (q_{tot}) in the soil, q_{tot}, can be defined as:

$$q_{tot} = q_{cond} + q_{w,conv} + q_{v,conv} \tag{1.7}$$

where q_{cond} is the conductive heat flux, $q_{w,conv}$ is the heat flux generated by liquid convection and $q_{v,conv}$ is the heat flux generated by vapor convection (Brandl 2006).

1.2.1.2 Mass transfer mechanism in soil

In embankments, compacted soil is unsaturated, it contains grain particles, water and air in porous pattern. The grain particles of soil are supposed to be static whereas water and vapor phases can move through the soil under thermo-hydraulic solicitations. The liquid water and vapor transfers in a porous media occur due to the soil temperature and

moisture content gradient. The flow rate for unsaturated soils can be given by Darcy's law. This law expresses that the water flow rate (u_w) through soil directly depends on the hydraulic head gradient (h_{head}), given as:

$$u_w = -k_r(S)\nabla h_{head} \tag{1.8}$$

where, k_r is the soil relative hydraulic conductivity which is a function of the suction (S) (Zhai and Rahardjo 2015). There are different models such as empirical, statistical, correlation and regression models to estimate the relative hydraulic conductivity (Fredlund et al. 2012). Among them the Mualem's equation (Mualem 1976) is used usually for calculating of the relative hydraulic conductivity as following:

$$k_r = \begin{cases} k_s S_e^{1/2}(1-(1-S_e^{n/n-1})^m)^2 & H_p < 0 \\ 1 & H_p \geq 0 \end{cases} \tag{1.9}$$

where k_r is the relative hydraulic conductivity, k_s is the saturated hydraulic conductivity ($m.s^{-1}$), Se is relative saturation, H_P is water potential or suction head (m), n and m=1-1/n are empirical parameters of van Genuchten model.

The relative saturation (Se) is calculated using van Genuchten model as following:

$$S_e = \frac{\theta - \theta_{sat}}{\theta_{sat} - \theta_{res}} = \begin{cases} \frac{1}{(1+|\alpha H_p|^n)^m} & H_p < 0 \\ 1 & H_p \geq 0 \end{cases} \tag{1.10}$$

where θ is volumetric water content, θ_{sat} and θ_{res} are saturated and residual volumetric water content respectively, α is related to the inverse of the air entry suction (m^{-1}).

Besides the mass transfer due to the moisture gradient in soil, several researchers reported that the hydraulic conductivity of soil increases by temperature increasing, While, the soil's ability to retain the water decreases. The effect of temperature variation on soil's hydraulic properties is described in detail in section 1.3.1.

Therefore, the mass transfer can be described by dividing it into two parts: mass transfer by vapor and mass transfer by water. The volumetric vapor flux coupled with temperature can be given as:

$$Q_v = -D_{Tv}\nabla T - D_{\Theta v}\nabla\Theta \tag{1.11}$$

where Q_v is the volumetric vapor flux ($m^3.m^{-2}.s^{-1}$), D_{Tv} is the thermal vapor moisture diffusivity ($m^2.s^{-1}.K^{-1}$), $D_{\Theta v}$ is the isothermal vapor moisture diffusivity ($m^2.s^{-1}$).

The volumetric liquid flux (Q_v) can be obtained if the temperature influence on the liquid transfer is considered:

$$Q_l = -D_{Tl}\nabla T - D_{\Theta l}\nabla\Theta - k_r\bar{i} \tag{1.12}$$

where D_{Tl} is the thermal liquid moisture diffusivity ($m^2.s^{-1}.K^{-1}$), $D_{\Theta l}$ is the isothermal liquid moisture diffusivity ($m^2.s^{-1}$), k_r is the relative hydraulic conductivity and i is the unit vector in the vertical direction.

Therefore, the total moisture transfer flux can be obtained:

$$Q_{total} = Q_v + Q_l \tag{1.13}$$

1.2.2 Soil thermal properties

The main soil thermal properties which affect the capacity of thermal energy storage and control the heat flow through a soil matrix are: thermal conductivity, volumetric heat capacity and thermal diffusivity. These parameters can be obtained indirectly with steady-state or transient-state methods by measuring the rise or fall of the temperature in response to a heat flux (Abu-Hamdeh et al. 2001; Kraemer and Chen 2014).

Steady-state method like hot plate method measures the thermal properties when the heat flux through the sample remains unchanged over time. Transient methods are used to measure the thermal properties during the unsteady-state heat transfer process. The thermal needle probe and infrared thermal imaging methods are often used to measure the thermal conductivity and thermal diffusivity of soil samples in the laboratory and field, respectively (Bilskie 1994; Coquard et al. 2006; Barry-Macaulay et al. 2013).

The soil's thermal properties change according to its physical and hydro-mechanical properties, such as the mineral composition, degree of saturation, and dry density. In the following, the soil thermal properties are defined and their evolution due to the physical

and hydro-mechanical properties are explained.

Thermal conductivity is the capacity of the material to conduct heat through the soil and it is calculated by the following equation:

$$\lambda = \frac{QL}{A\Delta T} \tag{1.14}$$

where λ is thermal conductivity ($W.m^{-1}.K^{-1}$), Q is the heat flow ($J.s^{-1}$), L is the thickness of material (m), A is cross section of material (m^2) and ΔT is the temperature gradient (K). Soil thermal conductivity is significantly influenced by the mineral composition, the degree of saturation and the dry density of the soil. For example, sands with high quartz content generally have a greater thermal conductivity (Zhang and Wang 2017). With increasing density, the solid particles are better packed into a unit volume and the number of contact points between the particles increases. These contact points provide a larger heat flow path, thus the soil thermal conductivity increases as shown in Figure 1.11a (Penner et al. 1975; Salomone and Kovacs 1984; Tang et al. 2008).

Lu et al. (2014) have presented a comprehensive experimental study to estimate the relationship between the thermal conductivity and water content for a silty loam soil (Figure 1.11b). When moisture is added to a soil, a thin water film develops which bridges the gaps between the soil particles. This bridging increases the effective contact area between the soil particles, and increases the heat flow and results in a higher thermal conductivity. The increase in thermal conductivity due to the water content increase was also validated numerically by Li et al. (2017) using a methodology based on least-squares finite element method on a loamy sand.

Volumetric heat capacity express the capacity of soil to store the heat while the system is under a temperature gradient. Volumetric heat capacity depends on soil density and soil specific heat. It can be calculated by the following equation:

$$C_v = \rho.c_p \tag{1.15}$$

where C_v is the volumetric heat capacity ($J.m^{-3}.K^{-1}$), ρ is the soil density ($kg.m^{-3}$) and c_p is the soil specific heat ($J.K^{-1}$).

Abu-Hamdeh (2003) carried out experimental tests to measure the soil volumetric heat

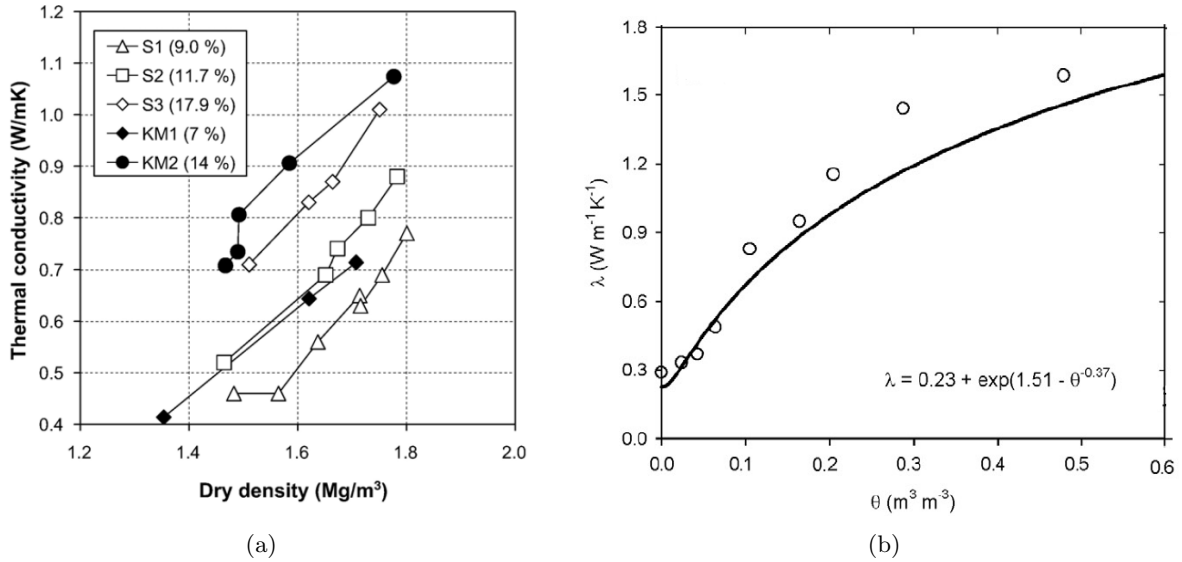

(a) (b)

Figure 1.11: Variation of thermal condactivity against (a) dry density for a compacted bentonite (Tang et al. 2008), (b) water content for a silty loam soil (Lu et al. 2014).

capacity of clay and sandy soils at different densities and water contents. The results showed that, volumetric heat capacity increased with increasing the dry density and the water content (Figure 1.12).

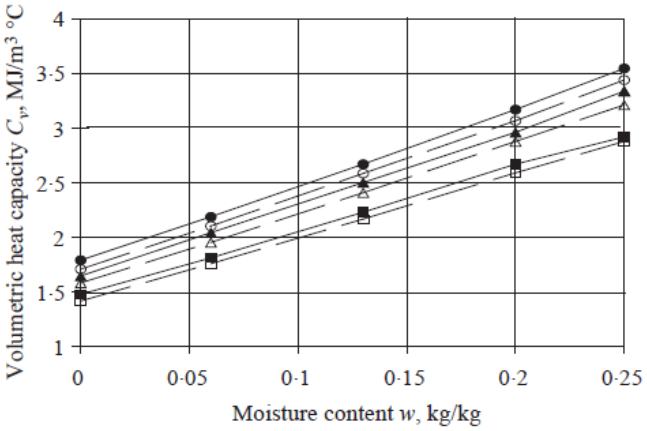

Figure 1.12: Volumetric heat capacity as a function of moisture content for clay soil at the bulk densities : ■, 1200 $kg.m^{-3}$, ▲, 1300 $kg.m^{-3}$ and • , 1400 $kg.m^{-3}$ (Abu-Hamdeh 2003).

Thermal diffusivity is a physical quantity that characterizes the capacity of a material to transmit a temperature signal from one point to another point. Thermal diffusivity is described as a ratio of thermal conductivity (λ) per volumetric heat capacity (C_v) (Equation 1.16):

$$\alpha = \frac{\lambda}{C_v} \tag{1.16}$$

where α is the thermal diffusivity ($m^2.s^{-1}$).

Similar to the heat capacity and thermal conductivity, thermal diffusivity depends on the soil water content and density. Thermal conductivity and volumetric heat capacity increase linearly with water content but thermal diffusivity increases until a given water content, after that it decreases slightly (Dec 2006, Figure 1.13).

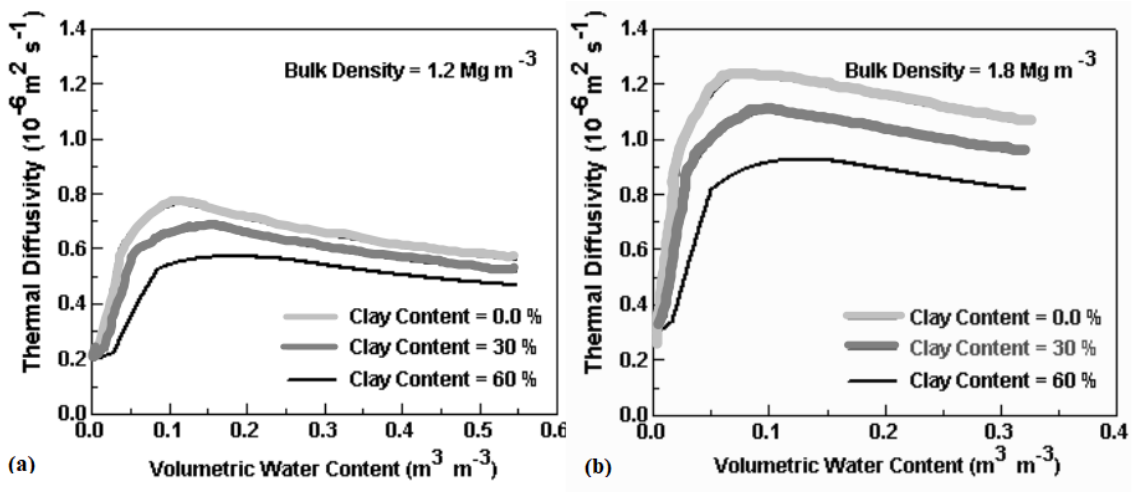

Figure 1.13: Thermal diffusivity variation against clay content, soil water content, and density for mineral soils (Dec 2006).

1.2.3 Effect of temperature on soil thermal properties

Some researchers observed that temperature variations could change the soil's thermal properties. This evaluation may affect the capacity of heat storage in compacted soils.

Eslami (2014) investigated the evolution of thermal properties of a compacted illitic clay with the variation of density, water content and temperature in the range of 1 to 70 $°C$ along the compaction curve (Figure 1.14). This author showed that, increasing the temperature of soil samples from 1 to 70 $°C$ causes an increase in the thermal conductivity which is more significant in the dry side of the compaction curve. On the contrary, the temperature increase has a negligible effect on thermal conductivity in the wet side of compaction curve (Figure 1.14a). Thermal volumetric capacity increases with increasing the water content and density, but temperature variation has no remarkable effect on this parameter. Thermal diffusivity is under the role of thermal volumetric capacity and conductivity that showed an increasing trend with temperature increase in the dry side of the compaction curve but after the optimum value of water content, it tends to decrease slightly (Figure 1.14b).

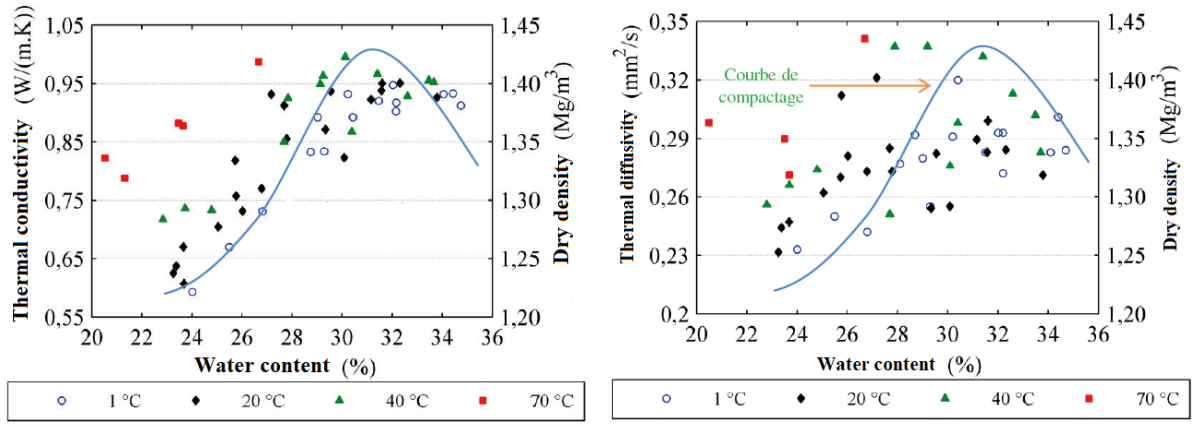

(a) (b)

Figure 1.14: Evolution of thermal properties of a compacted illitic clay with variation of the density, the water content and the temperature (Eslami 2014).

In another study, Mengistu et al. (2017) investigated the influence of temperature variations from 0 to 60 ^{0}C on the thermal properties of two aeolian soils (Clovelly and Hutton) in South Africa. Several soil samples were prepared at different water contents (0, 8, 16, 22, 40%). The results showed that the volumetric heat capacity of different samples slightly increases with temperature increase, whatever their water content were. The thermal conductivity showed an increasing trend with temperature increase at the water contents of 0, 8, and 16% while for the water content of 22% and saturated state (40%) it decreased with temperature increase (Figure 1.15). Therefore the soil thermal properties change with temperature variation and strongly depend on the value of soil water content and soil density.

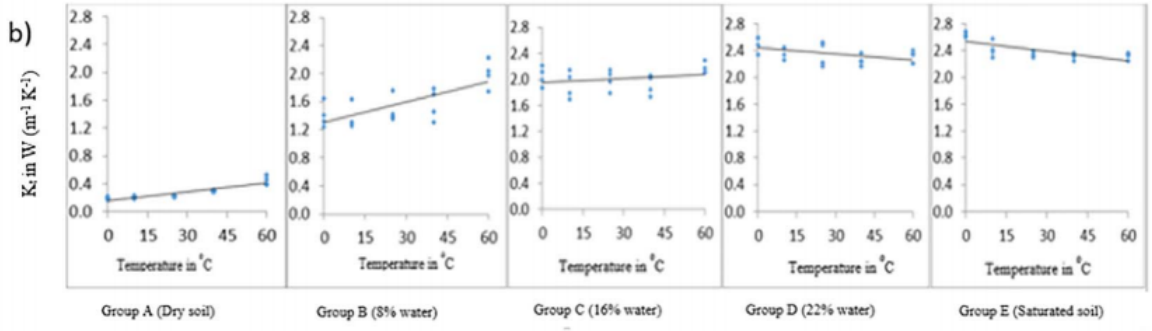

Figure 1.15: Evolution of thermal conductivity of aeolian soils with the variation of water content and temperature, K is the thermal conductivity (Mengistu et al. 2017).

1.2.4 Summary of expected thermal properties to store thermal energy in compacted soil

The performances of thermal energy storage in compacted soil is strongly dependent on soil thermal properties, soil compaction parameters (w and ρ_d) and horizontal heat exchanger shapes and patterns. Soil thermal properties are affected by various soil properties such as; soil mineralogy, density, water content, and temperature. These variations have complicated the measurement of soil thermal properties. Therefore, according to different studies, to increase the thermal efficiency of the systems for thermal energy storage the following aspects are needed:

• Appropriate soil compaction level relative to the density and water content to achieve the good thermal performance;

• A soil with high specific heat capacity, a medium thermal conductivity and a low thermal diffusivity to optimize the amount of stored thermal energy;

• Appropriate method to measure the thermal properties over time in storage system;

• A suitable shape and depths of heat exchanger loops;

• A suitable air or water flow rate through the loops;

• A suitable material to insulate this system and reduce the heat loss and soil thermal properties change due to the soil-atmosphere interaction.

1.3 Effect of temperature on the hydro-mechanical behavior of soil

When the serviceability of the embankments as a thermal energy storage medium starts, the compacted soil will be subjected to seasonal temperature variations. These temperature variations modify the thermo-hydro-mechanical behavior of the compacted soil. To prevent damage and ensure the long-term structure stability, the effect of the temperature variation on the hydro-mechanical behavior of the compacted soil should be investigated. In this section, first, the effect of temperature on hydraulic properties is described. Then consolidation behavior, such as soil thermal volumetric response, preconsolidation pressure, and the compressibility parameters, is discussed. Finally, the impact of thermal solicitations on the shear parameters such as cohesion and friction angle, is presented.

1.3.1 Effect of temperature on hydraulic properties

The evolution of hydraulic properties, such as hydraulic conductivity and water retention curve under non-isothermal conditions is investigated by several researchers (Cho et al. 1999; Bouazza et al. 2008; Ye et al. 2013). These authors said that the hydraulic conductivity increases with temperature increasing. Delage et al. (2011) studied the effect of temperature in the range of 20 to 90 °C on hydraulic conductivity of Boom clay. According to the results of triaxial tests, by heating, the hydraulic conductivity increased from 2.5 10^{-12} to 6.2 10^{-12} $m.s^{-1}$ whereas the porosity decreased from 39% to 37.2%. By cooling, the hydraulic conductivity decreased whereas porosity remained unchanged (Figure 1.16). They pointed out that these results may be due to the coupled effect of changes in water properties and porosity due to the temperature variation. However, Morin and Silva (1984) and Abuel-Naga et al. (2005) reported that the impact of the soil volume change due to the temperature variation is too small to be considered as a reason for the change of hydraulic conductivity at elevated temperature (90 °C). With temperature increase, the viscosity of water decreases and leads to an increase in the soil hydraulic conductivity (Hillel 1980).

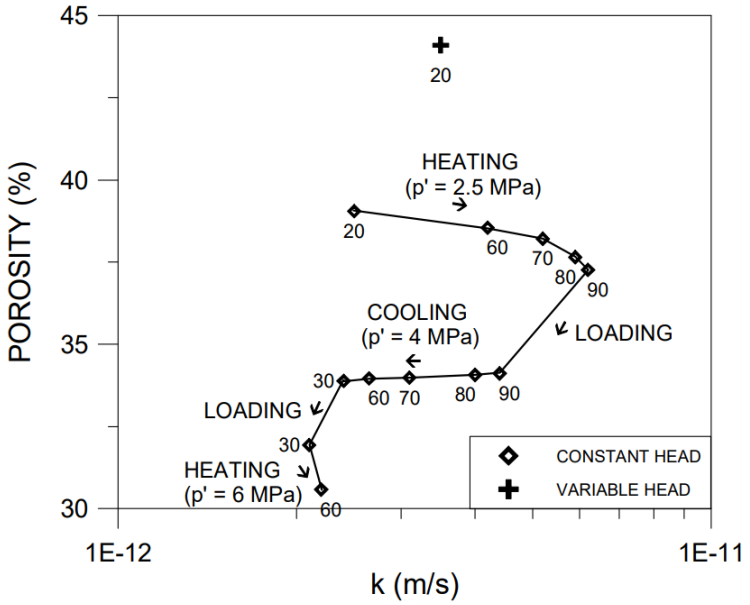

Figure 1.16: Hydraulic conductivity tests performed on a sample of Boom clay at various temperatures and stresses (Delage et al. 2011).

Based on the hydraulic conductivity test results at different elevated an equation proposed by Delage et al. (2011) to show temperature dependent of water viscosity by

determining the intrinsic permeability K (m^2):

$$k = \frac{K\gamma_w(T)}{\mu(T)} \tag{1.17}$$

where k is the hydraulic conductivity $(m.s^{-1})$, γ_w is the unit weight of water $(kN.m^{-3})$, μ is the water viscosity $(Pa.s)$ and T is the temperature (K). According to the literature, the viscosity of water in effective porosity decreases at higher temperature (equation 1.18, Hillel 1980):

$$\mu = -0.000046575Ln(T) + 0000239138 \tag{1.18}$$

Therefore the temperature dependence of water viscosity can be one of the reasons for hydraulic conductivity variations upon thermal solicitations.

In unsaturated state, Tang and Cui (2005) studied the temperature effect on water retention of compacted sodium bentonite using the vapor equilibrium technique at two different temperatures 20 and 80 ^oC. Their results showed that the water content decreases with increasing temperature for the same suction. Romero et al. (2001) obtained the same trend on the Boom clay using the vapor equilibrium method (Figure 1.17). They showed that a temperature increase, reduced the ability of the soil to retain the water. This variation may originate from the change in the surface tension of water, the pore water chemistry of the clay and an irreversible modification of the clay network.

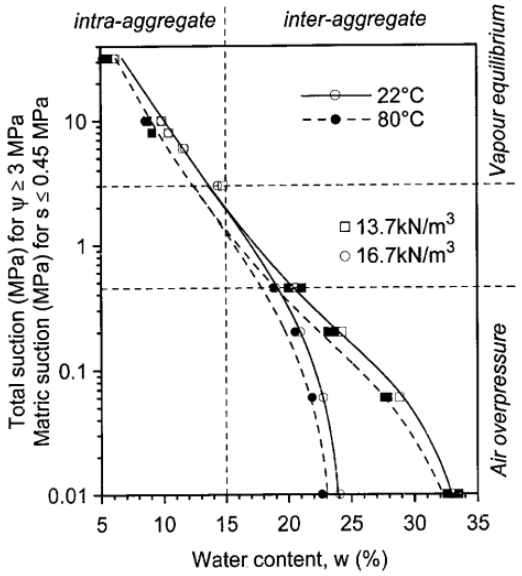

Figure 1.17: Water retention curves for different temperatures (Romero et al. 2001).

1.3.2 Effect of temperature on consolidation behavior

1.3.2.1 Thermal volumetric response

The thermal volumetric response of a soil strongly depends on the heating-cooling drainage conditions. In this part, the studies performed in drained conditions are first discussed afterwards the undrained response is presented.

In drained conditions, the thermal volumetric response of soil depends on the soil nature, the stress history quantified using the overconsolidation ratio (OCR) and the thermal variations history (number of temperature cycles). Several studies reported that the soils in highly overconsolidation state (OCR$\geq$2) exhibits a thermal reversible expansion during heating and subsequent cooling (Baldi et al. 1988; Di Donna 2014; Shetty et al. 2019). For example, Figure 1.18, presents the results of Baldi et al. (1988) in highly overconsolidated state (OCR=8) for a Boom clay soil. The reversible behavior of the overconsolidated sample could be due to the thermo-elastic expansion and contraction of the solid skeleton (Delage et al. 2004). The soils, slightly overconsolidated (OCR$\leq$2) and normally consolidated (NC) exhibits a contraction when the soil temperature increases (Baldi et al. 1988; Hueckel et al. 1998; n.d.). Then, during the subsequent cooling, different observations are reported (Figure 1.18). In some studies, a small part of the deformation is recovered (Hueckel et al. 1998; Shetty et al. 2019) while in other studies the contraction proceeded (Baldi et al. 1988; Di Donna 2014).

Different studies investigated the impact of several temperature cycles on the volumetric deformation of the soils (Di Donna 2014; Ma et al. 2017). The reversible behavior of the thermal volume change in the overconsolidated state is mentioned even after several heating-cooling cycles (Figure 1.19a, OC sample). In NC state, several studies have shown that the first heating-cooling cycle induces most of the irreversible volume change. The subsequent cycles with the same magnitude and range produce small increments of irreversible deformation that decreases cycle after cycle, revealing an accommodation phenomenon (Campanella and Mitchell 1968; Hueckel et al. 1998; Di Donna 2014). The results for NC state are presented in Figure 1.19b. Recently, Ma et al. (2017) reported that the volumetric deformation of soil in NC states was mainly during the first cycles. After 4 or 5 thermal cycles the deformation will be established and no significant change

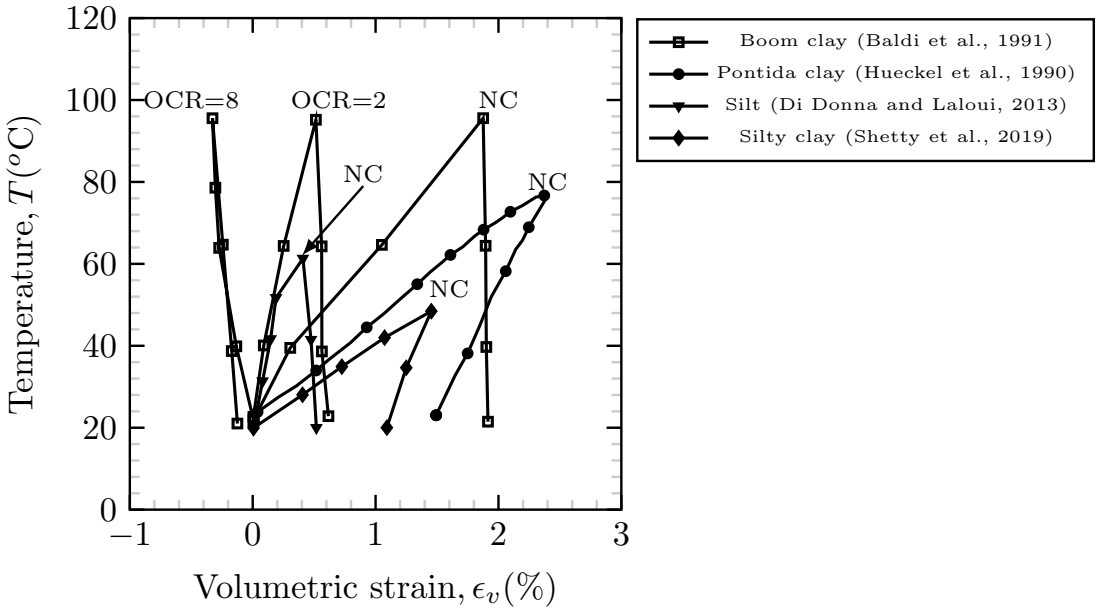

Figure 1.18: The thermal volumetric strain of soils during drained heating (contraction is positive).

was observed. Many researchers reported that the plastic deformation during thermal cy-

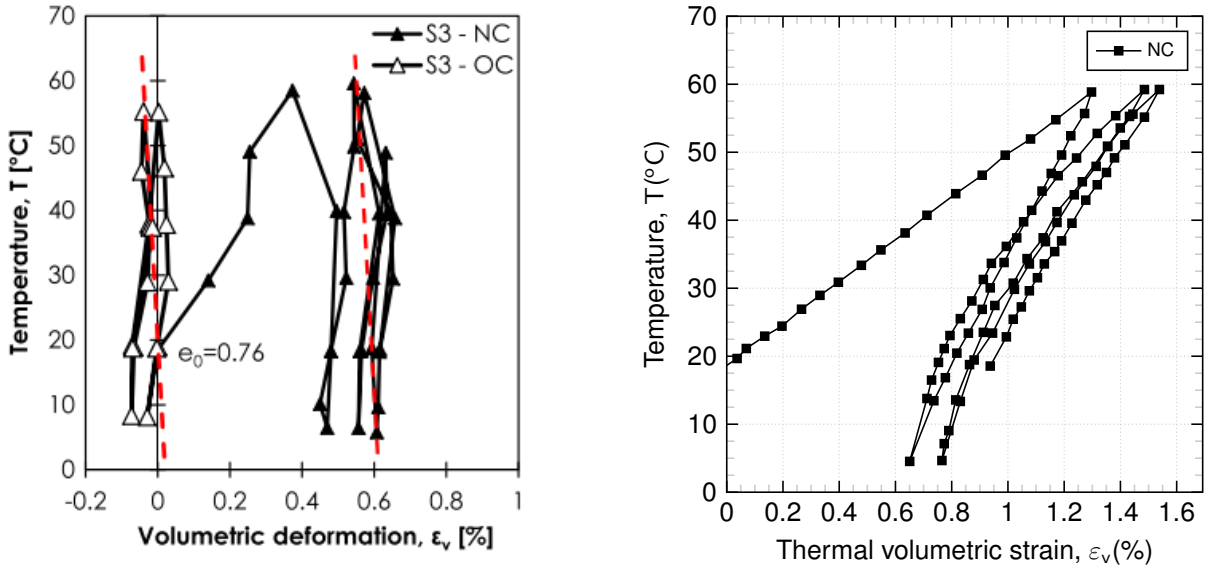

(a) (b)

Figure 1.19: Soil volumetric response during heating and cooling cycles (contraction is positive) (a) silty soil (Di Donna 2014) (b) Illite (modified from Campanella and Mitchell 1968) .

cles in NC conditions occurred due to: the dissipation of the pore water generation caused by heating; the degradation of the adsorbed water layer in clayey particles; the contrasted thermal response of the different mineral and water phase (Baldi et al. 1988; Campanella and Mitchell 1968; Shetty et al. 2019). Di Donna and Laloui (2013) explained that, this thermo-plastic deformation may be due to the decrease in frictional strength at the inter

particle contacts which causes particle rearrangements. Some researchers supposed that the amount of thermal volumetric change depends on the plasticity index of the soil. The soil with higher plasticity index shows more thermo-plasticity deformation (Delage et al. 2000; Abuel-Naga et al. 2007; Ghaaowd et al. 2015).

In undrained conditions, thermal loading induces pore pressure generation. This effect was studied by different researchers using temperature controlled triaxial devices (Campanella and Mitchell 1968; ESRIG 1969; Moritz 1995). They observed that, with temperature increase, the pore water pressure increases. Campanella and Mitchell (1968) proposed a theoretical model to estimate the variation of pore water pressure (Δu) due to the temperature variation as following:

$$\Delta u = \frac{n\Delta T(\alpha_s - \alpha_w) + \alpha_{st}\Delta T}{m_v - nm_w} \tag{1.19}$$

where n is the porosity, α_s and α_w are the coefficient of the volumetric thermal expansion of the solid particles and water respectively, α_{st} is the physic-chemical coefficient of thermal expansion of the structure, m_v and m_w are the compressibility of the structure of the sample and water respectively. This equation shows that the variation of the pore water pressure depends on the porosity, the temperature variation, the difference between the coefficient of thermal expansion of the solid particles and water, the volume deformation due to the physic-chemical effects and finally the compressibility of the soil sample structure due to the difference in the thermal expansion coefficient of water and solid particles.

Burghignoli et al. (2000) used a modified triaxial cell to investigate the thermo-hydro-mechanical behavior of a clayey soil at a temperature range of 20 to 50 °C (Figure 1.20a).

In accordance with previous studies, they reported that in undrained conditions, the pore water pressure increases with temperature rise for normally consolidated samples (paths a-b, c-d and e-f). Whereas by cooling the pore water pressure decreases (paths g-h and o-p in Figure 1.20b). At the end of the heating and cooling path, the temperature was kept constant and the pore water pressure increases slightly (paths b-c, h-i and p-q) (Figure 1.20b). They reported that the pore pressure variation during cooling and heating may be due to the different responses of water and solid skeleton to temperature variation

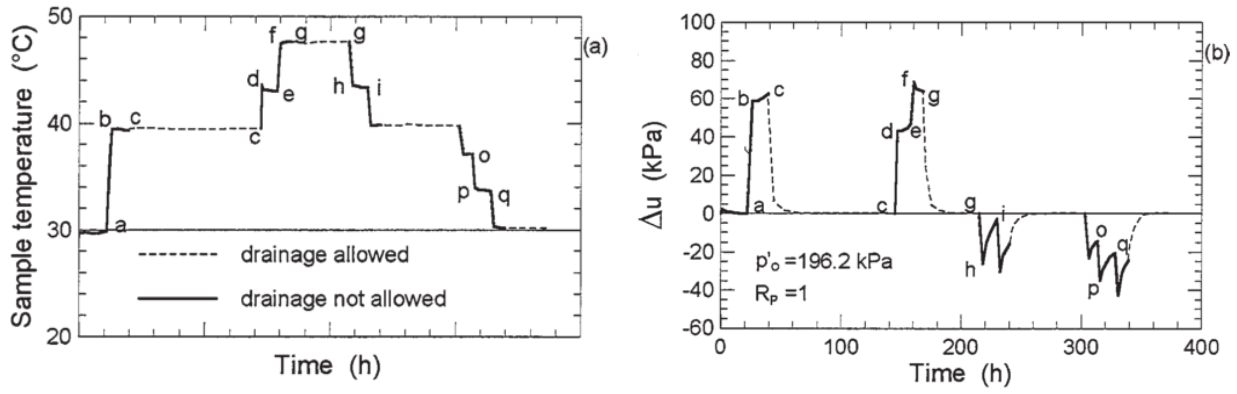

(a) (b)

Figure 1.20: (a) temperature variation over the time (b) pore water pressure changing in undrained condition (Burghignoli et al. 2000).

and the nature of the soil.

1.3.2.2 Effect of temperature on preconsolidation pressure

Preconsolidation pressure is the maximum effective stress that the soil has ever supported and is defined as the limit between the elastic and plastic domains. Several studies show that the preconsolidation pressure decreases with temperature increase in saturated conditions (Tidfors and Sällfors 1989; Eriksson 1989; Moritz 1995; Tang et al. 2007; Di Donna 2014; Jarad 2016). Laloui and Cekerevac (2003) summarized the results of different studies to show a nonlinear descending relationship between preconsolidation pressure and temperature (Figure 1.21). This evolution can be linked to the soil thermal softening due to the temperature-dependent properties of water and changing in the fabric pore structure (Baldi et al. 1988; Mon et al. 2013). Previous parts it has explained that with temperature increase, the viscosity of water decreases and leads to an increase in the soil hydraulic conductivity. Indeed, at high temperatures, the pore water drains easier and increases the particle contacts.

1.3.2.3 Effect of temperature on the compression and swelling indices

Several investigations exist on temperature effects on the slope of the normal compression lines which is defined as compression index (C_c) and the slope of the unloading lines which is defined as swelling index (C_s) (Cekerevac and Laloui 2004; François et al. 2007; Di Donna 2014) . All these researchers reported that, there is almost no significant change

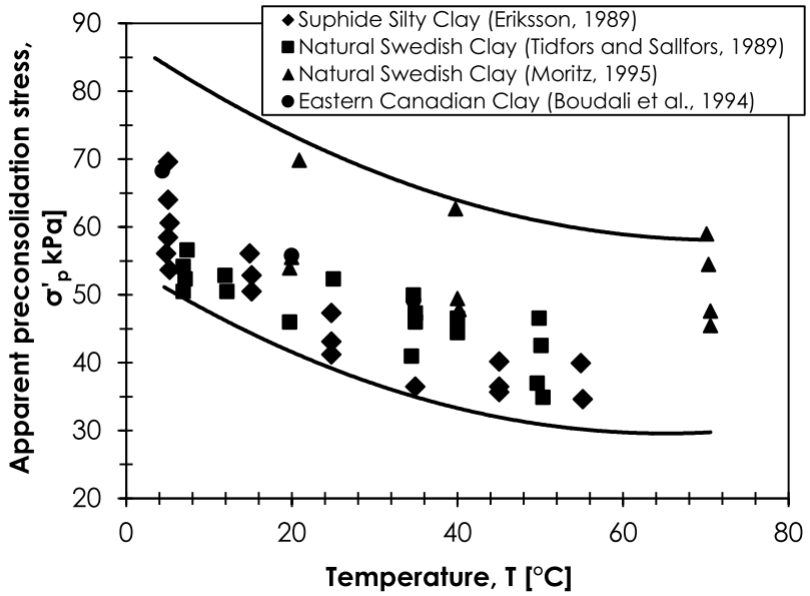

Figure 1.21: Evolution of the apparent preconsolidation pressure with temperature variation in the saturated state (Figure from Di Donna 2014).

for compression index (C_c) and swelling index (C_s) with temperature variations in the range of 20 to 90 °C (Figure 1.22). These observations are in agreement with the study of Kaddouri et al. (2019) who showed that the compression (C_c) and the swelling indices (C_s) are not influenced by temperature variations (5, 22, 50 and 70 °C) using a temperature controlled oedometric cell for a saturated clayey soil (Figure 1.22).

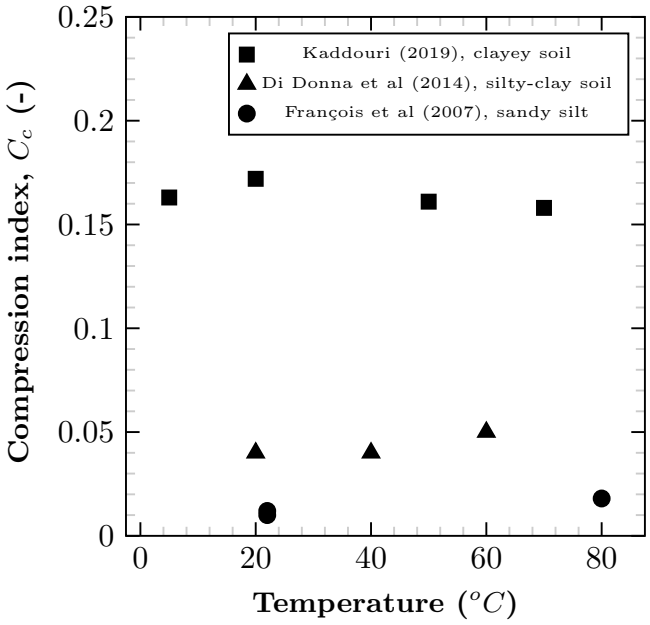

Figure 1.22: Evolution of the compression index at different temperatures.

1.3.3 Effect of temperature on shear parameters

Shear resistance of soils at non-isothermal conditions was intensively studied by several researchers regarding its importance in structural safety of geostructures dealing with thermal solicitations (Mitchell 1964; Murayama 1969; Hueckel and Baldi 1990; Kuntiwattanakul et al. 1995; Hueckel et al. 1998; Cekerevac and Laloui 2004; Abuel-Naga et al. 2006; Yavari 2014; Liu et al. 2018; Maghsoodi 2020; Maghsoodi et al. 2020a; Maghsoodi et al. 2021; Maghsoodi et al. 2020c). Due to the complex interactions of soil constituents under temperature variations, different results have been obtained but all these studies show that, the thermal and stress history greatly influences the shear resistance of soils.

For highly overconsolidated clays, Hueckel and Baldi (1990), by performing drained triaxial tests on Pontida clay, reported that the shear strength tends to decrease with temperature increase from 20 to 95 ^{o}C (Figure 1.23a). The authors concluded that this behavior may be due to the reduction of the elastic domain that was previously demonstrated (see section 1.3.2.2). For slightly overconsolidated sample (OCR=1.5) Cekerevac and Laloui (2004) reported no significant evolution for kaolin samples for temperature increase from 22 to 90^{o}C (Figure 1.23a).

In normally consolidated conditions, Cekerevac and Laloui (2004) performed drained triaxial tests at different temperatures (22 and 90^{o}C) with an initial confining pressure of 600 kPa. The results indicate that NC samples tested at high temperatures reached higher shear strength (Figure 1.23b). However, at large strains the shear stresses for all temperatures tend to the same critical state. These results for NC samples are in agreement with the results of Abuel-Naga et al. (2006) who found an increase of shear strength with drained heating (Figure 1.23b) on NC soft Bangkok clay. (n.d.), using a temperature controlled direct shear device, also showed that the shear strength of NC kaolin clay increased with a temperature increase from 22 to 60 ^oC but for the sandy soil it was almost independent of the temperature.

Several studies have been performed to investigate the effect of temperature on cohesion, friction angle or critical state coefficient (M) of soils. The effect of temperature on the friction angle was reported to be negligible in several studies (Moritz 1995; Cekerevac and Laloui 2004; n.d., Figure 1.24). But there are different results on the cohesion varia-

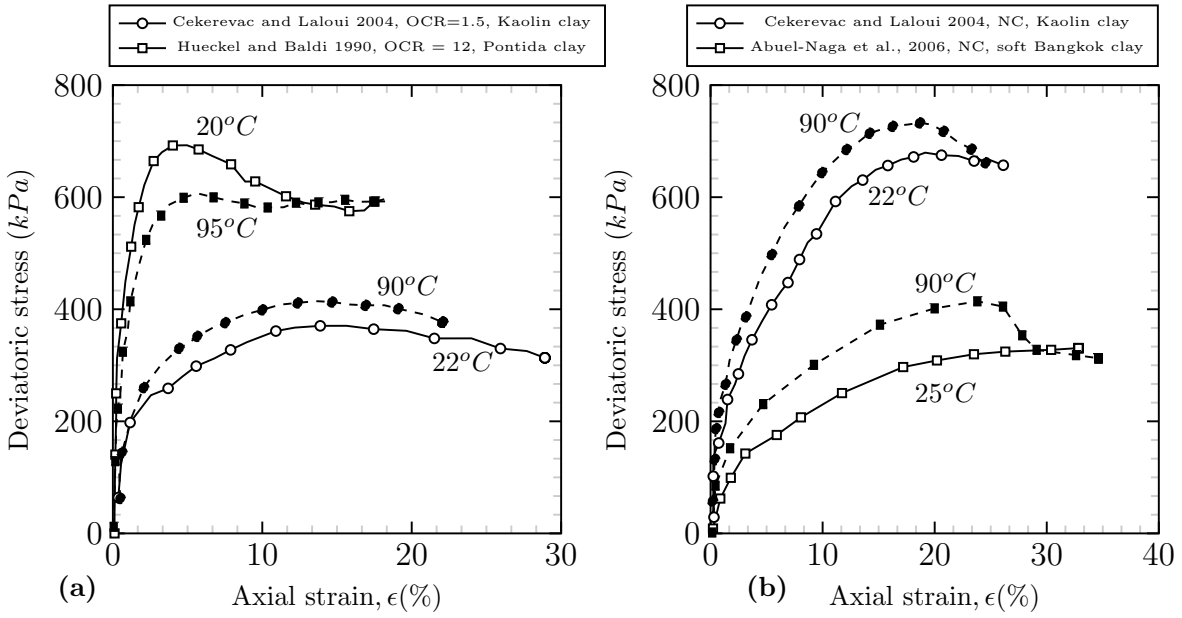

Figure 1.23: Drained triaxial tests at different temperatures for (a) overconsolidated samples (b) normally consolidated samples

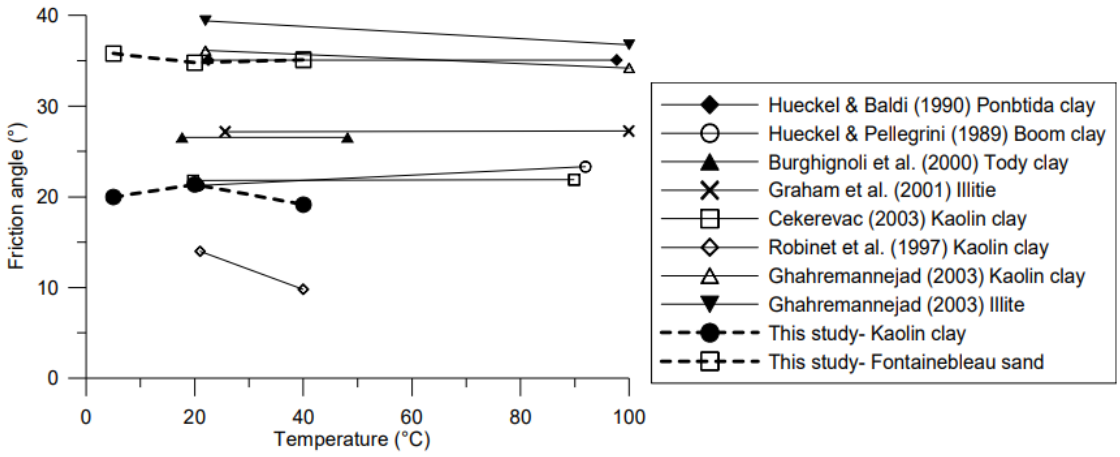

Figure 1.24: Effect of the temperature on friction angle for different soil types (Yavari 2014).

tion due to temperature variation. Yavari (2014) by conducting direct shear test at three temperatures (5, 20, and 40 ^oC) found that the cohesion of clay was almost unchanged. On the contrary, (n.d.) found that the temperature increase from 22 to 60 ^oC increases the cohesion by 35% for a kaolin clay using a temperature controlled direct shear device. Therefore, it can be concluded that the shear characteristic evolution due to the temperature variation depends on several parameters such as material characteristics (soil nature), experimental condition, overconsolidation ratio and thermo-mechanical path.

1.3.4 Conclusion of temperature effect on hydro-mechanical soil behavior

In order to identify the effect of temperature on hydro-mechanical soil behavior, several conclusion are noted as follows:

• increase in hydraulic conductivity and decrease in water retention capacity due to heating;

• reversible and irreversible volumetric deformations due to the temperature cycles in overconsolidated and normally consolidated states respectively;

• decrease in the preconsolidation pressure with temperature increase;

• the compression index and swelling index were independent of temperature variation;

• in normally consolidated state, the shear strength increases with temperature increase, and with increasing the OCR ratio the effect of temperature could be complicated.

1.4 Numerical thermo-hydro-mechanical investigation

To evaluate the thermal efficiency and mechanical performance of thermal energy storage systems, numerical simulations using finite element and finite difference tools are currently utilized in different studies. Generally in these models, the simulations consider a homogeneous soil medium with constant thermal properties and the heat transfer is modeled by conduction with solid particles of soil (Jradi et al. 2017; Asgari et al. 2020). However, in soils, the thermal properties will change by temperature, physical and hydraulic properties variations. To study these variations, fully coupled thermo-hydro-mechanical behavior of these types of structures should be investigated. Thus a comprehensive model should contain several aspects such as water transfer simulation in an unsaturated soil medium; variation of soil thermal properties due to changes in soil physical properties; and a constitutive law to describe the mechanical behavior modifications due to suction and temperature variations. In this section the theoretical equations for a thermo-hydraulic simulation are first explained. Then, the different constitutive models to take into account the effect of suction and temperature variations on the mechanical performance of soil are presented.

1.4.1 Thermo-hydraulic theoretical equations

The theoretical equation and influencing parameters such as heat and mass transfer and soil thermal properties to perform a coupled thermo-hydraulic simulation are explained in detail in section 1.2. Generally in the thermo-hydrulic sumulation the heat transfer on the ground surface is neglected. But due to the horizontal position of heat exchangers, the meteorological condition like the seasonal hydrothermal variations on the ground surface can change the efficiency of this system. Also in an embankment, the compacted soil is in interaction with atmosphere from top and the lateral surface sides. Therefore it is better to consider the soil-atmosphere interaction in coupled thermo-hydraulic simulation. In this study a validated 3D model by Tang and Nowamooz (2020) which considers the energy and water balance on the ground surface to evaluate the horizontal heat exchanger performance in field conditions using a finite element tool (COMSOL) is presented in detail. This model contains different parts as following:

- the soil surface energy balance;
- the soil surface water balance;
- the hydrothermal transfer in subsurface soil.

1.4.1.1 Soil surface energy balance

Energy balance on the ground surface is written as (Chalhoub et al. 2017)

$$R_n + H - LE - G = 0 \tag{1.20}$$

where R_n is the net radiation heat flux ($W.m^{-2}$), H is the sensible heat flux ($W.m^{-2}$), LE is the latent heat flux ($W.m^{-2}$), G is the ground heat flux which represents the total heat flow through the ground surface ($W.m^{-2}$) (Figure 1.25).

The net radiation and and the sensitive heat flux can be positive, when the heat flux is into the ground and can be negative, when the heat flux out from the ground. Therefore to obtained the ground heat flux, the net radiation heat flux, the sensitive heat flux and the latent heat flux should be calculated separately.

The net radiation is defined as the difference between the total incoming and outgoing radiations. The approach of Gan (2014) was used which consider the both air and

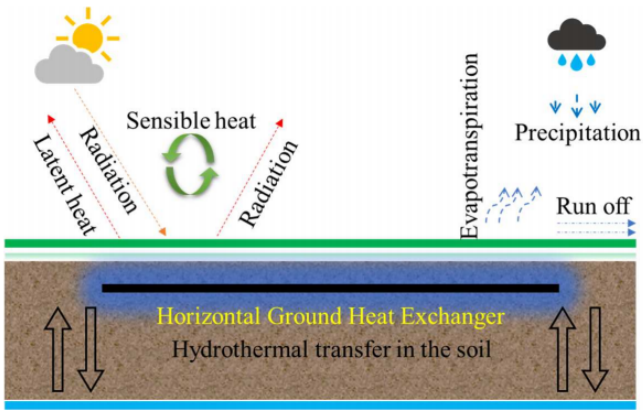

Figure 1.25: Shallow horizontal heat exchanger and the considered mechanism of the energy and water transfer in the ground (Tang and Nowamooz 2020).

soil temperatures.

$$R_n = (1 - a_l)R_s + (R_a - \varepsilon\sigma T_s^4) \tag{1.21}$$

where a_l is the surface albedo, R_s is the shortwave radiation $(W.m^{-2})$, R_a is the incoming longwave radiation $(W.m^{-2})$, $\varepsilon\sigma T_s^4$ is the outcoming longwave radiation $(W.m^{-2})$, ε is the soil surface emissivity, σ is Stephan-Boltzman constant $(W.m^{-2}.k^{-4})$, T_s is the soil temperature (K). The net long wave radiation is given by:

$$R_a - \varepsilon\sigma T_S^4 = -\sigma\varepsilon(T_s^4 - T_{sky}^4) \tag{1.22}$$

where T_{sky} is the sky temperature (K) that is a temperature that indicated the long wave radiation exchanges with the sky (Adelard et al., 1998). This parameters is controlled by cloud cover c_c and air temperature T_a (K) and is defined as following (Cole 1976):

$$T_{sky}^4 = 9.36 \times 10^{-6}(1 - c_c)T_a^6 + c_c[(1 - 0.84.c_c)(0.52 + 0.16.e^{8.45(1-(273.15/T_a))}) + 0.84.c_c]T_a^4 \tag{1.23}$$

The sensible heat flux is the heat transfer by conduction between the ambient air and the ground surface (Liu et al. 2007):

$$H = \rho_a C_{P-a}(T_a - T_s)/r_a \tag{1.24}$$

$$r_a = \frac{ln(\frac{Z_m - d}{Z_{om}}).ln(\frac{Z_m - d}{Z_{oh}})}{k^2 u_{wind}} \tag{1.25}$$

where Z_m is the height where the meteorological parameters are measured (m), d is the displacement height (m), Z_{om} is the roughness length for momentum (m), Z_{oh} is the roughness length for water vapor (m), k is the von Karman constant, and u_{wind} is the wind speed $(m.s^{-1})$.

The latent heat flux (LE) contains the latent heat vaporization of water and the actual evaporation, E, which can be obtained by following equation $(mm.s^{-1})$ (Monteith 1965):

$$E = P.[1 + (E_p/P)^{-2}]^{1/2} \tag{1.26}$$

where P is the rainfall rate $(mm.s^{-1})$, E_p is the evaporation potential $(mm.s^{-1})$ which can be calculated by Penman-Monteith equation as following (Monteith 1965):

$$E_p = \frac{1}{L}[\frac{\Delta.R_n + \rho_a C_{P-a}(e_S - e_a)/r_a}{\Delta + \gamma(1 + r_c/r_a)}] \tag{1.27}$$

where Δ is the slope of the saturation vapor pressure curve $(k.Pa.K^{-1})$, e_S is the saturation vapor pressure (kPa), e_a is the actual vapor pressure (kPa), γ is the psychrometric constant $(k.Pa.K^{-1})$, r_c is the crop canopy resistance $(s.m^{-1})$. Evaporation potential parameters and descriptions are presented in Table 1.1.

Table 1.1: Evaporation potential parameters and description.

Evaporation potential parameters	Description
$\Delta = 4098e_s/(T_a - 35.85)^2$	T_a is the air temperature
$e_s = 0.61.exp(17.27(T_a - 273.15)/(T_a - 35.85))$	T_a is the air temperature
$e_a = RH.e_s/100$	RH is air humidity RH
$\gamma = C_{P-a}.P_{at}/(L.r_{mw})$	P_{at} is the atmospheric pressure (Pa), r_{mw} is the molecular weight of water vapor to dry air
$r_c = r_l/(0.5.LAI)$	r_l is the stomatal resistance of a single leaf $(s.m^{-1})$ LAI is the leaf area index

1.4.1.2 Soil surface water balance

The precipitation (P) is the only water source, which is kept balanced with water run off (W_r), actual evaporation (E), and infiltration (W_i) through the land surface. Therefore:

$$P = W_r + E + W_i \tag{1.28}$$

1.4.1.3 Hydrothermal transfer in subsurface soil

To calculate the water potential with space and time, the Richards equation is considered as following:

$$\rho_w.\Psi.\frac{dH_P}{dt} + [-K.k_r.\nabla.\rho_w.(H_P + D + H_k)] \tag{1.29}$$

where ρ_w is the water density ($kg.m^{-3}$), Ψ is the specific moisture capacity (m^{-1}), H_p is the suction head (m), t is the time (s), K is the saturated hydraulic conductivity ($m.s^{-1}$), k_r is the relative hydraulic conductivity, D is the elevation head (m), H_k is the kinetic head (m). Equation 1.9 and 1.10 in section 1.2.1.2 can be used to calculated the relative hydraulic conductivity and its parameters.

As is discussed the soil thermal properties change with soil density and water content. Based on laboratory results, equations 1.30 and 1.31 proposed respectively by Nikoosokhan et al. (2016) and Tang and Nowamooz (2018a) to calculated the soil thermal conductivity and volumetric heat capacity relatice to soil density and saturation degree.

$$k_s = (0.443x_s + 0.081\gamma_d)\frac{(4.4x_s + 0.4)S_r}{1 + (4.4x_s - 0.6)S_r} + 0.087x_s + 0.019\gamma_d \tag{1.30}$$

where x_s, γ_d, and S_r are the soil sand content, dry unit weight ($kN.m^{-3}$) and saturation, respectively.

$$C_{v-s} = (4.18 - 0.095\gamma_d - 0.3x_s)S_r + 0.09\gamma_d - 0.2x_s \tag{1.31}$$

Therefore, to estimate the thermal efficiency of a soil under thermo-hydraulic variation the following investigations are required:

• find the in-situ meteorological data such as α_1, ε, σ, ρ_a, C_{p-a}, z_m, h_c, k, L, P_{at}, r_{mw} and r_1 to consider the soil-atmosphere interaction.

• laboratory measurement of hydraulic conductivity in saturated and unsaturated state to obtained K and k_r.

• laboratory measurement of the soil suction at different water contents to obtained water retention curve characteristics α, m and n.

• laboratory measurement of the soil thermal properties to validate the equations that will be used in thermo-hydraulic simulation model.

• find soil compaction characteristic (γ_d, w_{opt}) and soil sand content x_s.

Once the parameters of the presented model are obtained, the thermal performance of a system contains horizontal heat exchanger loops can be performed.

1.4.2 Thermo-mechanical constitutive models in saturated state

Several constitutive models were proposed to take into account the effect of temperature on the mechanical behavior of soils in the saturated state (Hueckel and Borsetto 1990; Cui et al. 2000; Graham et al. 2001; Hueckel et al. 2009; Laloui and François 2009b; Hamidi and Khazaei 2010; Yao and Zhou 2013). Hueckel and Borsetto (1990) were the first to propose a thermo-elasto-plastic constitutive model by modified the Cam-Clay model. In this model, the evolution of the yield limit has been considered based on the variation of the preconsolidation pressure with temperature. Cui et al. (2000) developed this model by considering the effect of temperature on the overconsolidated soils. Laloui and Cekerevac (2003) proposed another elasto-plastic model based on the principle of decrease in the elastic domain upon heating and the thermal volumetric change in normally and overconsolidated states. The detail of Laloui and Cekerevac (2003) model is presented in this study.

As is shown in figure 1.26a the isotropic yield limit decreases upon heating. The temperature dependence of preconsolidation can be described as the following:

$$P_c^{'}(T) = P_{c_0}^{'}(1 - \gamma_T log\frac{T}{T_0}) \tag{1.32}$$

where P'_{C_0} is the preconsolidation stress at a reference temperature T_0, γ_T is a material parameter describing the evolution of P'_c and T.

Therefore the elastic domain decreases and the thermo-elastic deformation (ϵ_v^{Te}) before reaching apparent preconsolidation pressure at a given temperature is described as following:

$$\epsilon_v^{Te} = \beta(T - T_0) + \frac{p' - p'_0}{K} \tag{1.33}$$

where β is the volumetric thermal dilation coefficient, $(T - T_0)$ is the temperature difference, p' and p'_0 are the current and the initial effective mean stress respectively and K is the bulk elastic modulus is given by:

$$K = K_{ref}(\frac{p'}{p'_{ref}})^n \tag{1.34}$$

where K_{ref} is the bulk elastic modulus at a reference pressure, p' is effective vertical stress, p'_{ref} is the value of the mean effective pressure at which the elastic modulus is measured and n is the non-linear elasticity exponent.

Once the preconsolidation is exceeded the plastic deformation occurs. The relation between preconsolidation pressure (P'_c) and volumetric plastic strain (ϵ_v^p) can be expressed as:

$$P'_c = P'_c(T)exp(\beta\epsilon_v^p) \tag{1.35}$$

where $P'_c(T)$ is the preconsolidation stress at a given temperature T and β is the plastic compressibility (the slope of the plastic domain of the ϵ_v $\log P'$).

As described in section 1.3.2.1, the soil in overconsolidation condition under constant vertical stress provides an expansion of volume upon heating and with subsequent cooling, this expansion is dissipated. This thermo-elastic (ϵ_v^{Te}) behavior is calculated using equation 1.33. For the normally consolidated soils, a volumetric plastic strain is observed upon heating. The thermal plastic strain induced a reduction in the void ratio of the soil. An equation is proposed to calculate the rate of thermo-plastic strain ($\dot{\varepsilon}_v^p(NC)$):

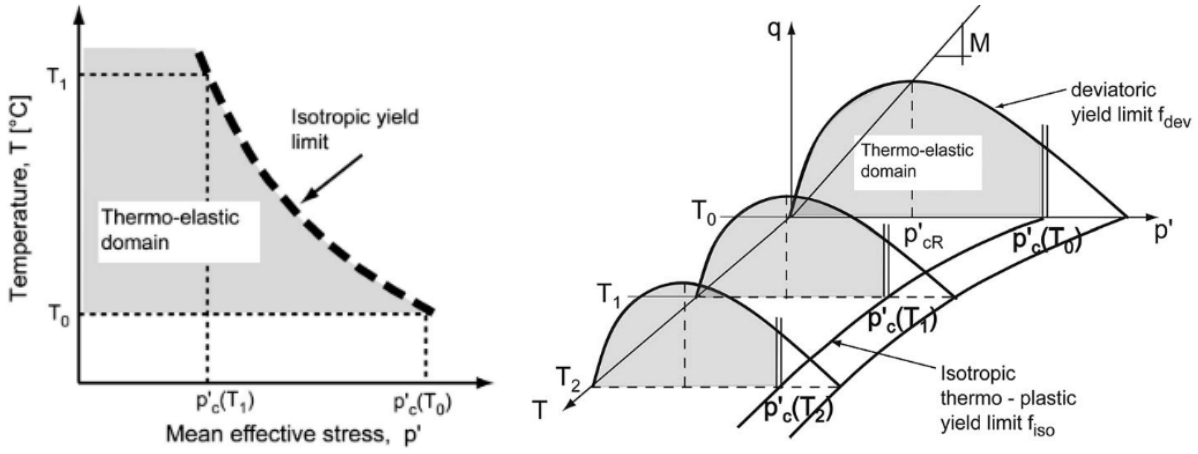

(a) (b)

Figure 1.26: (a) isotropic thermoplastic yield limit (b) coupled thermoplastic yield limits (Laloui and François 2009a).

$$\dot{\varepsilon}_v^p(NC) = \frac{\gamma \dot{T}}{2.303\beta T[1 - \gamma log(T/T_0)]} \tag{1.36}$$

where $\dot{T}$ is temperature rate.

To express the isotropic thermo-plastic yield limit in the isothermal condition the following equation is usually used:

$$f = P^{'} - P_c^{'} \tag{1.37}$$

Due to the temperature dependency of preconsolidation pressure ($P_c^{'}$) the isotropic thermo-plastic yield limit is thus given by (Figure 1.26):

$$f = P^{'} - P_{c_0}^{'}(1 - \gamma_T log\frac{T}{T_0})exp(\beta\epsilon_v^p) \tag{1.38}$$

1.4.3 Thermo-mechanical constitutive models in unsaturated state

Alonso et al. (1990) has proposed a constitutive model named Barcelona Basic Model (an extension of the Cam-Clay model) to describe the variation of the soil volume and shear resistance in unsaturated state. This model based on the principle of the increase in pre-consolidation pressure and consequently increase in the elastic domain causes an increase in the suction. The elasto-plastic model of Alonso et al. (1990) showed two different surfaces: SI (Suction Increase: the loading surface that manages plasticization due to suction

increase) and LC (Loading Collapse: the load surface that manages plasticization due to stress increase) (Figure 1.27a).

For a soil sample subjected to a stress increment dp under constant suction, the elastic volume deformation ($d\varepsilon^e_{vp}$) is given by:

$$d\varepsilon^e_{vp} = \frac{\kappa}{v}\frac{dp}{p} \tag{1.39}$$

where, v is the specific volume (1+e(void ratio)), κ is the elastic slope of the compressibility curve and p is the applied pressure (kPa).

When the preconsolidation stress p_0 is reached, the total volume deformation $d\epsilon^t_{vp}$ is determined by:

$$d\epsilon^t_{vp} = \frac{\lambda(s)}{v}\frac{dp_0}{p_0} \tag{1.40}$$

where, $\lambda(s)$ is the plastic slope of the compressibility curve for a constant suction and is given by:

$$\lambda(s) = \lambda(0)((1-r)exp(-\beta s) + r) \tag{1.41}$$

where $\lambda(0)$ is the plastic slope of the compressibility curve in the saturated state, r is the coefficient related to the maximum stiffness of soil, β is the coefficient which controls the rate of compressibility decrease.

Therefore the plastic deformation is given by:

$$d\epsilon^p_{vp} = d\epsilon^t_{vp} - d\epsilon^e_{vp} = \frac{\lambda(s)-\kappa}{v}\frac{dp_0}{p_0} \tag{1.42}$$

The variation of volume for a soil sample subjected to a suction variation ds under constant stress is divided in tow different domains: elastic and plastic variation. The variation of the volume in elastic domain ($d\epsilon^e_{vs}$) is:

$$d\epsilon^e_{vs} = \frac{\kappa}{v}\frac{ds}{s+p_{atm}} \tag{1.43}$$

where, s is the suction (kPa) and p_{atm} is the atmospheric pressure (kPa).

When suction of s_0 is reached, the total volume deformation ($d\epsilon^t_{vs}$) is determined by:

$$d\epsilon_{vs}^{t} = \frac{\lambda(s)}{v}\frac{ds_0}{s_0 + p_{at}} \tag{1.44}$$

Therefore the variation of the volume deformation in plastic domain ($d\epsilon_{vs}^{p}$) is:

$$d\epsilon_{vs}^{p} = d\epsilon_{vs}^{t} - d\epsilon_{vs}^{e} = \frac{\lambda(s) - \kappa}{v}\frac{ds_0}{s_0 + p_{at}} \tag{1.45}$$

The load area LC is expressed by the following equation:

$$\frac{p_0(s)}{p_c} = \left(\frac{p_0^*}{p_c}\right)^{\frac{\lambda(0)-\kappa}{\lambda(s)-\kappa}} \tag{1.46}$$

where p_c is the reference pressure (kPa), p_0^* is the preconsolidation pressure in saturation conditions (kPa), $p_0(s)$ is the preconsolidation pressure for a constant suction (kPa) (Figure 1.27).

The preconsolidation pressure in the saturated state (p_0^*) is temperature dependent and a description has been proposed by Wu et al. (2004) which is as following:

$$p_0^*(\varepsilon_v^p, T) = p_0^*(\varepsilon_v^p) + \alpha_1 \Delta T + \alpha_2 \Delta T|\Delta T| \tag{1.47}$$

where, ε_v^p is volumetric plastic strain, α_1 and α_2 are the coefficients that depend on the thermal sensitivity of the soil.

Thus the evaluation of preconsolidation pressure with temperature and suction variations is given by:

$$\frac{p_0(s,T)}{p_c} = \left(\frac{p_0^*(\varepsilon_v^p, T)}{p_c}\right)^{\frac{\lambda(0)-\kappa}{\lambda(s)-\kappa}} \tag{1.48}$$

The plastic slope of the compressibility curve changes with suction and temperature and is written as:

$$\lambda(s,T) = \lambda(0,T_r)((1-r)exp(-\beta s) + r) + \beta_1 \Delta T + \beta_2 \Delta T|\Delta T| \tag{1.49}$$

where T_r is the reference temperature, β_1 and β_2 are the empirical coefficients.

Therefore, the major axis of the ellipse in unsaturated soil will span the segment $-p_s$

to $p_0(s,T)$ and the surface area of the state is given by the following expression:

$$q^2 - M^2(p + p_s)(p_0(s,T) - p) = 0 \tag{1.50}$$

where, p_s is the triaxial extension strength and M is the slope of the fracture surface in the plan (p-q). The state surface in space (p-q-s) is shown in Figure 1.28.

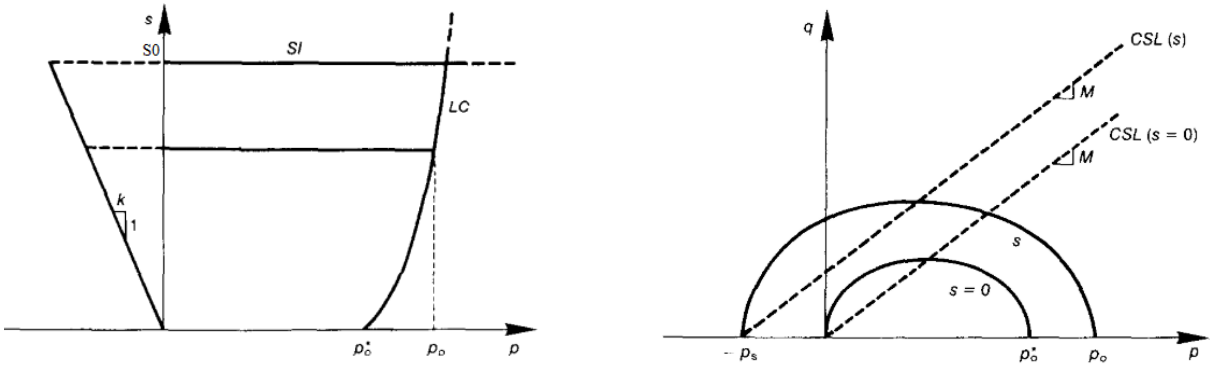

(a) (b)

Figure 1.27: (a) loading surface in LC and SI plane (b) yield surface in p-q (Alonso et al. 1990).

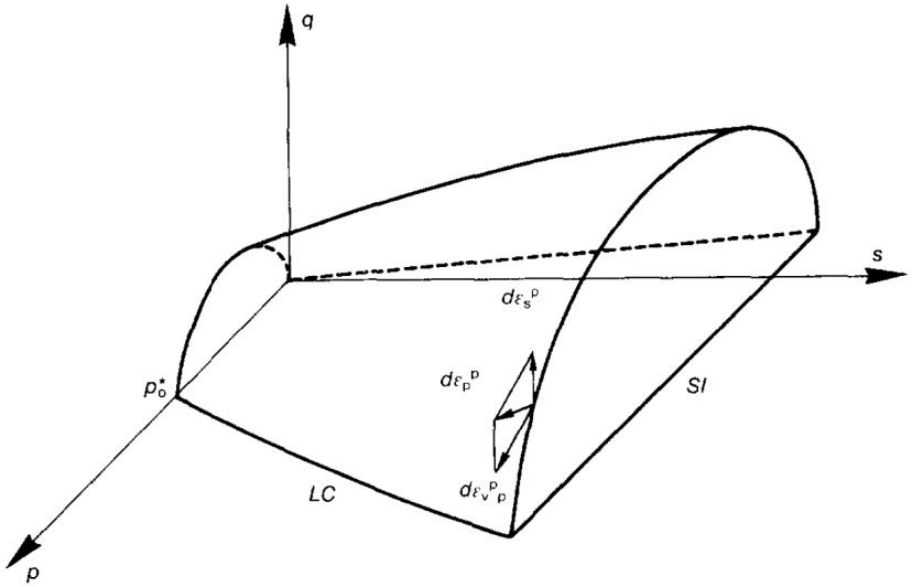

Figure 1.28: Yield surfaces in p,q,s stress space (Alonso et al. 1999).

Therefore, to estimate the thermo-hydro-mechanical behavior of a soil under suction and thermal solicitation the following laboratory tests are required:

• isotropic loading/unloading tests at different temperatures in saturated state to determine $P_c'(T)$ or $p_0^*(\varepsilon_v^p, T)$, γ_T, β, α_1, α_2 and $\lambda(0, T_r)$.

• applied temperature cycles under a constant load to determine K and n.

• isotropic loading/unloading tests with controlled suction and temperature to determine k, β, β_1, β_2, $\gamma(s)$, $\gamma(s,T)$ and r.

• applied drying/humidification cycles under a constant load to determine s_o.

• shear tests at constant suction to determine M.

The set up of these tests requires advanced experimental devices that allow controlling suction and temperature (suction and temperature controlled triaxial or oedometric devices). Once the parameters of the presented model for saturated and unsaturated state are calculated, the use of the models is simple and allows to model most of the phenomena observed experimentally.

1.4.4 Application of numerical models

Jradi et al. (2017) have carried out a comprehensive investigation on thermal energy storage under a residential building. They conducted a numerical simulation considering the conduction heat transfers. This study shows the efficiency of the air source heat pump (ASHP) combined with a solar power system as a basis for seasonal thermal energy storage. As can be seen in Figure 1.29 the U-shape loops were placed horizontally inside the soil beneath the residential building. The heat produced by the solar panels was used for 2 different aspects: the first, the electric power generated will be used directly for electrical and thermal demands. Second, the heat will be used to provide hot water inside the loops. The charging phase occurs in summer. During winter, when the solar system is not able to produce enough electricity to provide the heating need, the heat stored in the compacted soil is discharged through discharging loops.

The area of soil-based thermal storage was 225 m^2 and the storage volume was 900 m^3. A 20 cm thick insulation material insulated the storage medium from 3 different sides (upper and lateral sides). The bottom of the storage medium was not insulated. Figure 1.30a shows the variation of storage medium temperature for one year. The thermal store temperature increased progressively from 27 ^oC in April to 82 ^oC in November and then started to reduce. The heat is stored until October and then will be used to cover the deficit in the heating need. Figure 1.30b shows that a huge heat loss occurred at the bottom of the storage.

Boukelia (2016b) investigated the thermal efficiency of an embankment to store ther-

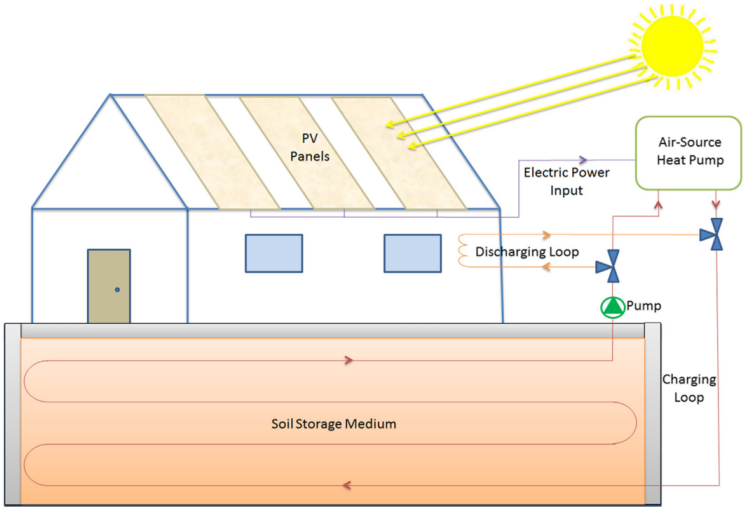

Figure 1.29: underground seasonal thermal energy storage (Jradi et al. 2017).

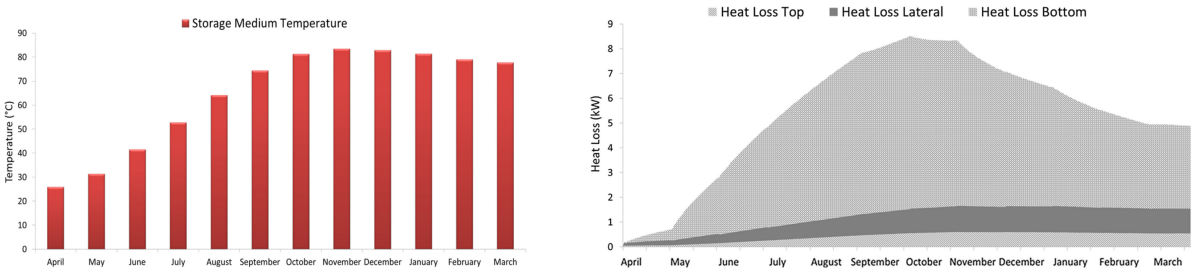

(a) (b)

Figure 1.30: (a) temperature variation of storage medium during the one year (b) heat loss from the underground storage medium (Jradi et al. 2017).

mal energy using horizontal heat exchanger loops by conducting the coupled thermo-hydraulic numerical simulations with a finite element tool (Code-Bright). The aim of this study was to investigate the suitable position of horizontal heat exchanger loops in an embankment with 10 m of high, 10 m of crest width and 1/2 for slope. The distance between two probes varies from 1 to 3 m and the distance from the last probe to the surface of the slope varied from 1 to 11.5 m. This system was considered to store solar energy during summer to be used during winter. Therefore, in summer, a constant temperature of 25 or 50 ^oC was imposed in the loops. In the autumn this system is supposed in relaxation. In winter, when the demand for thermal energy is high a constant temperature of 5 ^oC was imposed to the heat exchanger tubes. As a consequence, the heat which has been stored during summer is extracted. After several simulations, the optimal distance between probes to avoid excessive implementation of tubes was found to be 3 m. To avoid the heat loss due to the soil atmosphere intersection the optimal distance between probes

and the slope of the embankment was 11.5 m. Figure 1.31 indicated the temperature evolution for one year in different elevation points in the embankment configuration with a constant temperature of 50 ^oC. During summer, the temperature increases; during autumn the temperature slightly decreased toward an equilibrium; then throughout winter the temperature decreases and during spring, it reaches almost the initial temperature (12 ^oC). Even if temperature imposed, to the probes is 50 ^oC, the temperature of soil close to the probes only reached 38 ^oC. At the end of the autumn the temperature was about 25 ^oC. Therefore, about 13 ^oC of heat loss has occurred. To reduce heat loss during relaxation season insulation should be taken into account in the design stage.

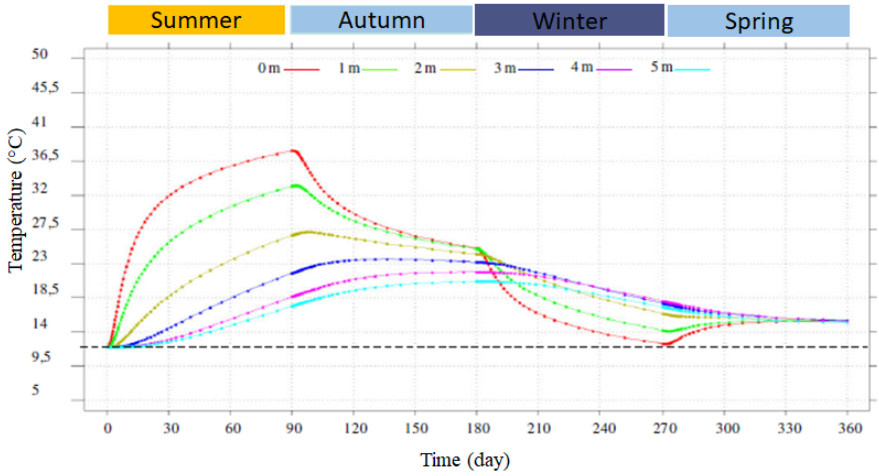

Figure 1.31: Temperature variation of storage medium during one year (Boukelia 2016b).

1.5 Conclusions

Literature review was conducted to introduce the different methods to store thermal energy inside soils. The thermal storage in embankments was presented as a new method which contribute in renewable energy production. Two important aspects of this structure; thermal efficiency and mechanical performance were discussed as well.

The efficiency of thermal energy storage in compacted soil is strongly dependent on soil thermal properties, soil compaction level and horizontal heat exchanger shapes and patterns. Soil thermal properties are affected by various soil properties such as; water content, mineralogy, density and temperature. However, compacted soils are usually unsaturated; therefore, reliable estimations and measurements of unsaturated compacted

soil thermal properties are important in the efficiency analysis of these structures. There is however no available method to follow in real-time, the evolution of these parameters in the field. Therefore, a method to develop and adapt an in-situ estimation of the thermal properties of soil is needed, to evaluate the long-term thermal efficiency of thermal energy storage in embankments or other configurations.

Once the compacted soil was selected, due to the its capacity for thermal energy storage, the thermo-hydro-mechanical behavior under monotonic and seasonally temperature variation should be investigated in laboratory. Based on most of the investigations that have focused on the effect of temperature (20 to 90 °C) on hydro-mechanical behavior of soil, it was observed that the soil behavior is dependent on temperature variation, stress history of the soil (NC or OC) and soil nature. Although in the extensive existing literature, effect of cooling, and heating-cooling cycles are poorly understood. Therefore, the effect of monotonic and cyclic temperature variation consolidation and shear parameters should be studied. These experimental results will be modeled and then used in numerical simulation to estimate the structure stability under non-isothermal conditions.

For numerical modeling of thermal energy storage, the theoretical equations to simulate the thermo-hydraulic behavior of soil considering soil-atmosphere interaction were explained in detail. Two important constitutive models to simulate the thermo-mechanical behavior of soil under non-isothermal condition were presented to introduce the necessary input parameters. These numerical modeling required different input parameters that should be first obtained in laboratory. For the mechanical simulation, when the effect of temperature on mechanical parameters is experimentally negligible, thus the thermal performance of the structure is a more important aspect than its mechanical part and it should be investigated numerically.

Chapter 2

Measurement of the thermal properties of unsaturated compacted soil by the transfer function estimation method

Abstract: Thermal energy storage in embankments can be considered a new economically efficient and environmentally friendly technology in geotechnical engineering. In these structures, horizontal heat exchanger loops can be installed inside different layers of compacted soil to store heat in the medium during the summer to be extracted during the winter. Compacted soils are usually unsaturated; therefore, reliable estimates and measurements of unsaturated compacted soil thermal properties, such as the volumetric heat capacity, thermal conductivity, and thermal diffusivity, are important in the efficiency analysis of these structures. However, there is no available method to characterize the evolution of these parameters over time in compacted soil.

In this study, several temperature sensors were placed inside different layers of unsaturated compacted soil in a cylindrical container (height of 0.8 m and diameter of 0.6 m) to monitor imposed temperature cycle variations. An inverse analytical model based on the one-dimensional radial heat conduction equation is proposed to estimate the thermal diffusivity using the temperature variation between two temperature sensors. The volumetric heat capacity was measured with a calorimeter in the laboratory, enabling estimation of the thermal conductivity of the compacted soil. Then, this estimated thermal conductivity was compared with the thermal conductivity values measured with two different methods (one steady-state and one transient-state method). The estimated ther-

mal conductivity was close to the value measured with the transient-state method. It was demonstrated that steady-state methods are not suitable for the measurement of thermal conductivities as high as 2.5 $W.m^{-1}.K^{-1}$ since thermal contact resistances are no longer negligible.

Keywords: Soil thermal properties, transfer function, unsaturated compacted soil, inverse analytical model.

2.1 Introduction

In recent years, due to the depletion of fossil resources and their negative impact on the environment, there is a tendency towards using renewable energy. Among the different types of renewable energies, solar energy provides an abundant, clean and safe energy source. The supply of this energy is periodic, following yearly and daily cycles (Stojanović and Akander 2010). Various techniques have been developed to store solar energy in a proper medium for use in high-demand periods. Thermal energy storage is a technique that can be described as the short- or long-term storage of thermal energy by heating a storage medium. Seasonal thermal energy storage stores solar energy that is diffused in the summer for space heating in the winter (H Abedin and A Rosen 2011). Thermal energy can be stored by inserting vertical or horizontal heat exchanger loops into a storage medium. Several studies have shown that seasonal thermal energy storage is a pertinent technique that has been used in geologic storage media, such as soil, due to its appropriate thermal properties and ease of access (Xu et al. 2014; Li et al. 2018).

In geotechnical engineering, different types of structures are made of unsaturated compacted soil, for example, road and rail embankments and dikes. Generally, these linear structures contain several layers of unsaturated compacted soils. Horizontal heat exchanger loops can easily be installed in these layers during the construction phase (Figure 2.1; Jradi et al. 2017; Boukelia et al. 2019).

However, the cyclic temperature variations in these structures could modify the thermo-hydro-mechanical (THM) behaviour of the soil, and these variations may consequently affect the expected mechanical performance of the structures and heat storage efficiency (Romero et al. 2001; François et al. 2007; Uchaipichat and Khalili 2009). Therefore, a

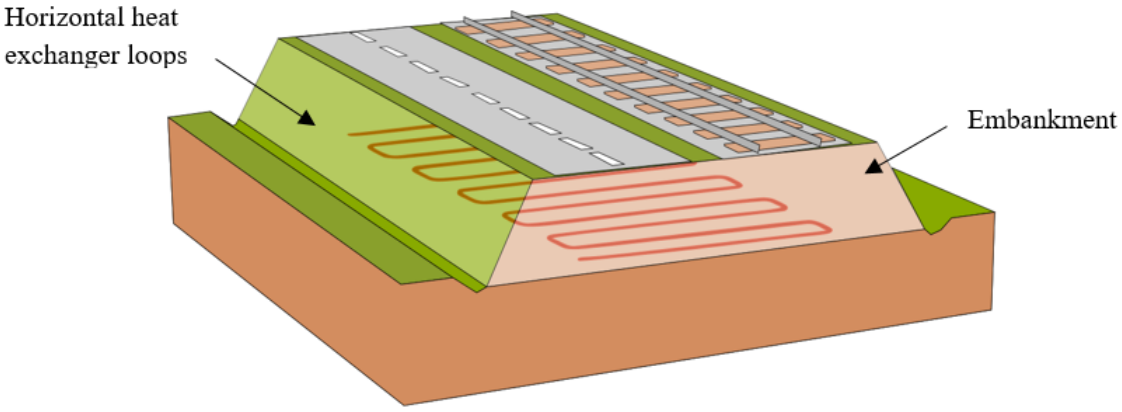

Figure 2.1: Forecast embankment thermal storage.

more comprehensive understanding of the following aspects is needed:

1) Determination of the thermal characteristics of unsaturated compacted soil to optimize the heat storage energy amount.

2) Examination of the effect of temperature variations on the THM behaviour of unsaturated compacted soil.

3) Investigation of the interaction between unsaturated compacted soil and heat exchanger loops.

This study focuses on the thermal parameters of unsaturated compacted soil to optimize the efficiency of thermal storage structures. The thermal properties that affect the heat storage capacity are the volumetric heat capacity C_v $(J.m^{-3}.K^{-1})$, the thermal conductivity λ $(W.m^{-1}.K^{-1})$ and the thermal diffusivity α $(m^2.s^{-1})$. The relationship between these thermal properties is as follows:

$$\alpha = \frac{\lambda}{C_v} \tag{2.1}$$

The soil thermal properties change according to its physical and hydro-mechanical properties, such as the mineral composition, degree of saturation and dry density (Penner et al. 1975; Abu-Hamdeh and Reeder 2000; Ekwue et al. 2006). The variation of these properties coupled with the thermal solicitations in unsaturated soil can reach a high level of complexity, which causes difficulties in evaluating the thermal properties of these soils (Jahangir et al. 2018). Additionally, in an unsaturated medium, due to such a complex multiphase medium, heat is transferred by three different modes: conduction through the

solid particles, convection through the gaseous and liquid phases, and radiation at the particle surfaces. However, due to the complex combination of these phases in unsaturated soil, most of the measurement and estimation methods applied to unsaturated soil to measure its thermal properties are based on the solution of a one-dimensional heat conduction equation assuming a homogeneous soil (Ukrainczyk 2009; Kodikara et al. 2011; Rajeev and Kodikara 2016).

The thermal properties of soils can be measured indirectly with steady-state or transient-state methods by measuring the rise or fall of the temperature in response to a heat flux (Abu-Hamdeh et al. 2001; Kraemer and Chen 2014). Steady-state methods are used to measure thermal properties when the heat transfer flux through the sample remains unchanged over time. The reference steady-state method to measure the thermal conductivity is the guarded hot plate method, which is performed on samples with a minimum cross-section of 0.3 x 0.3 m^2 (Barry-Macaulay et al. 2013; Dieye et al. 2017). The centred hot plate method enables measurement of the thermal conductivity of smaller samples, with a 0.1 x 0.1 m^2 cross-section (Jannot et al. 2010; Jannot et al. 2016).

Transient methods are used to measure thermal properties during the unsteady-state heat transfer process. The thermal needle probe and infrared thermal imaging methods are often used to measure the thermal conductivity and thermal diffusivity of soil samples in the laboratory and field, respectively (Bilskie 1994; Coquard et al. 2006; Kodikara et al. 2011; Barry-Macaulay et al. 2013). However, these transient methods only obtain a single reading at the corresponding time and cannot measure the temperature profile along the soil depth in the field, which is the inherent limitation of these techniques (Rajeev and Kodikara 2016).

In the field, the thermal diffusivity can also be estimated by monitoring the temperature of the soil via a thermal response test (Asrar and Kanemasu 1983; Gehlin and Hellström 2000). The thermal response test is commonly used to estimate the thermal properties of saturated soils based on the inlet and outlet temperatures of vertical heat exchanger loops, which are inserted several tens of metres into the ground (Gehlin and Nordell 2003; Beier 2018).

The temperature monitoring method, using different temperature sensors at different depths, has been proposed to estimate the thermal diffusivity of unsaturated soils near the

ground surface (Adams et al. 1976; Horton et al. 1983; Rajeev and Kodikara 2016). Based on these methods, different analytical and numerical models were proposed to predict the heat transfer function and consequently the apparent thermal diffusivity of the medium from the observed temperature variations.

Gao et al. (2009) and Rajeev and Kodikara (2016) used simplified analytical models under the hypothesis of a sinusoidal temperature variation in the soil surface (sinusoidal boundary condition), which is not always valid in thermal energy storage since the duration of the cooling period is not necessarily as long as the heating period. This type of temperature monitoring method was also used by Ukrainczyk (2009) to estimate the thermal diffusivity of complex materials. In their study, a numerical inverse solution for one-dimensional heat conduction was used, which is more complex than the direct analytical model and was only used in the laboratory.

Jannot and Degiovanni (2013) proposed a simple inverse analytical model to estimate the thermal properties of powders or granular materials. In this method, the transfer function is not dependent on the shape and intensity of the heat flux or the external boundary condition (such as the soil surface in the field). In this temperature/temperature method, first, the transfer function between two recorded temperatures is modelled, and then an associated inverse analytical model is proposed to estimate the thermal diffusivity. To our knowledge, this analytical model has never been applied to unsaturated compacted soils. In this study, this analytical model is adapted and applied to estimate the thermal diffusivity (α) of unsaturated compacted soil by monitoring the temperature of a large-scale sample when subjected to temperature variation cycles. Then, the volumetric heat capacity, C_v, was measured in the laboratory to estimate the thermal conductivity λ using Eq. (2.1). The estimated thermal conductivity was then compared with the thermal conductivities that were measured in the laboratory via two other classical methods (the transient-state and steady-state methods). If the estimated thermal conductivity validated, this method could enable system efficiency estimation of possible future applications of thermal energy storage in compacted soils such as embankments or other configurations.

2.2 Materials and methods

In this section, the properties of the studied material are first presented, and then the different methods used to estimate the thermal properties of unsaturated compacted soil are detailed.

2.2.1 Material properties

The tested soil was extracted from the Paris region in France. X-ray diffractogram analysis revealed that the soil contains 81% quartz, 7% dolomite, 5% calcite, 5% clay minerals and 3% feldspar (Boukelia 2016b). This material was dried, pulverized and passed through a 2 mm sieve before being used for the various experiments. According to the particle-size distribution, almost 20% of the soil particles were smaller than 2 μm, and 41% were smaller than 80 μm (Figure 2.2a). With a liquid limit (LL) of 27% and a plastic limit (PL) of 21%, the plasticity index (PI) was 6% (AFNOR 1993). The standard Proctor curve of the material (AFNOR 1999a) showed an optimum water content (w_{opt}) of 16% and a maximum dry density (ρ_d) of 1.81 $Mg.m^{-3}$ (Figure 2.2b).

The material was classified as a sandy lean clay, CL, according to the Unified Soil Classification System (ASTM 2000) and as A1 in the French standard for soil classification (GTR 2000).

To optimize the efficiency of thermal embankment storage, the variation of the thermal properties of the soil with the dry density and degree of saturation were investigated. In accordance with the literature, Bristow (1998) and Smits et al. (2010) observed that thermal properties increased with an increase in the degree of saturation or dry density. Boukelia (2016b) showed that the maximum values of the thermal conductivity and volumetric heat capacity of the studied soil were reached at a water content of 16.3% and a dry density of 1.79 $Mg.m^{-3}$. However, this compaction state could not be reached in the large-scale experimental container. As a consequence, the reference compaction state in this study was a water content of 16.3% and a dry density of 1.72 $Mg.m^{-3}$.

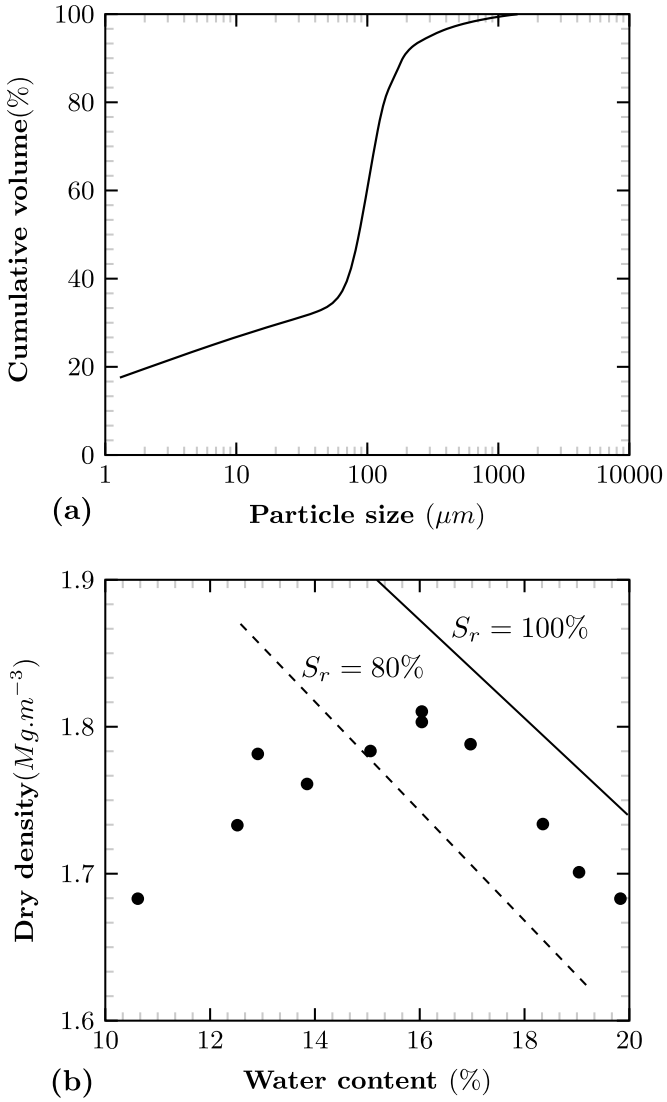

Figure 2.2: Characteristics of the studied soil: (a) particle size distribution and (b) compaction curve, Sr: The degree of saturation.

2.2.2 Transfer function estimation method (TFEM)

To prepare the sample for temperature monitoring, the soil was compacted in a container with a height of 0.8 m and a diameter of 0.6 m with a pneumatic compactor (Figure 2.3a). This large-scale sample was realized to reproduce the in-situ conditions. The compactor applied dynamic forces on a metallic plate, which was 0.04 m thick and 0.6 m in diameter, placed on top of the material to ensure homogeneous soil compaction. To ensure a homogeneous density the massif, compaction was performed in eleven 0.07 m thick layers.

Five temperature sensors, PT100 (6 mm in diameter and 60 mm in length), were

positioned in different layers of the compacted soil (T3 to T7, Figure 2.3a) and plugged into a data logger to monitor the temperature variations inside the compacted soil. The temperature was recorded every 50 s using the five temperature sensors. To induce cyclic variations of the temperature, an ethylene glycol-water solution was circulated through a stainless steel tube which was welded to the outside of the container (Figure 2.3c). A heating-cooling system (Vulcatherm thermoregulator, with a 6 kW heating capacity) imposed three successive heating-cooling cycles in the range of 20 to 50 ^oC (Figure 2.3d). Thermal equilibrium was reached for each step before changing, and the entire test lasted one week. Insulating sleeves were placed around the tube to reduce the amount of heat exchange with the surrounding atmosphere. Plastic film was placed on top of the container to preserve the initial water content. Finally, the entire device was placed in a box made of 0.04 m thick extruded polystyrene plates to reinforce the thermal insulation effect (Figure 2.3c).

2.2.3 Water content and density profile measurements

Six cores with a diameter of 28 mm were positioned on a concentric circle with a diameter half the size of that of the container (Figure 2.3b). The 630-mm-length cores were divided into small segments to measure the water content and density of the material as a function of depth. The measurements for two of the cores were conducted at the beginning of the test (20 a-b), and the measurements for two other cores were carried out at the end of the first heating cycle (50 a-b), while the two remaining cores were analysed at the end of the test (20 c-d) (Figure 2.3b, 2.3d). These results allowed us to assess the initial homogeneity of the sample and to evaluate any variations due to the temperature changes.

2.2.4 Other methods for measuring the thermal properties

To validate the proposed TFEM method, the thermal properties were measured by other methods.

A micro-differential scanning calorimeter (DSC, SETARAM μdsc3) was used to measure the specific heat (C_{dry}) of dry soil at different temperatures.

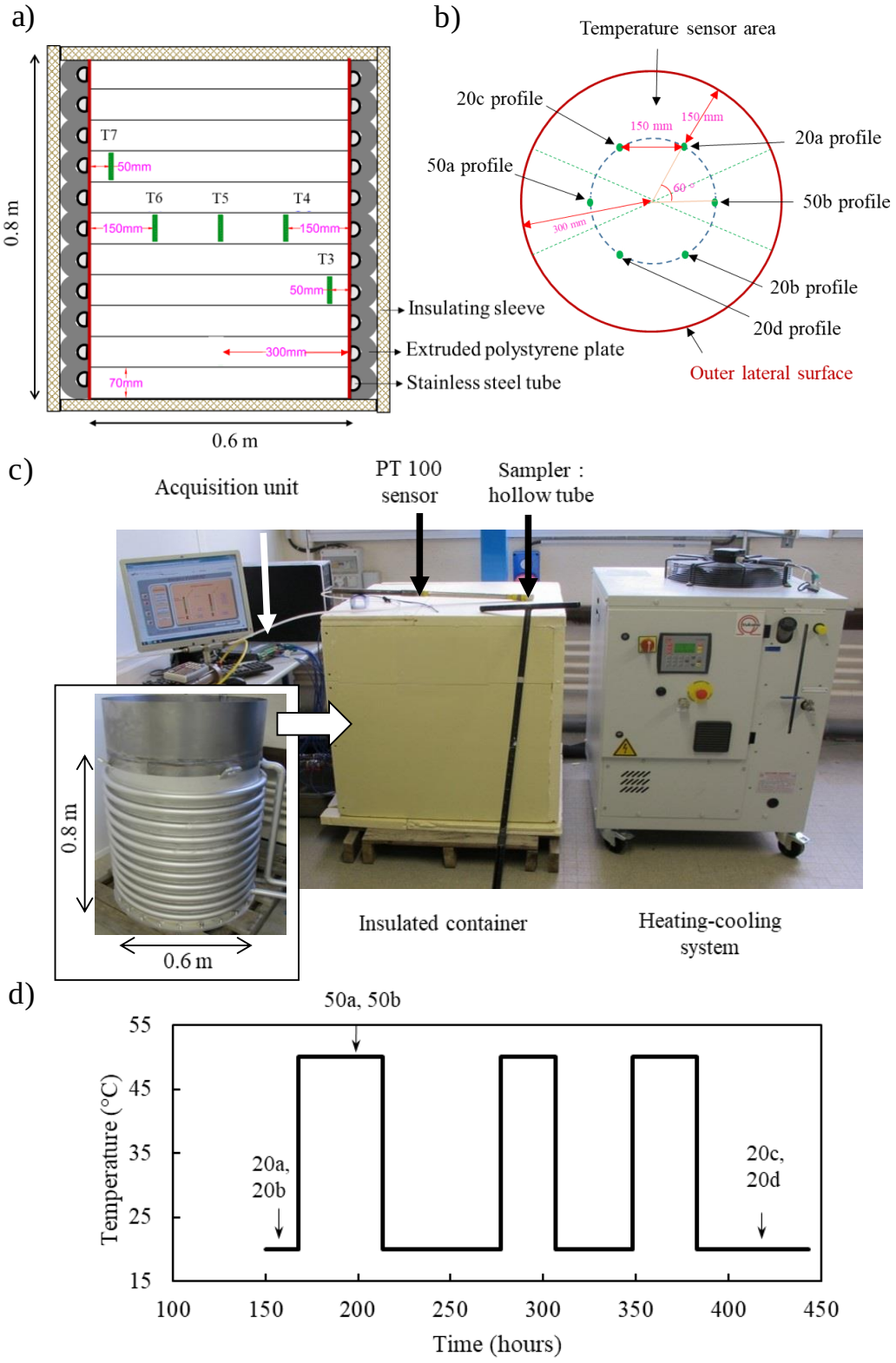

Figure 2.3: Details of the developed laboratory model a) cross sectional view of the thermo-regulated metric scale container and the place of the temperature sensors (T3 to T7) b) top view of the thermo-regulated metric scale container and the position of the cores profiles: 20 a-b: two cores before first heating, 50 a-b: two cores after the first heating and 20 c-d: two cores after the third heating and cooling cycle c) experimental setup d) three temperature cycles imposed using heating and cooling system and cores section times.

The specific heat (C_p) of soil at a certain mass water content (w) can be deduced by:

$$C_p = \frac{C_{dry} + wC_{water}}{1 + w} \tag{2.2}$$

where C_{water} is the specific heat of pure water ($C_{water} = 4180\ J.kg^{-1}.K^{-1}$ at 20 ^{o}C).

The volumetric heat capacity C_v ($J.m^{-3}.K^{-1}$) is then given by:

$$C_v = \rho C_p \tag{2.3}$$

where ρ is the density of wet soil ($Kg.m^{-3}$).

The thermal conductivity was also measured by two other methods: Transient-state method: a KD2 Pro Analyser and a single-needle probe (TR-1) with a 2.4 mm diameter and 100 mm length were used to measure the thermal conductivity of the compacted soil samples. This method is a transient-state technique that measures the thermal conductivity through the transient line heat source method (Devices et al. 2016). The single-needle probe (TR-1) was covered with a thin layer of grease to improve the contact between the probe and the soil. Then, it was inserted into the sample that was already compacted in three layers at the desired water content and dry density in a standard Proctor mould with a 0.116 m height and 0.101 m diameter. A waiting time of 15 min was allowed before each test so that the equilibrium temperature between the probe and the soil was reached. The presented values are the mean values of 4 tests performed at different locations in the sample. The thermal conductivity measurement range of this probe is from 0.2 to 4 $W.m^{-1}.K^{-1}$ with an accuracy of $\pm 10\%$ (Devices et al. 2016).

Steady-state method: the centred hot plate method (Jannot et al. 2010; Jannot et al. 2016) is a steady-state method that consists of inserting a thin planar heating element between the soil and a reference material of known thermal conductivity (Figure 2.4). A constant heat flux is produced by the heating element. The soil samples were compacted in a special mould (0.1 x 0.1 x 0.02 m^3) via the static compaction method (Figure 2.5a and 2.5b). The assembly was inserted between two aluminium plates that were maintained at a constant temperature (T_0=15 ^{o}C) and placed in a climatic chamber (Ta= 23 ^{o}C) (Figure 2.5c).

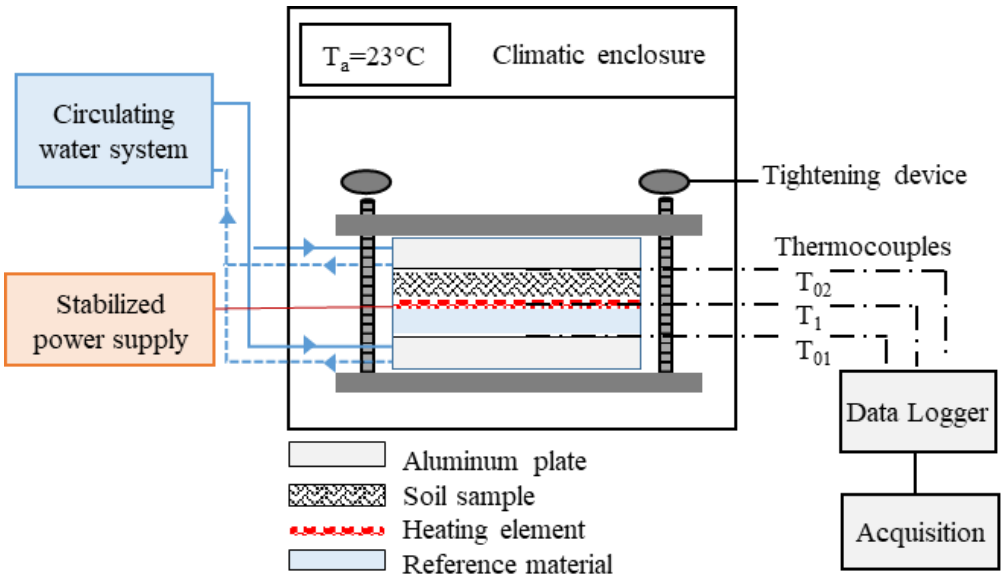

Figure 2.4: Scheme of hot plate device; where T_1 is the temperature of heating element, T_{01} and T_{02} are temperatures of the aluminum plates and T_a is the temperature of the air.

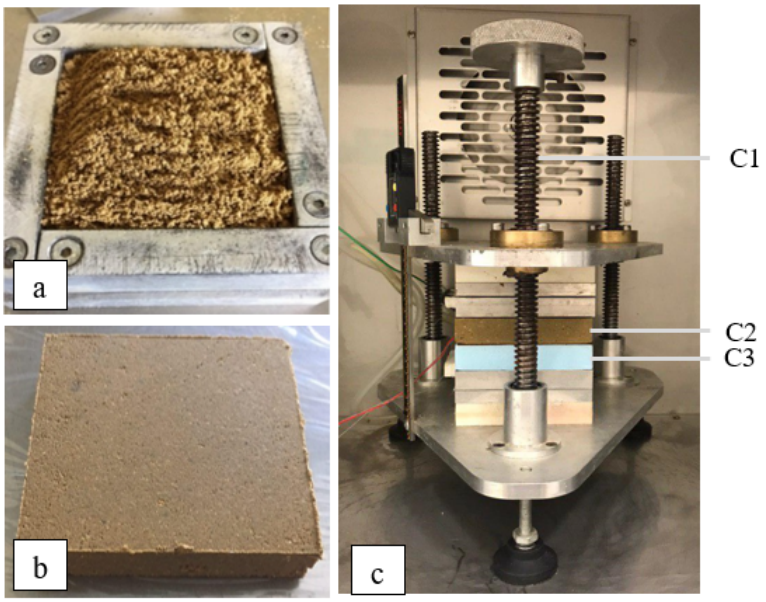

Figure 2.5: a) mold of sample preparation for centred hot plate tests b) compacted soil sample for centred hot plate test c) test assembly C1) Manually Compressing screw (Tightening device) C2) soil sample C3) reference material.

2.3 Modelling

2.3.1 The TFEM method

In this part, the inverse analytical model based on the one-dimensional solution of the Fourier heat balance equation is used to estimate the thermal diffusivity of the compacted soil based on the temperature variations between two temperature sensors.

The estimate of thermal diffusivity α ($m^2.s^{-1}$) is based on the estimation of the transfer function between the inlet and outlet temperatures inside the cylindrical sample. In this study, the heat flux is applied to the external surface of the cylindrical sample and as mentioned in the introduction, the transfer function is not dependent on the shape and intensity of the heat flux or the external boundary condition (Jannot and Degiovanni 2013). The following hypotheses are considered in this model:

- The initial temperature of the compacted soil inside the container is uniform;
- The heat transfer is 1D; and
- Mass transfer is neglected.

The inverse method is expressed by the following equations. The transient heat conduction in the radial direction in cylindrical coordinates is:

$$\frac{\partial^2 T}{\partial r^2} + \frac{1}{r}\frac{\partial T}{\partial r} = \frac{1}{\alpha}\frac{\partial T}{\partial t} \tag{2.4}$$

With the following boundary conditions:

$$\begin{cases} T(r, t = 0) = T_i, 0 \leq r \leq R \\ T(R, t) = T_0(t) \end{cases} \tag{2.5}$$

where T is the temperature (K), r is the radius (m) (the distance of the temperature sensors from the axis of the container), α is the thermal diffusivity ($m^2.s^{-1}$), t is the time (s), R is the radius of the container (m) and T_i is the initial temperature of the sample (K).

The following applies:

$$\overline{T} = T - T_i \tag{2.6}$$

The Laplace transform of Eq. (4) results in Eq. (7), where p is the Laplace parameter (s^{-1}), Θ(r,p) is the Laplace transform of $\overline{T}(t)$ and α is the thermal diffusivity ($m^2.s^{-1}$):

$$\frac{\partial^2 \Theta}{\partial r^2} + \frac{1}{r}\frac{\partial \Theta}{\partial r} = \frac{P}{\alpha}\Theta \tag{2.7}$$

This equation may also be written as:

$$\frac{\partial^2 \Theta}{\partial u^2} + \frac{1}{u}\frac{\partial \Theta}{\partial u} = \Theta \tag{2.8}$$

with:

$$u = \sqrt{\frac{p}{\alpha}} r = qr \tag{2.9}$$

The general solution of this equation is (Jannot and Degiovanni 2018):

$$\Theta(r,p) = AI_0(qr) + BK_0(qr) \tag{2.10}$$

where I_0 is the modified Bessel function of the first kind of order 0, K_0 is the modified Bessel function of the second kind of order 0, and A and B are constants.

The heat flux is null for r=0 so B=0 since $\lim_{r\to 0} K_0(qr) = 0$.

Hence:

$$\Theta(r,p) = AI_0(qr) \tag{2.11}$$

The Laplace transform H_p of the transfer function $F(t,\alpha)$ (s^{-1}) between the two temperatures $\overline{T}(r_2)$ and $\overline{T}(r_1)$ with $r_2 > r_1$ is :

$$H_p = \frac{\Theta(r_2,p)}{\Theta(r_1,p)} = \frac{I_0(qr_2)}{I_0(qr_1)} \tag{2.12}$$

This function only depends on the thermal diffusivity.

$$\Theta(r_1,p) = \frac{I_0(qr_2)}{I_0(qr_1)} \times (r_2,p) \tag{2.13}$$

$$\overline{T}(r_1,t) = \mathcal{L}^{-1}\left[\frac{I_0(qr_1)}{I_0(qr_2)}\right] \otimes \overline{T}(r_2,t) \tag{2.14}$$

where $\otimes$ is the convolution operator.

The thermal diffusivity α is estimated by minimizing the sum of the squared differences between the experimental curve $\overline{T}(r_1)$ and the modelled curve calculated by the relationship of the following type:

$$\overline{T}r_{1model} = \overline{T}r_{2experimental} \otimes F(t,\alpha) with : F(t,\alpha) = \mathcal{L}^{-1}[H(p,\alpha)] \tag{2.15}$$

Minimization of the sum of the squared deviations is carried out with the Levenberg-Marquart algorithm, and the function F(t,α) is calculated with the inverse Laplace transform of Eq. (2.12) and the De Hoog et al. (1982) algorithm . As indicated in Eqs. (2.14) and (2.15), this analytical model depends on the thermal diffusivity and the transient temperature variations at distances r1 and r2 from the axis of the cylindrical sample. The temperature variations at different distances from the centre of the container were obtained from the experiments carried out in the laboratory.

2.3.2 Single-needle probe method

In this method, a heat flux is applied from a single stainless steel needle probe for a period of time, t_h (approximately 30 s), and then the cooling phase starts when the heat flux is stopped. For both the heating and cooling phases, the temperature variations are monitored every second. These temperature variations are then fit to the equations below (Devices et al. 2016).

The temperature during the heating phase:

$$T_h = m_0 + m_2 t + m_3 ln(t) \tag{2.16}$$

The temperature during the cooling phase

$$T_c = m_1 + m_2 t + m_3 ln[\frac{t}{t - t_h}] \tag{2.17}$$

where T is the temperature (K), t is the time, m_0 and m_1 are the ambient temperatures of the heating and cooling phases (K), respectively, m_2 is the rate of the background temperature drift (K.s^{-1}), and m_3 is the slope of the line relating the temperature rise to the logarithm of the temperature (K). Since Eqs. (2.16) and (2.17) are log time approximations, only the final 2/3 of the data collected are used for fitting, and the early time data are neglected during the heating and cooling phases (Bristow 1998). Finally,

the thermal conductivity is calculated using the following equation:

$$\lambda = \frac{Q}{4\pi m_3} \tag{2.18}$$

where λ is the thermal conductivity ($W.m^{-1}.K^{-1}$) and Q is the applied heat input rate per unit length ($W.m^{-1}$).

2.3.3 The centred hot plate method

The heat flux φ (W) produced in the heating element can be written as:

$$\varphi = \frac{\lambda_{ref}}{e_{ref}}(T_1 - T_{01}) + \frac{T_1 - T_{02}}{R_s} \tag{2.19}$$

where λ_{ref} and e_{ref} are the thermal conductivity ($W.m^{-1}.K^{-1}$) and thickness (m), respectively, of the reference material, T_1 is the temperature of the heating element (K), T_{01} and T_{02} are the temperatures of the aluminium plates (K) and R_s is the global thermal resistance ($K.m^2.W^{-1}$). The global thermal resistance (sample and contact resistance) is given by:

$$R_s = \frac{T_1 - T_{02}}{\varphi\frac{\lambda_{ref}}{e_{ref}}(T_1 - T_{01})} \tag{2.20}$$

and

$$R_s = \frac{e_s}{\lambda_s} + R_{c1} + R_{c2} \tag{2.21}$$

where R_{c1} and R_{c2} are the thermal contact resistances on each side of the sample ($K.m^2.W^{-1}$). The thermal conductivity may be calculated as follows:

$$\lambda_s = \frac{e_s}{R_s - R_{c1} - R_{c2}} \tag{2.22}$$

Neglecting these thermal contact resistances, one can deduce the following:

$$\lambda_s = \frac{e_s}{R_s} \tag{2.23}$$

where λ_s is the soil thermal conductivity ($W.m^{-1}.K^{-1}$) and e_s is the thickness of the soil sample (m).

2.4 Results and discussion

In the following, the homogeneity of the compacted soil is first verified, and then, the temperature monitoring data inside the compacted soil and the inverse analytical model were used to estimate the thermal diffusivity. Thereafter, the volumetric heat capacity of the material was measured via the micro-calorimeter test to estimate the thermal conductivity of the compacted soil.

2.4.1 Water content and density profiles

The water content (w) and dry density (ρ_d) of the compacted soil were measured as a function of the depth (from 200 to 580 mm depth) in six cores (Figure 2.6). At the initial state (20a-b), the mean water content was 16.3%, and the mean dry density was 1.72 $Mg.m^{-3}$.

The water content was measured before starting the thermal cycles (20a-b), and the values were close to the initial water content (16.3%) (Figure 2.6a). After the first heating cycle, there is a water content gradient in terms of the radius of the cylindrical samples, and the water content at the wall of the cylindrical sample near the heat flux decreased, while the water content at the centre of cylindrical sample increased (50a-b). Consequently, the water content measurement at a radius of R/2 (R is the radius of the container) is slightly lower than the initial water content (-0.41%). At the end of the cycles, after the temperature has stabilized (20c-d Figure 2.3), the water gradient has dissipated, and the water content at a radius of R/2 becomes equal to the initial value of 16.3%.

2.4.2 Sensitivity analysis of the TFEM method

The initial temperature of the compacted soil was 20 ^{o}C, and the soil was subjected to three heating cycles to 50 ^{o}C. The temperature variations were imposed through the outer lateral surface of the container, and the temperature variations were recorded by the different temperature sensors at the different positions in the container (see section 2.2.2 and Figure 2.3a for further details). Figure 2.7 shows the temperature records of the temperature sensors T3, T4, T5, T6, and T7. The time to reach equilibrium is different

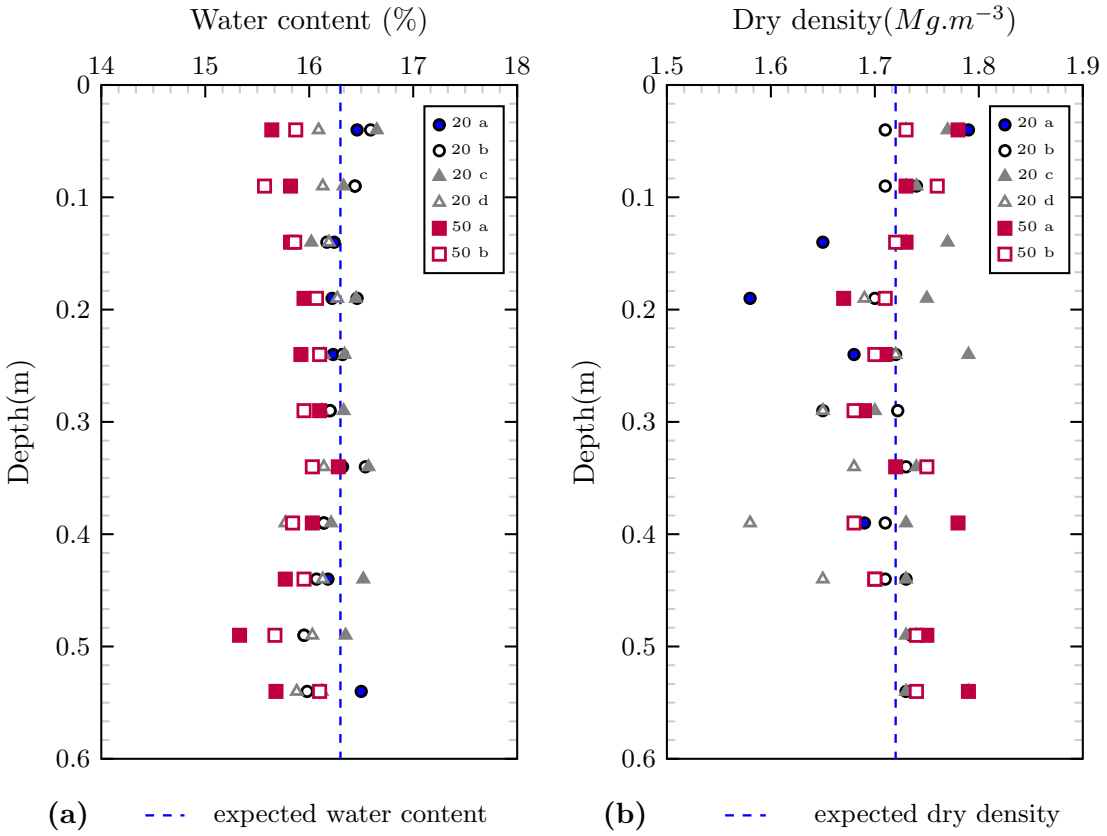

Figure 2.6: (a) water content profiles (b) dry density profiles along the depth of the container.

according to the distance between the temperature sensor and the source of the heat flux. Thus, temperature sensors T7 and T3, which were closer to the source, reached equilibrium quicker than the other temperature sensors that were further away.

As mentioned in the previous section (2.3.1), the analytical model was based on the temperature, the time, the thermal diffusivity and the distance from the centre of the container. First, the uniqueness of the solution was verified, and then the standard deviation and the errors due to the temperature and distance variations from the axis of the container were calculated.

2.4.2.1 Influence of the initial value of the thermal diffusivity

To verify the uniqueness of the solution, the analytical model was applied with several initial thermal diffusivities. In Eq. (2.15), the temperature variations recorded by the T6 sensor were used as Tr_2 and the T5 values as Tr_1. The analytical model has been applied with different initial thermal diffusivities (α) of 5.10^{-7}, 8.10^{-7} and 10.10^{-7} $m^2.s^{-1}$. For each test, the thermal diffusivity converges towards the same value, namely, $8.6.10^{-7}$

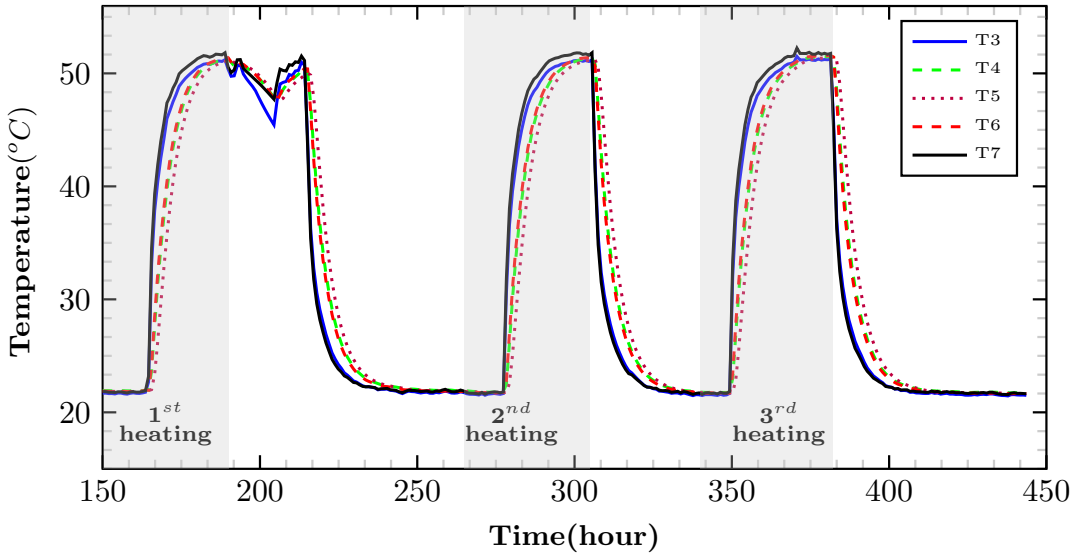

Figure 2.7: Temperature variations in the compacted soil at various locations in the container: three heating-cooling cycles (20-50-20 ^{o}C).

$m^2.s^{-1}$. The results showed that the value of the estimated thermal diffusivity was independent of its initial value. In the following, an average value of 8.10^{-7} $m^2.s^{-1}$ was considered as the initial value of the thermal diffusivity.

2.4.2.2 Influence of the uncertainty of the temperature variations

To estimate the influence of the uncertainty of the temperature variations on the results, the following process was performed:

- A random noise measurement with a standard deviation of $\pm$ 0.1 ^{o}C was added to each temperature measurement.
- The analytical model was applied considering these noisy temperatures.

This process was repeated 100 times for each sensor couple. The mean value and the standard deviation were calculated for the first heating cycle (Table 2.1). The results showed that a standard deviation of 0.1 ^{o}C of the temperature values has a negligible standard deviation (less than 0.05%) for the thermal diffusivity estimation.

2.4.2.3 Influence of the distance variations on thermal diffusivity estimation

The main uncertainty of the model is related to the distances of the temperature sensors to the centre of the container. In the laboratory, the relative positions of the temperature sensors inside the container were accurately known, but in the field, the initial position of

Table 2.1: Standard deviation evaluation consideing a 0.1 ^{o}C error on the temperature measure and errores due to the the variation of the distance (0.001 m) between the temperature sensors from the axis of container. r_1 and r_2 are the distance of the sensors from the axis of the container.

Tr_2	Tr_1	r_2 (m)	r_1 (m)	α $(10^{-7}m^2.s^{-1})$		Standard deviation %	Error %
				Estimated	Mean		
T3	T4	0.25	0.15	10.08	10.08	0.05	2
T3	T5	0.25	0	10.24	10.24	0.03	1
T4	T5	0.15	0	10.49	10.49	0.03	2
T6	T5	0.15	0	8.68	8.68	0.04	1
T7	T5	0.25	0	9.21	9.21	0.02	0
T7	T6	0.25	0.15	9.52	9.52	0.04	1

each temperature sensor may change over time throughout their setting in the soil layer and throughout the length of the structure. To estimate the influence of a distance error, the following process has been carried out:

- Estimation of the thermal diffusivity with nominal values r_1 and r_2.
- Estimation of the thermal diffusivity with the following pairs of radii $(r_1+\delta r, r_2+\delta r)$,$(r_1+\delta r, r_2-\delta r)$,$(r_1-\delta r, r_2+\delta r)$,and $(r_1-\delta r, r_2-\delta r)$, where δr is the distance error (10^{-3} m).

The maximum deviation between these 4 estimated thermal diffusivity values and the first one has been considered as the estimated error. The process was applied to each pair of probes (Table 2.1). The accuracy of the estimation of the thermal diffusivity is less than 2% for any pair of temperature sensors.

It should be noted that an error as high as 10 mm in the position of temperature sensor T5 (r_1 =0) would have a negligible influence on the estimated α (a deviation less than 0.5%). This is because I_0 (r=0)=0 and the derivative of I_0 at the vicinity of 0 is small. In contrast, an error of 5 mm in the position of temperature sensor T6 (r_2 =0.15 m) led to an error of 6.8%. Consequently, the position of the temperature sensors must be accurately known to use this method. In some cases, (such as for T6), the method could lead to a significant estimation error.

2.4.3 Thermal properties estimated with the TFEM

The thermal diffusivity value α ($m^2.s^{-1}$) for each section between 2 temperature sensors (Tr_2 and Tr_1) is listed in Table 2.2. The average thermal diffusivity was 9.6 x 10^{-7} $m^2.s^{-1}$ for the first heating cycle and 9.4 x 10^{-7} $m^2.s^{-1}$ for the second and third heating cycles.

Busby (2015) estimates the thermal properties of different types of soil by utilizing a British database of meteorological soil temperature measurements obtained at a depth of 1 m. The range of the thermal diffusivity values (5 x $10^{-7} \leq \alpha \leq 10^{-6}$ $m^2.s^{-1}$) reported by Busby (2015) was consistent with the thermal diffusivity values determined in this study for soils with similar characteristics.

Figure 2.8a shows the difference recorded between the T5 and T6 measurements, and Figure 2.8b compares the experimental records with the simulation results considering the estimated parameters for the first cycle. The differences are much smaller than 0.02 ^{o}C for a maximum temperature increase of 27 ^{o}C, which shows a good agreement between the experimental measurements and the analytical model results and validates the applicability of the 1D heat conduction model.

Table 2.2: Estimated thermal diffusivity $\alpha(m^2.s^{-1})$ of compacted soil using TFEM and thermal conductivity $\lambda(W.m^{-1}.K^{-1})$ using α and $C_v(J.m^{-3}.K^{-1})$ measured by calorimetry; r_1 and r_2 are the distance of the sensors from the axis of the container.

Tr_2	Tr_1	r_2 (m)	r_1 (m)	C_v $(J.m^{-3}.K^{-1})$	1^{st} cycle		2^{st} and 3^{st} cycles	
					$10^{-7}\alpha$ $(m^2.s^{-1})$	λ $(W.m^{-1}.K^{-1})$	$10^{-7}\alpha$ $(m^2.s^{-1})$	λ $(W.m^{-1}.K^{-1})$
T3	T4	0.25	0.15		10.0	2.64	9.9	2.61
T3	T5	0.25	0		10.2	2.69	10.0	2.64
T4	T5	0.15	0		10.4	2.74	10.3	2.71
T6	T5	0.15	0	2.64×10^6	8.6	2.27	8.4	2.21
T7	T5	0.25	0		9.2	2.43	9.0	2.37
T7	T6	0.25	0.15		9.5	2.5	9.3	2.45

The dry specific heat, C_{dry}, of the dry material as a function of the temperature was measured with a micro-calorimeter. The results are plotted in Figure 2.9. Then, considering the initial water content (16.3%) of the tested samples, the specific heat, C_p, of the soil was calculated at 20 ^{o}C using Eq. (2.2): C_p=1322 J.kg^{-1}.K^{-1}. The volumetric heat capacity evaluated was finally calculated with Eq. (2.3): C_v = 2.64 x 10^6 J.m^{-3}.K^{-1}.

Then, this value of the volumetric heat capacity (C_v = 2.64 x 10^6 J.m^{-3}.K^{-1}) was used to calculate the thermal conductivity λ (W.m^{-1}.K^{-1}) for each cycle using Eq. (2.1). Table 2.2 summarizes the thermal conductivity values calculated for all cycles. The average value for the first cycle was 2.51±0.23 W.m^{-1}.K^{-1}, and the average value for the second cycle was the same as the third one: 2.47±0.25 W.m^{-1}.K^{-1}.

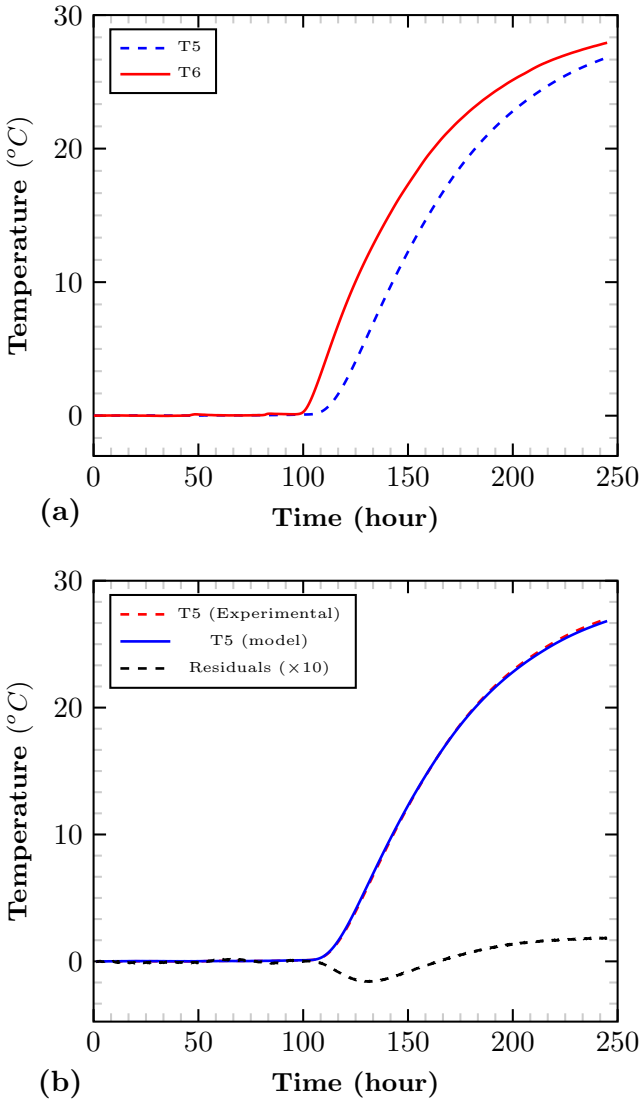

Figure 2.8: (a) temperature evolution recorded by T5 and T6 sensors during the first heating cycle (b) comparison between the experimental and the model values for T5 evolution.

2.4.4 Comparison with the other measurement methods

In this section, the results of the soil thermal conductivity measurements with the needle probe (KD2 pro) and centred hot plate methods are presented. The thermal conductivity of the two samples was measured with the needle-probe device (KD2 pro). The average thermal conductivity of the samples was approximately 2.46 $W.m^{-1}.K^{-1}$ (Table 2.3).

Two tests were performed with the centred hot plate method (Table 2.3). The first test lasted 2 days, and the second test lasted 6 days. T_1 denotes the temperature of the heating element controlled by the electrical intensity. During the tests, the temperature of the heating element (T_1) was 24.3 ± 0.76 ^{o}C, and the temperature of the aluminium

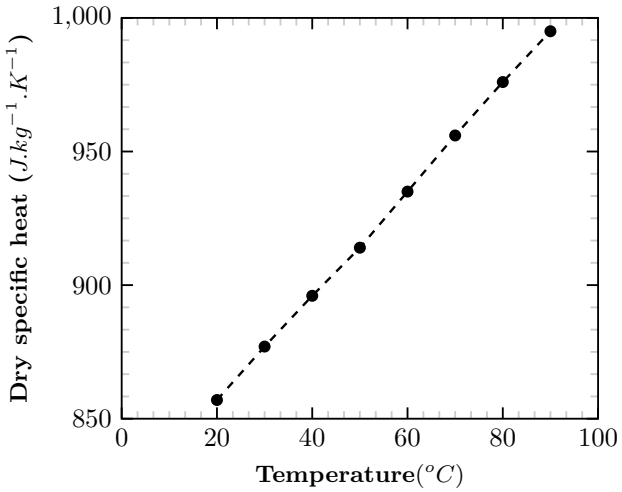

Figure 2.9: Dry specific heat variation (C_{dry}) of the dried soil according to the temperature.

Table 2.3: Thermal conductivity $\lambda(W.m^{-1}.K^{-1})$ Measurement of the compacted soil with the single needle probe and centred hot plate method.

Method	Single needle probe		Centred hot plate				
Nb.	T ^oC	λ $(W.m^{-1}.K^{-1})$	e (m)	T_1	T_{01} (^oC)	T_{02}	λ $(W.m^{-1}.K^{-1})$
1	23.25	2.42	0.02	23.58	15.30	13.86	1.9
2	20.98	2.50	0.02	25.10	16.51	14.97	2.05
Mean value		2.46					1.97

plates (T_{01} and T_{02}) was 14.5 ± 0.5 ^{o}C (Table 2.3). The temperature differences between the heating element and the aluminium plates induced a one-dimensional heat flow from the heating element through the sample towards the aluminium plate. The temperature of the surrounding air in all the tests was kept constant at 23 ^{o}C to ensure 1D heat transfer at the centre of the sample. The variation of the thermal conductivity with time for the second test is presented in Figure 2.10. After one day, the thermal conductivity decreased. This decrease can be explained by considering the water evaporation under heating, as the sample water content decreased from 16.3% to 14.66% during the second test. Under that condition, the average thermal conductivity of the compacted soil for both tests was 1.97 W.m^{-1}.K^{-1}.

The estimated values of the thermal conductivity measured by the TFEM method (2.51 W.m^{-1}.K^{-1}) and by the single-needle probe method (2.46 W.m^{-1}.K^{-1}) are very close (2% deviation). In contrast, the deviation between the values obtained by the TFEM method and the centred hot plate method (1.97 W.m^{-1}.K^{-1}) is quite high (greater than 20%).

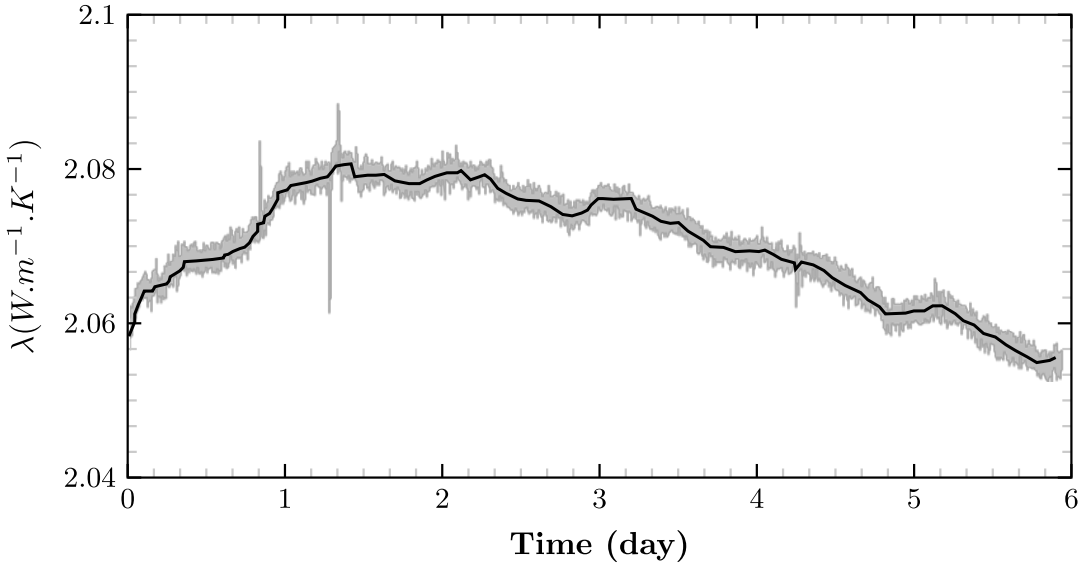

Figure 2.10: Variation of the thermal conductivity λ (W.m^{-1}.K^{-1}) during a centred hot plate test on the compacted soil.

In the compacted soil the heterogeneity plays an important role on the value of the thermal conductivity. The compacted soil is anisotropic, with a higher thermal conductivity in the radial direction (Midttømme et al. 1998: Low et al. 2015). Due to the sample preparation method, in this study, several layers were statically compacted in order to reach the desired density and homogeneity. The thermal conductivity estimated and measured parallel to the layering (in the metric scale container and with the thermal needle probe) were found to be higher than that measured perpendicular to the layering (in centred hot plate). Therefore, it can be concluded that the soil anisotropy could be an influencing factor on the axial and radial direction measurements.

Other difference between these values originated in measurement methods. In centred hot plate method, the thermal resistance between the heat element and the soil sample is neglected. A thin layer of the air between the soil sample and the heat element, could provide a thermal resistance (Jannot et al. 2016). Therefore, this thermal resistance reduces the heat flux through the soil sample and consequently reduces the soil thermal conductivity. The thermal resistance of the soil sample is approximately R_s=$e_s/\lambda_s \approx$ 0.02/2.5≈8x10^{-3} K.m^2.W^{-1} for a sample thickness of e=0.02 m.

Assuming an air layer with a thickness of e_{air}=0.025 mm on each side of the sample, the total thermal contact resistance is R_{c1}+R_{c2}=2e_{air}/λ_{air}=2 x 2.5 x 10 $^{-5}$/0.025=2 x 10 $^{-4}$ K.m^2.W^{-1}. The estimated value with Eq. (2.23) is λ_s=1.97 W.m^{-1}.K^{-1}. Considering

the estimated value of $R_{c1}+R_{c2}$ and using Eq. (2.22), one obtains: λ_s=2.45 W.m^{-1}.K^{-1}. This value is close to the values obtained with the two transient-state methods. One can conclude that steady-state methods are not suitable for the measurement of thermal conductivities as high as 2.45 W.m^{-1}.K^{-1}.

Also the centred hot plate is a steady state method and the time to reach temperature equilibrium (48 to 144 hours) is higher than transient-state method (10 minutes). During the time consuming test for centred hot plate, the water content decreases. The water plays a bridge role between the soil particles increasing the heat transfer and consequently increasing the effective contact area between the soil particles (Salomone and Kovacs 1984). As a result, the heat transfer is smaller in the sample with low water content. In the metric scale container, the water content of the compacted soil varied slightly. This condition was close to the transient-state method as the measurement is relatively quick and the initial condition does not change. The dimension of the samples could also explain these difference. The transient-state and centred hot plate measurements are performed on small-scale samples, whereas the estimated thermal conductivity was calculated from large-scale soil sample. The large-scale samples present more heterogeneity in terms of soil characteristics like mineralogy, granulometry, water content, density. therefore, the measurement values are an average of all these varieties.

2.5 Conclusions

In this study, the thermal properties of an unsaturated compacted soil were investigated. The thermal diffusivity was estimated via a new "temperature/temperature" method based on the estimation of a heat transfer function. One of the main benefits of this method is that it only requires temperature time series measurements at two locations.

The thermal conductivity was then estimated based on the estimated values of the thermal diffusivity and the volumetric heat capacity measured by calorimetry and then compared with the values obtained with two other methods (a transient-state method and a steady-state method). The inverse analytical model, generally used to characterize granular powders, was applied to unsaturated compacted soils in this study. The results showed that this simple analytical model has a good agreement (2% deviation) with the

experimental results obtained with the transient-state method and the single-needle probe method. In contrast, we have demonstrated that steady-state methods are not suited for this type of material since thermal contact resistances are no longer negligible compared to the sample thermal resistance.

In this method, the shape and intensity of the heat flux or the external boundary condition have not been considered, but the hypothesis of transient heat conduction in the radial direction in cylindrical coordinates should be considered. As is generally done, mass transfer is not considered in this model. The main uncertainty of the model is related to the distances of the temperature sensors to the centre of the container, so the distance between two sensors must be accurately measured.

The main advantage of this method is its application to in situ measurements. In this analytical model, heat conduction should be applied in the radial direction in cylindrical coordinates. The radial heat flux can be conducted experimentally, from the outer surface of a cylindrical container (as in this study), but under in situ conditions, the radial heat flux can be applied by just considering the cylindrical shape of heat exchanger loops (from the surface of the tubes towards an arbitrary cylindrical surface). In the field, only two temperature sensors should be placed at different distances from the heat exchanger tubes to monitor the temperature variations; therefore, thermal properties at any time can be estimated. Consequently, this method could enable system efficiency estimation of possible future applications of thermal energy storage in compacted soils such as embankments or other configurations.

Chapter 3

Effect of monotonic and cyclic temperature variations on the mechanical behavior of a compacted soil

Abstract: Settlement and slope stability of an embankment are mechanical aspects that play a major role in structural safety. Due to the tendency towards renewable energy, the embankments can be considered as a suitable medium for thermal energy storage. Using horizontal heat exchanger tubes, the thermal energy will be stored in different compacted soil layers in an embankment. Therefore, this structure can be subjected to daily and seasonally temperature variations due to heat extraction. Cyclic temperature variation can modify the mechanical behavior of compacted soils. Thus this study aims to investigate the effect of monotonic and temperature cycles in the range of 5 to 50 ^oC, on consolidation parameters and shear characteristics of a compacted sandy lean clay. To achieve this, temperature-controlled oedometric and direct shear tests were performed. Results showed that the effect of heating and cooling on mechanical properties is more pronounced under vertical stresses higher than the preconsolidation pressure. By heating, the normal consolidation line shifted to the left and consequently, the apparent preconsolidation decreased. Compression and swelling indexes could be considered independent of temperature variation. Due to the temperature cycles, the volumetric response of the compacted soil in oedometric and shear tests was stress history-dependent. Results of the direct shear tests showed that by temperature variation (heating/cooling and temperature cycles) the cohesion increased and the friction angle remained unchanged.

Keywords: Embankment, thermal energy storage, compacted soil, Thermo-Hydro-Mechanical behavior, temperature-controlled oedometer tests, temperature-controlled direct shear tests.

3.1 Introduction

To limit the environmental impact of the production of needed energy, the energy geostructures could provide new and clean solutions to the important issue of global warming for the years to come. These solutions still need to be further studied to provide appropriate techniques for both domestic and industrial energy needs.

Solar energy is an infinite, clean, and affordable source, it has a great potential to produce renewable thermal and electrical energy. Several technologies convert solar energy into a utilizable kind of energy for human needs like space heating. For example, solar energy storage consists of heat storage in a proper medium during summer to be preserved and later discharged for utilization in the winter (Stojanović and Akander 2010; H Abedin and A Rosen 2011). Several studies have demonstrated that the thermal energy storage in soils is a pertinent technique, due to their appropriate thermal properties and ease of access (Gan 2013; Beier and Holloway 2015).

In geotechnical engineering, different types of structures are made of compacted soils, such as roads and rail embankments. These linear structures contain several layers of compacted soils. To store the heat in an embankment in summer, and extract it in winter (or vice versa), the horizontal heat exchanger loops can be easily installed in these layers during the construction phase (Boukelia 2016a; Jradi et al. 2017).

Generally, the soils and earthen structures are exposed to external daily and seasonally temperature variations. When the serviceability of these structures as thermal energy storage medium starts, they will be subjected in addition to internal seasonal temperature variations. The temperature variation in soil storage mediums can fluctuate in the range of 10 to 50 ^oC (Hesaraki et al. 2015). These temperature variations could modify the thermo-hydro-mechanical (THM) behavior of compacted soil (Cekerevac and Laloui 2004; Uchaipichat and Khalili 2009). To prevent any damage, such as settlement and slope failure, and also to ensure the long-term structural stability of these energy structures,

the effect of temperature variation on their mechanical behavior should be investigated.

Compacted soils are initially set up in an unsaturated state close to the saturation state (degree of saturation between 85 to 95%). During their service life and thermal exploitation, the water content and the temperature are changing simultaneously.

Among different types of external solicitations, it is well known that landslides, settlements, and disorders of all kinds occur generally as a result of intense rainfall and seepage in embankments (Iverson and Major 1987; Rahardjo et al. 2001; Thibbotuwawa and Weerasekera 2013). Usually, the rainfall decreases the suction and increases the hydraulic conductivity in these unsaturated soils, this accelerates the soil saturation and the pore water pressure increase. As a result, the shear strength and factor of safety of the slope decrease (Rahardjo et al. 2001; Liu et al. 2017; Li et al. 2019). Based on the aforementioned statements, this study focuses on investigating the thermo-hydro-mechanical behavior of saturated compacted soil, as in embankments, the saturated state is clearly the most critical one.

In this context, for energy geostructures, a better understanding of the effect of monotonic and cyclic temperature variations on mechanical behavior such as consolidation and shear characteristics of compacted soil is of great importance.

Several researchers investigated the effect of temperature variations on consolidation and volumetric behavior of different types of soils under different stress paths (Tidfors and Sällfors 1989; Eriksson 1989; Moritz 1995; Burghignoli et al. 2000; Cekerevac and Laloui 2004; Uchaipichat and Khalili 2009). These investigations indicated that the effect of temperature on THM behavior of soils depends on the soil nature; the stress history and the thermal variation path.

Regarding the consolidation behavior, heated specimens exhibit a plastic behavior earlier compared to unheated ones, afterwards the elastic domain size reduces and shows a clear soil softening (Tidfors and Sällfors 1989). Thus, the preconsolidation pressure ($\sigma_p^{'}$) which is defined as the limit between the elastic and plastic domain, decreases upon heating (Cekerevac and Laloui 2004; Abuel-Naga et al. 2005). The effect of temperature variation on the compression and swelling indices (C_c and C_s) are found to be negligible in the temperature ranges from 20 to 90 ^oC (Cekerevac and Laloui 2004; Di Donna 2014).

In terms of volumetric behavior under temperature cycles, the soil initially in the

normally consolidated state (NC) exhibits a contraction when temperature increases (Burghignoli et al. 2000; Cekerevac and Laloui 2004). However, different observations are reported during the following cooling. In some studies, cooling removes a small part of the thermal contraction caused by heating (Shetty et al. 2019), but in others, during cooling the thermal contraction continues to increase (Campanella and Mitchell 1968; Di Donna and Laloui 2013). Ma et al. (2017) reported that the thermal contraction becomes smaller after 4 or 5 successive heating and cooling cycles.

The soil in an overconsolidated state exhibits a thermal expansion during heating and with subsequent cooling, a reversible behavior is observed. Therefore, the thermal expansion with heating is dissipated (Di Donna and Laloui 2013; Shetty et al. 2019). This reversible behavior was observed with further heating and cooling cycles.

Based on most of the investigations that have focused on the study of the effect of temperature variations between 20 to 90 ^oC, it can be concluded that the preconsolidation pressure is a temperature dependent parameter and decreases with heating. But despite the importance of this parameter in thermal energy storage systems, its variations due to cooling and several heating-cooling cycles are poorly understood.

The other important mechanical characteristics of an energy structure such as a road embankment are shear parameters: shear strength (τ), cohesion (c), and friction angle (φ). Although their dependency on temperature variations has been studied in recent years, the results are still controversial. For natural soil, using a temperature-controlled triaxial device in undrained conditions Moritz (1995) has observed a decrease of shear strength due to a temperature increase from 8 to 70 ^oC. Yavari (2014), by performing direct shear tests, showed that for Fontainebleau sand and both normally and overconsolidated kaolin clay, the shear strengths were almost independent of temperature (5 to 40 ^oC). Maghsoodi et al. (2020b) using a temperature controlled direct shear device, showed that the shear strength of Normally consolidated kaolin clay increased with a temperature increase from 22 to 60 ^oC, but no temperature dependence was measured for the Fontainbleau sand.

The effect of temperature on friction angle (φ) was reported to be negligible in several studies (Moritz 1995; Cekerevac and Laloui 2004; Maghsoodi et al. 2020b). But there are different results for the cohesion (c) variation upon heating and cooling cycles. Yavari (2014) found that the cohesion of a kaolin clay at three different temperatures (5, 20, and

40 ^oC) is almost unchanged. On the contrary Maghsoodi et al. (2020b) found that the temperature increase from 22 to 60 ^oC increases the cohesion from 17.2 to 23 kPa for kaolin clay and decreased it from 17.2 to 11 kPa for cooling from 22 to 5 ^oC.

Very few studies have investigated the impact of thermal cycles on shear characteristics. For example, Yazdani et al. (2019) have investigated the effect of temperature cycles on shear characteristics. Their study is mostly focused on soil-structure interface mechanical behavior. Therefore, the effect of several temperature cycles on the shear behavior of soils needs to be investigated.

The shear characteristics evolution due to the monotonic and cyclic temperature variations depends on several parameters such as material characteristics and soil nature, overconsolidation ratio, experimental conditions, and thermo-mechanical paths. But the results are not numerous enough, and there are still many unanswered questions on this subject.

This experimental study aims to investigate the thermo-mechanical behavior of a compacted sandy lean clay that is currently used in embankment constructions, in the saturated state under different stress paths. Temperature-controlled oedometer and direct shear devices were used to perform consolidation and shear tests under monotonic and cyclic temperature variations. The main aspects of the thermo-mechanical behavior of the compacted soil that are tackled in this study are to investigate the effect of cooling (20 to 5 ^oC), heating (20 to 50 ^oC), and thermal cycles (5-50 ^oC) on consolidation and shear characteristics.

3.2 Soil properties, devices, and specimen preparation

3.2.1 Soil properties

The tested soil was extracted from the Paris region in France. X-ray diffractograms analysis reveals that it contains 81% quartz, 7% dolomite, 5% calcite, 5% clayey materials, and 3% feldspar (Boukelia 2016a). This material was dried, pulverized, and sieved through a 2 mm sieve before being used for various experiments. According to the particle-size distribution tests, almost 20% of the particles of the soil were smaller than 2 μm, and 41% were smaller than 80 μm (Figure 3.1). With a liquid limit (LL) of 27% and a plastic limit

(PL) of 21%, the plasticity index (PI) was 6% (AFNOR 1993). The standard Proctor test results showed an optimum water content (w_{opt}) of 16% and a maximum dry density (ρ_d) of 1.81 Mg.m^{-3} (Table 3.1).

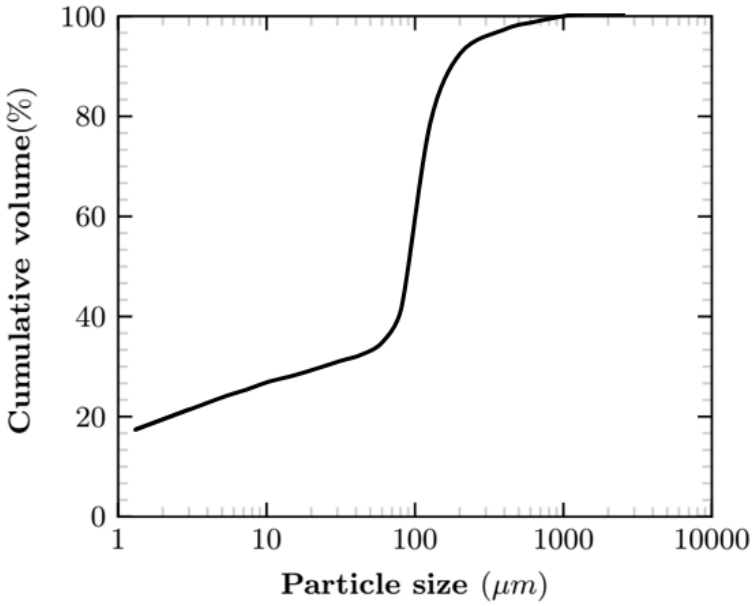

Figure 3.1: Particle size distribution (Boukelia 2016a)

Table 3.1: Characteristics of the studied soil

Properties	Amount
Plasticity limit (%)	20.5
Liquidity limit (%)	27.2
Plasticity index (%)	6.6
w_{opt} (%)	16.1
ρ_d (Mg/m^3)	1.8
Class of soil	CL
Thermal conductivity (W/m.K)	2.46
Volumetric heat capacity (J/k.m^3)	2.64
Thermal diffusivity (m^2/s)	9.6×10^{-7}

The material was classified as sandy lean clay, CL, according to the Unified Soil Classification System (ASTM 2000). In this study, the soil specimens were prepared at a water content (w) of 16.3% and a dry density ρ_d of 1.79 $Mg.m^{-3}$ in accordance with the optimal thermal condition defined by Boukelia (2016a). The dry soil was wetted up to the desired water content by adding the distilled water and stored in plastic bags for almost 3 days before being compacted in the cells for each test.

3.2.2 Device and specimen preparation: oedometric tests

A temperature-controlled oedometric device was used to investigate the effect of temperature on the consolidation behavior of the studied compacted soil. The system included a cylindrical cell of stainless steel (70 mm in diameter) and a piston to apply the vertical stress using a load frame (Figure 3.2). The vertical deformation of the specimen was measured using a linear variable differential transducer (LVDT) with an accuracy of 10^{-5} m. To impose the desired temperature, a heating-cooling device circulated fluid in the spiral tubes around the soil specimen, and a K-type thermocouple was placed in the bottom part of the oedometer cell to measure the temperature of the specimen during the tests. The system comprised also a volume/pressure controller to control the pore water pressure at the base of the specimen. To minimize the thermal losses, the oedometric cell was insulated with a polystyrene box. To maintain a constantly saturated state during tests, a continuous water supply was maintained.

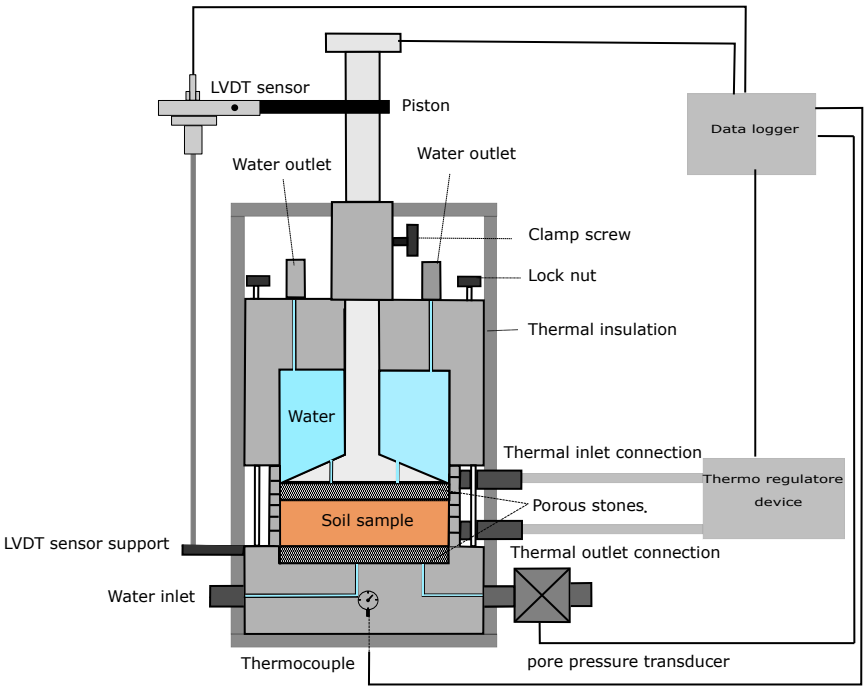

Figure 3.2: Temperature-controlled oedometric device.

Thermal calibration was performed to take into account the effect of temperature on different parts of the device and corrections were applied to the results. The thermal deformation of the oedometric cell was observed by measuring the vertical displacement of the piston during cycles of heating and cooling under 10 kPa of vertical stress. The

device was first heated from 20 ^oC to 50 ^oC, and then was cooled up to 5 ^oC and finally was heated up to 20 ^oC in steps of 10 ^oC. Figure 3.3 shows the relationship between the measured thermal vertical displacement (Δh_T) of the oedometric cell using LVDT at different applied temperature. The heating caused dilation in the oedometric cell, while cooling caused a contraction. A linear equation can be determined as follows:

$$\Delta h_T = -0.0026\Delta T + 0.05 \tag{3.1}$$

Where ΔT is temperature variation (^oC).

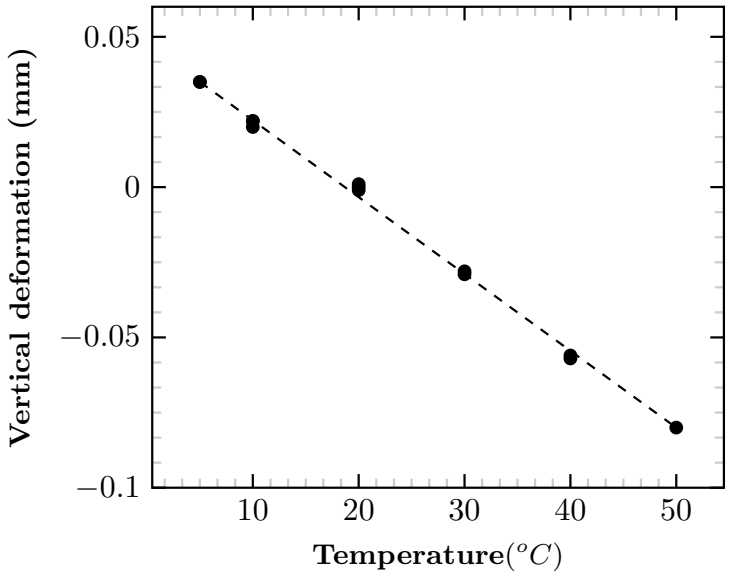

Figure 3.3: Temperature-controlled oedometric device.

The abovementioned relationship was used to obtain the correct measurements of the sample deformation during temperature variations by following equation:

$$\Delta h_{T(sample)} = \Delta h_{T(sample+cell)} - \Delta h_{T(cell)} \tag{3.2}$$

where $\Delta h_{T(sample+cell)}$ is the measured total displacement during heating or cooling phases.

To perform oedometric tests, the soil at the water content 16.3% was compacted directly in the oedometric cell (70 mm in diameter and 20 mm in height) to reach the target dry density of 1.79 $Mg.m^{-3}$. Then, the saturation phase was started by applying a backwater pressure of 9 kPa through the bottom part of the oedometric cell (through

the water inlet, in Figure 3.2). The saturation phase was performed at 20 ^oC under 9 kPa of vertical stress. To check the saturation state, the hydraulic conductivity was measured over a long time (7 days) to achieve an equilibrium state, and also the water content of several samples was measured after several days. Afterward, different thermo-mechanical paths were applied, they are presented in detail in section 3.3.1.

3.2.3 Device and specimen preparation: direct shear tests

The temperature-controlled direct shear device contains a shear box (60 x 60 x 30 mm) that is placed inside a container filled with water to maintain the saturation state of the samples (Figure 3.4). The heating-cooling system circulates fluid at the desired temperature under the container. The temperature is checked using 3 different thermocouples placed: in the upper half of the shear box; in the lower half of the shear box and the container. A piston applies the normal stress σ_n (kPa) on the top of the soil specimen using a load frame. The shear displacement and the normal displacement were measured using two linear variable differential transducers (LVDT) (Figure 3.4). To obtain the real volume change of the soil sample, the thermal calibration of the different parts of the device was performed.

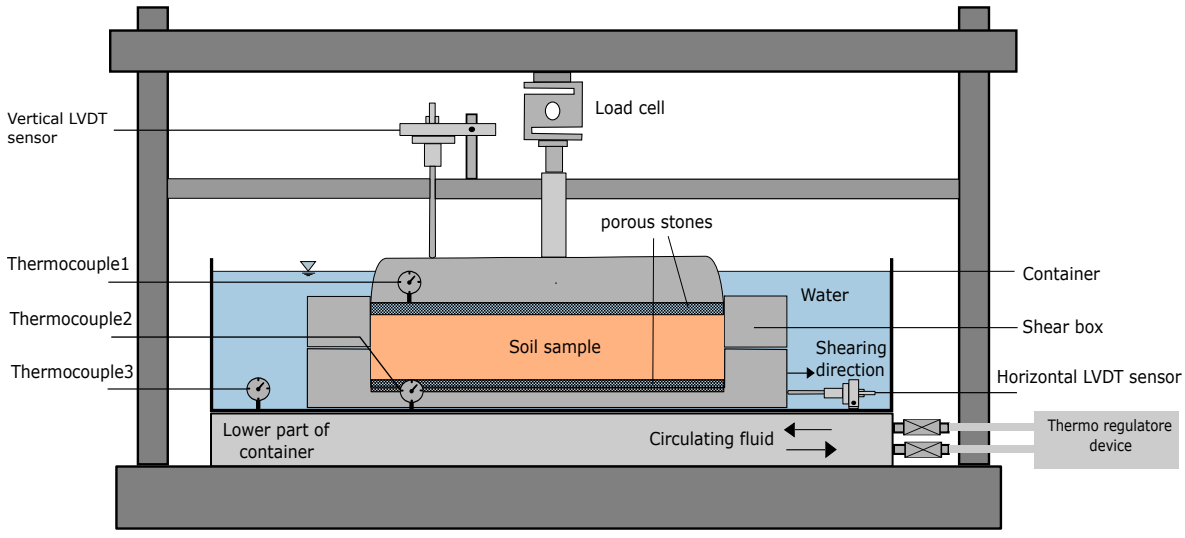

Figure 3.4: Temperature-controlled direct shear device.

Before direct shear tests, the soil at the initial water content (16.3%) was compacted directly in the shear box at the density of 1.79 $Mg.m^{-3}$. The specimens were saturated by leaving them inside a water container at 20 ^oC. The saturation level was checked by

measuring the water content of different specimens after several days. After one week, the measured water content was close to the estimated water content of a saturation state. This duration was repeated for all the samples.

3.3 Experimental programs

The experimental programs to take into account the effect of cooling (20 to 5 ^oC), heating (20 to 50 ^oC), and several heating-cooling cycles in the range of 5 to 50 ^oC on consolidation and shear behavior are presented in the following.

3.3.1 Consolidation program

3.3.1.1 Monotonic thermo-mechanical paths

Standard oedometric tests were conducted at different temperatures to investigate the effect of temperature on the consolidation parameters as compression index (C_c), swelling index (C_s), and apparent preconsolidation pressure ($\sigma_p^{'}$). After the saturation phase, one reference standard oedometric test at 20 ^oC was performed (test number 1 in Table 3.2). The specimen was loaded by applying successive vertical effective stress increments in different steps in the range of 9 to 1600 kPa and then was unloaded to 100 kPa. For oedometric tests at different temperatures, the soil specimen was cooled from 20 to 5 ^oC or heated up from 20 to 50 ^oC with a heating/cooling rate of 5 ^oC/h after the saturation phase. The heating/cooling rate was slow enough to avoid excess pore water pressure generation due to the temperature variation. Then the complete oedometric tests were performed (tests number 2-3 in Table 3.2).

3.3.1.2 Cyclic thermo-mechanical paths

The tests numbers 4 to 7 in Table 3.2 were supposed to reproduce the volumetric response of compacted soil element in different depths of an embankment which is under internal and external seasonal temperature variations.

Therefore, to simulate the effect of external seasonal temperature variation due to the soil-atmosphere interaction, compacted soil sample in test number 4 (Table 3.2) was

Table 3.2: Experimental programme for consolidation tests (L=loading, U=unloading, C=cooling, H=heating and TC = thermal cycles).

Test number	Test type	Temperature (^oC)	Vertical effective stress (kPa)	OCR before TC	TC (^oC)
1	L-U	20	9-1600-100	-	-
2	C-L-U	5	9-1600-100	-	-
3	H-L-U	50	9-1600-100	-	-
4	L-TC	20	9	8	5-50
5	L-TC	20	9-170	1	5-50
6	L-TC	20	9-400	1	20-50
7	L-U-TC	20	9-1600-100	16	20-50

subjected to 4 temperature cycles in the range of 5 to 50 ^oC after saturation phase under 9 kPa. The thermal load (heating and cooling) was applied by successive increments of ΔT=10 ^oC (5 ^oC/h).

The test numbers 5 to 7 consider the effect of internal temperature variation due to the heat transfer from a horizontal heat exchanger that is commonly horizontal installed at $2m$ from the base. Considering $10m$ height embankment, the total effective vertical stress is 170 kPa (20.8 $kN.m^{-3}$ x 8 m). Therefore, test number 5 (Table 3.2) was thus done by applying the effective vertical stress from 9 to 170 kPa, and then 4 temperature cycles (5 to 50 ^oC) were applied. Besides these conditions, during the lifetime of the embankment, the compacted soil may be loaded or unloaded. Test number 6 (Table 3.2) simulated a subsequent loading of the compacted soil. Therefore, the soil sample was vertically loaded from 9 to 400 kPa and then 4 temperature cycles (20 to 50 ^oC) were applied (test number 6 in Table 3.2). To reach a highly overconsolidation state (OCR=16) four temperature cycles in the range of 20 to 50 ^oC were applied after a loading (1600 kPa) and unloading of 100 kPa (test number 7 in table 3.2).

3.3.2 Direct shear program

3.3.2.1 Monotonic thermo-mechanical paths

The direct shear tests at different temperatures were conducted to investigate the effect of the cooling and heating on shear parameters. After the saturation phase at 20 ^oC, the normal stress was applied to the compacted soil (paths $0-1$ in Figure 3.5). Three values

of initial normal stresses ($\sigma_n^{'}$=50, 100, 200 kPa) were chosen. These values correspond to the soil pressure in the depths of 2.5 m, 5 m, and 10 m in an embankment assuming a density of 20.8 $kN.m^{-3}$. After the consolidation phase, the shear test at 20 ^oC was done (paths $1-2$ in Figure 3.5, tests 1-3, Table 3.3). From the settlement curve and the time required for the specimen to achieve 50 percent of its consolidation under the maximum normal stress (t_{50}) a shearing rate of 0.02 $mm.min^{-1}$ was calculated (Astm 1994). This slow rate applied for the shear test was supposed to ensure drained conditions during shearing. To take into account the effect of temperature variation on shear parameters, after the consolidation phase, the cooling or heating phase was applied (paths $1-1^{'}$ and $1-1^{''}$ in Figure 3.5). Finally, when the soil volumetric variation stabilized, the specimens were sheared with a rate of 0.02 $mm.min^{-1}$ (paths $1^{'}-2^{'}$ and $1^{''}-2^{''}$ in Figure 3.5, tests 4-10, Table 3.3).

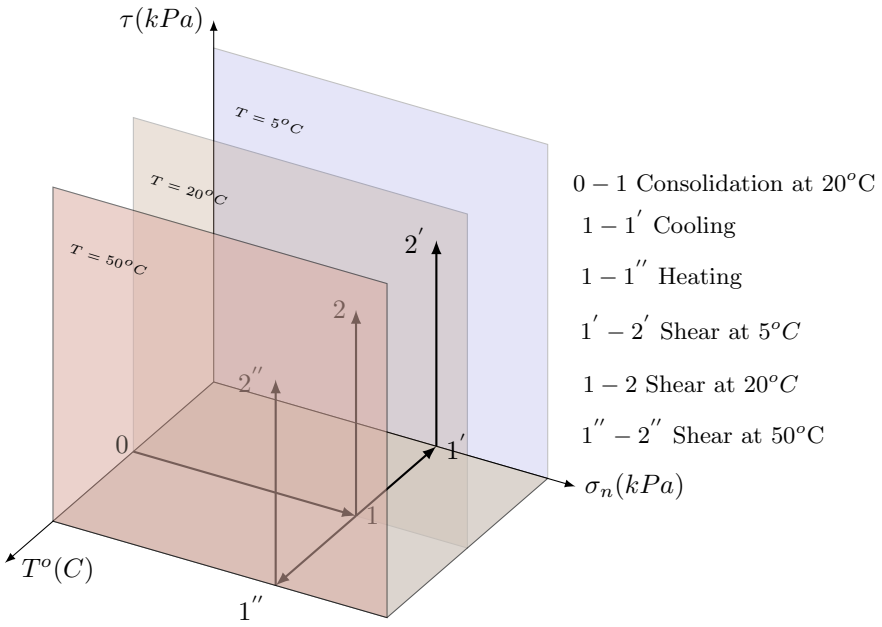

Figure 3.5: Thermo-mechanical path for direct shear tests at different temperatures.

3.3.2.2 Cyclic thermo-mechanical paths

The thermal cycles under constant normal stress were performed on compacted soil specimens in the direct shear box to evaluate the variation of shear parameters (cohesion and friction angle) after the thermal cycles. As the monotonic thermo-mechanical path, after the saturation phase at 20 ^oC, three normal stresses ($\sigma_n^{'}$=50, 100, 200 kPa) were applied

on different compacted soil specimens at 20 ^oC. After the consolidation phase, 5 thermal cycles in the range of 5 to 50 ^oC were applied by a successive increment of ΔT=10 ^oC (5 ^oC/h). After thermal cycles, when the thermal volume change stabilized, the specimens were sheared at 20 ^oC with a displacement rate of 0.02 $mm.min^{-1}$ (tests 11 to 13, Table 3.3).

Table 3.3: Experimental programme for direct shear test (TC=thermal cycles)

Test number	Density (Mg/m^3)	Type	Temperature ^oC	effective normal stress (kPa)
1	1.77	Loading-Shearing	20	50
2	1.76	Loading-Shearing	20	100
3	1.76	Loading-Shearing	20	200
4	1.75	Loading-Cooling-Shearing	5	50
5	1.76	Loading-Cooling-Shearing	5	100
6	1.77	Loading-Cooling-Shearing	5	100
7	1.76	Loading-Cooling-Shearing	5	200
8	1.75	Loading-Heating-Shearing	50	50
9	1.77	Loading-Heating-Shearing	50	100
10	1.76	Loading-Heating-Shearing	50	200
11	1.78	Loading-TC-Shearing	20 (5-50)	50
12	1.78	Loading-TC-Shearing	20 (5-50)	100
13	1.78	Loading-TC-Shearing	20 (5-50)	200

3.4 Experimental results

This part presents the results from oedometric and direct shear tests under different thermo-mechanical paths. The following part will be dedicated to the scientific discussion.

3.4.1 Thermo-mechanical results for oedometric tests

3.4.1.1 Monotonic thermo-mechanical oedometric results

Three standard oedometric tests at different temperatures were carried out (5, 20, and 50 ^oC). The void ratios for all of the specimens after saturation remained unchanged due to the zero swelling potential of this compacted soil. The void ratio variations after cooling and heating were negligible.

Figures 3.6a and b show the normalized settlement and void ratio variations against the vertical effective stresses at different temperatures respectively. The results show that, with temperature increase at vertical stresses higher than 100 kPa, the vertical displacement increased, and at the same time the void ratio decreased (Figure 3.6b). These results show that the heated soil becomes more compressible and the soil capability to support a vertical stress decreases, as a consequence the normal consolidation line moves to the left. Therefore, for the studied soil, the consolidation behavior could be considered as temperature-dependent and with temperature increase, a thermal softening could be expected.

Table 3.4: Consolidation parameters of studied soil at different temperatures.

Temperature ^oC	Initial void ratio	C_c	C_s (unloading)	$\sigma_p^{'}$ (kPa)
5	0.516	0.035	0.01	80
20	0.517	0.037	0.01	75
50	0.518	0.040	0.013	65

From the results obtained in standard oedometric tests at different temperatures (Figure 3.6b), the slope of the normal compression lines defined as compression index ($C_c = \Delta e/\Delta log\sigma_v^{'}$), and the slope of the unloading lines defined as a swelling index ($C_s = \Delta e/\Delta log\sigma_v^{'}$) were obtained and are presented in the Table 3.4. Figure 3.7a shows their variation with temperature appears as they changed very slightly with temperature variation.

The apparent preconsolidation pressure $\sigma_p^{'}$ was evaluated using the Casagrande method (Casagrande 1936) for each standard oedometric curves at each temperatures (5, 20, 50

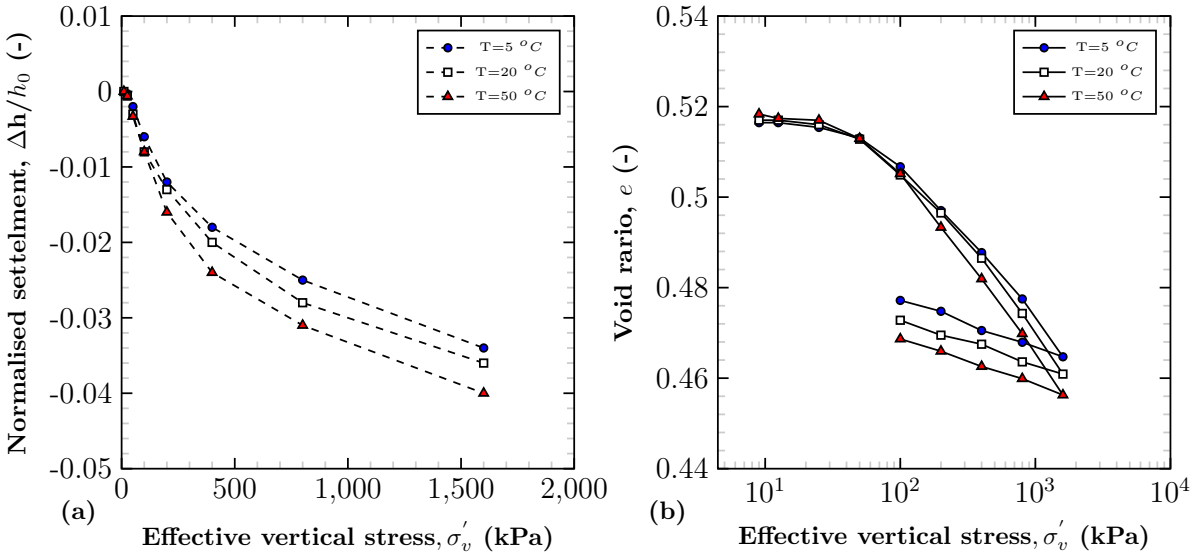

Figure 3.6: (a) normalized settlement and (b) void ratio variations against effective vertical stress at different temperatures.

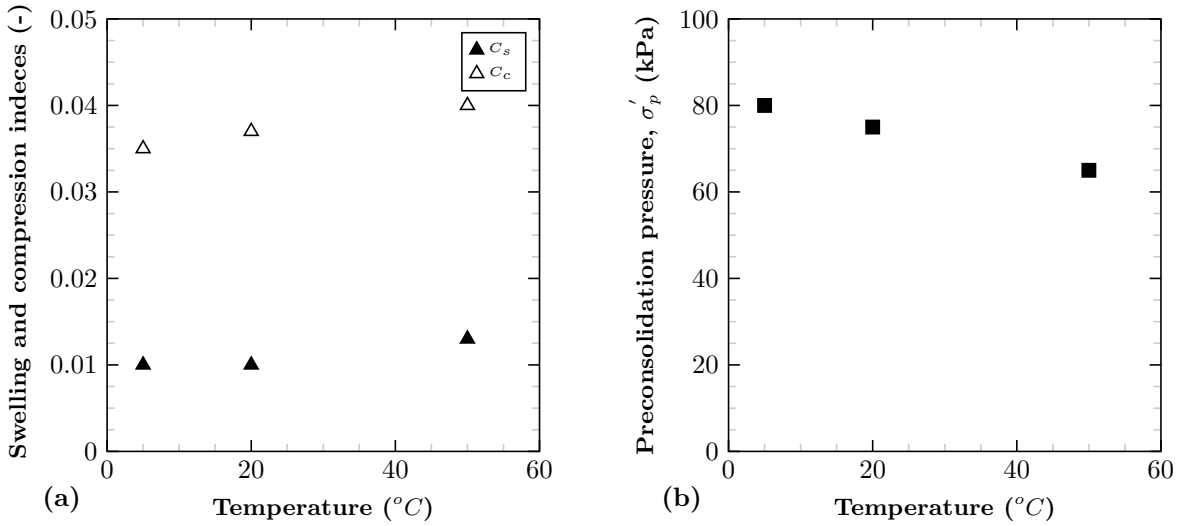

Figure 3.7: (a) Effect of temperature on the swelling index C_s and compression index C_c, (b) Effect of temperature on preconsolidation pressure ($\sigma_p^{'}$).

^oC) (Figure 3.6b). The results presented in Table 3.4 and their relationship are plotted in Figure 3.7b. The preconsolidation pressure $\sigma_p^{'}$ reached 80, 75, and 65 kPa at 5, 20 to 50 ^oC respectively.

From the results of void ratio variations against vertical stress the hydraulic conductivity was calculated for each load increment at different temperatures using the following equation:

$$k = C_v m_v \gamma_w \tag{3.3}$$

where k is the hydraulic conductivity ($m.s^{-1}$), C_v is the coefficient of consolidation, m_v is the coefficient of volume compressibility and γ_w is the unit weight of water at a given temperature.

Figure 3.8 shows that when the vertical effective stress increased, the hydraulic conductivity decreased due to the increasing density and decreasing void ratio. At a constant effective vertical stress, the hydraulic conductivity increased as temperature increases.

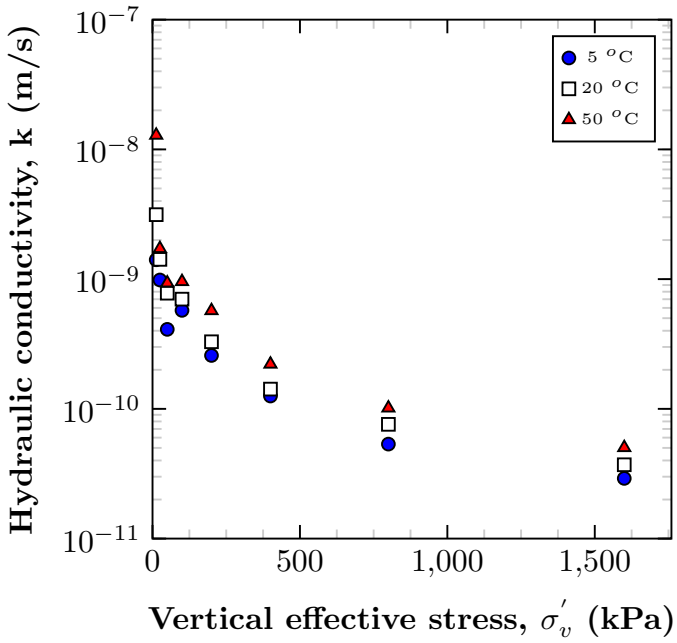

Figure 3.8: Effect of the temperature on hydraulic conductivity (k).

3.4.1.2 Thermal cycles effect on the volumetric variation of studied compacted soil

The results of volumetric variation against temperature cycles under 9 kPa are presented in Figure 3.9a (test number 4, Table 3.2). With heating from 20 to 50 ^oC the volumetric response was almost negligible whereas, during cooling from 50 to 5 ^oC the sample dilated slightly. With further temperature cycles, the soil specimen showed a thermo-elastic response and the volumetric variations were reversible. This reversible behavior could correspond to the thermo-elastic expansion and contraction of the solid skeleton.

Under 170 kPa the soil was in normally consolidated condition and after first heating (20 to 50 ^oC), the specimen contracted as a volume decrease of 0.13% was observed (Figure 3.9a). To determine the elastic or plastic nature of thermal loading, after heating, the sample is cooled down to 5 ^{o}C and the volume of the specimen slightly decreased (0.17%).

The volume variations during the first thermal cycle (20-50-5 ^oC) were irreversible. But this thermal contraction decreased cycle by cycle and after four thermal cycles, the deformation was stabilized and an elastic behavior was reached. In Figure 3.9a, it appears that the part of the curve under 20 ^0C is superimposed. In the following, the temperature cycles were applied in the range of 20 to 50 ^0C.

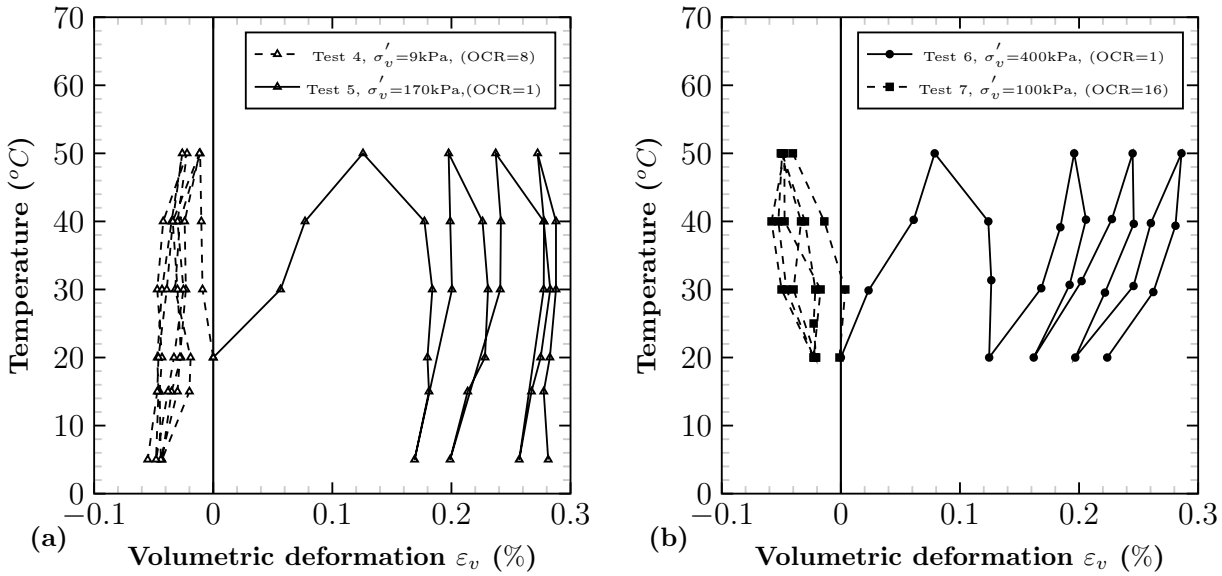

Figure 3.9: Volumetric deformation during thermal cycles under a) 9 kPa (test 4, OCR=8) and 170 kPa(test 5, OCR=1) b) 400 kPa(test 6, OCR=1) and 100 kPa (test 7, OCR=16)

After thermally induced volume changes verification for effective in-situ stress states, two extreme cases were applied. In test number 6 under 400 kPa (NC state), 4 thermal cycles (20 to 50 ^oC) exhibited a thermal plastic contraction increasing when the number of thermal cycles increased (Figure 3.9b). In highly OC state (OCR=16) in test number 7 (Table 3.2), again 4 thermal cycles in the range of 20 to 50 ^oC were applied. In this state, after a slight deformation, the soil specimen showed a reversible volumetric response (Figure 3.9b).

The elastoplastic deformation due to the thermal cycles at OC (at 9 kPa) and NC (at 170 and 400 kPa) states leads to a void ratio variation at constant vertical stress. To compare the effect of thermal cycles on soil with a reference oedometric test at 20 ^oC, the evolution of normalized void ratios versus effective vertical stress for both types of tests with thermal cycles and reference oedometric tests, are depicted in Figure 3.10. Figure 3.10a shows that the void ratio increased after the thermal cycles under 9 kPa (OC state). To detect the effect of this variation on the subsequent loading, the specimen was then

loaded vertically. The whole curve is slightly higher than the reference test (black points). The slope of the consolidation line (C_c=0.036) was the same as the reference test, and the temperature cycles had a negligible effect on the apparent preconsolidation pressure.

Figure 3.10b and 3.10 c show the void ratio variations for applied thermal cycles under 170 and 400 kPa respectively (test 5 and 6, Table 3.2). The void ratios, before applying thermal cycles, coincided with the reference oedometric test at 20 ^oC. After thermal cycles, the void ratio in NC state decreased for both tests. These variations are due to the thermally induced plastic deformation that can be considered as a thermal hardening. These void ratios corresponded to a void ratio in higher vertical stress for the reference test at 20 ^oC. For instance, in Figure 3.10c the normalized void ratio after thermal cycles under 400 kPa was 0.93 which corresponds to vertical stress of 600 kPa for the reference test at 20 ^oC (blue point in Figure 3.10 c). Therefore, when the specimen is subjected to thermal cycles it behaves like an over-consolidated soil. After this loading, the specimens were loaded vertically and the void ratios for both tests reached the same void ratio as the reference test. The slope of the subsequent loading line after thermal cycles (slope of ac line in Figure 3.10c) is 0.021 while the slope for the normal consolidation line at 20 ^oC is 0.037.

3.4.2 Thermo-mechanical results for direct shear test

3.4.2.1 Monotonic thermo-mechanical direct shear results

In this section, the effect of cooling and heating on shear characteristics is investigated. In temperature-controlled direct shear tests, after the saturation phase, the consolidation phase was started and the specimen was loaded vertically at three different normal stresses $\sigma_n^{'}$=50, 100, and 200 kPa at 20 ^oC. After this consolidation phase, a heating or cooling phase (5 ^oC/h), was applied to the compacted soil specimens. The cooling phase was conducted from 20 to 5 ^oC and the heating phase from 20 to 50 ^oC. The results showed that the cooling phase had a negligible effect on the volumetric deformation of the specimens whereas during heating, the specimens contracted and the volumes of the specimens decreased slightly. Figure 3.11a shows the volumetric deformation due to the heating in the shear box. The volume of the specimens decreased by 0.07, 0.12, and 0.14%

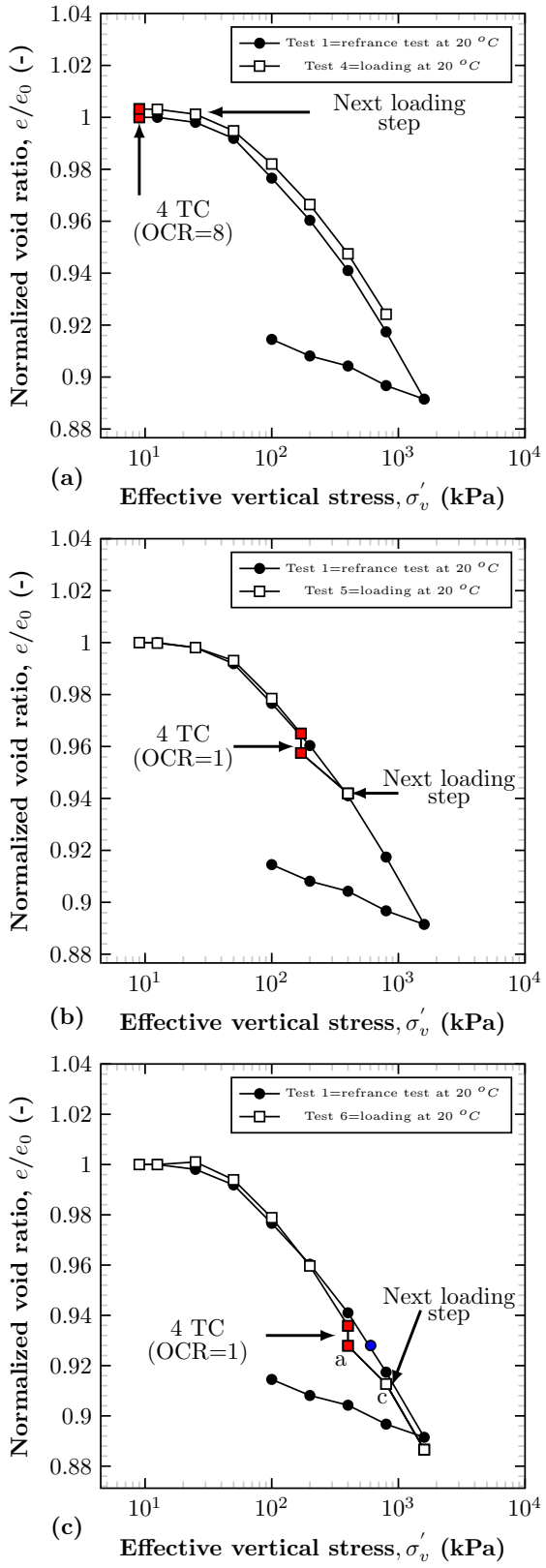

Figure 3.10: Void ratios variation after thermal cycles under (a)9 kPa (b) 170 kPa (b) 400 kPa, TC=temperature cycles.

for the normal stresses of 50, 100, and 200 kPa respectively.

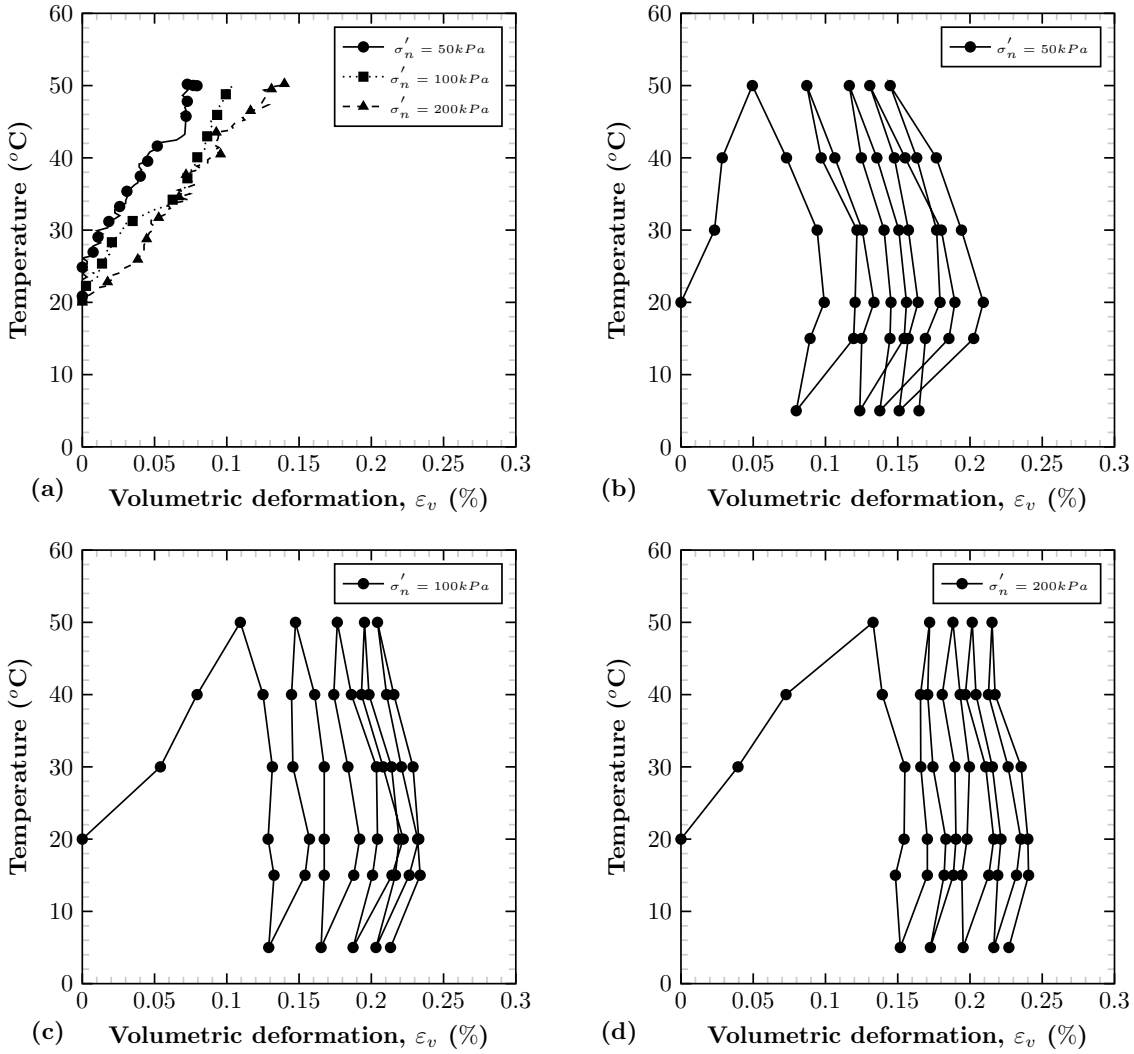

Figure 3.11: Thermal volumetric deformation (a) during heating from 20 to 50 °C (b), (c) and (d) during 5 thermal cycles at $\sigma_n^{'}$ = 50, 100 and 200 respectively.

When the thermal volumetric deformation stabilized, the compacted soil was sheared with a rate of 0.02 mm/min. Figure 3.12 shows the variation of the shear strength against shear displacement for $\sigma_n^{'}$=50, 100, and 200 kPa at 5, 20, and 50 ^oC. To ensure the quality of the results, several tests were duplicated, for example, the test under $\sigma_n^{'}$=100 kPa at 5 ^oC (Figure 3.12b). Under normal effective stress of 50 kPa, the shear strengths increased slightly by heating and cooling (Figure 3.12a). However, the heated and cooled specimens showed a higher dilatation than the specimen at 20 ^oC (Figure 3.12d). Under 100 kPa, the shear strength increased slightly by heating whereas cooling had a negligible effect on the shear strength (Figure 3.12b). The heated and cooled specimens showed a higher dilatation than the specimen at 20 ^oC (Figure 3.12e). Under 200 kPa, the shear stress was

not affected by heating whereas cooling reduced it by 9% (Figure 3.12c). For these samples during shearing, the soil specimen slightly contracted at first, then this contraction was followed by a negligible dilatation (Figure 3.12f).

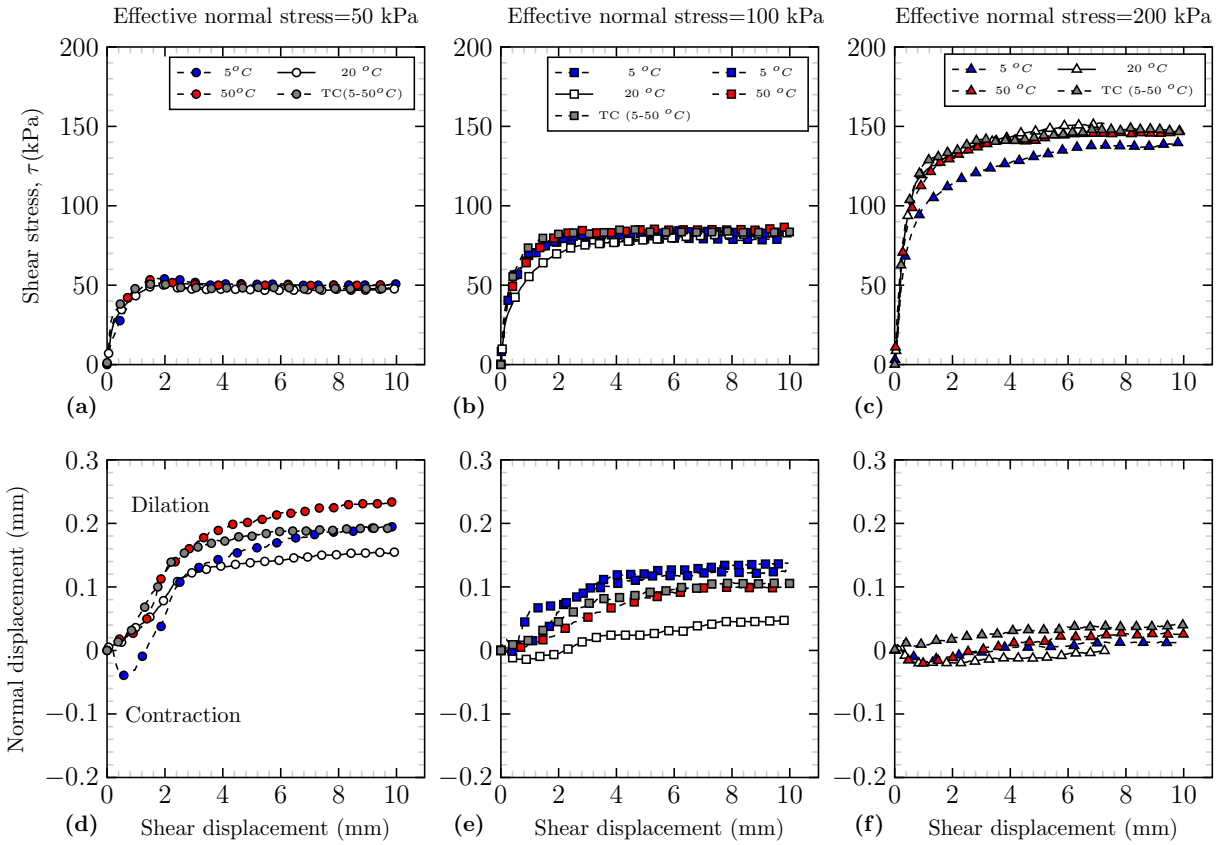

Figure 3.12: Effect of temperature on shear stress and normal displacement at three different effective normal stresses a-d) 50 kPa b-e) 100 kPa and c-f) 200 kPa, TC=temperature cycles.

To obtain the shear characteristics (cohesion, c and friction angle φ), the shear stress corresponding to 10% of the sample length was taken for each test and is presented in Table 3.5. Figure 3.13 shows the Mohr-Coulomb plane for the studied soil at different temperatures. The results show that cooling ($\Delta T = -15^oC$) changed the shear characteristics: the cohesion increased from 13.0 to 20.5 kPa and the friction angles decreased slightly from 34.4^o to 30.5^o. The heating ($\Delta T = +30^oC$) increased slightly the cohesion by 4 kPa (from 13.0 to 17.4) and the friction angle was not affected.

It can be concluded that the thermal volumetric deformation during heating did not affect the shear strength but cooling decreased it and this behavior was more pronounced under high normal stresses. Regarding the volumetric variation during the shear phase, at low normal effective stresses, the compacted soil tended to dilate. However, with

Table 3.5: Shear characteristics of studied soil for different temperatures.

T (^oC)	τ (kPa)			c (kPa)	φ (^{o})
	$\sigma_n^{'}$= 50 kPa	$\sigma_n^{'}$=100 kPa	$\sigma_n^{'}$=200 kPa		
5	49.7	79.0	137.0	20.6	30.5
20	48.0	80.5	150.5	13.0	34.4
50	49.8	84.7	149.5	17.4	33.5
TC(5-50)	48.6	83.7	146.0	17.4	33.0

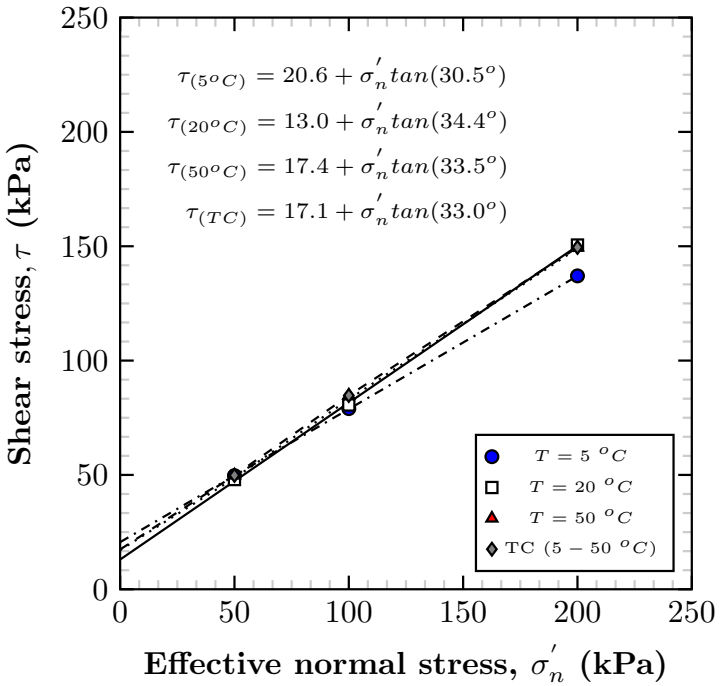

Figure 3.13: Shear stress against effective normal stress at T = 5 ^oC, T = 20 ^oC, T = 50 ^oC and after 5 TC (temperature cycles, 5-50 ^oC).

increasing the normal stress, this tendency is fading.

3.4.2.2 Cyclic thermo-mechanical direct shear results

For thermal cyclic tests after saturation, the same normal stresses as monotonic section ($\sigma_n^{'}$=50, 100, and 200 kPa) were applied. After reaching the desired normal stress, the compacted soil samples were subjected to temperature cycles: they were first heated up from 20 to 50 ^{o}C then cooled down from 50 to 5 ^{o}C and subsequently followed by 4 temperature cycles from 5 to 50 ^{o}C.

Figure 3.11b, c, and d show the volumetric deformation due to the temperature cycles under each normal stress. The compacted soil upon heating from 20 to 50 ^oC contracted by 0.05, 0.11, and 0.14% under normal stress of 50, 100, and 200 kPa respectively. This

order of magnitude is coherent with the results of monotonic thermo-mechanical paths as is shown in Figure 3.11a. After that, the samples cooled down to 5 ^{o}C and slightly contracted. The contraction of the sample upon the first heating was found to be irreversible. The first cycle caused a higher contraction compared to subsequent cycles (Figure 3.11b, c, and d). The final thermal contractions after 5 thermal cycles were 0.16%, 0.21% and 0.22% under 50, 100 and 200 kPa respectively. When the thermal volumetric deformation stabilized, the samples were sheared (0.02 mm/min) at 20 ^{o}C (Figure 3.12). The shear stress corresponding to 10% of the sample length in table 3.5 showed that the temperature cycles have slightly increased the shear strength of the compacted soil under normal stresses of 50 and 100 kPa while it decreased slightly under 200 kPa compared to reference tests at 20 ^{o}C. This shear stress variation as well as the volumetric response of the cyclic tests follows the same trend as the monotonic tests at 50 ^{o}C (Figure 3.12). In both tests, with increasing the normal stress, the dilative response under lower normal stress (50 and 100 kPa) tends towards a contractive one under higher vertical stress (200 kPa). The Mohr-Coulomb plane after temperature cycles showed that the cohesion increased by 4 kPa (from 13.0 to 17.4 kPa) and the friction angle remained unchanged compared to the reference test at 20 ^oC (Table 3.5). The variation of the cohesion was the same as the test at 50 ^oC. If the volumetric deformation due to heating will be one reason for the shear increase, it can be concluded that the first heating has a significant impact on the shearing response.

3.5 Discussion

3.5.1 Temperature effect on consolidation parameters

In terms of consolidation behavior, temperature variations had a negligible effect on the compression index (C_c) and swelling index (C_s) of the studied compacted soil but they had an impact on apparent preconsolidation pressure ($\sigma_p^{'}$). The decrease of $\sigma_p^{'}$ with increasing temperature leads to a shrinkage of the elastic domain. The observed results are in accordance with those of other authors on saturated natural and compacted soil samples (François et al. 2007; Kaddouri et al. 2019).

The decrease in the elastic domain could be linked to the soil thermal softening that

was observed in e-log $\sigma_v^{'}$ curves. It could be due to the temperature-dependent properties of water and changes in the fabric of pores structure (Baldi et al. 1988; Mon et al. 2013). Indeed, with temperature increase, the viscosity of water decreases and leads to an increase in soil hydraulic conductivity (Delage et al. 2011; Di Donna 2014). As a consequence, at higher temperatures, the pore water drains easier, and the particle contact increases. This thermal softening causes the normal consolidation line shifts to the left and consequently the apparent preconsolidation pressure decreases (Tidfors and Sällfors 1989; Shariatmadari and Saeidijam 2012).

3.5.2 Volumetric response due to the temperature cycles

The thermo-elastoplastic volumetric response of the compacted soil due to temperature cycles under different verticaal stresses was found to be state-dependent (OC or NC). Whatever the vertical stresses, in the overconsolidated state, the elastic volumetric deformation was induced whereas in normally consolidated states, for both oedometric and shear tests, a significant thermal plastic strain was observed during the first temperature cycle (Figures 3.9 and 3.11). After the first cycle, subsequent cycles induced lower thermal plastic strain. In NC state, the sample is subjected to the maximum experienced vertical stress, and simultaneously, the thermal load is applied which imposes additional energy to the system. The energy dissipation can be associated with an increase in pore water drainage or particle rearrangement. Campanella and Mitchell (1968), Baldi et al. (1988), Di Donna and Laloui (2013) and Shetty et al. (2019) observed the same type of thermo-plastic strain induced by heating-cooling cycles, in NC clayey and silty clay soils. Some researchers reported that the amount of thermal volumetric change depends on the plasticity index (PI) of the soil (Abuel-Naga et al. 2007; Ghaaowd et al. 2015). The soil with higher plasticity index shows more thermo-plastic deformation due to the degradation of the adsorbed water layer in clay particles (Delage et al. 2000). Di Donna and Laloui (2013) reported a volumetric deformation of 0.6% for natural silty clay soils with a plasticity index of 18% while, for the studied soil in this paper, the volumetric deformation was 0.15% with a plasticity index of 6.6%.

3.5.3 Temperature cycles effect on consolidation parameters

The compacted soil in NC state after being subjected to thermal cycles (under 170 and 400 kPa), was reloaded vertically at 20 ^{o}C. After thermal plastic deformation and void ratio decrease, the compacted soil shows less compressibility with subsequent loading (slope of ac is less than the compression index, C_c at 20 ^{o}C, Figure 3.10C). This behavior can be due to the increase in the stiffness and hardness of the soil caused by thermal cycles. While by subsequent loading the void ratio converged to the void ratio of the reference oedometric test at 20 ^oC (Figure 3.10b and 3.10c). This means that the impact of thermal plastic deformation of the compacted soil in NC state disappears upon subsequent loading. This observation is corroborated with the findings reported by Di Donna and Laloui (2013) and Shetty et al. (2019) who have studied the effect of thermal cycles on the thermal volumetric change of silty clay soil.

3.5.4 Heating or cooling and temperature cycles effect on shear characteristics

In terms of structural stability of an embankment made of studied compacted soil, the friction angle was not affected by temperature variation which has been confirmed by several studies on other soils in the literature (Hueckel and Baldi 1990; Burghignoli et al. 2000; Ghahremannejad 2003; Cekerevac and Laloui 2004; Maghsoodi et al. 2020b). The induced thermal volumetric deformation during heating or temperature cycles slightly increased the cohesion. Cooling decreased the shear stress under higher normal stresses and consequently, the cohesion increased by 7.6 kPa.

In consolidation and shear behavior, two different behavior was observed. Regarding the consolidation behavior, on one hand, the heated compacted soil showed a softening behavior, on the other hand, the shear stress slightly increased. The increase in cohesion can be related to the thermal volumetric contraction that occurred in the heating phase which densified the samples. For compacted soil at a lower temperature (5 ^oC) oedometric tests showed lower settlement during the consolidation phase, moreover, the shear test results showed that the compacted soil under high normal stress has low shear strength. This could be explained by the fact that the links between soil particles in low

temperatures at the microstructural level could become more fragile and consequently the strength could decrease. Further investigations on the microstructure of heated and cooled specimens are necessary to confirm this explanation.

Regarding the volumetric response during shearing, the dilatation is the result of two different events: (i) rolling and sliding of soil particles (ii) normal stress-induced contraction. The soil particle rearrangements caused a disorder and result in a volume augmentation, whereas the contraction process decreases the soil volume. When the normal stress is relatively small, the soil particle rolling and the subsequent disorder are dominant. In high normal stresses, the contraction becomes more dominant and the particle rearrangement is confined (Yavari et al. 2016; Zhao et al. 2017; Kouakou et al. 2020). Therefore, the dilatation decreases with normal stress increase. Considering the temperature effect on volumetric behavior during shearing, it should be noted that no clear trend was observed. Yavari et al. (2016) mentioned that, in the direct shear test, only a very thin layer of soil is subjected to shear and the normal displacement corresponds to the change in volume of the sheared zone. The thickness of this layer can vary from one test to another and could explain this unclear trend on volumetric behavior caused by temperature variation.

3.5.5 Engineering implications of results

Based on thermo-mechanical paths in this study, it can be confirmed that in the construction phase the horizontal heat exchanger loops can be placed in different depths in an embankment. The experimental results showed that the temperature variations, either monotonic heating or cooling or temperature cycles increase the soil cohesion that is advantageous for bearing capacity and embankment slopes stability. In terms of consolidation behavior in thermal charging and discharging seasons, when the compacted soil is exposed to monotonic temperature variations, due to the very small differences in compression index at different temperatures, the effect of temperature on the embankment global settlement can be considered negligible. Furthermore, the volumetric response under different vertical stresses (50 to 200 kPa) at different embankment depths (2.5 to 10 m) due to heating and temperature cycles could be also small enough to be neglected.

Thus, it can be concluded that the effect of temperature on the global mechanical

behavior of the studied compacted soil with temperature variation range from 5 to 50 ^oC could be negligible. It should be noted that the embankment is in interaction with the atmosphere from its top and lateral surfaces, the thermal efficiency of the structure could be affected due to the heat losses. Consequently, it is better to place the heat exchangers far from the top and lateral surfaces. The tests in this study were performed at an initial optimal compaction state for thermal properties (w=16.3 and $\rho_d = 1.79 Mg.m^{-3}$). This initial soil condition could affect thermo-hydro-mechanical responses to the temperature variation. Therefore, the initial soil compaction state should take into account the optimal thermal soil properties.

3.6 Conclusions

This study investigated the consolidation and shear behavior of compacted sandy lean clay subjected to the monotonic and cyclic temperature variations. This type of soil is frequently used for embankment application in France. It should be noted that these tests were performed in the saturated state which underestimates soil mechanical properties. The temperature-controlled oedometric and direct-shear devices were used to perform non-isothermal tests.

Based on the results of the oedometric test, the following conclusions can be drawn:

• the heated compacted soil shows a softening behavior, in contrast, cooled compacted soil shows hardening behavior;

• the compression index and swelling index were unchanged with temperature variation;

• the apparent preconsolidation pressure decreased with heating and increased with cooling;

• the volumetric response of compacted soil depends on the stress history. In an over-consolidated state, a reversible deformation was observed, and in a normally consolidated state the temperature cycles induced a thermal plastic contraction;

• the compacted soil subjected to temperature cycles showed a hardening behavior.

The results of direct shear tests showed that heating from 20 to 50 ^oC and temperature cycles had a negligible effect on shear characteristics whereas cooling from 20 to 5 ^oC decreased the shear stress at higher normal stresses (200 kPa).

These results are essential in designing the energy geostructures in a similar range of temperatures. Further work should be performed to investigate the microstructural behavior of studied soil due to heating or cooling. Moreover, in terms of thermal efficiency behavior, a numerical simulation will be performed to investigate the suitable position of horizontal heat exchanger loops due to the heat loss caused by soil-atmospheric interaction.

Chapter 4

A numerical study into effects of soil compaction and heat storage on thermal performance of a Horizontal Ground Heat Exchanger

Abstract: The good capacity of the numerical simulations makes possible to bring some further responses on the backfill soil selection and its installation depth in the Horizontal Ground Heat Exchanger (HGHE). Therefore, a well-known backfill soil was considered to be used as substitutive material. The hydrothermal properties of the backfill material were estimated in laboratory and then injected in a numerical framework considering the atmosphere-soil-HGHE interaction. Numerical simulations were performed for a HGHE installed in the compacted backfill soil and the local natural soil. The simulation results showed that the compacted backfill soil improves by 8.5% the system performance compared to local uncompacted soil. Two heat storage scenarios at three different installation depths were also investigated. The results showed that an inlet fluid temperature of 50 ^oC in summer increased highly the system performance by 13.7% to 41.4%, while the improvement was less significant (0% to 4.8%) for the ambient inlet temperature scenario. A deeper installation depth increased also the system performance.

Keywords: Horizontal Ground Heat Exchanger; Numerical simulations; Atmosphere-soil-HGHE interaction; Backfill soil; Installation depth; System Performance.

4.1 Introduction

Shallow geothermal energy is one of the many sources of renewable energy, and it can be easily accessed all around the world (H Abedin and A Rosen 2011; Shortall et al. 2015; Sangi and Müller 2018). The temperature of the ground can be exploited during winter using a ground source heat pump for space heating and during summer for cooling needs. To increase the efficiency of shallow geothermal energy the solar energy can be stored during summer to increase the temperature of the ground (Xu et al. 2014; Lee et al. 2018; Lahoori, Jannot, Rosin-Paumier, Boukelia and Masrouri 2020). Generally, open and closed heat exchangers are available for the exploitation of shallow geothermal energy (Florides and Kalogirou 2007), which are then served as low-potential sources of thermal energy for heat pumps (Adamovsky et al. 2015). Horizontal Ground Heat Exchanger (HGHE) is one of those closed loop heat exchangers. Compared to Vertical Ground Heat Exchanger (VGHE), it is more cost effective although it requires more installation space (Self et al. 2013; Lahoori, Rosin-Paumier, Stoltz and Jannot 2020).

Due to the shallow installation depth (conventionally between 1.0 and 2.0 m), HGHE is also more sensitive to the meteorological condition (Gonzalez et al. 2012; Habibi and Hakkaki-Fard 2018). The experimental investigations showed that the thermal performance depends on the depth of HGHE installation (Beier and Holloway 2015). At deeper position, the soil thermal properties are not affected by the daily and seasonally ambient temperature variation. The results reported by Elminshawy et al. (2017) showed that the thermal performance of the horizontal system highly depends on the soil compaction state (water content and density) and air flow rate. By increasing density, the solid particles are better packed into a unit volume and the number of contact points between the particles increases (Penner et al. 1975; Abu-Hamdeh and Reeder 2000). These contact points provide a larger heat transfer by conduction which causes the temperature variation between the inlet and outlet airflow. These observations are in agreement with the study of Hurtado et al. (2012) which investigated the capacity of a compacted soil to store thermal energy from the chimney power plant using an analytical model based on a finite volume procedure. They mentioned that the output power energy was increased by 10% when the soil compaction increased from loose to dense level.

Since the experimental investigations are time and money consuming, the thermal performance of horizontal heat exchanger loops in soils has been numerically investigated using finite element and finite difference tools in different studies. Normally in these models, the simulation is done by considering a homogeneous soil mass with constant thermal properties and the heat transfer is modeled by conduction using solid particles of soil (Jradi et al. 2017). However, in unsaturated compacted soils, the thermal properties will change by temperature variations, soil physical and hydraulic properties. Therefore, a comprehensive investigation is a thermo-hydraulic simulation with consideration of the mass transfer by vapor and liquid flows (Gan 2013; Gao et al. 2016; Boukelia 2016b; Li et al. 2018; Li et al. 2018). Asgari et al. (2020) showed that the thermal performance of the linear and slinky types of HGHE increases by increasing the number of layers arrangement in the ground. For the spiral type exchangers, the thermal performance did not change with increasing the number of layers. Boukelia (2016b) investigated the heat lost in a seasonal storage system in an embankment using HGHE by conducting the coupled thermo-hydraulic numerical simulations with a finite element tool (Code-Bright). The author observed that when the inlet temperature in the HGHE during summer was 50 ^oC, the temperature of the soil close to the probes reached 38 ^oC. At the end of the autumn when the thermal extraction season started, the temperature was about 25 ^oC, therefore, about 13 ^oC of heat loss has been occurred. Jradi et al. (2017) showed the efficiency of the Air Source Heat Pump (ASHP) combined with a solar power system as a basis for seasonal thermal energy storage. They showed also that a huge heat loss occurred after storage seasons. Therefore, to increase the thermal performance of a medium to store thermal energy, the insulation material covering the soil might be a good option and it can be taken into account in the design stage.

Another challenging issue is the consideration of the atmosphere-soil-HGHE interaction in the prediction of the system performance. Tang and Nowamooz (2020) proposed a numerical simulation framework to evaluate the HGHE performance in field conditions by considering energy and water balance on the land surface. They showed in their simulations that the consideration of the atmosphere-soil-HGHE interaction underestimates highly the outlet temperature especially for the horizontal systems installed close to the soil surface up to a difference of 48%.

The good capacity of the numerical framework considering the atmosphere-soil-HGHE interaction makes possible to bring some further responses on the backfill soil characteristics and the installation depth rarely studied so far. This point is very crucial for the thermal performance of the horizontal systems. Modeling the surface soil may significantly improve the system performance, and also avoid the cost of HGHE installation at deeper depths.

In this context, this investigation aims to visualize how the soil backfill and its installation depth influence the HGHE performance. Therefore, a compacted backfill soil that its hydrothermal behavior has been experimentally investigated is considered. Then, hydrothermal properties of the compacted soil are estimated and embedded in the numerical framework considering the atmosphere-soil-HGHE interaction. The HGHE is usually used to extract geothermal energy, but in this study, two different thermal energy storage scenarios are also investigated.

4.2 Hydrothermal behavior of the studied soil

The studied soil is frequently used as the backfill soil in France. The material was classified as sandy lean clay, CL, according to the Unified Soil Classification System (ASTM 2000). Regarding the X-ray diffractograms analysis the compacted soil contains 81% quartz, 7% dolomite, 5% calcite, 5% clayey materials and 3% feldspar. According to the particle-size distribution, almost 20% of the particles of the soil were smaller than 2 μm corresponding to the clay content, and 59% were higher than 0.05 mm corresponding to the sand content (x_s). With a liquid limit (LL) of 27% and a plastic limit (PL) of 21%, the plasticity index (PI) was 6%. The backfill soil is compacted at a water content of 16.3% to reach a dry density of 1.72 $Mg.m^{-3}$ as a reference state.

Figure 4.1 shows the variation of the water content with the suction for the compacted soil at its reference state. The van Genuchten equation (Van Genuchten 1980) is used to model the Soil Water Retention Curve (SWRC):

$$w = w_r + \frac{w_{sat} - w_r}{(1 + (\alpha s)^n)^m} \tag{4.1}$$

where w is the soil water content at the suction s; w_{sat} and w_r are the saturated water

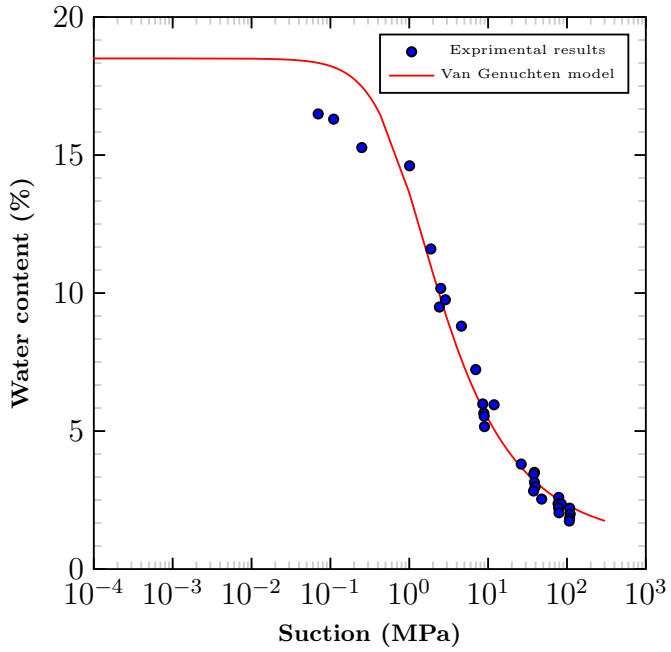

Figure 4.1: SWRC of the studied compacted backfill soil at reference compaction state (w=16.3% an ρ_d=1.72 $Mg.m^{-3}$)

content and the residual water content; α is a parameter related to the air entry suction; m and n are the model constant parameters with $m = 1 - 1/n$. Table 4.1 summarizes the main parameters of the SWRC used for the studied soil.

Table 4.1: Hydrothermal properties of the studied soil.

Application	$K(m.s^{-1})$	$I(-)$	$\alpha(m^{-1})$	$n(-)$	$w_r(-)$	$x_s(-)\%$	$\rho_s(Mg.m^{-3})$
Compacted backfill soil	1.10^{-9}	0.5	0.0134	1.52	0.01	0.62	2.60

Figure 4.2 shows the variation of the hydraulic conductivity of the studied material with suction. The hydraulic conductivity was measured in saturated conditions with triaxial device and in the unsaturated state with the Wind method (Wind 1966). A combined equation of Van Genuchten (1980) and (Mualem, 1976) is used to calculate hydraulic conductivity with suction:

$$k = K(S_e)^l(1 - (1 - S_e^{1/m})^m)^2 \tag{4.2}$$

$$S_e = \frac{w - w_r}{w_{sat} - w_r} \tag{4.3}$$

where K is the saturated hydraulic conductivity, S_e is the relative saturation of the soil and l is the pore connectivity parameter. These fitted parameters of Mualem-van Genuchten equation are also summarized in Table 4.1.

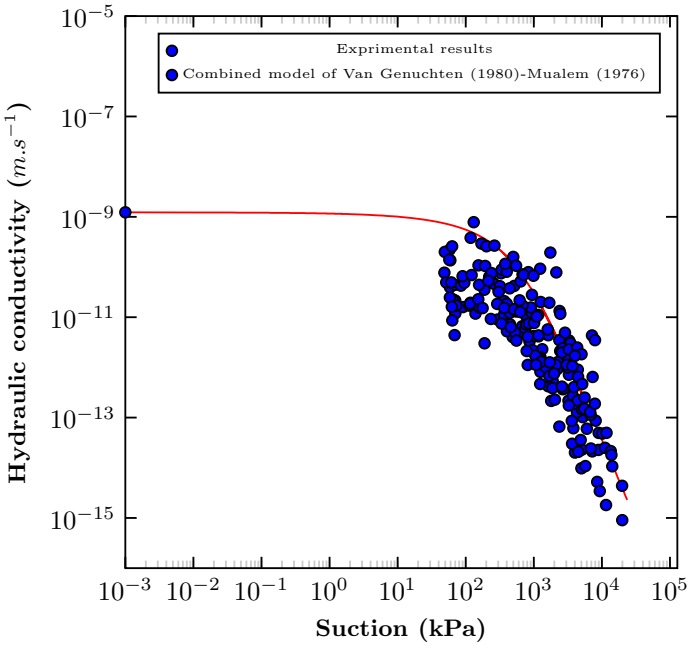

Figure 4.2: Hydraulic conductivity of the studied backfill soil.

The thermal properties were defined for the reference compaction state of the studied material. The thermal conductivity and volumetric heat capacity were measured by KD2 Pro method (Devices et al. 2016). These values are 2.46 $W.m^{-1}.K^{-1}$ and 3.25.10^6 $J.m^{-3}.K^{-1}$ respectively.

The approach proposed by Nowamooz et al. (2015) and Nikoosokhan et al. (2015) is used to model the soil thermal conductivity:

$$k_s = (0.443x_s + 0.081\gamma_d)\frac{(4.4x_s + 0.4)S_r}{1 + (4.4x_s - 0.6)S_r} + 0.087x_s + 0.019\gamma_d \tag{4.4}$$

where x_s, γ_d, and S_r are the soil sand content, dry unit weight ($kN.m^{-3}$) and degree of saturation, respectively.

The approach proposed by Tang and Nowamooz (2018a) and Tang and Nowamooz (2018b) is also used to calculate the soil volumetric heat capacity:

$$C_{v-s} = (4.18 - 0.095\gamma_d - 0.3x_s)S_r + 0.09\gamma_d - 0.2x_s \tag{4.5}$$

4.3 General conditions of the numerical simulations

General geotechnical, meteorological, hydrothermal and system conditions are given in this section.

4.3.1 Geotechnical conditions

The studied geometry has a length of 30 m, a width of 12 m and a height of 20 m. This deep geometry is selected to have no hydrothermal impact of the seasonal metrological condition on the bottom boundary. A slinky-type HGHE with 0.03 m of inner diameter and 0.036 m of outer diameter is installed 1 m below surface, covered with the backfill soil compacted at dry densities of 1.72 $Mg.m^{-3}$.

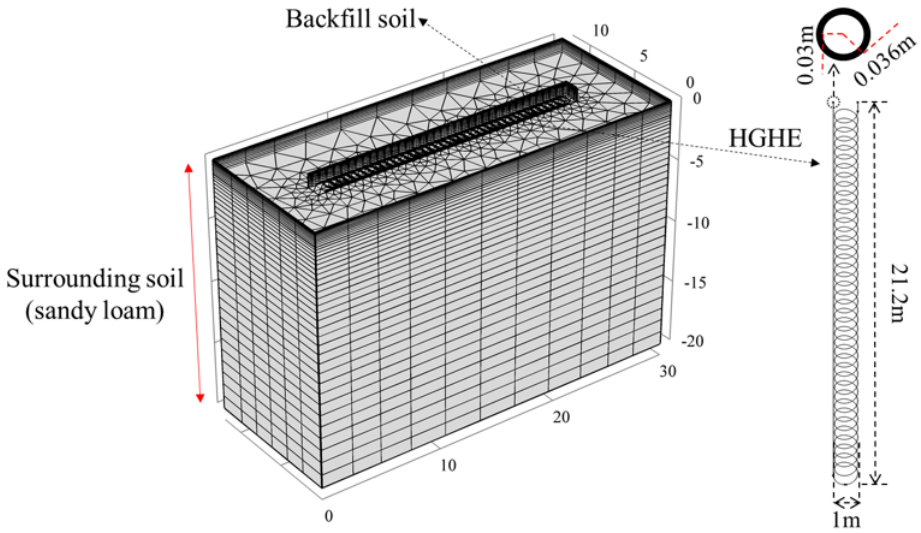

Figure 4.3: Geometry and its mesh for the numerical simulations.

We considered that the HGHE system and its backfill are installed in Alsace region in France in June. The local natural soil surrounding the HGHE till 1 m of depth (installation depth) is completely replaced by the backfill soil (Figure 4.3). The local soil is mainly constituted of sandy loam and its hydrothermal properties are listed in Table 4.2.

Table 4.2: Hydrothermal properties of the subsurface soils.

Application	$K(m.s^{-1})$	$I(-)$	$\alpha(m^{-1})$	n(-)	$w_s(-)$	$w_r(-)$	$x_s(-)$	$\rho_s(Mg.m^{-3})$	$\rho_d(Mg.m^{-3})$
Sandy loam	$1.78.10^{-5}$	0.5	2.60	1.52	0.39	0.02	0.80	2.62	1.60

A swept mesh is deployed to obtain reasonable computation time. It should be noted that the generated meshes are denser in the shallow depths since the shallow ground is more sensitive to hydrothermal fluctuation on the land surface. In addition, the meshes around the HGHE are also denser due to the steep temperature and suction gradients (Choi and Ooka 2016). The geometry and its mesh are shown in Figure 4.3.

4.3.2 Boundary and meteorological conditions

The temperature gradient at the bottom boundary is set 0.142 $K.m^{-1}$ (Baillieux et al. 2013), and the extra water from the precipitation is drained at the bottom boundary. The groundwater level is set constant at the depth of 7.5 m in the whole year. No hydrothermal flow is imposed on the lateral boundaries.

The meteorological condition corresponds to the local condition with the installation time in June (Tang and Nowamooz 2018b; Tang and Nowamooz 2019). The parameters for the soil surface energy balance are reported in Table 4.5 in Appendix. Figure 4.4a and Figure 4.4b present the ambient temperatures and the shortwave radiation for one year represented by a simplified sinusoidal curve.

At the site, there is no obvious seasonal fluctuation of cloud cover, wind speed, precipitation and air humidity with time. Therefore, an average cloud cover of 0.41, an average wind speed of 2 $m.s^{-1}$, an average monthly precipitation of 55.7 mm, and an average air humidity of 83% are applied in the numerical simulation model to capture the main meteorological condition of the local site.

For the surface water balance, 20% of precipitation run off, and the other 80% participate into evapotranspiration or infiltration.

4.3.3 Initial hydrothermal conditions

An equilibrium method is used to obtain the initial hydrothermal profiles at its installation time in the end of summer. Figure 4.5 shows the suction and temperature profiles at this

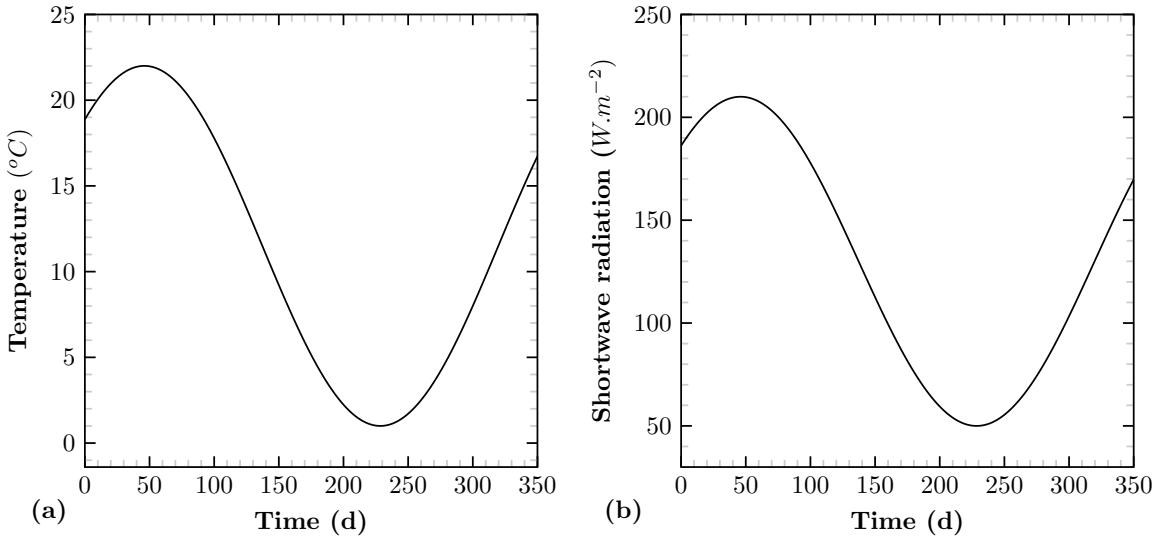

Figure 4.4: Simplified local meteorological condition: (a) ambient temperature fluctuation for one year and (b) shortwave radiation fluctuation for one year.

time.

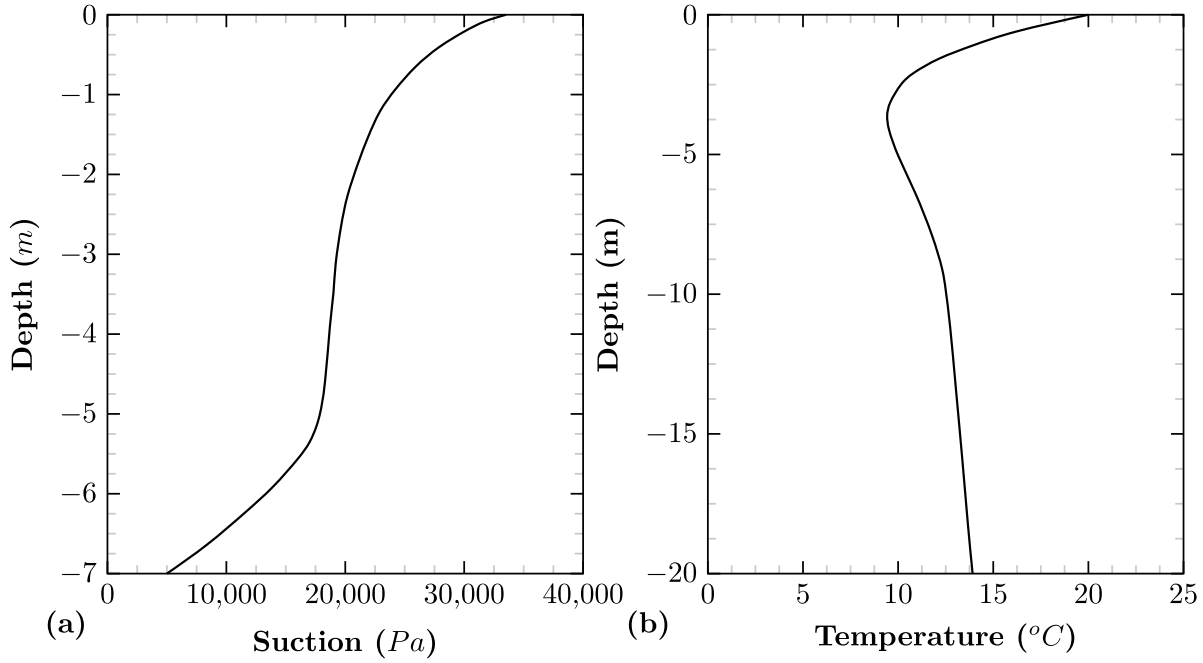

Figure 4.5: Initial hydrothermal profiles: (a) suction profile and (b) temperature profile.

4.3.4 Pipe and its carrying fluid

The pipe is a High-Density Polyethylene Pipe (HDPE) with the thermal conductivity of 0.4 $W.m^{-1}.K^{-1}$. Propylene Glycol (PG) with a volume concentration of 25% is selected as

the carrying fluid. It has a dynamic viscosity of 0.0055 $Pa.s$, a density of 1026 $kg.m^{-3}$, a thermal conductivity of 0.45 $W.m^{-1}.K^{-1}$ and a specific heat capacity of 3974 $J.kg^{-1}.K^{-1}$ (Casasso and Sethi 2014). The carrying fluid velocity is 0.5 $m.s^{-1}$ during the operation period.

4.4 Comparison of performances of HGHE installed in the local and compacted backfill soils

The numerical simulations consider the atmosphere-soil-HGHE interaction in its framework. Tang and Nowamooz (2020) proposed a numerical framework for the atmosphere-soil-HGHE interaction. To avoid the repetition of the numerical framework, some principal equations of this numerical framework are reported in Appendix (Table 4.4). To show the suitable hydro-thermal efficiency of backfill material, the performance of installed HGHE is also compared to the same system installed in the local sandy loam (Tang and Nowamooz 2018a). The system has been designed to extract the shallow geothermal energy. Therefore, a heating scenario is considered according to the local climate condition presented in section 3.2. The HGHE works from the end of Autumn season up to the end of Winter season (Figure 4.4a). During working times, a fluid with the inlet temperature of 1 ^oC circulated through the HGHE to exploit the geothermal energy. The inlet temperature of 1 ^oC is conventionally selected because of the thermal performance of the HGHE system. The HGHE is installed in compacted backfill and local soil in which their hydrothermal properties were presented in Tables 4.1 and 4.2 respectively.

During the service time of the HGHE, the Total Extracted Energy (TEE) can be obtained with time (t) by the following equation:

$$TEE = \int A\rho_f u_f C_{p-f}(T_{out} - T_{in})dt \tag{4.6}$$

where T_{in} is the fluid inlet temperature (^oC), T_{out} is the fluid outlet temperature (^oC), A is the pipe inner cross-sectional area (m^2), ρ_f is the fluid density ($kg.m^{-3}$), C_{p-f} is the fluid specific heat capacity ($J.kg^{-1}.K^{-1}$) and u_f is the fluid flowing velocity ($m.s^{-1}$).

The mesh number and time step verifications for the model are additionally brought

out. Four mesh numbers indicating 38826, 53654, 78383 and 117866 are taken into account. Five time steps representing 1.5, 1.25, 1, 0.75 and 0.5 days are compared to choose the optimal one. The results show that there is a decrease accuracy of the TEE with the decrease of mesh number and increase of time step. The results show that the accuracy of the numerical simulation model could be satisfied with the mesh number of 78383 and the time step of 1 day (Figure 4.6).

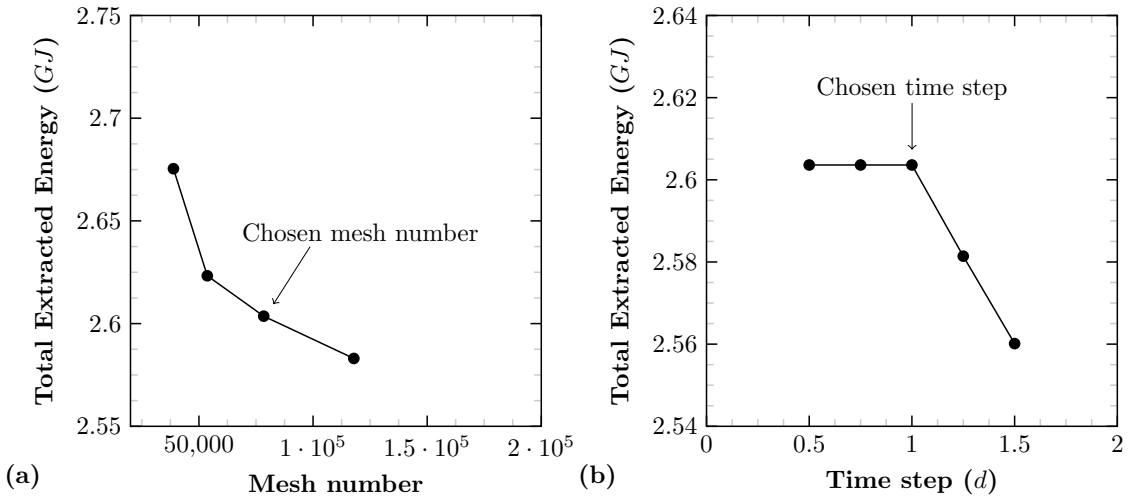

Figure 4.6: (a) mesh number and (b) time step verifications for the numerical simulation model.

Figure 4.7a shows the TEE of the HGHE during its annual working period for the local and backfill soils. It shows that the installed HGHE can extract 2.95 GJ and 2.49 GJ of energy after 1 year respectively for backfill and local soil. It shows that the backfill soil increases 18.5% the system performance which is mainly due to its higher initial hydro-thermal properties (Figure 4.7b).

4.5 Heat storage effect on the performance of HGHE installed in the compacted backfill soil

In this section, the effect of thermal energy storage during summer on the HGHE performance installed in compacted backfill soil is investigated. The results are compared to the original system with no heat storage (called Nsto scenario in this section). Several installation depths are also tested in the numerical simulations.

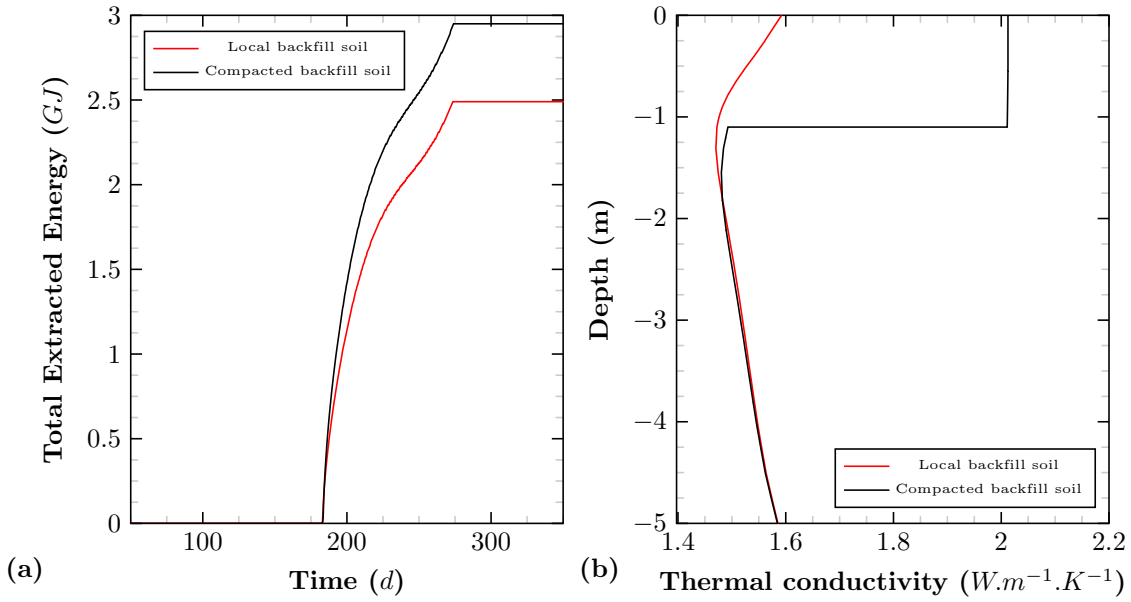

Figure 4.7: (a) the extracted energy with time during the service period of the HGHE for backfill and local soils installed at the depth of 1 m, (b) the initial thermal conductivity profiles for the backfill and local soils.

4.5.1 Studied scenarios and installation depths

The context of thermal energy storage increases the performance of the HGHE by increasing the temperature of ground. Therefore, during summer, a fluid with higher temperature than the ground can circulate through the HGHE to exchange the temperature with surrounding soil. The stored heat is expected to be released during winter. The stored energy during summer season is extracted by a circulating fluid with a temperature of 1 ^oC in the HGHE during winter. The system stops working at the end of Winter.

To store thermal energy in soil during summer season and use it in winter, two different scenarios are investigated in this study:

a) First scenario (StoA)

A reservoir of carrying fluid is exposed to exterior temperature and then the carrying fluid circulates in HGHE during summer. Therefore, the inlet temperature in 3 months of summer is the ambient temperature (scenario StoA) as presented in Figure 4.8 (temperatures of 0 to 92 days). This system is in relaxation in Autumn (from 92nd to 183rd day), therefore no fluid flow will be circulated through the system. When Winter comes (from 183rd to 274th day), a fluid flow with inlet temperature of 1 ^oC will be circulated. Again the system is in relaxation in Spring (from 274rd to 365th day) (Table 4.3).

b) Second scenario(Sto50)

Solar panels absorb the solar energy and the energy can be used to heat the subsurface soil in summer while a fluid with a constant inlet temperature is circulating in the HGHE. Therefore, the inlet temperature in 3 months of summer is a constant temperature of 50 ^oC (Sto50) as presented in Figure 4.8. The system works the same way as the ambient temperature storage scenario except that the inlet temperature is 50 ^oC in Summer season (Table 4.3).

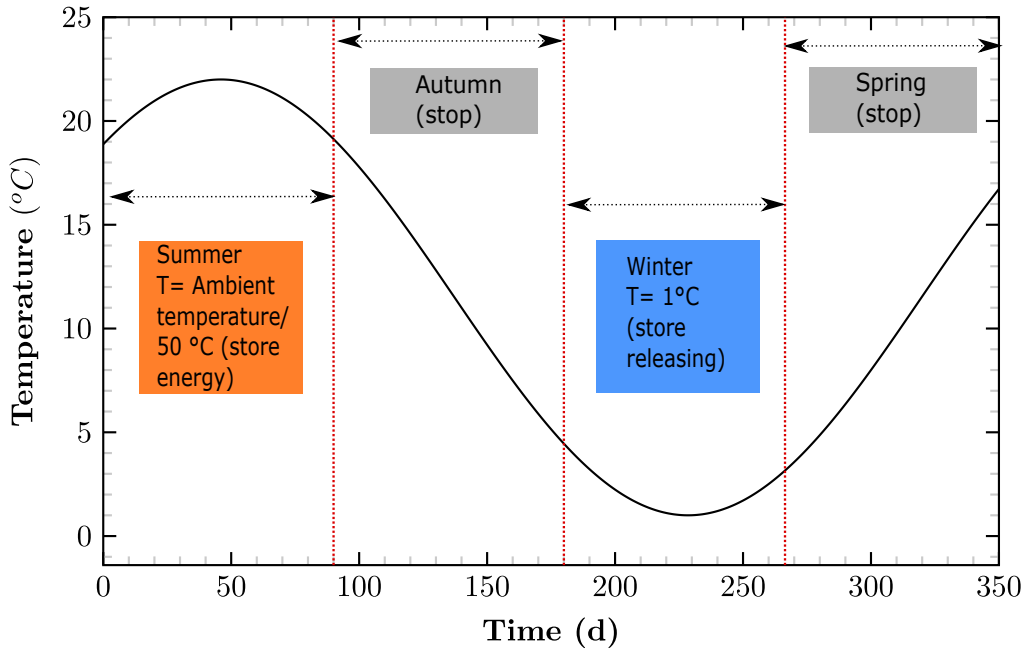

Figure 4.8: Operation mode for the HGHE over one year.

Table 4.3: Imposed temperature of inlet fluid for StoA and Sto50.

Scenario	Summer (0 to 92^{th} days)	Autumn (92^{nd} to 183^{rd} day)	Winter (183^{rd} to 274^{th} day)	Spring (274^{rd} to 365^{th} day)
StoA	Ambient temperature Figure 4.4a	Relaxation	1 ^oC	Relaxation
Sto50	50 ^oC	Relaxation	1 ^oC	Relaxation

Due to the interaction with ground surface, the stored energy during relaxation seasons is dissipated into the atmosphere. If the HGHE is installed close to the land surface, a higher amount of stored energy can be dissipated. Therefore, three depths of 1, 1.5 and 2 m beneath land surface are investigated for both scenarios to study the influence of installation depth on the HGHE performance.

4.5.2 Simulation results

a) Scenario 1 (StoA) compared to scenario with no heat storage (Nsto)

Figure 4.9 shows the pipe outlet temperature with time at the installation depths of 1, 1.5 and 2 m for the first scenario (StoA) compared to the outlet temperatures of the original HGHE with no heat storage (Nsto) presented in section 4.4. The figure shows the fluid outlet temperature decreases abruptly with the working of the HGHE. Afterwards, the fluid temperature generally decreases and starts to increase with warmer climate. In addition, the figure shows that outlet temperature increases slightly by depth.

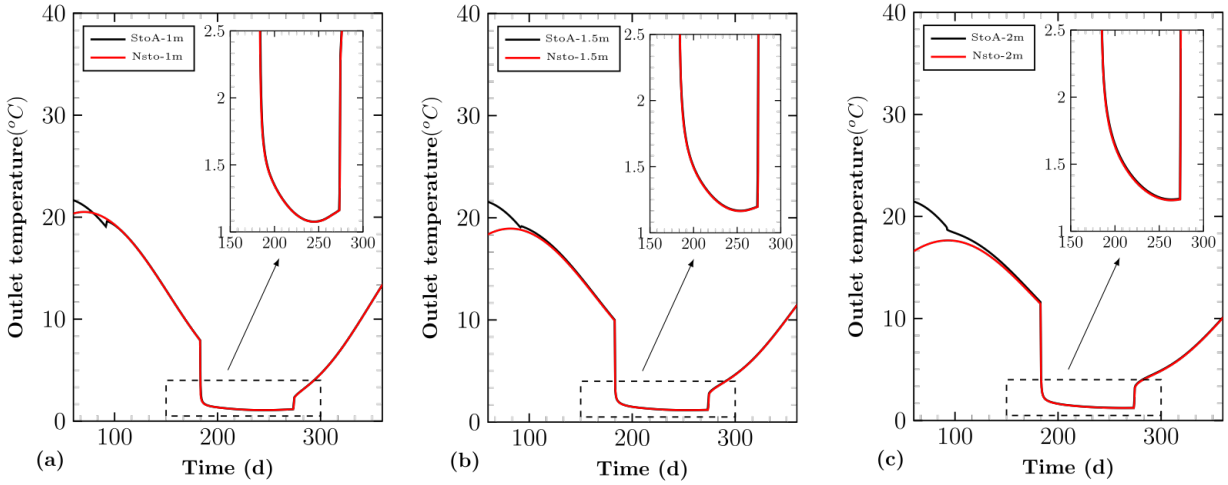

Figure 4.9: Outlet temperature comparison of the storage scenario (ambient temperature) and the non-storage scenario for three installation depths (a) 1m, (b) 1.5m and (c) 2m.

b) Scenario 2 (Sto50) compared to scenario with no heat storage (Nsto)

Figure 4.10 shows the outlet temperature for the second storage scenario (Sto50) at three installation depths compared to the outlet temperatures of the original HGHE with no heat storage (Nsto) presented in section 4.4. The figure shows that the ground temperature is obviously improved in summer, and the deeper the installation depth, the larger difference between the outlet temperatures of the scenario considering and non-considering the energy storage in summer.

4.6 Comparison of different studied scenarios

The surrounding temperatures of the HGHE installed at the depth of 2 m in the end of Summer, Autumn and Winter are shown in Figure 4.11. The figure shows that the soil

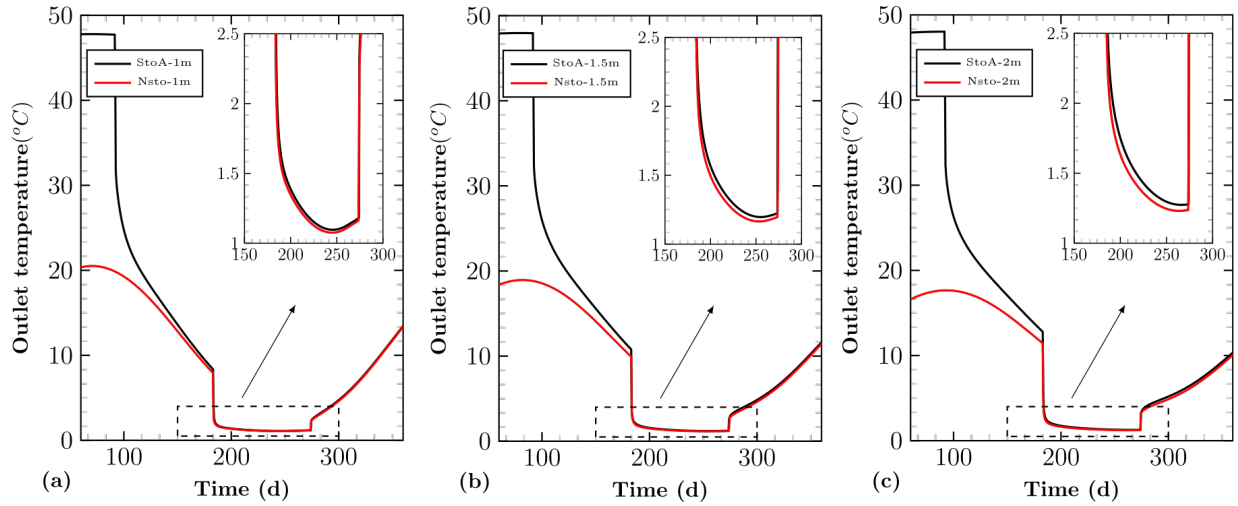

Figure 4.10: Outlet temperature comparison of the storage scenario (50 ^oC of inlet temperature during summer) and the non-storage scenario for three installation depths (a) 1m, (b) 1.5m and (c) 2m.

temperature has been clearly improved in the scenario with 50 ^oC of fluid inlet temperature in Summer (Sto50), while the surrounding temperature improves negligibly with the ambient temperature storage scenario (StoA). Specifically, soil temperature has been improved 27 ^oC and 3 ^oC respectively at the depth of 2 m at the end of Summer and Autumn with the energy storage scenario (Sto50).

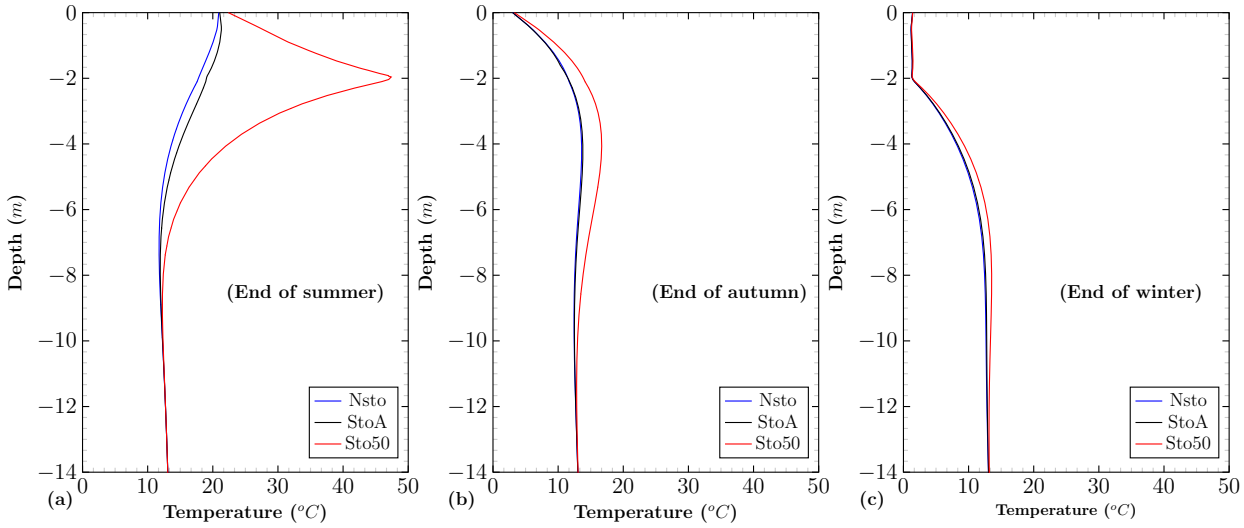

Figure 4.11: Temperature profiles at the end of (a) Summer , (b) Autumn and (c) Winter.

By using equation 4.6, the corresponding extracted energies can be exploited with time for both scenarios as presented in Figure 4.12. The results show that the heat storage can improve the TEE and the improvement increases with depth in both scenarios. This increase is more evident for the scenario Sto50. Specifically, for the installation depth of

$1m$, this increase is 0.34 GJ (13.7%) compared to 0.0 GJ (0.0%). When the installation depth increases from 1 to 2 m, the final improvement of the TEE increases from 0.0 GJ to 0.12 GJ (0.0 to 4.8%) for the first scenario StoA (Figure 4.12a) while it increases form 0.34 GJ to 1.03 GJ (13.7 to 41.4%) for the second scenario (Sto50).

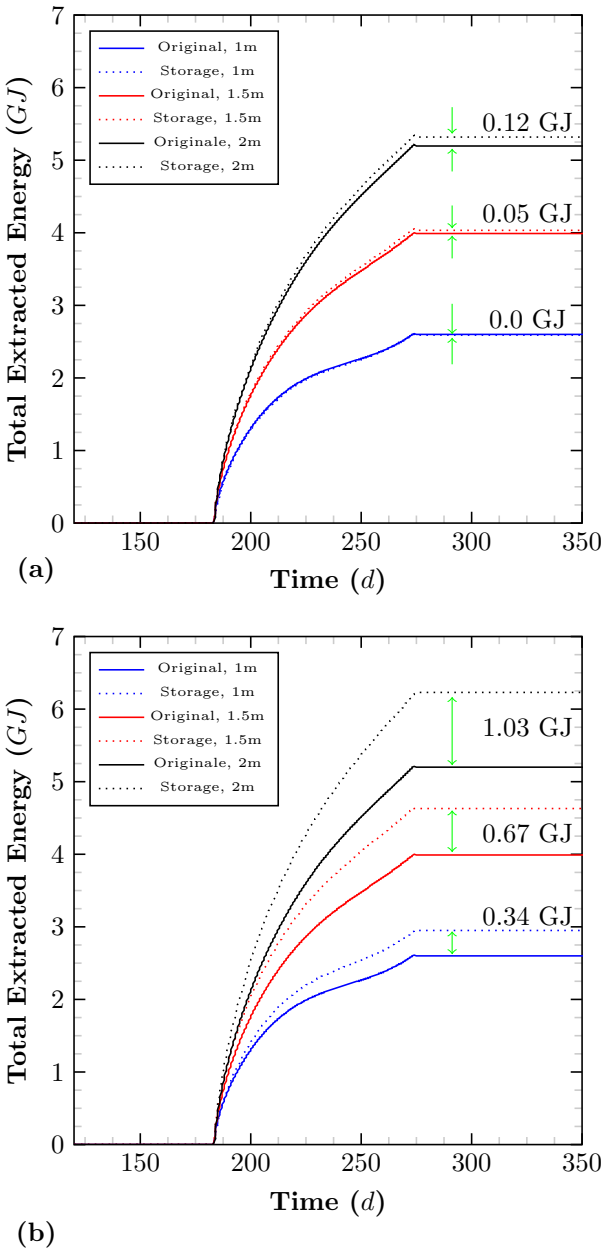

Figure 4.12: Total extracted energy with time of (a) first scenario (StoA) and (b) second scenario (Sto50) compared to the original HGHE system (Nsto).

Figure 4.13 compares the annual TEE values of the aforementioned heat storage scenarios (StoA and Sto50) with the TEE values of the original scenario without heat storage (Nsto). The figure shows that the HGHE can be highly improved by adopting an inlet

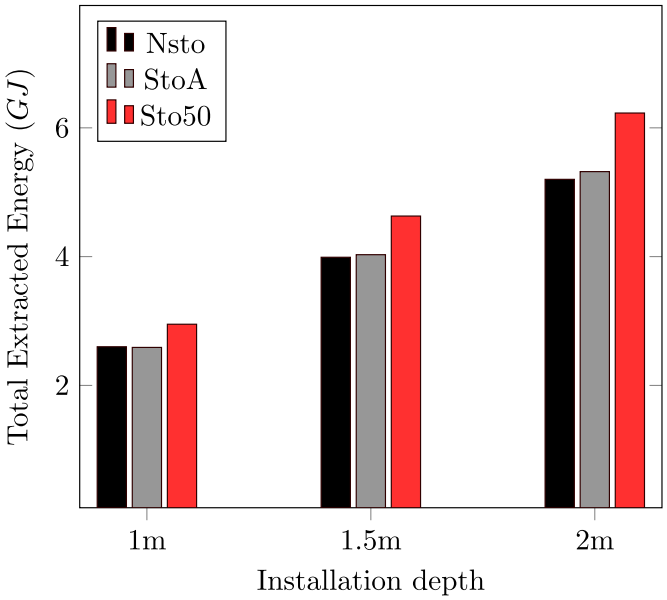

Figure 4.13: Comparison between the heat storage scenarios (StoA and Sto50) with non-storage scenario (Nsto) at three different installation depths.

fluid temperature of 50^oC in summer while the ambient inlet temperature produces less amelioration in the HGHE performance.

4.7 Conclusions

This work brings some responses on the selection of the backfill material and its installation depth in a HGHE system. A well-known backfill soil was used to improve the performance of an HGHE system installed in the east of France. The hydrothermal properties of the backfill soil were first injected in a numerical framework considering the atmosphere-soil-HGHE interaction. The simulations results showed that the backfill material provided an increase 18.5% in the HGHE performance compared to the existing local soil. To improve the HGHE performance, two heat storage scenarios at three different installation depths were studied. The results showed that an inlet fluid temperature of 50 ^oC in summer increased highly the system performance (13.7 to 41.4%) while the improvement was less significant (0 to 4.8%) for the ambient inlet temperature. A deeper installation depth increased the total extracted energy (TEE) but increases the installation costs. In this study have focused only on one metrological region and further analysis are still necessary to combine the meteorological conditions to the selection of the backfill materials used in the HGHE systems.

4.8 Appendix

Governing Equations

Figure 4.14 shows a schematic diagram of the concerning phenomenon in HGHE engineering. The necessary governing equations considering the atmosphere-soil-HGHE interaction are constituted of 4 parts: a) the soil surface energy balance; b) the soil surface water balance; c) the hydrothermal transfer in subsurface soil and d) the heat transfer in pipe. All these equations were already published in Tang and Nowamooz (2020). A summary of these equations is presented in Table 4.4.

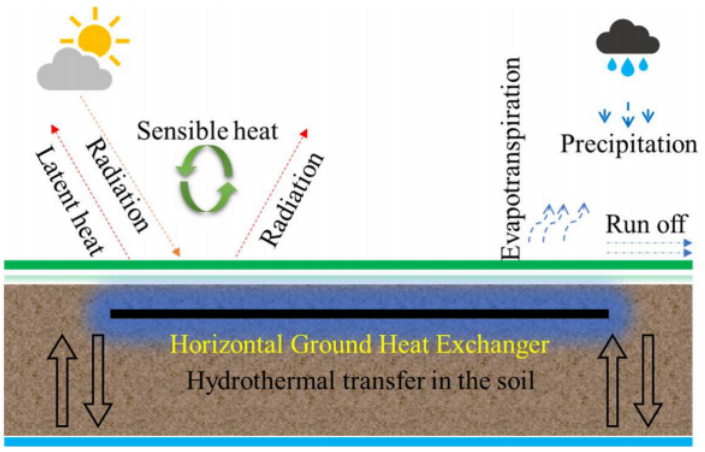

Figure 4.14: Comparison between the heat storage scenarios (StoA and Sto50) with non-storage scenario (Nsto) at three different installation depths.

In Table 4.4, R_n is the net radiation heat flux ($W.m^{-2}$), H is the sensible heat flux ($W.m^{-2}$), LE is the latent heat flux ($W.m^{-2}$), G is the ground heat flux ($W.m^{-2}$), a_l is the surface albedo, R_s is the shortwave radiation ($W.m^{-2}$), R_a is the incoming longwave radiation ($W.m^{-2}$), $\varepsilon\sigma T_s^4$ is the outcoming longwave radiation ($W.m^{-2}$), ε is the soil surface emissivity, σ is Stephan-Boltzman constant ($W.m^{-2}.k^{-4}$), T_s is the soil temperature (K), ρ_a is the air density ($kg.m^{-3}$), C_{P-a} is the air specific heat capacity ($J.kg^{-1}.K^{-1}$), r_a is the aerodynamic resistance to heat transfer ($s.m^{-1}$), P is the rainfall rate ($mm.s^{-1}$), E_p is the evaporation potential ($mm.s^{-1}$), LAI is the leaf area index, h_c is the displacement height is linear o the vegetation height (m), W_r is the water run off, E is the actual evaporation, W_i is the infiltration, ρ_w is the water density ($kg.m^{-3}$), Ψ is the specific moisture capacity (m^{-1}), H_p is the suction head (m), t is the time (s), K is the saturated hydraulic conductivity ($m.s^{-1}$), k_r is the relative hydraulic conductivity, D is the elevation head

Table 4.4: Principal equations of atmosphere-soil-HGHE interaction.

Type of interaction	Principal equation
soil surface energy balance (Turc 1954; Pike 1964; Monteith 1965; Allen et al. 1989; Gerrits et al. 2009; Chalhoub et al. 2017; Chen and Buchberger 2018)	$R_n + H - LE - G = 0$ $R_n = (1 - a_l)R_s + (R_a - \varepsilon\sigma T_s^4)$ $H = \rho_a C_{P-a}(T_a - T_s)/r_a$ $E = P.[1 + (E_p/P)^{-2}]^{1/2}$ LAI=24.h_c for clipped grass or LAI=5.5+1.5 ln h_c for other crops
Soil surface water balance (Dietrich et al. 2016)	$P = W_r + E + W_i$
Richard equation for hydraulic transfer is soil (Wind 1966; Mualem 1976; Van Genuchten 1980)	$\rho_w.\Psi.\frac{dH_P}{dt} + [-K.k_r.\nabla.\rho_w.(H_P + D + H_k)] = 0$
Hydrothermal transfer in subsurface soil (Nowamooz et al. 2015; Nikoosokhan et al. 2015; Tang and Nowamooz 2018a; Tang and Nowamooz 2018b)	$\rho_s C_{p-s}\frac{dT_s}{dt} = \nabla.(k_s \nabla T_s) + \nabla.(\rho_s C_{p-s} u_w T_s) + Q_s$
Heat transfer in pipe	$A\rho_f C_{p-f}\frac{dT_f}{dt} + A\rho_f C_{p-f} u_f.\nabla T_f = \nabla.Ak_f\nabla.T_f + f_D\frac{\rho_f A}{2d_h}\lvert u_f\rvert u_f^2 + Q_{wall}$ $Q_{wall} = h_{int}.Z.(T_{i-p} - T_f)$

Table 4.5: Parameters for the soil surface energy balance.

Parameter	Description	Value	Unit
al	Albedo	0.25	-
ε	Soil emissivity	0.97	-
σ	Stephan-Boltzman constant	5.67×10^{-8}	$W.m^{-2}.K^{-4}$
ρ_a	Air density	1.25	$kg.m^{-3}$
C_{p-a}	Air specific heat capacity	1.00×10^3	$J.kg^{-1}.K^{-1}$
z_m	Height to collect the meteorological data	2.00	m
h_c	Grass height	0.06	m
k	von Karman constant	0.41	-
L	Latent heat of vaporization	2.26	$J.kg^{-1}$
p_{at}	Atmospheric pressure	102000	Pa
r_{mw}	Molecular weight of water vapor to dry air	0.62	-
r_1	Stomatal resistance of a single leaf	100	$s.m^{-1}$

(m), H_k is the kinetic head (m), ρ_s is the soil density $(kg.m^{-3})$, C_{p-s} is the soil heat capacity $(J.kg^{-1}.K^{-1})$, C_{p-w} is the water specific heat capacity $(J.kg^{-1}.K^{-1})$, u_w is the water velocity in soil $(m.s^{-1})$, Q_s is the soil heat source $(W.m^{-3})$, A is the pipe inner cross-sectional area (m^2), ρ_f is the fluid density $(kg.m^{-3})$, C_{p-f} is the fluid specific heat capacity $(J.kg^{-1}.K^{-1})$, T_f is the fluid temperature (^oC), u_f is the fluid flowing velocity $(m.s^{-1})$,

k_f is the fluid thermal conductivity ($W.m^{-1}.K^{-1}$), f_D is the Darcy friction factor, d_h is the hydraulic diameter (m) and Q_{wall} is the energy from the surrounding media ($W.m^{-1}$), h_{int} is the film heat transfer coefficient ($W.m^{-2}.K^{-1}$), Z is the pipe inner perimeter (m) and T_{i-p} is the inner pipe temperature (^oC).

General conclusion and perspectives

Due to the severe environmental impact of non-clean sources of energy, in recent years, research has been conducted to investigate and propose new technologies to exploit green and renewable sources of energy. Among these technologies, utilization of solar energy can be mentioned. Thermal energy storage in soils using horizontal heat exchangers was known as a preferable method compared to the others. To avoid the time-consuming process of land occupying and construction phase, placing the horizontal heat exchanger in different compacted soil layers in embankments are considered in literature.

In this thesis different methods to store the thermal energy in the ground were presented in the first chapter, afterwards they were compared in terms of cost and environmental impact. Then, the study was focused on investigation of thermal and mechanical performances of an embankment to store thermal energy. The thermal performance of compacted soil was found to be dependent on the soil compaction state. The soil thermal properties change with the density and water content. The measurement and estimation of thermal properties are more difficult in compacted soil which is unsaturated and contains different phases. In the wet side of compaction curve, with density and water content increase, the soil thermal properties increase. Consequently, an inverse analytical model to estimate the thermal properties of a compacted soil was proposed in Chapter II. The thermal diffusivity was estimated via a new "temperature/temperature" method based on the estimation of a heat transfer function. One of the main benefits of this method is that it only requires temperature-time series measurements at two different locations.

The thermal conductivity was then estimated using the estimated value of thermal diffusivity and the volumetric heat capacity was measured by calorimetry and then compared with the values obtained with two other methods (a transient-state method and a steady-state method). The results showed that this simple analytical model has a good

agreement (2% deviation) with the experimental results obtained with the transient-state method. In contrast, the steady-state methods are not suited for this type of material since thermal contact resistances are no longer negligible compared to the sample thermal resistance.

In the proposed analytical model, the shape and intensity of the heat flux or the external boundary conditions have not been considered, but the hypothesis of transient heat conduction in the radial direction in cylindrical coordinates should be considered. As is generally done, mass transfer is not considered in this model. The sensitivity analysis of this model showed that this model is sensitive to the distance between two sensors, so the distance between two sensors must be accurately measured.

It can be concluded that by in situ temperature monitoring in the soil medium using two temperature sensors, the soil thermal properties can be estimated using this analytical model at any time. For example, in an embankment, during the heat storage season, the radial heat flux can be applied by considering the cylindrical shape of heat exchanger loops (from the surface of the tubes towards an arbitrary cylindrical surface). Then two temperature sensors should be placed at different distances from the heat exchanger tubes to monitor the temperature. Therefore, this method could enable system efficiency estimation of possible future applications of thermal energy storage in embankments or other configurations.

When the initial compacted state of the soil regarding its optimal thermal properties are selected, the mechanical performance of compacted soil during its lifetime in an embankment should be investigated. The evaluation of the mechanical properties for the studied soil was carried out in Chapter III. This chapter presents the experimental results to investigate the consolidation and shear behavior of a compacted soil subjected to the monotonic (5, 20, and 50 ^oC) and cyclic temperature variations (5 to 50 ^oC) using temperature-controlled oedometric and direct-shear devices. It should be noted that these tests were performed in the saturated state which shows a more critical stability state than the unsaturated soil. Based on oedometric test results; the compression and swelling indexes were unchanged with temperature variation; the apparent pre-consolidation pressure decreased with heating and increased with cooling, the volumetric response of compacted soil due to the temperature cycles was dependent on stress history. In over-consolidated

state a reversible deformation was observed and in normally consolidated state the temperature cycles induced a thermal plastic contraction. Thus it can be concluded that, in terms of consolidation behavior in thermal charging and discharging seasons, when the compacted soil is exposed to monotonic temperature variations, due to very small differences in compression index at different temperatures, the effect of temperature on the embankment's global settlement can be considered negligible. Furthermore, the volumetric response under different vertical stresses (50 to 200 kPa) at different embankment depths (2.5 to 10 m) due to the temperature cycles could be also small enough to be neglected.

The results of direct shear tests showed heating from 20 to 50 ^oC and temperature cycles (5 to 50 ^oC) had a negligible effect on shear characteristics whereas cooling from 20 to 5 ^oC decreased the shear stress at higher normal stresses (200 kPa). Whereas, in all other paths, the cohesion increased and the friction angles remained unchanged that is advantageous for bearing capacity and embankment slopes stability. Therefore, based on thermo-mechanical paths studied in this research work, it can be concluded that in the construction phase, the horizontal heat exchanger loops can be placed in different depths in an embankment.

It should be noted that due to the soil-atmosphere interaction from the top and lateral surfaces in the embankments the heat loss could be considerable. Therefore, the suitable installation depths and also an insulation material should be envisaged in the design stage. Chapter IV evaluates the thermal performance of a compacted backfill soil using a validated hydro-thermal numerical simulation considering the atmosphere-soil interaction and installation depth of horizontal ground heat exchangers. The simulations result on a soil from Alsace region (France) showed that the compacted backfill soil increased by 18.5% the thermal performance of the horizontal heat exchanger compared to the natural uncompacted soil. To improve the thermal performances of the system, two heat storage scenarios at three different installation depths were studied. The results showed that an inlet fluid temperature of 50 ^oC in summer increases highly the system performance (13.7 to 41.4%) while the improvement is less significant (0 to 4.8%) for the ambient inlet temperature. A considerable amount of heat loss was observed during thermal charging and discharging seasons. A deeper installation depth increases the total extracted energy

but increases the installation costs.

The following points can be proposed for further investigations on thermal energy storage in an embankment:

• In thermal properties determination tests (centered hot plate test) and temperature monitoring in the container, water migration due to the temperature gradient was observed. This migration impacts the thermo-mechanical performance of the compacted soil. Therefore, further investigations are needed to study quantitatively the water migration caused by temperature variations (for example by Magnetic resonance imaging (MRI).

• In-depth studies of micro-structural behavior of a compacted soil are needed for better understanding of the evolution of mechanical characteristics due to the temperature variations.

• The thermo-hydro-mechanical behavior of compacted soil in unsaturated state should be investigate to assess the positive contribution of unsaturated state to the overall stability of the system .

• The exact embankment geometry should be considered to estimate the thermal performance by taking into account the soil-atmosphere interaction.

• Different shapes and arrangements of horizontal heat exchanger loops and different inlet heat fluxes should be modeled in numerical simulations.

• The overall thermal performance of an insulation material can be studied to reduce the heat lost during thermal charging and discharging seasons. For example, the geotextile materials can be a good proposition for insulation of the soil (see appendix A dedicated to the evaluation of the geotextile thermal properties as an insulation layer for an embankment).

• The thermal and mechanical performances of the embankment can be well understood by performing coupled thermo-hydro-mechanical numerical modelling.

• The investigation of the thermo-hydro-mechanical behavior of different natural and also treated soils can help to reduce cost of transportation from cutting to banking.

• The realization of an in-situ compacted backfill soil equipped by different sensors to measure temperature, water content and displacement over long time could be helpful for a better understanding of the thermal and mechanical performances of an embankment

to store the thermal energy.

Appendix A

Thermal conductivity of nonwoven needle-punched geotextiles: effect of stress and moisture

Abstract: This paper explores the use of geotextiles, as insulation material for energy geostructures made of compacted soil. This work is based on measurements of the thermal conductivity of four nonwoven needle-punched geotextiles of varying thicknesses made from virgin or recycled fibres. These values were measured using the hot-plate method. Then, to assess the use of these geotextiles under a covering soil layer, compression tests were performed. For each sample, the relation between thickness and vertical stress was thus established. The thermal conductivities varied from 0.04 to 0.06 $W.m^{-1}.K^{-1}$ depending on the geotextile type and the compression stress applied. Subsequent measurements focused on the thermal conductivity of a bilayer compacted soil plus geotextile. Results revealed a water migration towards the geotextile and therefore a larger thermal conductivity. These results highlighted the main importance of compression load and moisture environment in the use of geotextiles as insulation products.

Keywords: Geosynthetics, Geotextiles, Insulation, Energy geostructures, Thermal conductivity.

A.1 Introduction

In geotechnical engineering, different types of structures are made of compacted soils, for example, road, rail embankments and dikes. Recent prospects studied show the opportunity to insert horizontal heat exchanger loops in these layers during the construction phase (Boukelia 2016a; Lahoori, Jannot, Rosin-Paumier, Boukelia and Masrouri 2020). The circulation of a fluid in these heat exchanger loops make it possible to store thermal energy in the compacted soil during warm season, to be preserved and later discharged for utilization in the demanded period (Xu et al. 2014; Jradi et al. 2017; Li et al. 2018). This type of thermal energy storage is successfully used in soils or rocks (Stojanović and Akander 2010; Cao 2010; H Abedin and A Rosen 2011).

The challenge, in case of seasonally thermal energy storage, is to decrease heat loss to optimize the potential heat storage (Fantucci et al. 2015; Lahoori, Rosin-Paumier, Jannot, Boukelia and Masrouri 2020). To address this challenge, mineral wood, fibreglass, cellulose and polystyrene are often used as an insulation layer overthermal energy systems (Schmidt et al. 2003). However, for thermal energy storage in compacted soils, the insulation material should be thin, easy to spread and effectively resistant to external loads. These factors have led to the consideration of geosynthetics, and particularly nonwoven needle-punched geotextiles, for use in heat-storage systems.

Over the last four decades, the use of synthetics or natural geosynthetics has grown in civil-engineering applications, for example to provide functions like drainage, filtration, separation or reinforcement (EN ISO 10318-1, AFNOR 2015). The capacity of geosynthetics to provide heat insulation was shown by Bouazza et al. (2017) in the case of composite liners of landfills barriers. To investigate their insulating capacity, their thermal properties (e.g. thermal conductivity, diffusivity and volumetric thermal capacity) must be known. Methods to measure thermal conductivity fall into two categories: steady-state methods and transient methods (see for example the review of Vieira et al. 2017). A typical steady-state method is the hot plate method, which is commonly used to measure the thermal conductivity of flat, homogeneous and insulating materials (Al-Ajlan 2006; Ali et al. 2016; Jannot et al. 2016). This method consists of establishing a steady temperature gradient over a known sample thickness and controlling the heat flow from one side

to the other; it allows the thermal conductivity to be measured at different temperatures and for different thicknesses.

Few measurements of the thermal conductivity of geotextiles, and more specifically of nonwoven needle-punched Geotextiles, have been reported in the literature. Singh and Bouazza (2013) indicated that the thermal conductivity of nonwoven polyester geotextiles under 2 kPa of vertical stress ranged from 0.07 to 0.83 $W.m^{-1}.K^{-1}$ and was a function of water content, immersion time in water and surface treatment. However, very few results have been reported for geotextile thermal behavior under mechanical loads. Different studies show even though that the properties of geotextiles like thickness, porosity, permittivity, transmissivity and pore sizes are affected by vertical stress (Palmeira and Gardoni 2002), these parameters evolutions may have a huge impact on thermal conductivities of geotextiles. A few studies performed thermal conductivity analysis on geosynthetic clay liners under different vertical stress. Ali et al. (2016) showed that their thermal conductivity increased in thermal conductivity with increasing vertical stress whatever it water content.

The aim of this paper is to assess whether a geotextile may be used as an insulation layer in situations where geotextiles are subjected to vertical stress and exposed to moisture. For this purpose, a hot-plate apparatus was used to measure the thermal conductivity of various nonwoven needle-punched geotextiles. This study considers geotextiles with various density (i.e. mass per unit area), thickness and fibre type (recycled vs virgin). Then, other experiments investigate how vertical stress and moisture affect the thermal conductivity of geotextiles. Finally, the thermal conductivity of a soil-geotextile assembly was measured and discussed.

A.2 Materials and methods

A.2.1 Physical properties of geotextiles

Geotextiles are manufactured from various types of fibres (i.e. virgin vs recycled, natural vs synthetic) and with different assemblages, such as non-woven, needle-punched, or heat bonded. The present study used four types of needle-punched geotextiles with different fibre types and thicknesses (R1, R2, V1 and V2). Types R1 and R2 consisted of synthetic

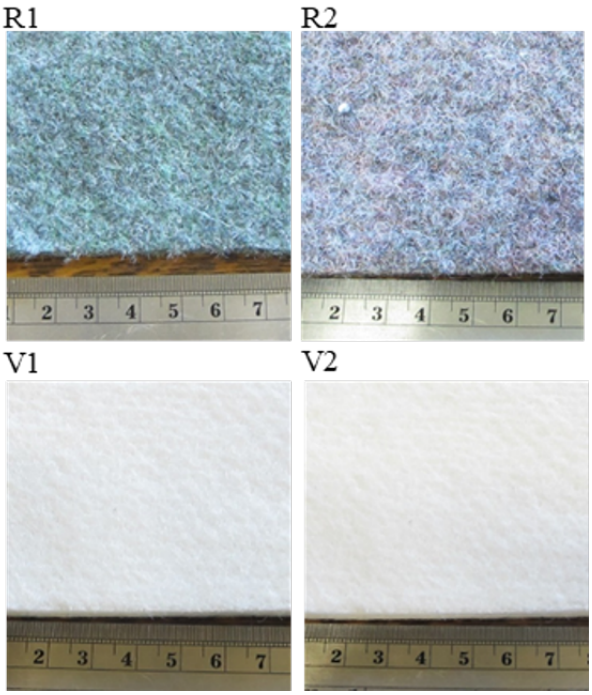

Figure A.1: Appearance of the four geotextiles.

recycled fibres (mixture of polypropylene and polyester fibres) and types V1 and V2 consisted of synthetic polypropylene virgin fibres (Figure A.1). Prior to testing, the geotextiles were die cut into specimens measuring 0.1 m $\times$0.1 m. The thicknesses of ten samples of each geotextile were measured, according to EN ISO 9863-1 (AFNOR 2016), under vertical stresses of 2, 20 and 200 kPa respectively (Table A.1). The mass of specimens makes it possible to calculate their initial dry density. Under a vertical stress of 2 kPa, the bulk densities of the materials are 104.1, 124.2, 121 and 152.1 $kg.m^{-3}$ for types R1, R2, V2 and V1, respectively Types R2 and V2 have similar thickness and mass per unit area, whereas type V1 is thicker and denser. Type R1 is finer (only 3.7 mm thick under 2 kPa of vertical stress), but its density is similar to that of types R2 and V2. Figure A.2 shows the geotextile density variation as a function of it thickness. The evolution of density is non-linear, as suggested by the density equation that is the ratio of the mass to the volume.

A.2.2 Soil properties

The studied compacted soil is a sandy lean clay extracted from the Paris region. Boukelia et al. (2019) provide a complete characterization of the soil, the main characteristics are

Table A.1: Properties of nonwoven needle-punched geotextiles.

Ref.	Type of fibers	Thickness $10^{-3}(m)$			Mass per unit area	Bulk density at 2 kPa
		at 2 kPa	at 20 kPa	at 200 kPa	$g.m^{-2}$	$(kg.m^{-3})$
$R1$	Recycled	3.670±0.110	3.000±0.212	1.817±0.100	382.1±19.9	104.1±0.1
$R2$	Recycled	7.113±0.408	5.903±0.346	3.692±0.308	883.4±67.7	124.2±0.1
$V1$	Virgin	7.940±0.141	7.091±0.154	5.396±0.269	1207.6±61.7	152.1±0.2
$V2$	Virgin	6.824±0.118	6.082±0.130	3.851±0.110	825.6±28.2	121.0±0.1

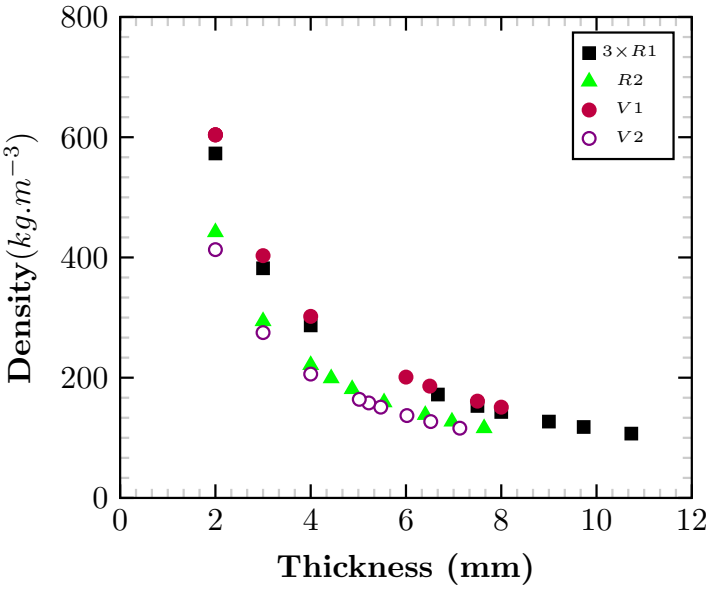

Figure A.2: Density of geotextiles as a function of thickness.

presented in Table A.2. A particle-size analysis of this soil classifies it as a fine soil, as 41% of the sample passed through a 80 μm sieve and 20% passed through a 2 μm sieve. The maximal dry density is 1.8 $Mg.m^{-3}$ from the proctor compaction test and the optimal water content is 16.1%. In this study, the soil samples were compacted into moulds with an initial water content of 16.3% and a dry density of 1.72 $Mg.m^{-3}$, which corresponds to the optimum thermal condition for the energy storage (Boukelia et al. 2019).

A.2.3 Thermal parameters

The geotextile thermal conductivities were measured using a steady-state method whereas a transient method was also used to measure the thermal conductivities of the soil samples.

Table A.2: Soil properties

Atterberg limits following NF P94-051 (AFNOR 1993)	
Plastic limit (%)	20.5
Liquid limit (%)	27.2
Plasticity Index	6.6
Normal proctor following NF P94-093 (AFNOR 1999b)	
w_{opt} (%)	16.1
ρ_d $(Mg.m^{-3})$	1.80

A.2.3.1 Hot-plate device (steady-state method)

Figure A.3 shows the hot-plate apparatus, which consisted of a thin planar heating element inserted between two identical samples of size 0.1 m × 0.1 m. This assembly was inserted between two aluminium plates maintained at constant temperature ($T_{01} = T_{02} = 15^oC$) by a circulating-water system (Figure A.3), and the entire system was placed in a climatic enclosure Binder KBF115 at a fixed temperature of 23 ^oC.

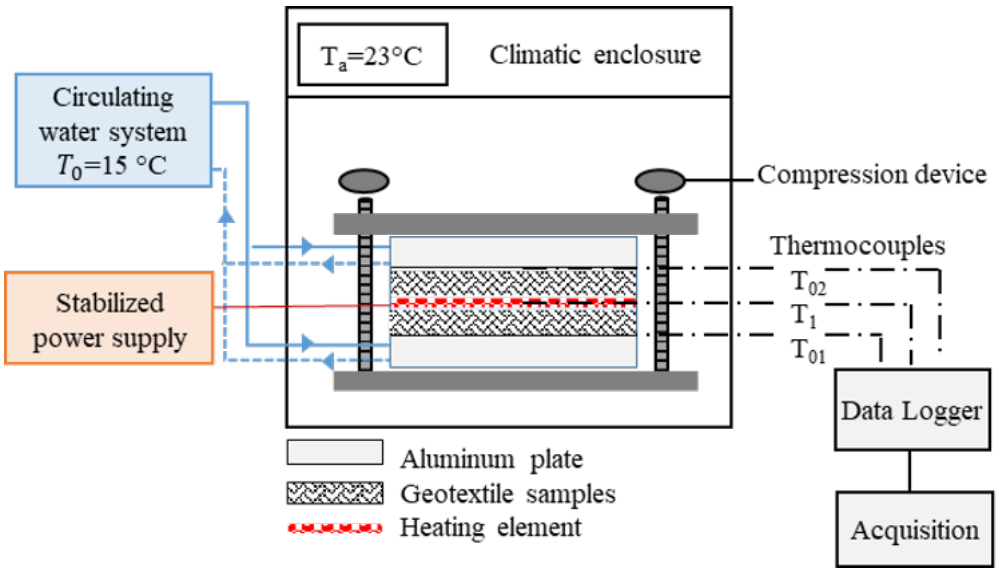

Figure A.3: Schematic drawing of hot-plate device, where T_1 is the temperature of the heating element, T_{01} and T_{02} are the temperatures of the aluminium plates and T_a is the air temperature.

A heat flow rate step with a heat flux of ϕ_0 $(W.m^{-2})$ was applied to the heating element using stabilized power supply (Tektronix PWS2185) with controlled intensity (I). The temperature T_1 at the center of the heating element was measured as well as the temperature on the opposite side of each specimen (denoted T_{01} and T_{02}, respectively). At thermal equilibrium, and assuming one-dimensional heat flux at the centre of the system,

the heat flux ϕ_0 is related to the ratio of the electrical resistance R (Ω) of the heating element and to its surface area S (m^2) as follows:

$$\phi_0 = \frac{\lambda(\Delta T_1 + \Delta T_2)}{e} = \frac{R}{S} I^2 \quad with \quad \frac{R}{S} = 3980 \Omega.m^{-2} \tag{A.1}$$

The thermal conductivity λ ($W.m^{-1}.K^{-1}$) and the thermal resistance R_{th} ($W.K^{-1}$) are obtained using:

$$\lambda = \frac{e\phi_0}{\Delta T_1 + \Delta T_2} \tag{A.2}$$

$$R_{th} = \frac{e}{\lambda} \tag{A.3}$$

with

$$\Delta T_1 = T_1 - T_{01} \quad and \quad \Delta T_2 = T_1 - T_{02} \tag{A.4}$$

In these equations, e is the sample thickness, ϕ_0 is the heat flux and ΔT_1 and ΔT_2 are the temperature differences recorded between the two sides of the sample at the end of the test.

To measure the thermal conductivity and thermal resistance of each geotextile sample, two samples of the same geotextile were placed on each face of the heating element (see Figure A.4, configuration a). A compression device allowed us to perform hot-plate tests with geotextiles of varying thicknesses (Figure A.5c).

In other configurations (Figures A.4b– A.4d), a reference material with known thermal conductivity λ_0 and thickness e_0 was placed in the lower half of the sample. In these cases, the thermal conductivity λ ($W.m^{-1}.K^{-1}$) is obtained using:

$$\lambda = \frac{e}{\Delta T_2}(\phi_0 - \frac{\lambda_0 \Delta T_1}{e_0}) \tag{A.5}$$

where

$$\phi_0 = \frac{\lambda_0 \Delta T_1}{e_0} + \frac{\lambda \Delta T_2}{e} \tag{A.6}$$

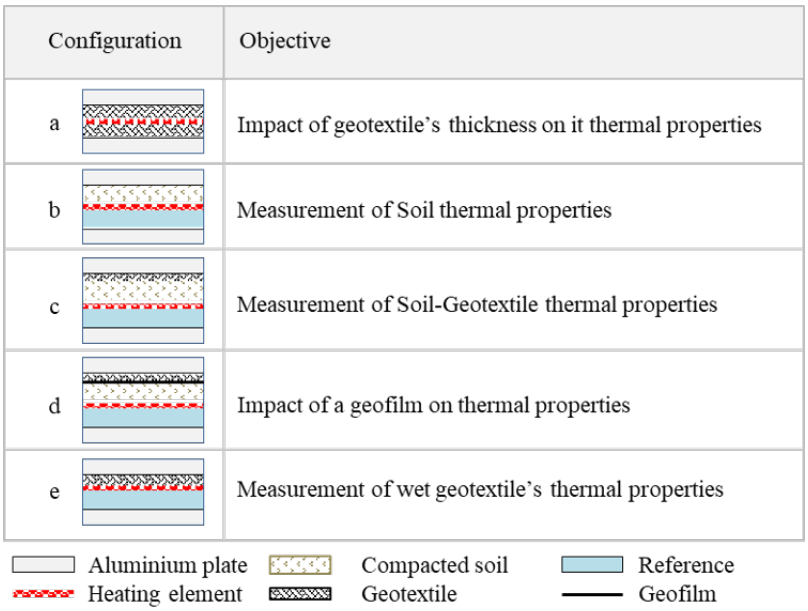

Figure A.4: Sample arrangement in hot-plate device: (a) geotextiles, (b) soil-geotextile, (c) wet geotextile and (d) soil-geotextile with geofilm.

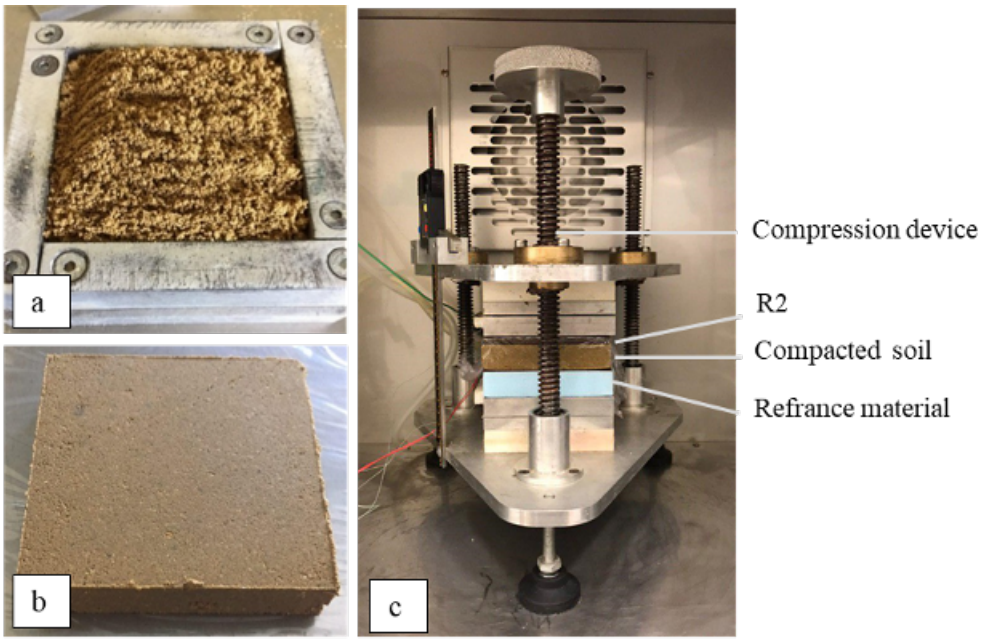

Figure A.5: (a) mould for hot-plate test (b) soil sample for hot-plate device (c) sample placement in hot-plate device.

Equations (A.2) and (A.5) are obtained by assuming that the thermal contact resistance of each side of the samples is negligible compared with the thermal resistance of the sample. This is justified because the samples tested always included a layer of geotextile with a low thermal conductivity. In configuration b, the soil and geotextile were wrapped together in a plastic film to measure their thermal parameters for the case of direct contact. The soil at the desired water content was compacted in a $0.1 \times 0.1 \times 0.02\ m^3$ mould (Figures A.5a and A.5b). Configuration c was used to measure the thermal parameters of wet geotextiles. Finally, configuration d is similar to configuration b except that a 0.05-mm-thick geofilm was placed between the soil and the geotextile. The estimated thermal resistance of the geofilm (in configuration d) was $R_{geofilm} = \frac{5 \times 10^{-3}}{0.3} = 1.6 \times 10^{-4} W.K^{-1}$, with $\lambda_{geofilm} = 0.3\ W.m^{-1}.K^{-1}$, which is negligible compared with the thermal resistance of the geotextile samples.

A.2.3.2 Thermal needle probe (transient method)

The hot-plate device cannot be used to measure the thermal conductivity of the soil (thermal conductivity $\lambda \cong 2\ W.m^{-1}.K^{-1}$ because the thermal-contact resistance is not negligible compared with the thermal resistance of the sample. Instead, a thermal-needle-probe method (KD2 Pro thermal properties analyser, Decagon) is used to measure the thermal conductivity of the soil samples. This transient technique measures the increase in temperature at a given distance from a heat source inserted in the sample (Zhao et al. 2016). The sensor TR-1 consists of single needle 2.4 mm in diameter and 100 mm long and measures the thermal conductivity λ from 0.2 to 4 $W.m^{-1}.K^{-1}$.

The soil samples were compacted with the target water content and dry density in a mould 0.116 m deep and 0.101 m in diameter (Figure A.6). To optimize the thermal contact between sensor needle and the TR-1 probe, a thin layer of thermal grease (Arctiv Silver 5 – High-density polysynthetic silver thermal compound) covered the needle before being inserted into the sample. The sensor was given 15 minutes before each test to reach the thermal equilibrium with the soil. Four tests were done in different locations in each sample, with the mean of the results being reported as the thermal conductivity of the sample.

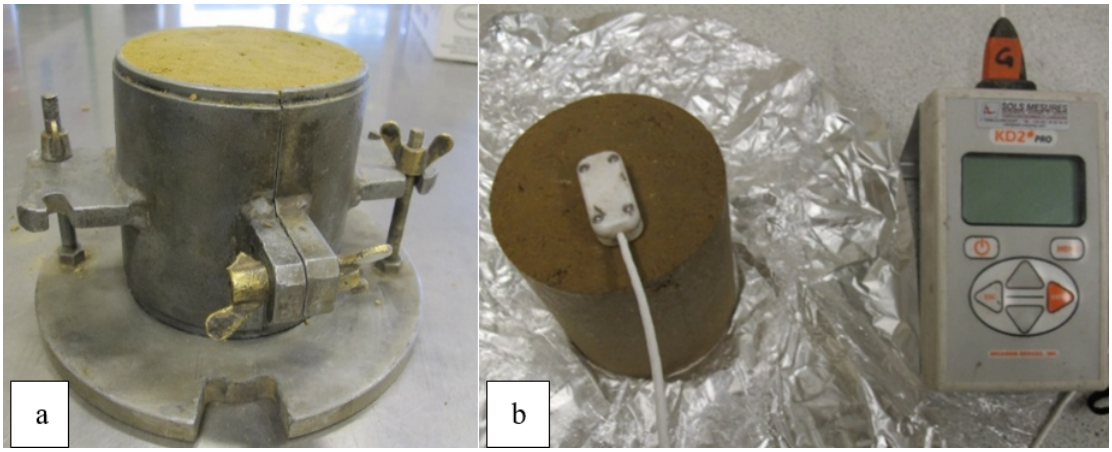

Figure A.6: (a) soil sample in Proctor mould, (b) measurement of thermal conductivity of soil with hot-wire device.

A.2.4 Compression test

The compression test consists in measuring the reduction in thickness of the various geotextiles as a function of vertical stress applied by a mechanical press (C45105; 100 kN maximum strength). The geotextiles were placed between two 0.1×0.1 m^2 metal plates to ensure homogeneous compression. The vertical stress was recorded all along the 1.08 min^{-1} displacement. The creep phenomenon was neglected because its influence on the geotextile thermal properties was considered to be negligible.

A.3 Experimental results and discussion

A.3.1 Geotextile thermal conductivity vs. thickness

The thermal conductivity and resistance of geotextile samples were measured using the hot-plate device.

The thermal conductivity and resistance of geotextile samples were measured using the hot-plate device. During the tests, the temperature T_1 of the heating element was close to 25 ^oC, and the temperatures T_{01} and T_{02} of the aluminium plates were near 15 ^oC (Table A.3). The temperature difference between heating element and aluminium plate caused a one-dimensional heat flow from the heating element through the sample to the aluminium plates. For all tests, the temperature of the surrounding air was held at about 23 ^oC to ensure one-dimensional heat flow at the sample centre (Jannot et al. 2016). In this study, the thermal resistance of the tested specimens was sufficient to neglect the resistance at

Table A.3: Thermal conductivity and resistance of geotextiles of various thicknesses measured using the hot-plate device.

Material	e (10^{-3})	T_1 (^oC)	T_{01} (^oC)	T_{02} (^oC)	λ $(W.m^{-1}.K^{-1})$	R_{th} $(W.K^{-1})$
3xR1	10.73	24.94	14.97	15.33	0.042	0.255
	9.73	25.32	15.88	15.29	0.043	0.226
	9.00	25.28	14.94	15.35	0.045	0.199
	8.00	25.09	14.94	15.34	0.046	0.173
	7.50	25.5	15.00	15.40	0.047	0.160
	6.67	24.76	15.04	15.47	0.047	0.142
R2	7.64	25.02	14.55	14.93	0.043	0.179
	6.96	24.99	14.69	15.07	0.043	0.161
	6.40	24.99	14.68	15.05	0.045	0.143
	5.54	25.33	14.71	15.11	0.047	0.118
	4.87	25.03	14.77	15.18	0.055	0.885
	4.43	24.79	14.94	15.37	0.064	0.695
V1	8.50	25.39	15.05	15.45	0.050	0.160
	8.00	25.18	15.13	15.53	0.053	0.141
	7.49	24.61	15.1	15.52	0.056	0.116
	6.50	24.98	15.14	15.58	0.059	0.101
V2	7.13	25.45	14.14	13.19	0.044	0.162
	6.52	24.82	14.19	13.93	0.049	0.134
	6.02	24.77	14.2	13.94	0.050	0.121
	5.47	24.67	14.22	13.95	0.050	0.109
	5.22	25.05	14.22	13.95	0.050	0.104
	5.02	24.76	14.22	13.93	0.051	0.982

the interface between the heating element and the specimens. Although samples R2, V1 and V2 geotextiles were sufficiently thick to neglect thermal contact resistance, sample R1 geotextile was thinner, so its thermal contact resistance cannot be neglected and it could not be tested in a single layer. Consequently, three layers of R1 geotextile were stacked for the measurement to give an initial thickness of 10.73 mm.

Several tests were done in which the samples were compressed to various thicknesses; the results are reported in Table A.3 and displayed in Figures A.7a and A.7b. All the thermal conductivities measurements of the various types of geotextile increases when their thickness decreases. The extremum values are 0.042 to 0.064 $W.m^{-1}.K^{-1}$ (Figure A.7a). Because the air thermal conductivity is lower than the resin thermal conductivity, the compressed geotextile, denser, exhibits a higher thermal conductivity.

Figure A.7b shows the geotextile thermal conductivity as a function of their normalized thickness e/e_0 to focus on other parameters than the initial thickness differences. According to their similar densities, the curves for V2, R1 and R2 geotextiles are expected to be

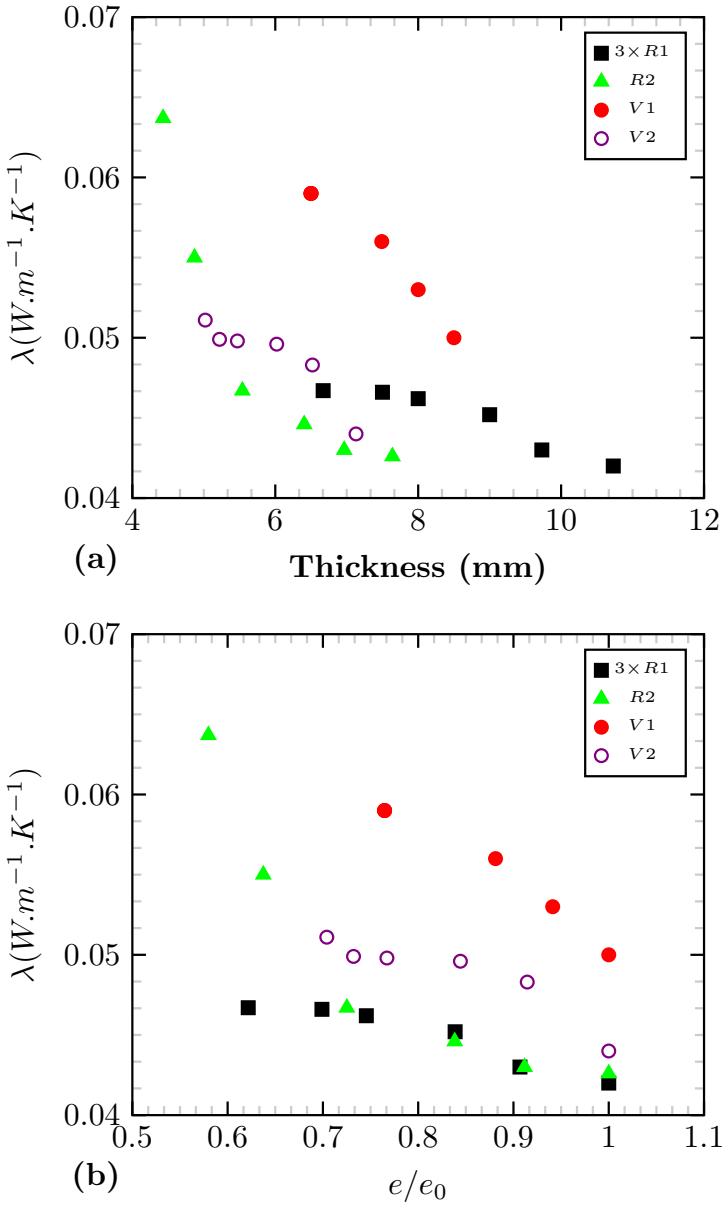

Figure A.7: Thermal conductivity of geotextiles as a function of (a) thickness and (b) normalized sample thickness. Measurements were made using the hot-plate device.

superimposed. However, the thermal conductivities of geotextiles V2 are higher than R2's ones. This difference can be partly explained by the fibre's nature. Indeed, the thermal conductivity of polypropylene resin (base constituent of V2) is 0.22 $W.m^{-1}.K^{-1}$ whereas the thermal conductivity of polyester resin is only 0.19 $W.m^{-1}.K^{-1}$. As a consequence, considering the thicknesses of the various products at a same density (using Figure A.2), the thermal conductivities of R1 and R2 geotextiles, made of a mixture of polypropylene and polyester, are lower than those of V1 and V2 (see Figure A.7a).

The thermal conductivity of geotextile V1, ranged from 0.050 to 0.059 $W.m^{-1}.K^{-1}$., is consistent with it higher density. Geotextile V1 was the densest of all geotextiles tested (about 150 $kg.m^{-3}$, see Table A.1), and this higher solid content reduces the thermal insulation properties due to the higher solids particle available for heat conduction, as manifested by the larger initial thermal conductivity (λ=0.050 $W.m^{-1}.K^{-1}$) compared with the other samples.

All the geotextiles present an apparent linear relationship between thermal conductivity and thickness at higher thicknesses. However, as the relationship between the density and the thickness is non-linear (Figure A.2), the evolution of the thermal conductivity is also non-linear as evidenced for the R2 geotextile in the Figure A.7.

A.3.2 Thermal conductivity of geotextiles vs. vertical stress

Figures A.8a shows the results of the short-term compression tests and Figure A.8b plots the vertical stress as a function of normalized thicknesses e/e_0 . As expected, the denser geotextile V1 resists compression better than the other geotextiles. For example, under 60 kPa, V1 maintains 79% of its initial thickness whereas R2 and V2 maintain only 69% and 75% of their initial thickness, respectively. The initial thickness of the three layers of geotextile R1 is greater than that of the other geotextiles, but the thickness decreases strongly with stress. Under 60 kPa, the 3×R1 thickness is only 64% of its initial value. These results are consistent with the static thickness measurements (Table A.1), which were also short-term measurements. Therefore, the compression method at constant speed may be used to determine the reduction in thickness even if creep phenomenon is neglected.

For each geotextile, the hot-plate tests give the thermal conductivities at different

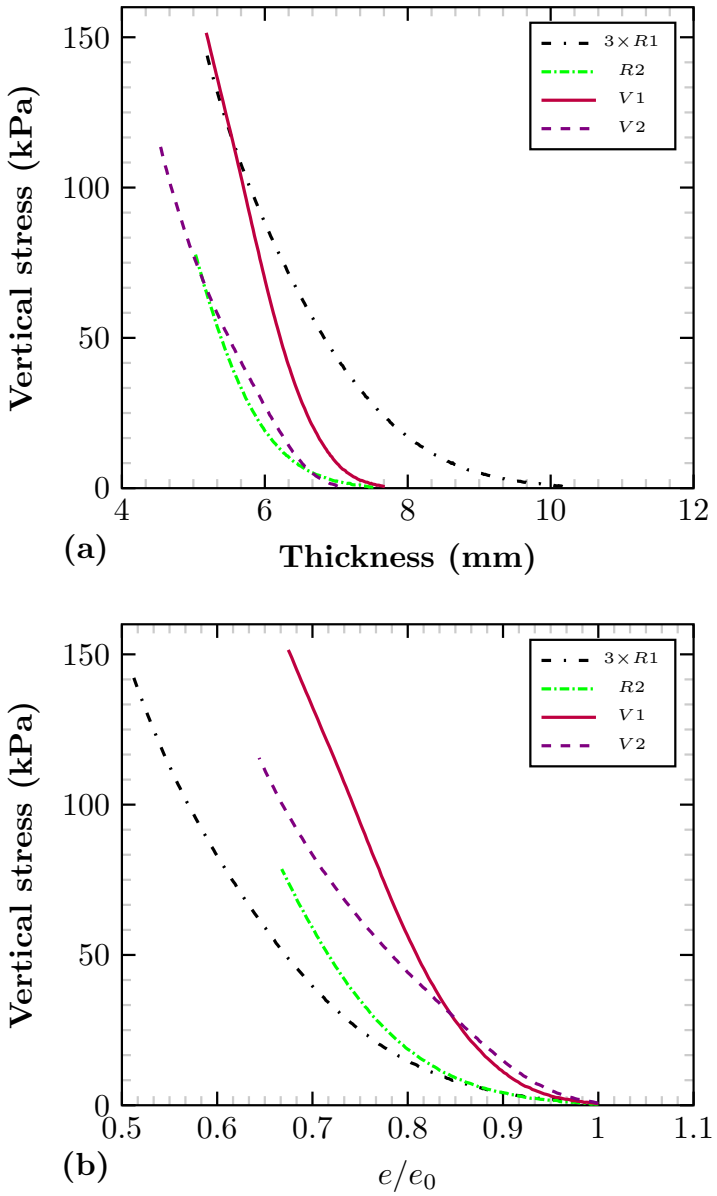

Figure A.8: Short-term vertical stress as a function of (a) thickness and (b) normalized sample thickness (creep phenomenon not measured).

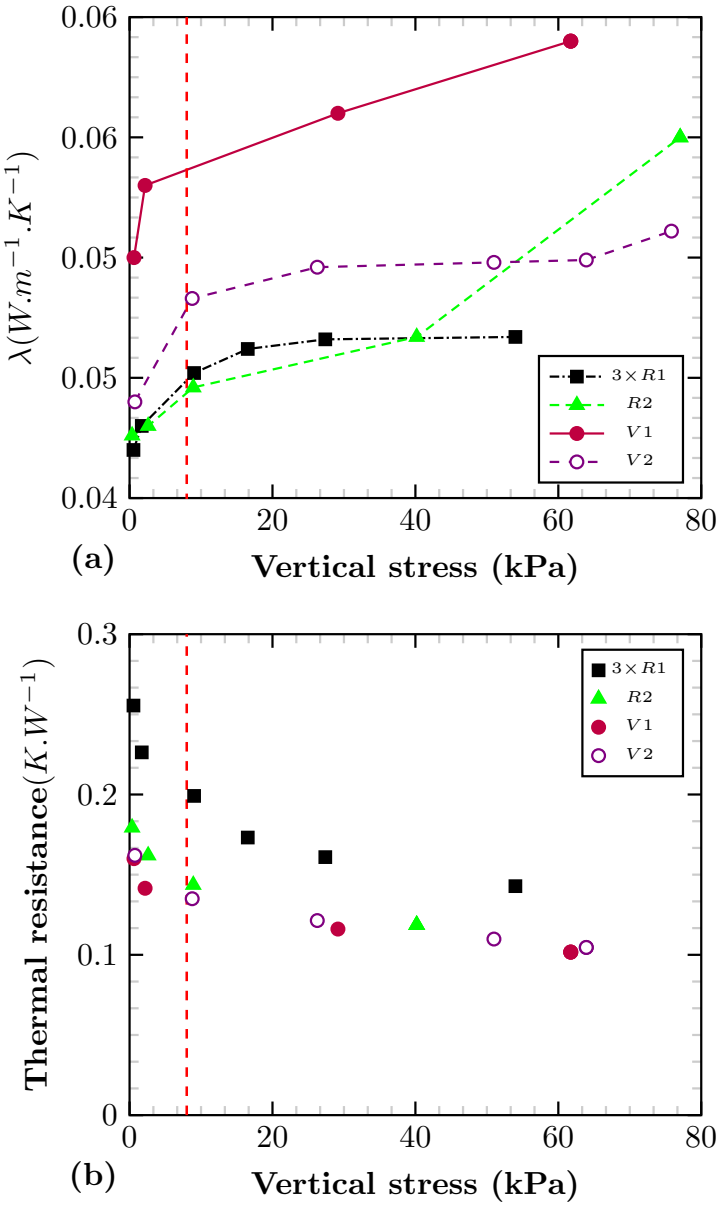

Figure A.9: (a) thermal conductivity and (b) calculated thermal resistance of geotextiles as a function of short-term vertical stress.

thicknesses (Figure A.7a) whereas the compression test links the vertical loads and the resulting thicknesses (Figure A.8a). These two curves were combined and presented in Figure A.9a as thermal conductivity variation versus vertical stress. As previously explained, increasing the vertical stress reduced the air content of the geotextiles, resulted in an increase of density, and consequently the thermal conductivity raised. These results are also consistent with the study of Ali et al. (2016) which indicate that the thermal conductivity of geosynthetic clay liners exhibit an increase with increasing vertical stress in the range of 0 to 100 kPa.

The non-linear relationship between density and thickness (Figure A.2) results in a faster increase of thermal conductivity at lower thicknesses (see for example R2 and V2 geotextiles). Moreover, the heat is mainly conducted along the fibres in the geotextiles, as a consequence, the thermal conduction is even greater since the fibres' contacts were frequent. Therefore it can be concluded that the geotextile texture may also impact the thermal conductivity.

Finally, knowing the thermal conductivity and thickness of a geotextile under a given stress, the thermal resistance of the geotextile can be calculated using Eq. (A.3). Figure A.9b shows that the thermal resistance decreases with increasing stress applied to the geotextile. This result allows us to calculate the expected thermal resistance of a geotextile under a covering layer. Considering a compacted soil layer (density 2 $Mg.m^{-3}$) with a thickness of 0.4 m, the vertical stress applied to the geotextile is of 8 kPa. The Figure A.9b shows that, on that conditions, the thermal resistances were of 0.199, 0.143, 0.134 and 0.141 $W.K^{-1}$ for samples 3×R1, R2, V2 and V1, respectively. As a result, 3×R1 sample has a higher thermal resistance but the setting up of three superimposed layers may cause stability problem on a sloping ground. Under that vertical stress, the thermal resistance of R2 and V1 are similar and V2 is a few lower than the other geotextiles.

A.3.3 Thermal conductivity of wet soil combined with geotextile

Table A.4 gives the results of thermal conductivity of compacted soil measured with the thermal-needle probe (KD2 Pro). The test was repeated twice at 20 ^{o}C. The average of the two measurements is 2.46 $W.m^{-1}.K^{-1}$. In this study to evaluate the thermal conductivity of soil-geotextile combinations, a theoretical approach was first conducted

Table A.4: Thermal conductivity of compacted soil measured by thermal-needle probe (KD2 Pro).

No.	T (^oC)	λ ($W.m^{-1}.K^{-1}$)
1	23.25	2.419
2	20.98	2.503

Table A.5: Equivalent thermal conductivity calculated with different soil and geotextile associations.

Simulation nb.	**Configuration**	**Thicknesses (m)**		**Thermal conductivities** ($W.m^{-1}.K^{-1}$)		
		e_{soil}	$e_{Geotextile}$	λ_{soil}	$\lambda_{Geotextile}$	$\lambda_{Eq.}$
1	unconfined	0.02	0.00744	2.46	0.042	0.148
2	confined	0.02	0.00600	2.46	0.046	0.181
3	hydric exchange	0.02	0.00744	2.46	0.120	0.391

and then experimental measurements were performed.

A.3.3.1 Theoretical estimation

If the thermal conductivities of the soil and geotextile are known, the following equation is used to estimate the equivalent thermal conductivity for a combination of soil and geotextile:

$$\lambda_{Eq} = \frac{e_{(soil+Geotex)}}{\frac{e_{soil}}{\lambda_{soil}} + \frac{e_{Geotex}}{\lambda_{Geotex}}} \tag{A.7}$$

where e_{soil} and e_{Geotex} are the thicknesses of the soil and the geotextile (m) and λ_{soil} and λ_{Geotex} are the thermal conductivities of the soil and the geotextile ($W.m^{-1}.K^{-1}$), respectively. Several simulations of the system were done using the input parameters listed in Table A.5. Given the initial thicknesses and thermal conductivities of the soil sample and geotextile R2 (simulation 1), the expected equivalent thermal conductivity is 0.148 $W.m^{-1}.K^{-1}$. Considering the compression of R2 under a 0.4 m soil layer, its equivalent thermal conductivity is 0.181 $W.m^{-1}.K^{-1}$. This value is assumed if mass transfer does not occur between the two materials and a perfect interface is maintained between soil and geotextile. Laboratory experiments are required to assess the consequences of an interaction (i.e. water transfer) between the soil and the geotextiles and/or of an interface with thermal resistance.

Table A.6: Thermal conductivity of compacted soil + geotextile measured with the hot-plate device.

Test nb.	Configuration (Fig. 5)	Material	e ($10^{-3}m$)	$T1$ (^oC)	$T2$ (^oC)	$T3$ (^oC)	λ ($W.m^{-1}.K^{-1}$)
1	b	Soil and R2	2.7	14.84	25.15	14.37	0.42
2	b	Soil and R2	2.7	15.31	25.25	14.86	0.51
3	c	Wet R2	7.4	15.03	24.65	15.31	0.12
4	c	Wet R2	7.3	15.53	25.03	14.98	0.12
5	d	Soil, geofilm and R2	2.8	14.9	24.64	14.8	0.14

A.3.3.2 Experimental measurement

To measure the thermal conductivity of the soil/geotextile (R2) bilayer, both materials were wrapped together in a cellophane film and placed in the hot-plate device (configuration b, Figure A.4). The average thermal conductivity from tests 1 and 2 (Table A.6) is 0.465 $W.m^{-1}.K^{-1}$, which is four times greater than the theoretical value (0.148 $W.m^{-1}.K^{-1}$). The difference comes from the generation of water flow from soil towards the geotextile. After the test, the soil and the geotextile were weighed. On one hand, the final mass of the geotextile was 30.55 g whereas its initial mass was only 8.5 g. On the other hand, the soil sample initially prepared at a water content of 16.3 % reached only 10.6 % at the end of the test. This difference might result from water absorption by the geotextile and/or water flow initiated by the heat flux from the soil towards the geotextile.

Immediately after finishing these tests, the wet geotextile was tested alone (configuration c, Figure A.4). The thermal conductivity was 0.12 $W.m^{-1}.K^{-1}$, which is three times larger than its initial value of 0.04 $W.m^{-1}.K^{-1}$ (Table A.6, test 3). A similar result was obtained from another geotextile R2 specimen sprayed with water to reach a total mass of 30 g (Table A.6, test 4).

Using λ_{R2}=0.12 $W.m^{-1}.K^{-1}$ in the equation for the wet geotextile R2 (Eq. (A.7), simulation 3, Table A.5), the equivalent thermal conductivity reached 0.391 $W.m^{-1}.K^{-1}$, which is close to the experimental value of 0.45 $W.m^{-1}.K^{-1}$. These results show how humidification affects the insulating efficiency of a geotextile. Because water thermal conductivity (0.6 $W.m^{-1}.K^{-1}$) is higher than the air (0.02 $W.m^{-1}.K^{-1}$), when air is replaced by water in the porosity of any material, it thermal conductivity increased.

Singh and Bouazza (2013) indicated that the thermal conductivities of the nonwoven continuous filament needle punched polyester dry geotextiles were in the range 0.07 to 0.13 $W.m^{-1}.K^{-1}$in the dry state in place of 0.41 to 0.83 $W.m^{-1}.K^{-1}$ after immersion in water. Ali et al. (2016) added that the variability of water distribution in partially hydrated geosynthetic clay liner has been identified as a factor, which may affect their thermal conductivity.

A.4 Conclusions

The primary goal of this study was to measure the thermal conductivity and resistance of nonwoven needle-punched geotextiles, taking into consideration the effect of an applied vertical stress in the short term. Although the geotextiles must be sufficiently dense to resist to a moderate vertical stress but this deformation lead to higher thermal conductivities. Several geotextiles with different densities and fibre composition (virgin or recycled) were tested. The thermal conductivities ranged from 0.04 to 0.06 $W.m^{-1}.K^{-1}$. In addition, the water content significantly affected the thermal parameters. The thermal conductivity of moistened geotextiles were three times larger than that of dry geotextiles. In the field, the geotextile may be moistened by precipitations and/or by vapour migration from the warm heat storage area. Consequently, a geotextile is suggested to be sandwiched between two geofilms before using as an isolation layer.

Appendix B

Résumé étendu

B.1 Introduction

Le stockage de chaleur dans des milieux tels que les aquifères (Lee 2010), les roches (Becattini et al. 2017), les sols naturels et compactés (Elminshawy et al. 2017) est susceptible de réduire la dépendance vis-à-vis des combustibles fossiles et de contribuer à la production d'énergie renouvelable. La chaleur est stockée pendant l'été, pour être conservée et utilisée pendant la période hivernale. La chaleur, par exemple issue de l'énergie solaire, peut être emmagasiné dans le sol grâce à des tubes placés à la verticale ou à l'horizontales. En raison du rapport coût-bénéfice et du moindre impact environnemental, l'échangeur de chaleur horizontal est plus avantageux que l'échangeur vertical, même s'il nécessite plus d'espace (Gan 2013). Dans ce contexte, les remblais présentent un grand potentiel d'intégration de ces échangeurs. En effet, les remblais sont constitués de couches de sol compactées les unes au-dessus des autres jusqu'à atteindre le niveau souhaité pour la construction de routes, d'autoroutes, de chemins de fer ou encore pour la construction d'un bâtiment. Ces ouvrages représentent des volumes importants de matériaux anthropisés pouvant être valorisés. Le premier chapitre de cette thèse a été consacré à la présentation du concept de stockage d'énergie thermique et aux questions connexes à ce sujet.

La bonne conception d'un remblai pour stocker l'énergie thermique nécessite de connaitre l'état de compactage du sol, ses propriétés thermiques et également la position des échangeurs de chaleur (profondeur, configuration et espacement). Les sols compactés sont généralement non saturés (degré de saturation entre 85 et 95%) ce qui complique l'estimation ou la mesure de leurs propriétés thermiques (la capacité thermique

volumétrique, la conductivité thermique et la diffusivité thermique) à l'état non saturé, a fortiori en cas de modification cyclique de sa température. Le développement d'une méthode d'estimation et de mesure fiable pour déterminer les propriétés thermiques du sol est important pour évaluer la faisabilité de ces structures. Ce point fait l'objet du chapitre 2 de cette thèse.

Si l'on considère un remblai support de stockage, le sol compacté sera soumis à des variations de température quotidiennes et saisonnières sur ses faces externes, et en son sein via les échangeurs de chaleur. Ces variations cycliques de température (5 à 50 ^oC) peuvent modifier les caractéristiques thermo-hydro-mécanique du sol compacté. Pour ce qui concerne sa stabilité, les réponses mécaniques les plus importants d'un remblai sont le tassement et la résistance au cisaillement. Plusieurs études ont montré que les variations de température peuvent entraîner des variations volumétriques du sol plus ou moins importantes selon le matériau et l'historique des contraintes du sol (Di Donna and Laloui 2013). Par conséquent, même si le sol compacté peut être sélectionné sur la base de ses performances thermiques, son comportement mécanique dans différents états (saturé et non saturé) et sous différentes contraintes (à différentes profondeurs) doit être étudié. Ces aspects sont au cœur des expérimentations décrites dans le chapitre 3 de cette thèse.

Afin de prévoir le comportement thermo-hydro-mécanique des remblais géothermiques, des études numériques peuvent être menées en utilisant des codes à éléments finis ou à différences finies. Cependant, le transfert de masse dans le sol dû à la variation de température n'est que rarement étudié. Souvent, le sol est supposé être homogène avec des propriétés thermiques constantes, alors que le transfert thermo-hydraulique est susceptible de modifier les propriétés thermiques et mécaniques des sols compactés. Par conséquent, au stade de la conception, une simulation thermo-hydro-mécanique couplée serait nécessaire pour étudier la stabilité et la faisabilité de la structure en tant que support de stockage. Un exemple de modélisation est proposé en chapitre 4 de cette thèse.

Ainsi, quatre chapitres sont développés dans cette étude pour aborder les aspects mentionnés ci-dessus. Les résultats de chaque chapitre sont résumés ci-après.

B.2 Etat de l'art sur le stockage de l'énergie thermique dans les sols

Le chapitre bibliographique est axé sur la compréhension de l'efficacité énergétique des systèmes de stockage de chaleur. Les mécanismes du transfert de chaleur et de masse ainsi que les propriétés thermiques du sol sont présentés en détail. L'évolution de ces propriétés en fonction de la composition physico-chimique des sols est également étudiée. Ensuite, une section répertorie et analyse les études portant sur les performances mécaniques de sols compactés soumis à des variations de température. Les propriétés hydriques, les paramètres de consolidation et la résistance au cisaillement du sol sont développés en particulier. Enfin, les modèles théoriques et constructifs existants qui pourraient être utilisés pour réaliser une simulation thermo-hydro-mécanique couplée du système de stockage sont présentés. Ce chapitre permet de souligner les questions les plus importantes concernant le stockage de l'énergie thermique dans un remblai qui ont servi de base aux travaux de recherche présentés dans les chapitres 2, 3 et 4.

B.3 Mesure des propriétés thermiques d'un sol compacté non saturé par la méthode d'estimation de la fonction de transfert

Afin d'estimer les propriétés thermiques d'un sol compacté à l'état non saturé en laboratoire, plusieurs capteurs de température (PT100) ont été mis en place en différents points d'un massif de sol compacté en 11 couches dans une cuve cylindrique thermorégulée (hauteur de 0,8 m et diamètre de 0,6 m) (Figure B.1). Le sol étudié est un limon typique des matériaux utilisés en France pour la construction de remblais. Trois cycles de température successifs sont appliqués sur les bords de la cuve dans un intervalle de 20 à 50 ^oC. Les températures sont enregistrées par les sondes tout au long des cycles.

Ensuite un modèle analytique inverse basé sur l'équation de conduction thermique radiale unidimensionnelle est proposé pour estimer la diffusivité thermique en utilisant la variation de température entre deux capteurs de température. La diffusivité thermique (α) estimée permet de calculer la conductivité thermique (λ) en utilisant l'équation 1. La

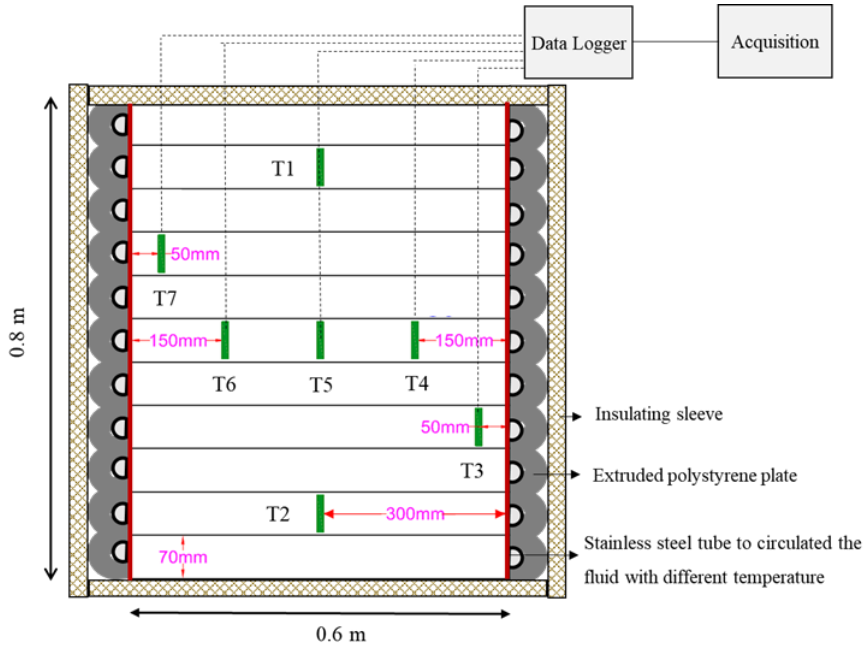

Figure B.1: Placement des sondes dans différentes couches de sol

Table B.1: Propriétés thermiques du sol compacté, T_{in} est la variation de température enregistrée par le capteur positionné près de la source de chaleur et T_{out} est la variation de température enregistrée par le capteur plus proche du centre de la cuve, R_{in} est la distance d'entrée depuis le centre du cylindre, R_{out} est la distance de sortie depuis le centre du cylindre.

Tr_2	Tr_1	r_2 (m)	r_1 (m)	C_v $(J.m^{-3}.K^{-1})$	1^{st} cycle		2^{st} and 3^{st} cycles	
					$10^{-7}\alpha$ $(m^2.s^{-1})$	λ $(W.m^{-1}.K^{-1})$	$10^{-7}\alpha$ $(m^2.s^{-1})$	λ $(W.m^{-1}.K^{-1})$
T3	T4	0.25	0.15	2.64×10^6	10.0	2.64	9.9	2.61
T4	T5	0.15	0		10.4	2.74	10.3	2.71

capacité thermique volumétrique (C_v) est mesurée en laboratoire.

$$\alpha = \frac{\lambda}{C_v} \tag{B.1}$$

Le tableau B.1 indique les valeurs des diffusivités thermiques et de la conductivité thermique pour deux sections sélectionnées au cours du premier et du deuxième chauffage.

Dans un second temps, la conductivité thermique calculée est comparée à deux méthodes classiques de laboratoire (une méthode en régime permanent et une méthode en régime transitoire). Les valeurs estimées de la conductivité thermique mesurée par la méthode numérique (2,51 $W.m^{-1}.K^{-1}$) et par la méthode du fil chaud (2,46 $W.m^{-1}.K^{-1}$) sont très proches (écart de 2%). En revanche, l'écart entre les valeurs obtenues par la méthode numérique et la méthode de la plaque chaude centrée (1,97 $W.m^{-1}.K^{-1}$) est plus élevé de

20%.

La faible valeur obtenue avec la méthode de la plaque chaude centrée peut s'expliquer par la présence d'une fine couche d'air entre l'éprouvette de sol et l'élément thermique qui constitue une résistance thermique (Jannot et al. 2010). Cela réduit le flux de chaleur à travers l'éprouvette de sol et réduit par conséquent la conductivité thermique du sol. De plus, la plaque chaude est une méthode à régime constant ainsi, le temps nécessaire pour atteindre l'équilibre de température (48 à 144 heures) est élevé, nettement supérieur à la durée d'un essai avec une méthode transitoire (10 minutes). Au cours de l'essai une migration de l'eau interstitielle peut se produire au sein de l'éprouvette voire une diminution de la teneur en eau.

Ainsi, en mesurant la température in situ à l'aide de deux capteurs de température, les propriétés thermiques du sol peuvent être estimées à tout moment à l'aide de ce modèle analytique. Par exemple, dans un remblai, pendant la saison de stockage de la chaleur, le flux thermique radial peut être appliqué en considérant la forme cylindrique des boucles d'échangeur de chaleur (de la surface des tubes vers une surface cylindrique arbitraire). Ensuite, deux capteurs de température doivent être placés à des distances différentes des tubes échangeurs de chaleur pour mesurer la température. La distance entre les deux capteurs doit être mesurée avec précision. Cette méthode pourrait donc permettre d'estimer l'efficacité du futur stockage de chaleur dans le sol.

B.4 Effet des variations de température monotones et cycliques sur le comportement mécanique d'un sol compacté

Ce chapitre présente les résultats d'essais expérimentaux pour étudier la consolidation et le comportement au cisaillement d'un sol compacté soumis à des variations de température monotones (5, 20 et 50 ^oC) et cycliques (5 à 50 ^oC) en utilisant des dispositifs œdométriques et de cisaillement direct à température contrôlée. D'après les résultats, présentés en figure B.2, l'indice de compression et l'indice de gonflement restent inchangés lors de l'augmentation de la température de 5 à 50 ^oC. En revanche la pression apparente de préconsolidation diminue.

La réponse volumétrique du sol compacté due aux cycles de température dépend de

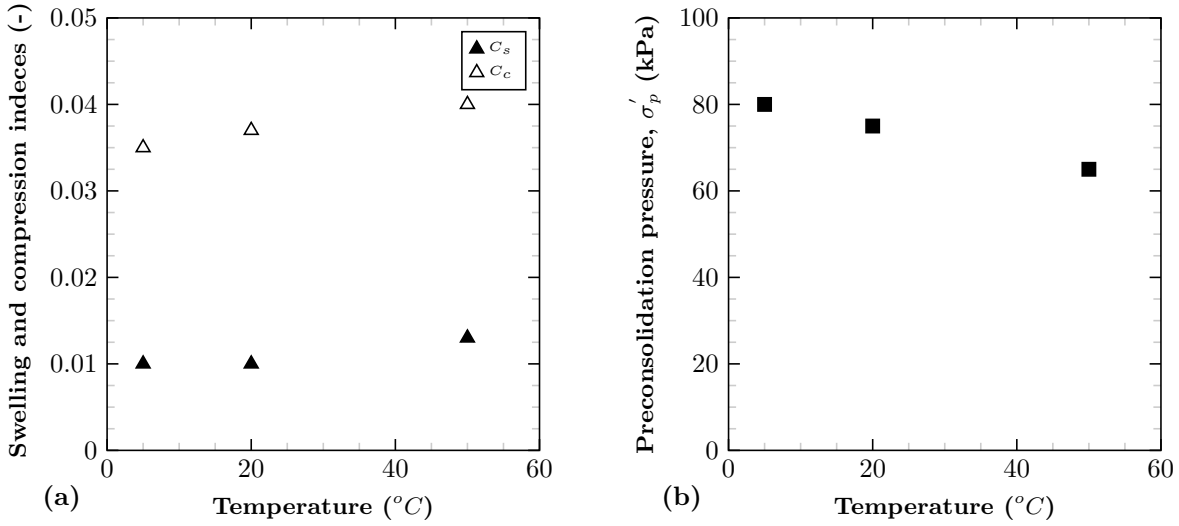

Figure B.2: (a) Effet de la température sur l'indice de gonflement C_s et l'indice de compression C_c, (b) Effet de la température sur la pression de préconsolidation ($\sigma_p^{'}$).

l'histoire de chargement du matériau. À l'état surconsolidé (OCR>1), une déformation réversible a été observée tandis qu'à l'état normalement consolidé (OCR=1), les cycles de température induisent une contraction plastique thermique (Figure B.3).

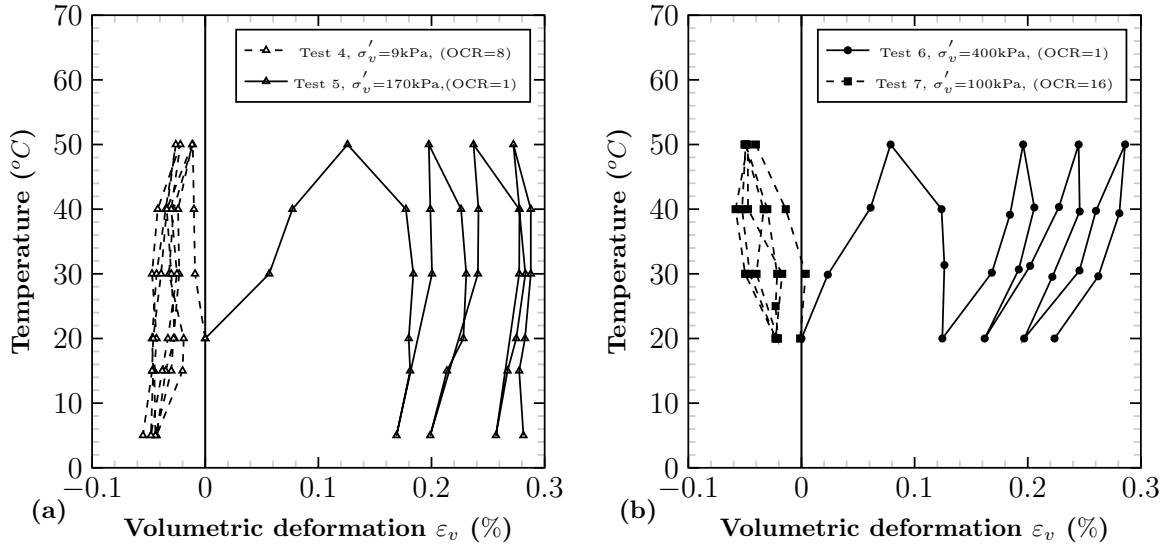

Figure B.3: Déformation volumétrique pendant les cycles thermiques sous a) 9 kPa (OCR=8) et 170 kPa (OCR=1) b) 400 kPa(OCR=1) et 100 kPa (OCR=16).

Les résultats des essais de cisaillement direct ont montré que le chauffage de 20 à 50 ^oC et les cycles de température (5 à 50 ^oC) ont un effet négligeable sur la résistance au cisaillement. En revanche, le refroidissement de 20 à 5 ^oC diminue la résistance au cisaillement sous des contraintes normales plus élevées (200 kPa). Quel que soit le chemin thermo-mécanique appliqué, la cohésion augmente légèrement en comparaison avec l'état

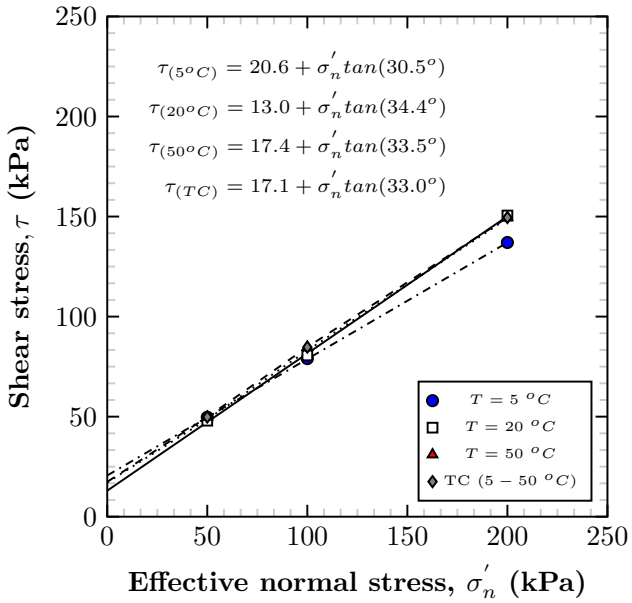

Figure B.4: Contrainte de cisaillement contre la contrainte normale effective à T = 5 ^oC, T = 20 ^oC, T = 50 ^oC et après 5 TC (cycles de température, 5-50 ^oC).

initial et les angles de frottement restent inchangés, ce qui est avantageux pour la portance et la stabilité des pentes des remblais (Figure B.4). Par conséquent, sur la base des trajectoires thermo-mécaniques étudiées dans ce travail de recherche, on peut conclure que dans la phase de construction, les boucles d'échangeurs de chaleur horizontales peuvent être placées à différentes profondeurs dans un remblai.

Toutefois, en raison des interactions sol-atmosphère le long des surfaces supérieures et latérales des remblais, la perte de chaleur pourrait être considérable. C'est la raison pour laquelle il convient de prévoir, dès la conception, d'adapter les profondeurs d'installation aux interactions attendues. De plus, l'ajout d'un matériau d'isolation pourrait s'avérer intéressant. L'utilisation d'outils numériques, tels que présentés dans la partie suivante, permet d'avancer sur ce point.

B.5 Calcul de performances d'un échangeur de chaleur horizontal en sol compacté

Le chapitre 5 évalue la performance thermique d'un sol de remblai compacté en utilisant une simulation numérique hydro-thermique validée qui tient compte de l'interaction atmosphère-sol et de la profondeur d'installation des échangeurs de chaleur horizontaux dans

le sol. Les simulations numériques apportent des précisions sur le choix du sol de remblai et la profondeur d'installation des échangeurs de chaleur. Le sol précédemment étudié est utilisé comme matériau de substitution du sol en place. Les propriétés hydriques et thermiques du matériau sont estimées en laboratoire, puis utilisées dans le code numérique choisi. Une attention particulière a été portée aux interactions atmosphère-sol et sol-échangeur.

Le modèle d'éléments finis utilisé est établi dans COMSOL, il tient compte:

- du bilan énergétique à la surface du sol (Chen and Buchberger 2018);
- du bilan hydrique à la surface du sol (Dietrich et al. 2016);
- du transfert hydrothermal dans le sol (Van Genuchten 1980) et
- du transfert de chaleur dans les tubes (Tang and Nowamooz 2020).

La comparaison des simulations numériques réalisées pour une installation dans le sol compacté et les matériaux locaux montre une amélioration de 18,5 % de la performance thermique lorsque l'échangeur est installé dans le sol compacté. Pour améliorer la performance thermique du système, deux scénarios de stockage de chaleur (StoA et Sto50) à trois profondeurs d'installation différentes (1, 1.50 et 2 m) ont été étudiées (Figure B.5).

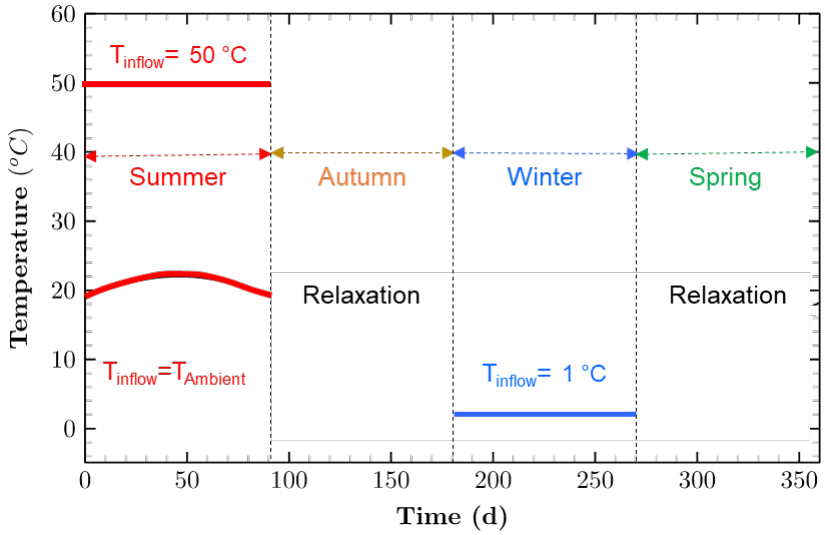

Figure B.5: Les deux scénarios de stockage différent seulement par la température d'entrée en été, elle est égale à la température ambiante dans le scénario StoA et de de 50 ^oC dans le scenario Sto50. En automne, le système était en relaxation; en hiver, la température d'entrée est de 1^oC et au printemps, le système est à nouveau en relation.

Les résultats montrent qu'une température du fluide d'entrée de 50 ^oC en été (Sto50) augmente fortement la performance du système (13,7 à 41,4%) alors que l'amélioration

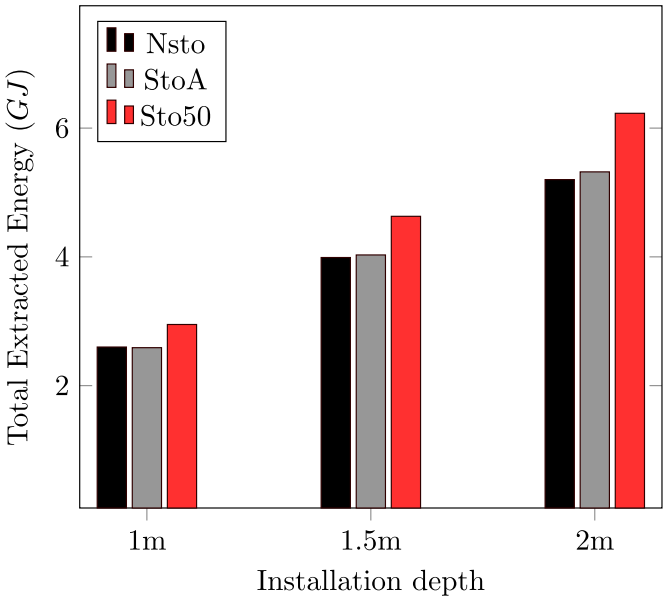

Figure B.6: Comparaison entre les scénarios de stockage de la chaleur (StoA et Sto50), et le scénario sans stockage (Nsto) à trois profondeurs d'installation différentes.

par rapport à un système sans stockage (NSto) est moins significative (0 à 4,8%) lorsque la température au cours de l'été correspond à la température ambiante (StoA) (Figure B.6). Par ailleurs, une perte de chaleur considérable a été observée pendant les saisons de relaxation et de déstockage. L'augmentation de la profondeur d'installation améliore la performance énergétique mais augmente également les coûts d'installation.

B.6 Conclusion

Dans cette thèse, différentes méthodes de stockage de l'énergie thermique dans le sol ont été présentées dans le premier chapitre, puis comparées. Le stockage de l'énergie thermique dans les sols à l'aide d'échangeurs de chaleur horizontaux est une méthode reconnue comme efficace et vertueuse pour l'environnement. Afin de pallier à son principal inconvénient qui est l'importante surface de sols occupée, son incorporation dans les remblais est étudiée. Pour cela, l'étude s'est concentrée sur les performances thermiques d'un remblai pour stocker de la chaleur.

La mesure des propriétés thermiques d'un sol non saturé est complexe, pour les déterminer in situ, un modèle analytique inverse est proposé en chapitre 2. La diffusivité thermique y est estimée par une méthode "température/température" basée sur l'estimation d'une fonction de transfert de chaleur. Cette méthode ne nécessite que des

mesures ponctuelles de température au cours du temps en deux endroits différents du massif. La conductivité thermique a ensuite été estimée à l'aide de la capacité thermique volumétrique mesurée par calorimétrie. Cette valeur a été comparée à la valeur obtenue avec une méthode à l'état transitoire et les résultats montrent écart de 2%.

Le principal avantage de cette méthode est son applicabilité pour les mesures in situ en tenant compte de la conduction thermique transitoire dans la direction radiale. Cela permettrait de contrôler l'efficacité des systèmes de stockage d'énergie thermique tels qu'un remblai ou d'autres configurations dans les sols.

Après avoir établi l'état de compactage du sol présentant des propriétés thermiques optimales pour le stockage, les performances mécaniques du sol compacté pendant la durée de vie du remblai ont été étudiées. Le chapitre 3 présente les dispositifs œdométriques et de cisaillement direct à température contrôlée utilisés pour étudier la consolidation et la résistance au cisaillement du sol compacté. L'effet de variations de température monotones (5, 20 et 50 ^oC) et cycliques (5 à 50 ^oC) a été mesuré sur des éprouvettes saturées, c'est à dire à l'état de stabilité le plus critique. D'après les résultats des essais œdométriques, l'effet de la température sur le tassement global du talus peut être considéré comme négligeable en raison de très faibles différences d'indice de compression.

Afin de simuler différentes profondeurs d'installation des échangeurs (2,5 à 10 m), des essais sont réalisés sous différentes contraintes verticales (50 à 200 kPa). Les variations de volumes mesurées au cours de l'application de cycles de variations de température sont très faibles et peuvent être considérées comme négligeable au-delà du 1er cycle.

Les résultats des essais de cisaillement direct ont montré que le chauffage de 20 à 50 ^oC et les cycles de température (5 à 50 ^oC) avaient un effet négligeable sur les caractéristiques de cisaillement, tandis que le refroidissement de 20 à 5 ^oC diminuait la contrainte de cisaillement critique si la contrainte normale atteignait 200 kPa. Ce résultat suggère qu't une surveillance des températures du massif au cours de la période hivernale est nécessaire.

Les résultats de simulations numériques ont montré que le sol de remblai compacté augmentait de 18,5% la performance thermique de l'échangeur de chaleur horizontal en comparaison avec un sol naturel non compacté (Alsace, France). Deux scénarios de stockage de chaleur à trois profondeurs d'installation différentes ont également été étudiés. Les résultats ont montré qu'une température du fluide d'entrée de 50 ^oC en été augmenterait

fortement la performance du système de 13,7% à 41,4%, alors que l'amélioration serait moins significative (0% à 4,8%) lorsque la température d'entrée correspond seulement à la température ambiante. De meilleures performances sont également obtenues lorsque l'échangeur est placé à une profondeur plus importante. Les simulations numériques, prenant en compte l'interaction sol-atmosphère, montrent que l'échangeur de chaleur horizontal doit être placé à une distance suffisante des surfaces supérieure et latérales du remblai pour limiter les pertes de chaleur afin de garantir un bon équilibre entre les apports et les pertes. Cette distance devra être calculée en fonction des capacités thermiques du sol utilisé et des conditions climatiques in situ.

Les points suivants peuvent être proposés pour des études plus approfondies sur le stockage de l'énergie thermique dans un remblai:

• Lors des tests de détermination des propriétés thermiques (test de la plaque chaude centrée) et au cours des essais en cuve thermo régulée, des migrations d'eau dues aux gradients de température ont été observées. Ces migrations pourraient affecter les performances thermomécaniques du sol compacté. Par conséquent, des recherches supplémentaires sont nécessaires pour étudier quantitativement la migration de l'eau causée par les variations de température, par exemple à l'aide de l'imagerie par résonance magnétique (IRM).

• Des études approfondies du comportement micro-structurel d'un sol compacté sont nécessaires pour mieux expliquer l'évolution des caractéristiques mécaniques dues aux variations de température.

• Le comportement thermo-hydro-mécanique du sol compacté à l'état non saturé doit être étudié pour évaluer la contribution positive de l'état non saturé à la stabilité globale du système. Dans ce contexte, une modélisation numérique thermo-hydro-mécanique couplée serait nécessaire.

• La poursuite du développement du modèle numérique qui prendrait en compte la géométrie exacte du remblai pourrait permettre d'estimer la performance thermique du système malgré les interactions sol-atmosphère.

• Les différentes formes et dispositions des boucles horizontales des échangeurs de chaleur pourraient être modélisées par des simulations numériques. De même, les flux de chaleur à l'entrée pourraient être affinés pour représenter au mieux les quantités de chaleurs apportées par des panneaux solaires par exemple.

• La performance thermique globale d'un matériau d'isolation peut être étudiée pour réduire les pertes de chaleur pendant les saisons de charge et de décharge thermiques. Par exemple, les géotextiles peuvent être une bonne solution pour l'isolation du sol (voir l'annexe A consacrée à l'évaluation des propriétés thermiques des géotextiles comme couche d'isolation pour un remblai).

• L'étude du comportement thermo-hydro-mécanique de différents sols naturels et traités pourrait contribuer à réduire les coûts de transport des matériaux de construction.

• La réalisation d'un remblai expérimental en sol compacté in situ équipé de différents capteurs pour mesurer la température, la teneur en eau et les déformations mécaniques serait recommandée pour une meilleure compréhension des performances thermiques et mécaniques d'un remblai pour stocker de la chaleur.

Bibliography

(n.d.).

Abu-Hamdeh, N. H. (2003). Thermal properties of soils as affected by density and water content, *Biosystems engineering* **86**(1): 97–102.

Abu-Hamdeh, N. H., Khdair, A. I. and Reeder, R. C. (2001). A comparison of two methods used to evaluate thermal conductivity for some soils, *International Journal of Heat and Mass Transfer* **44**(5): 1073–1078.

Abu-Hamdeh, N. H. and Reeder, R. C. (2000). Soil thermal conductivity effects of density, moisture, salt concentration, and organic matter, *Soil science society of America Journal* **64**(4): 1285–1290.

Abuel-Naga, H., Bergado, D., Bouazza, A. and Ramana, G. (2007). Volume change behaviour of saturated clays under drained heating conditions: experimental results and constitutive modeling, *Canadian Geotechnical Journal* **44**(8): 942–956.

Abuel-Naga, H., Bergado, D., Ramana, G., Grino, L., Rujivipat, P. and Thet, Y. (2006). Experimental evaluation of engineering behavior of soft bangkok clay under elevated temperature, *Journal of geotechnical and geoenvironmental engineering* **132**(7): 902–910.

Abuel-Naga, H., Bergado, D., Soralump, S. and Rujivipat, P. (2005). Thermal consolidation of soft bangkok clay, *Lowland Technology International Journal* **7**(1): 13–22.

Adamovsky, D., Neuberger, P. and Adamovsky, R. (2015). Changes in energy and temperature in the ground mass with horizontal heat exchangers—the energy source for heat pumps, *Energy and Buildings* **92**: 107–115.

Adams, W., Watts, G. and Mason, G. (1976). Estimation of thermal diffusivity from field observations of temperature as a function of time and depth, *American Mineralogist* **61**(7-8): 560–568.

AFNOR (1999a). Nf p 94-093 sols: Reconnaissance et essais détermination des références de compactage d 'un matériau. essai proctor normal-essai proctor modifié [soils: Investigation and testing. determination of the compaction characteristics of a soil. standard proctor test. modified proctor test].

AFNOR (2015). 10318-1: Geosynthetic - part 1: Terms and definitions., *European Committee for Standardization, Brussels.* .

AFNOR (2016). 9863-1: Geosynthetics - determination of thickness at specified pressures., *European Committee for Standardization, Brussels.* .

AFNOR, P. (1993). 94-051: Soil: investigation and testing, *Determination of Atterberg's limits, Liquid limit test using cassagrande apparatus, Plastic limit test on rolled thread* .

AFNOR, P. (1999b). 94-093: Soils: Investigation and testing-determination of the compaction characteristics of a soil-standard proctor test-modified proctor test, *Association Française de Normalisation* .

Al-Ajlan, S. A. (2006). Measurements of thermal properties of insulation materials by using transient plane source technique, *Applied thermal engineering* **26**(17-18): 2184–2191.

Ali, M. A., Bouazza, A., Singh, R. M., Gates, W. P. and Rowe, R. K. (2016). Thermal conductivity of geosynthetic clay liners, *Canadian Geotechnical Journal* **53**(9): 1510–1521.

Allen, R. G., Jensen, M. E., Wright, J. L. and Burman, R. D. (1989). Operational estimates of reference evapotranspiration, *Agronomy journal* **81**(4): 650–662.

Alonso, E. E., Gens, A. and Josa, A. (1990). A constitutive model for partially saturated soils, *Géotechnique* **40**(3): 405–430.

Alonso, E., Vaunat, J. and Gens, A. (1999). Modelling the mechanical behaviour of expansive clays, *Engineering geology* **54**(1-2): 173–183.

An, N. (2017). *Numerical investigation of soil-atmosphere interaction: application to embankments of treated soils*, PhD thesis.

Asgari, B., Habibi, M. and Hakkaki-Fard, A. (2020). Assessment and comparison of different arrangements of horizontal ground heat exchangers for high energy required applications, *Applied Thermal Engineering* **167**: 114770.

Asrar, G. and Kanemasu, E. (1983). Estimating thermal diffusivity near the soil surface using laplace transform: Uniform initial conditions 1, *Soil Science Society of America Journal* **47**(3): 397–401.

Astm, D. (1994). 3080-90: Standard test method for direct shear test of soils under consolidated drained conditions, *Annual book of ASTM standards* **4**: 290–295.

ASTM, E. (2000). Standard practice for classification of soils for engineering purposes (unified soil classification system), *Annual book of ASTM standards* .

Baillieux, P., Schill, E., Edel, J.-B. and Mauri, G. (2013). Localization of temperature anomalies in the upper rhine graben: insights from geophysics and neotectonic activity, *International Geology Review* **55**(14): 1744–1762.

Baldi, G., Hueckel, T. and Pellegrini, R. (1988). Thermal volume changes of the mineral–water system in low-porosity clay soils, *Canadian geotechnical journal* **25**(4): 807–825.

Barry-Macaulay, D., Bouazza, A., Singh, R. M., Wang, B. and Ranjith, P. (2013). Thermal conductivity of soils and rocks from the melbourne (australia) region, *Engineering Geology* **164**: 131–138.

Becattini, V., Motmans, T., Zappone, A., Madonna, C., Haselbacher, A. and Steinfeld, A. (2017). Experimental investigation of the thermal and mechanical stability of rocks for high-temperature thermal-energy storage, *Applied Energy* **203**: 373–389.

Beier, R. A. (2018). Use of temperature derivative to analyze thermal response tests on borehole heat exchangers, *Applied Thermal Engineering* **134**: 298–309.

Beier, R. A. and Holloway, W. A. (2015). Changes in the thermal performance of horizontal boreholes with time, *Applied Thermal Engineering* **78**: 1–8.

Bilskie, J. R. (1994). Dual probe methods for determining soil thermal properties: Numerical and laboratory study.

Bouazza, A., Abuel-Naga, H. M., Gates, W. and Laloui, L. (2008). Temperature effects on volume change and hydraulic properties of geosynthetic clay liners, *The First Pan American Geosynthetics Conference & Exhibition*, number CONF, Industrial Fabrics Association International (IFAI).

Bouazza, A., Ali, M. A., Rowe, R. K., Gates, W. P. and El-Zein, A. (2017). Heat mitigation in geosynthetic composite liners exposed to elevated temperatures, *Geotextiles and Geomembranes* **45**(5): 406–417.

Boukelia, A. (2016a). *Modélisations physique et numérique des géostructures énergétiques*, PhD thesis, Université de Lorraine.

Boukelia, A. (2016b). *Physical and numerical modeling of energy geostructures, PhD thesis.*, PhD thesis.

Boukelia, A., Eslami, H., Rosin-Paumier, S. and Masrouri, F. (2019). Effect of temperature and initial state on variation of thermal parameters of fine compacted soils, *European Journal of Environmental and Civil Engineering* **23**(9): 1125–1138.

Brandl, H. (2006). Energy foundations and other thermo-active ground structures, *Geotechnique* **56**(2): 81–122.

Bristow, K. L. (1998). Measurement of thermal properties and water content of unsaturated sandy soil using dual-probe heat-pulse probes, *Agricultural and forest meteorology* **89**(2): 75–84.

Burghignoli, A., Desideri, A. and Miliziano, S. (2000). A laboratory study on the thermomechanical behaviour of clayey soils, *Canadian Geotechnical Journal* **37**(4): 764–780.

Busby, J. (2015). Determination of thermal properties for horizontal ground collector loops.

Caljé, R. (2010). Future use of aquifer thermal energy storage below the historic centre of amsterdam, tu delft, masters, delft.

Campanella, R. G. and Mitchell, J. K. (1968). Influence of temperature variations on soil behavior, *Journal of Soil Mechanics & Foundations Div* .

Cao, S. (2010). State of the art thermal energy storage solutions for high performance buildings.

Casagrande, A. (1936). The determination of pre-consolidation load and it's practical significance, *Proc. Int. Conf. Soil Mech. Found. Eng. Cambridge, Mass., 1936*, Vol. 3, p. 60.

Casasso, A. and Sethi, R. (2014). Efficiency of closed loop geothermal heat pumps: a sensitivity analysis, *Renewable Energy* **62**: 737–746.

Cekerevac, C. and Laloui, L. (2004). Experimental study of thermal effects on the mechanical behaviour of a clay, *International journal for numerical and analytical methods in geomechanics* **28**(3): 209–228.

Chalhoub, M., Bernier, M., Coquet, Y. and Philippe, M. (2017). A simple heat and moisture transfer model to predict ground temperature for shallow ground heat exchangers, *Renewable energy* **103**: 295–307.

Chen, X. and Buchberger, S. G. (2018). Exploring the relationships between warm-season precipitation, potential evaporation, and "apparent" potential evaporation at site scale, *Hydrology and Earth System Sciences* **22**(8): 4535.

Cho, W., Lee, J. and Chun, K. (1999). The temperature effects on hydraulic conductivity of compacted bentonite, *Applied clay science* **14**(1-3): 47–58.

Choi, W. and Ooka, R. (2016). Effect of disturbance on thermal response test, part 2: Numerical study of applicability and limitation of infinite line source model for interpretation under disturbance from outdoor environment, *Renewable Energy* **85**: 1090–1105.

Cole, R. (1976). The longwave radiation incident upon the external surface of buildings.

Coquard, R., Baillis, D. and Quenard, D. (2006). Experimental and theoretical study of the hot-wire method applied to low-density thermal insulators, *International journal of heat and mass transfer* **49**(23-24): 4511–4524.

Cui, Y. J., Sultan, N. and Delage, P. (2000). A thermomechanical model for saturated clays, *Canadian Geotechnical Journal* **37**(3): 607–620.

De Hoog, F. R., Knight, J. and Stokes, A. (1982). An improved method for numerical inversion of laplace transforms, *SIAM Journal on Scientific and Statistical Computing* **3**(3): 357–366.

Dec, D. A. (2006). *Thermal properties in Luvisols under conventional and conservation tillage treatment*, PhD thesis, Christian-Albrechts Universität Kiel.

Delage, P., Cui, Y. J. and Sultan, N. (2004). On the thermal behaviour of boom clay, *Proceedings Eurosafe 2004 conference, Berlin, CD-Rom.*

Delage, P., Sultan, N. and Cui, Y. J. (2000). On the thermal consolidation of boom clay, *Canadian Geotechnical Journal* **37**(2): 343–354.

Delage, P., Sultan, N., Cui, Y.-J. and Ling, L. X. (2011). Permeability changes in boom clay with temperature, *arXiv preprint arXiv:1112.6396* .

Devices, D. et al. (2016). Kd2 pro thermal properties analyzer operator's manual, *Pullman, WA* .

Di Donna, A. (2014). *Thermo-mechanical aspects of energy piles*, PhD thesis.

Di Donna, A. and Laloui, L. (2013). Soil response under thermomechanical conditions imposed by energy geostructures, *Energy Geostructures: Innovation in Underground Engineering* pp. 3–21.

Dietrich, O., Fahle, M. and Seyfarth, M. (2016). Behavior of water balance components at sites with shallow groundwater tables: Possibilities and limitations of their simulation using different ways to control weighable groundwater lysimeters, *Agricultural Water Management* **163**: 75–89.

Dieye, Y., Sambou, V., Faye, M., Thiam, A., Adj, M. and Azilinon, D. (2017). Thermo-mechanical characterization of a building material based on typha australis, *Journal of Building Engineering* **9**: 142–146.

Drijver, B. and Willemsen, A. (2001). Groundwater as a heat source for geothermal heat pumps, *International summer school on direct application of geothermal energy, International Geothermal Association, Bad Urach, Germany, September* pp. 17–20.

Ekwue, E., Stone, R. and Bhagwat, D. (2006). Thermal conductivity of some compacted trinidadian soils as affected by peat content, *Biosystems engineering* **94**(3): 461–469.

Elminshawy, N. A., Siddiqui, F. R., Farooq, Q. U. and Addas, M. F. (2017). Experimental investigation on the performance of earth-air pipe heat exchanger for different soil compaction levels, *Applied Thermal Engineering* **124**: 1319–1327.

Eriksson, L. (1989). Temperature effects on consolidation properties of sulphide clays, *International Conference on Soil Mechanics and Foundation Engineering: 13/08/1989-18/08/1989*, Balkema Publishers, AA/Taylor & Francis The Netherlands, pp. 2087–2090.

Eslami, H. (2014). *Thermo-hydromechanical soil behavior in the neighborhood of energy geostructures*, PhD thesis.

ESRIG, M. I. (1969). Some temperature effects on soil compressibility and pore water pressure, *Special Report-Highway Research Board* (103): 231.

Fantucci, S., Lorenzati, A., Kazas, G., Levchenko, D. and Serale, G. (2015). Thermal energy storage with super insulating materials: a parametrical analysis, *Energy Procedia* **78**: 441–446.

Florides, G. and Kalogirou, S. (2007). Ground heat exchangers—a review of systems, models and applications, *Renewable energy* **32**(15): 2461–2478.

François, B., Salager, S., El Youssoufi, M., Ubals Picanyol, D., Laloui, L. and Saix, C. (2007). Compression tests on a sandy silt at different suction and temperature levels, *Computer applications in geotechnical engineering*, pp. 1–10.

Fredlund, D., Rahardjo, H. and Fredlund, M. (2012). Chapter 5: Soil–water characteristic curves for unsaturated soils, *Unsaturated Soil Mechanics in Engineering Practice* pp. 184–272.

Gan, G. (2013). Dynamic thermal modelling of horizontal ground-source heat pumps, *International Journal of Low-Carbon Technologies* **8**(2): 95–105.

Gan, G. (2014). Dynamic interactions between the ground heat exchanger and environments in earth–air tunnel ventilation of buildings, *Energy and buildings* **85**: 12–22.

Gao, L., Zhao, J. and Tang, Z. (2015). A review on borehole seasonal solar thermal energy storage, *Energy procedia* **70**: 209–218.

Gao, Y., Fan, R., Li, H., Liu, R., Lin, X., Guo, H. and Gao, Y. (2016). Thermal performance improvement of a horizontal ground-coupled heat exchanger by rainwater harvest, *Energy and Buildings* **110**: 302–313.

Gao, Z., Wang, L. and Horton, R. (2009). Comparison of six algorithms to determine the soil thermal diffusivity at a site in the loess plateau of china, *Hydrology and Earth System Sciences Discussions* **6**(2): 2247–2274.

Gehlin, S. and Hellström, G. (2000). Recent status of in-situ thermal response tests for btes applications in sweden, *Proc. Terrastock 2000* pp. 159–164.

Gehlin, S. and Nordell, B. (2003). Determining undisturbed ground temperature for thermal response test, *ASHRAE Transactions*, Vol. 109, pp. 151–156.

Gerrits, A., Savenije, H., Veling, E. and Pfister, L. (2009). Analytical derivation of the budyko curve based on rainfall characteristics and a simple evaporation model, *Water Resources Research* **45**(4).

Ghaaowd, I., Takai, A., Katsumi, T. and McCartney, J. S. (2015). Pore water pressure prediction for undrained heating of soils, *Environmental Geotechnics* **4**(2): 70–78.

Ghahremannejad, B. (2003). Thermo-mechanical behaviour of two reconstituted clays.

Girard, A., Gago, E. J., Muneer, T. and Caceres, G. (2015). Higher ground source heat pump cop in a residential building through the use of solar thermal collectors, *Renewable energy* **80**: 26–39.

Gonzalez, R. G., Verhoef, A., Vidale, P. L., Main, B., Gan, G. and Wu, Y. (2012). Interactions between the physical soil environment and a horizontal ground coupled heat pump, for a domestic site in the uk, *Renewable energy* **44**: 141–153.

Graham, J., Tanaka, N., Crilly, T. and Alfaro, M. (2001). Modified cam-clay modelling of temperature effects in clays, *Canadian geotechnical journal* **38**(3): 608–621.

GTR (2000). Réalisation des remblais et des couches de forme, *Laboratoire Central des Ponts et Chaussées, Paris* p. 102.

H Abedin, A. and A Rosen, M. (2011). A critical review of thermochemical energy storage systems, *The open renewable energy journal* **4**(1).

Habibi, M. and Hakkaki-Fard, A. (2018). Evaluation and improvement of the thermal performance of different types of horizontal ground heat exchangers based on techno-economic analysis, *Energy Conversion and Management* **171**: 1177–1192.

Hamidi, a. and Khazaei, C. (2010). A thermo-mechanical constitutive model for saturated clays, *International Journal of Geotechnical Engineering* **4**: 445–459.

Hesaraki, A., Holmberg, S. and Haghighat, F. (2015). Seasonal thermal energy storage with heat pumps and low temperatures in building projects—a comparative review, *Renewable and Sustainable Energy Reviews* **43**: 1199–1213.

Hillel, D. (1980). Fundamentals of soil physics academic, *San Diego, CA* .

Horton, R., Wierenga, P. and Nielsen, D. (1983). Evaluation of methods for determining the apparent thermal diffusivity of soil near the surface 1, *Soil Science Society of America Journal* **47**(1): 25–32.

Hueckel, T. and Baldi, G. (1990). Thermoplasticity of saturated clays: experimental constitutive study, *Journal of geotechnical engineering* **116**(12): 1778–1796.

Hueckel, T. and Borsetto, M. (1990). Thermoplasticity of saturated soils and shales: constitutive equations, *Journal of Geotechnical Engineering* **116**(12): 1765–1777.

Hueckel, T., François, B. and Laloui, L. (2009). Explaining thermal failure in saturated clays, *Géotechnique* **59**(3): 197–212.

Hueckel, T., Pellegrini, R. and Del Olmo, C. (1998). A constitutive study of thermo-elasto-plasticity of deep carbonatic clays, *International journal for numerical and analytical methods in geomechanics* **22**(7): 549–574.

Hurtado, F., Kaiser, A. and Zamora, B. (2012). Evaluation of the influence of soil thermal inertia on the performance of a solar chimney power plant, *Energy* **47**(1): 213–224.

Iverson, R. M. and Major, J. J. (1987). Rainfall, ground-water flow, and seasonal movement at minor creek landslide, northwestern california: Physical interpretation of empirical relations, *Geological Society of America Bulletin* **99**(4): 579–594.

Jahangir, M. H., Ghazvini, M., Pourfayaz, F. and Ahmadi, M. H. (2018). A numerical study into effects of intermittent pump operation on thermal storage in unsaturated porous media, *Applied Thermal Engineering* **138**: 110–121.

Jannot, Y. and Degiovanni, A. (2013). Thermal properties measurement of dry bulk materials with a cylindrical three layers device, *Review of Scientific Instruments* **84**(9): 094901.

Jannot, Y. and Degiovanni, A. (2018). *Thermal properties measurement of materials*, Wiley Online Library.

Jannot, Y., Degiovanni, A., Grigorova-Moutiers, V. and Godefroy, J. (2016). A passive guard for low thermal conductivity measurement of small samples by the hot plate method, *Measurement Science and Technology* **28**(1): 015008.

Jannot, Y., Felix, V. and Degiovanni, A. (2010). A centered hot plate method for measurement of thermal properties of thin insulating materials, *Measurement Science and technology* **21**(3): 035106.

Jarad, N. (2016). *Temperature impact on the consolidation and creep behaviour of compacted clayey soils*, PhD thesis, Université de Lorraine.

Jradi, M., Veje, C. and Jørgensen, B. (2017). Performance analysis of a soil-based thermal energy storage system using solar-driven air-source heat pump for danish buildings sector, *Applied Thermal Engineering* **114**: 360–373.

Kaddouri, Z., Cuisinier, O. and Masrouri, F. (2019). Influence of effective stress and temperature on the creep behavior of a saturated compacted clayey soil, *Geomechanics for Energy and the Environment* **17**: 106–114.

Kodikara, J., Rajeev, P. and Rhoden, N. J. (2011). Determination of thermal diffusivity of soil using infrared thermal imaging, *Canadian geotechnical journal* **48**(8): 1295–1302.

Kouakou, N., Cuisinier, O. and Masrouri, F. (2020). Estimation of the shear strength of coarse-grained soils with fine particles, *Transportation Geotechnics* **25**: 100407.

Kraemer, D. and Chen, G. (2014). A simple differential steady-state method to measure the thermal conductivity of solid bulk materials with high accuracy, *Review of Scientific Instruments* **85**(2): 025108.

Kuntiwattanakul, P., Towhata, I., Ohishi, K. and Seko, I. (1995). Temperature effects on undrained shear characteristics of clay, *Soils and Foundations* **35**(1): 147–162.

Lahoori, M., Jannot, Y., Rosin-Paumier, S., Boukelia, A. and Masrouri, F. (2020). Measurement of the thermal properties of unsaturated compacted soil by the transfer function estimation method, *Applied Thermal Engineering* **167**: 114795.

Lahoori, M., Rosin-Paumier, S., Jannot, Y., Boukelia, A. and Masrouri, F. (2020). Thermal energy storage in embankments: Investigation of the thermal properties of an unsaturated compacted soil, *E3S Web of Conferences*, Vol. 205, EDP Sciences, p. 07011.

Lahoori, M., Rosin-Paumier, S., Stoltz, G. and Jannot, Y. (2020). Thermal conductivity of nonwoven needle-punched geotextiles: effect of stress and moisture, *Geosynthetics International* pp. 1–9.

Laloui, L. and Cekerevac, C. (2003). Thermo-plasticity of clays: an isotropic yield mechanism, *Computers and Geotechnics* **30**(8): 649–660.

Laloui, L. and François, B. (2009a). Acmeg-t: soil thermoplasticity model, *Journal of engineering mechanics* **135**(9): 932–944.

Laloui, L. and François, B. (2009b). ACMEG-T: Soil Thermoplasticity Model, *Journal of Engineering Mechanics* **135**(9): 932–944.

Lee, C., You, J. and Park, H. (2018). In-situ response test of various borehole depths and heat injection rates at standing column well geothermal heat exchanger systems, *Energy and Buildings* **172**: 201–208.

Lee, K. S. (2010). A review on concepts, applications, and models of aquifer thermal energy storage systems, *Energies* **3**(6): 1320–1334.

Li, B., Xu, W. and Tong, F. (2017). Measuring thermal conductivity of soils based on least squares finite element method, *International Journal of Heat and Mass Transfer* **115**: 833–841.

Li, C., Cleall, P. J., Mao, J. and Muñoz-Criollo, J. J. (2018). Numerical simulation of ground source heat pump systems considering unsaturated soil properties and groundwater flow, *Applied Thermal Engineering* **139**: 307–316.

Li, Y., Xu, W., Wang, S., Wang, H. and Dai, Y. (2019). Slope stability analysis with reference to rainfall infiltration in the yongping copper mine, china., *Current Science (00113891)* **116**(4).

Liu, H., Liu, H., Xiao, Y. and McCartney, J. S. (2018). Effects of temperature on the shear strength of saturated sand, *Soils and Foundations* **58**(6): 1326–1338.

Liu, J., Yang, C., Gan, J., Liu, Y., Wei, L. and Xie, Q. (2017). Stability analysis of road embankment slope subjected to rainfall considering runoff-unsaturated seepage and unsaturated fluid–solid coupling, *International Journal of Civil Engineering* **15**(6): 865–876.

Liu, S., Lu, L., Mao, D. and Jia, L. (2007). Evaluating parameterizations of aerodynamic resistance to heat transfer using field measurements.

Low, J. E., Loveridge, F. A., Powrie, W. and Nicholson, D. (2015). A comparison of laboratory and in situ methods to determine soil thermal conductivity for energy foundations and other ground heat exchanger applications, *Acta geotechnica* **10**(2): 209–218.

Lu, Y., Lu, S., Horton, R. and Ren, T. (2014). An empirical model for estimating soil thermal conductivity from texture, water content, and bulk density, *Soil Science Society of America Journal* **78**(6): 1859–1868.

Ma, Q., Ng, C., Mašín, D. and Zhou, C. (2017). An approach for modelling volume change of fine-grained soil subjected to thermal cycles, *Canadian Geotechnical Journal* **54**(6): 896–901.

Maghsoodi, S. (2020). *Thermo-mechanical behavior of soil-structure interface under monotonic and cyclic loads in the context of energy geostructures*, PhD thesis, Université de Lorraine.

Maghsoodi, S., Cuisinier, O. and Masrouri, F. (2020a). Effect of temperature on the cyclic behavior of clay–structure interface, *Journal of Geotechnical and Geoenvironmental Engineering* **146**(10): 04020103.

Maghsoodi, S., Cuisinier, O. and Masrouri, F. (2020b). Thermal effects on mechanical behaviour of soil–structure interface, *Canadian geotechnical journal* **57**(1): 32–47.

Maghsoodi, S., Cuisinier, O. and Masrouri, F. (2020c). Thermal effects on one-way cyclic behaviour of clay-structure interface, *E3S Web of Conferences*, Vol. 205, EDP Sciences, p. 05001.

Maghsoodi, S., Cuisinier, O. and Masrouri, F. (2021). Non-isothermal soil-structure interface model basedon critical state theory, *Acta Geotechnica* pp. 1–21.
URL: *https://doi.org/10.1007/s11440-020-01133-1*

Mengistu, A. G., van Rensburg, L. D. and Mavimbela, S. S. (2017). The effect of soil water and temperature on thermal properties of two soils developed from aeolian sands in south africa, *Catena* **158**: 184–193.

Midttømme, K., Roaldset, E. and Aagaard, P. (1998). Thermal conductivity of selected claystones and mudstones from england, *Clay Minerals* **33**(1): 131–145.

Mitchell, J. K. (1964). Shearing resistance of soils as a rate process, *Journal of Soil Mechanics & Foundations Div* **90**(Proc. Paper 3773).

Mon, E. E., Hamamoto, S., Kawamoto, K., Komatsu, T. and Moldrup, P. (2013). Temperature effects on geotechnical properties of kaolin clay: simultaneous measurements of consolidation characteristics, shear stiffness, and permeability using a modified oedometer, *GSTF International Journal of Geological Sciences (JGS)* **1**(1).

Monteith, J. L. (1965). Evaporation and environment, *Symposia of the society for experimental biology*, Vol. 19, Cambridge University Press (CUP) Cambridge, pp. 205–234.

Morin, R. and Silva, A. J. (1984). The effects of high pressure and high temperature on some physical properties of ocean sediments, *Journal of Geophysical Research: Solid Earth* **89**(B1): 511–526.

Moritz, L. (1995). *Geotechnical properties of clay at elevated temperatures*, Vol. 47, Swedish Geotechnical Institute Linköping, Sweden.

Mualem, Y. (1976). A new model for predicting the hydraulic conductivity of unsaturated porous media, *Water resources research* **12**(3): 513–522.

Murayama (1969). Effect of temperature on the elasticity of clays, *Special Report 103, Washington D.C.* .

Nikoosokhan, S., Nowamooz, H. and Chazallon, C. (2015). Effect of dry density, soil texture and time-spatial variable water content on the soil thermal conductivity. geomech geoeng 11 (2): 149–158.

Nikoosokhan, S., Nowamooz, H. and Chazallon, C. (2016). Effect of dry density, soil texture and time-spatial variable water content on the soil thermal conductivity, *Geomechanics and Geoengineering* **11**(2): 149–158.

Nowamooz, H., Nikoosokhan, S., Lin, J. and Chazallon, C. (2015). Finite difference modeling of heat distribution in multilayer soils with time-spatial hydrothermal properties, *Renewable Energy* **76**: 7–15.

Olafsen Lackey, S., Myers, W. F., Christopherson, T. C. and Gottula, J. J. (2009). Nebraska grout task force in-situ study of grout material 2001-2006 and 2007 dye tests.

Palmeira, E. M. and Gardoni, M. G. (2002). Drainage and filtration properties of non-woven geotextiles under confinement using different experimental techniques, *Geotextiles and Geomembranes* **20**(2): 97–115.

Penner, E., Johnston, G. and Goodrich, L. (1975). Thermal conductivity laboratory studies of some mackenzie highway soils, *Canadian Geotechnical Journal* **12**(3): 271–288.

Pike, J. (1964). The estimation of annual run-off from meteorological data in a tropical climate, *Journal of Hydrology* **2**(2): 116–123.

Rahardjo, H., Li, X., Toll, D. G. and Leong, E. C. (2001). The effect of antecedent rainfall on slope stability, *Unsaturated Soil Concepts and Their Application in Geotechnical Practice*, Springer, pp. 371–399.

Rajeev, P. and Kodikara, J. (2016). Estimating apparent thermal diffusivity of soil using field temperature time series, *Geomechanics and Geoengineering* **11**(1): 28–46.

Romero, E., Gens, A. and Lloret, A. (2001). Temperature effects on the hydraulic behaviour of an unsaturated clay, *Unsaturated Soil Concepts and Their Application in Geotechnical Practice*, Springer, pp. 311–332.

Salomone, L. A. and Kovacs, W. D. (1984). Thermal resistivity of soils, *Journal of Geotechnical Engineering* **110**(3): 375–389.

Sangi, R. and Müller, D. (2018). Dynamic modelling and simulation of a slinky-coil horizontal ground heat exchanger using modelica, *Journal of Building Engineering* **16**: 159–168.

Schmidt, T., Mangold, D. and Müller-Steinhagen, H. (2003). Seasonal thermal energy storage in germany, *ISES solar world congress*, Vol. 14, p. 2003.

Self, S. J., Reddy, B. V. and Rosen, M. A. (2013). Geothermal heat pump systems: Status review and comparison with other heating options, *Applied energy* **101**: 341–348.

Shariatmadari, N. and Saeidijam, S. (2012). The effect of thermal history on thermo-mechanical behavior of bentonite-sand mixture, *International Journal of Civil Engineering* **10**(2): 162–167.

Shetty, R., Singh, D. and Ferrari, A. (2019). Volume change characteristics of fine-grained soils due to sequential thermo-mechanical stresses, *Engineering Geology* **253**: 47–54.

Shortall, R., Davidsdottir, B. and Axelsson, G. (2015). Geothermal energy for sustainable development: A review of sustainability impacts and assessment frameworks, *Renewable and sustainable energy reviews* **44**: 391–406.

Sibbitt, B., McClenahan, D., Djebbar, R., Thornton, J., Wong, B., Carriere, J. and Kokko, J. (2012). The performance of a high solar fraction seasonal storage district heating system–five years of operation, *Energy Procedia* **30**: 856–865.

Singh, R. M. and Bouazza, A. (2013). Thermal conductivity of geosynthetics, *Geotextiles and Geomembranes* **39**: 1–8.

Smits, K. M., Sakaki, T., Limsuwat, A. and Illangasekare, T. H. (2010). Thermal conductivity of sands under varying moisture and porosity in drainage–wetting cycles, *Vadose Zone Journal* **9**(1): 172–180.

Stojanović, B. and Akander, J. (2010). Build-up and long-term performance test of a full-scale solar-assisted heat pump system for residential heating in nordic climatic conditions, *Applied Thermal Engineering* **30**(2-3): 188–195.

Tang, A.-M. and Cui, Y.-J. (2005). Controlling suction by the vapour equilibrium technique at different temperatures and its application in determining the water retention properties of mx80 clay, *Canadian Geotechnical Journal* **42**(1): 287–296.

Tang, A.-M., Cui, Y.-J. and Barnel, N. (2007). A new isotropic cell for studying the thermo-mechanical behavior of unsaturated expansive clays.

Tang, A.-M., Cui, Y.-J. and Le, T.-T. (2008). A study on the thermal conductivity of compacted bentonites, *Applied Clay Science* **41**(3): 181–189.

Tang, F. and Nowamooz, H. (2018a). Hydro-thermal properties of the unsaturated soil, *Civil Infrastructures Confronting Severe Weathers and Climate Changes Conference*, Springer, pp. 18–26.

Tang, F. and Nowamooz, H. (2018b). Long-term performance of a shallow borehole heat exchanger installed in a geothermal field of alsace region, *Renewable Energy* **128**: 210–222.

Tang, F. and Nowamooz, H. (2019). Factors influencing the performance of shallow borehole heat exchanger, *Energy Conversion and Management* **181**: 571–583.

Tang, F. and Nowamooz, H. (2020). Outlet temperatures of a slinky-type horizontal ground heat exchanger with the atmosphere-soil interaction, *Renewable Energy* **146**: 705–718.

Thibbotuwawa, D. and Weerasekera, K. (2013). Study of stabilization of unstable area and development of mitigation measures for landslide at peradeniya, due to widening of town roads, *ENGINEER* **46**(02): 43–57.

Tidfors, M. and Sällfors, G. (1989). Temperature effect on preconsolidation pressure.

Turc, L. (1954). The water balance of soils. relation between precipitation, evaporation and flow, *Ann. Agron* **5**: 491–569.

Uchaipichat, A. and Khalili, N. (2009). Experimental investigation of thermo-hydro-mechanical behaviour of an unsaturated silt, *Géotechnique* **59**(4): 339–353.

Ukrainczyk, N. (2009). Thermal diffusivity estimation using numerical inverse solution for 1d heat conduction, *International journal of heat and mass transfer* **52**(25-26): 5675–5681.

Van Genuchten, M. T. (1980). A closed-form equation for predicting the hydraulic conductivity of unsaturated soils, *Soil science society of America journal* **44**(5): 892–898.

Vieira, A., Maranha, J., Christodoulides, P., Alberdi-Pagola, M., Loveridge, F., Nguyen, F., Florides, G., Radioti, G., Cecinato, F., Prodan, I. et al. (2017). Characterisation of ground thermal and thermo-mechanical behaviour for shallow geothermal energy applications, *Energies* **10**(12): 2044.

Wang, H. and Qi, C. (2008). Performance study of underground thermal storage in a solar-ground coupled heat pump system for residential buildings, *Energy and Buildings* **40**(7): 1278–1286.

Wigstrand, I. (2010). The ates project–a sustainable solution for stockholm-arlanda airport, *renewable energy* **2010**(30).

Wind, G. (1966). Capillary conductivity data estimated by a simple method, *Technical report*, [sn].

Wu, W., Li, X., Charlier, R. and Collin, F. (2004). A thermo-hydro-mechanical constitutive model and its numerical modelling for unsaturated soils, *Computers and Geotechnics* **31**(2): 155–167.

Xinguo, L., Jun, Z., Jian, W., Qiang, L., Yi-Ping, W. and Yan-Min, J. (2009). Application and experiment on solar-ground coupled heat pump with heat storage, *Solar Journal* **30**(12): 1658–1660.

Xu, J., Wang, R. and Li, Y. (2014). A review of available technologies for seasonal thermal energy storage, *Solar energy* **103**: 610–638.

Yao, Y. and Zhou, A. (2013). Non-isothermal unified hardening model: a thermo-elasto-plastic model for clays, *Geotechnique* **63**(15): 1328.

Yavari, N. (2014). *Aspects géotechniques des pieux de fondation énergétiques*, PhD thesis, Paris Est.

Yavari, N., Tang, A. M., Pereira, J.-M. and Hassen, G. (2016). Effect of temperature on the shear strength of soils and the soil–structure interface, *Canadian Geotechnical Journal* **53**(7): 1186–1194.

Yazdani, S., Helwany, S. and Olgun, G. (2019). Influence of temperature on soil–pile interface shear strength, *Geomechanics for Energy and the Environment* **18**: 69–78.

Ye, W.-M., Wan, M., Chen, B., Chen, Y., Cui, Y. and Wang, J. (2013). Temperature effects on the swelling pressure and saturated hydraulic conductivity of the compacted gmz01 bentonite, *Environmental Earth Sciences* **68**(1): 281–288.

Zhai, Q. and Rahardjo, H. (2015). Estimation of permeability function from the soil–water characteristic curve, *Engineering Geology* **199**: 148–156.

Zhang, N. and Wang, Z. (2017). Review of soil thermal conductivity and predictive models, *International Journal of Thermal Sciences* **117**: 172–183.

Zhao, D., Qian, X., Gu, X., Jajja, S. A. and Yang, R. (2016). Measurement techniques for thermal conductivity and interfacial thermal conductance of bulk and thin film materials, *Journal of Electronic Packaging* **138**(4).

Zhao, L., Yang, P., Zhang, L.-C. and Wang, J. (2017). Cyclic direct shear behaviors of an artificial frozen soil-structure interface under constant normal stress and sub-zero temperature, *Cold Regions Science and Technology* **133**: 70–81.